NASA CR-174,746

DOE/NASA/0309-1
NASA CR-174746
MTI 84TR58

DEVELOPMENT OF GAS-LUBRICATED PISTONS FOR HEAVY-DUTY DIESEL ENGINE TECHNOLOGY PROGRAM

Wilbur Shapiro
Mechanical Technology Incorporated

July 1984

Prepared for
NATIONAL AERONAUTICS AND SPACE ADMINISTRATION
Lewis Research Center
Cleveland, Ohio
Under Contract DEN 3-309

for
U.S. DEPARTMENT OF ENERGY
Conservation and Renewable Energy
Office of Vehicle and Engine R&D

DISCLAIMER

Printed in the United States of America

Available from
National Technical Information Service
U.S. Department of Commerce
5285 Port Royal Road
Springfield, VA 22161

NTIS price codes[1]
Printed copy: A10
Microfiche copy: A01

[1]Codes are used for pricing all publications. The code is determined by the number of pages in the publication. Information pertaining to the pricing codes can be found in the current issues of the following publications, which are generally available in most libraries: *Energy Research Abstracts (ERA), Government Reports Announcements* and Index (*GRA* and I): *Scientific Abstract Reports (STAR);* and publication, NTIS-PR-360 available from NTIS at the above address.

DOE/NASA/0309-1
NASA CR-174746
MTI 84TR58

DEVELOPMENT OF GAS-LUBRICATED PISTONS FOR HEAVY-DUTY DIESEL ENGINE TECHNOLOGY PROGRAM

Wilbur Shapiro
Mechanical Technology Incorporated
Latham, New York 12110

July 1984

Prepared for
NATIONAL AERONAUTICS AND SPACE ADMINISTRATION
Lewis Research Center
Cleveland, Ohio 44135
Under Contract DEN 3-309

for
U.S. DEPARTMENT OF ENERGY
Conservation and Renewable Energy
Office of Vehicle and Engine R&D
Washington, D.C. 20585
Under Interagency Agreement DE-A101-80CS50194

TABLE OF CONTENTS

TABLE OF CONTENTS (Cont'd)

LIST OF FIGURES

LIST OF FIGURES (Cont'd)

LIST OF FIGURES (Cont'd)

LIST OF FIGURES (Cont'd)

LIST OF TABLES

EXECUTIVE SUMMARY

Gas-lubricated piston rings are one alternative for adiabatic diesel engines. The high temperatures involved preclude utilization of conventional lubricants and piston rings. Mechanical Technology Incorporated (MTI) and the Cummins Engine Company began development of gas-lubricated pistons in 1977. Concepts were formulated, designs completed and hardware produced. Static testing of the hardware was conducted by MTI under the sponsorship of the Department of Energy with NASA Lewis Research Center acting as the monitoring agency. This report principally describes the results of the test program.

Because of the necessity to operate with very small clearances (in the range of 1.5 to 8 microns), the piston ring must have the capability to produce a self-adjusting clearance that responds to the pressures imposed in the fluid film. One means to accomplish self- adjusting clearances is to sector the ring into a number of freely moving segments that are preloaded against the cylinder liner by supply gas from the combustion chamber and to provide a hydrostatic balancing fluid film utilizing the same source of fluid. A comprehensive description of the ring system is given in Section 2. A rig was produced for evaluating fluid film performance of the rings under varying operating conditions. Results of the test program are provided in Section 4.

In general, the segmented ring configuration tested was deficient in overall performance and would not be acceptable for the application. The principal difficulty was the inability of all segments of a ring set to form a fluid film when exposed to internal pre-load. The problem is due to the delicate moment balance necessary to prevent the segments from overturning combined with the small operating films required.

Optimism was produced by some of the sectors that did form a film and performed well in almost every respect, including capability to accept external loads in the range of 6,000 N, in addition to preloads of approximately 30,000 N.

Flow levels were high (50-60 kg/hr) but could be reduced by more advanced configurations. Approximately 30% of the flow is attributable to leakage between sectors. Target flow levels are in the range of 15 Kg/hr. or approxi-

mately 7 percent of the intake volume. These flow levels are achievable by employing a solid breathable liner with solid pistons. (See Section 7).

Approximate gas bearing theories that were applied to the design of the segmented rings are not precise enough especially with respect to pad inclination angle and fluid-film righting moments. Comprehensive gas-bearing computer codes that model the geometry accurately are required. Although more accurate analysis is required, analysis alone will not be sufficient to produce an optimum design. The close clearances and high pressures involved are beyond what has been verified with contemporary gas-bearing theory and further complexities are introduced by elastic and thermal distortion. Thus, further efforts will require extensive, well instrumented experimentation, and it can be expected that first-generation successful configuration will be produced by a combined theoretical, empirical process.

Recessed configurations were proven to be better for the application than inherently compensated geometries. The advantages of recesses include:

1. Improved liftoff, especially against pre-load because the incoming gas can enter the film more easily.

2. Superior load capacity and stiffness as compared to inherently compensated geometries.

Recesses may produce slightly greater flow requirements and are more prone to pneumatic hammer. However, flow differences can be small and pneumatic hammer is mitigated by friction and damping in the support structure.

Care must be exercised in the design process to ensure that inlet flow restrictions in the pad geometry are minimized to assure the fluid can adequately enter the film. Also, provision for adequate orifice discharge length is important to assure proper operation of the orifice restrictor element.

Some cursory examinations were given to other configurations with the general label of "breathable liner". In these configurations, solid piston designs are coupled with flexible liners that elastically deflect to form a fluid film under hydrostatic pressurization. These configurations afford the mechanical

simplicity required for mass produced engines, and indications are that they will perform acceptably. Breathable liners are the recommended future direction for continued development of gas-lubricated piston rings.

It is concluded that gas-lubricated piston rings are feasible for engines such as the adiabatic diesel, but considerable development work remains, not only for fluid film generation, but in applying material combinations that can withstand momentary high-speed rubs and avoiding contamination of small restrictor elements from combustion gases.

1.0 INTRODUCTION

The adiabatic diesel engine concept shows promise for significantly improving efficiency over present-day diesel engine designs. However, a number of technological developments are needed in order that the predicted performance can be fully realized in practice.

A major problem area is a practical method for sealing the engine combustion chamber gases and supporting the pistons in their housings under the hostile environment generated by the high operating temperatures in an adiabatic engine. It is expected that adiabatic diesel engine temperatures will be of the order of 700° C or greater; inasmuch as the use of conventional oil-lubricated piston rings will not be suitable in this situation, novel methods need to be evolved to accomplish the piston sealing function.

Sealing and load-support mechanism based on gas lubrication offer possible approaches for treating the problem. Because of the availability of high-pressure gas from the combustion chamber itself, the mechanism of hydrostatic support for the piston rings appears particularly suitable. A small portion of the high-pressure combustion gases can be channeled through suitable supply lines and restrictors into the interface between the piston-ring face and the cylinder liner. By design, a very small clearance (of the order of 1.5 to 8 microns) is provided between the ring face and liner, which controls the rate of gas leakage past the ring and allows the ring to reciprocate without contacting the liner. The high- pressure supply gas can generate a net restoring force on the piston ring by altering the pressure distribution within the gas film whenever an external force tends to displace the ring from its concentric position within the liner. Thus, hydrostatic lubrication affords a possible means for maintaining a clearance between the ring face and liner when the ring is subjected to side loads transmitted through the piston (compression, combustion, expansion) and when side loads are not transmitted (intake, exhaust).

Preliminary operating specifications for the adiabatic diesel engine are indicated on Table 1-1 below:

TABLE 1-1

ADIABATIC DIESEL ENGINE PRELIMINARY SPECIFICATIONS

Stroke	15.24 cm (6 in.)
Diameter	15.24 cm (6 in.)
Speed	219.9 rad/s (2100 rpm) at rated power 157.1 rad/s (1500 rpm) at peak torque
Peak Pressures	12.33 MPa (1789 psia) at rated power 14.33 MPa (2079 psia) at peak torque
Average Temperature	316° C (601° F)
Maximum Load	13,344 N (3,000 lbs)
M.E.P.	2.478 MPa (359.4 psia)

The piston size was subsequently reduced to 5.5 inches, which was the diameter utilized for the static test rig. The maximum load is a momentary load that occurs within a 30 degree crank angle range.

Under a prior program with the Cummins Engine Company of Columbus, Indiana, prototype hydrostatic rings and a static test rig had been designed and manufactured. This report describes the results of a static test program intended to establish performance of a particular hydrostatic ring configuration. It also presents advanced configurations that indicate promise for future development.

2.0 DESCRIPTION OF THE HYDROSTATIC PISTON RING

To be viable, the hydrostatic piston must operate with very small clearances (1.5 - 8 microns) so that leakage and blowby is maintained within acceptable limits, and that adequate stiffness is provided by the gas film. It would be difficult to manufacture rigid pistons and liners within the clearance tolerance requirements and if it were possible to produce the required clearance, it would not be maintained due to thermal distortions occurring in the cylinder and piston. Therefore, the system of piston and liner must be designed to provide a self-adjusting clearance in response to the pressure in the film.

The sectored ring concept is comprised of a number of circumferential sectors or segments fitted together in the ring groove of the piston (see Figure 2-1). Gas from a high-pressure reservoir is supplied through a series of circumferentially located restrictor holes into the interface between the ring face and cylinder liner. The reservoir is re-energized once each time during the 4 strokes of a cycle when the combustion chamber gas pressure is at its maximum. During the compression and expansion strokes, the rings will be forced against the piston, so the side loads can be accepted without consuming the gas film. The segmented ring configuration was selected to effect self-generation of the gas film thickness between the ring face and liner, and to compensate for any ring wear that may occur as a result of rubbing contact with the liner.

The principle of operation of the hydrostatically supported piston ring is as follows. The piston ring is designed to operate at some axisymmetric radial clearance by force and moment balancing of the ring segments. With no supply of fluid to the interface through a restrictor, the pressure change along the fluid film from the high-pressure combustion chamber to the crank end is nearly linear. This is shown schematically in Figure 2-2 by the curve marked "without restrictor". In such a case, the fluid film has no stiffness inasmuch as the fluid film pressure profile does not change as a result of changes in the radial clearance. On the other hand, the introduction of a supply of restrictor compensated high-pressure gas within the interface makes the pressure distribution sensitive to changes in clearance, thereby making possible the generation of a restoring force to counteract the force tending to alter the clearance. When operating at equilibrium design conditions, the pressure distribution in a hydrostatically supported ring takes the form indicated by the curve marked

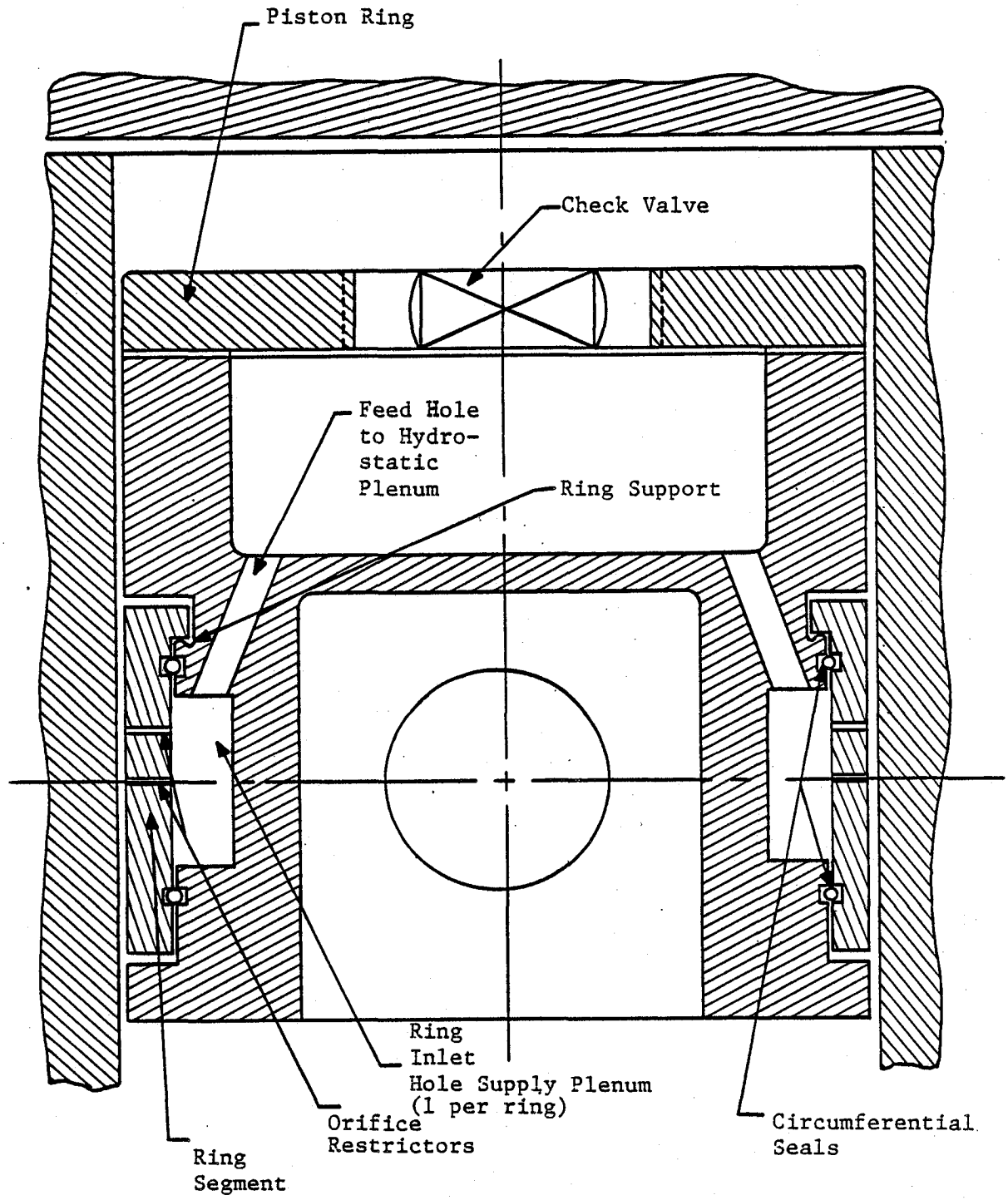

Figure 2-1 Segmented Piston-Ring Configuration

821618

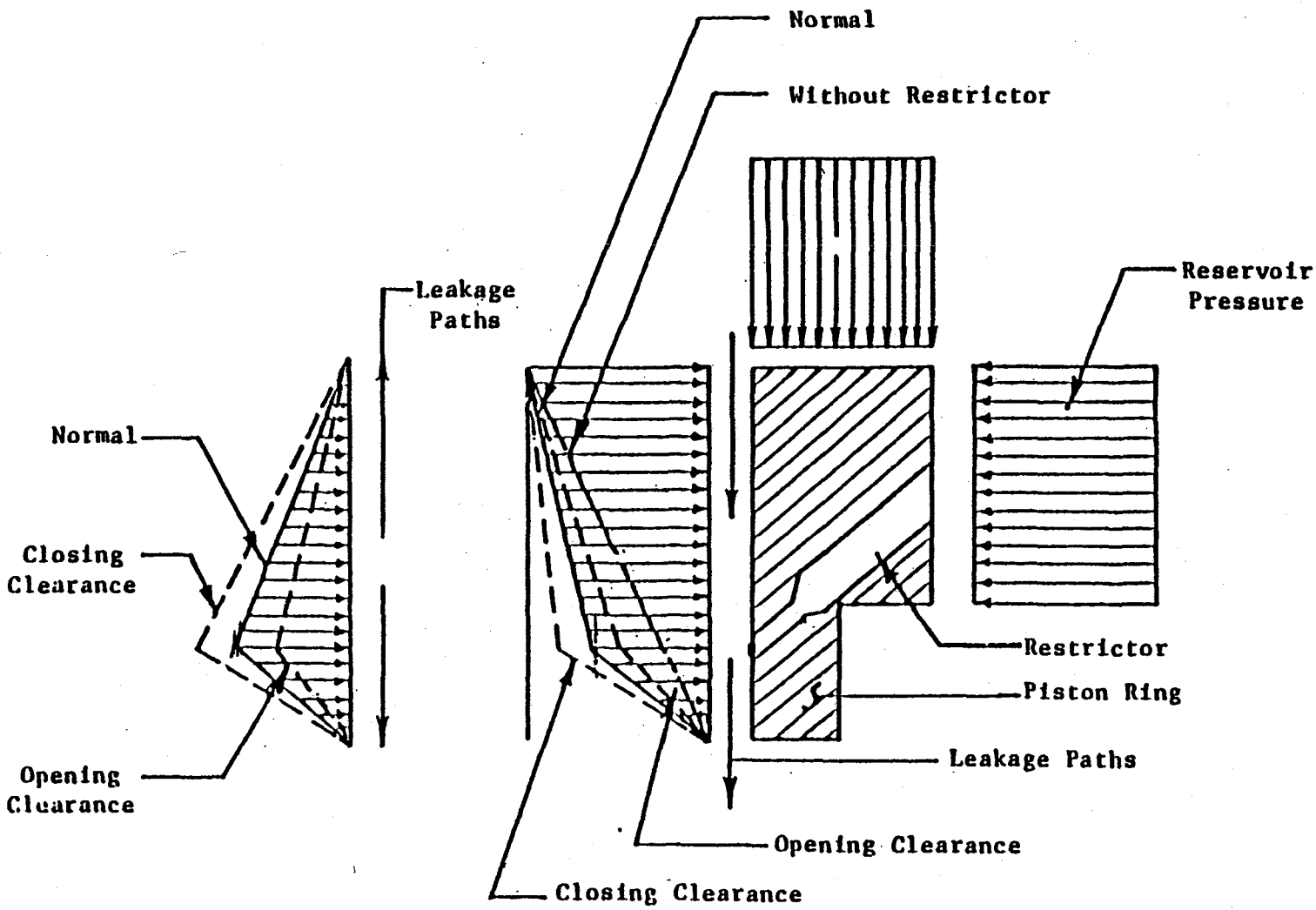

Figure 2-2 Pressure Distribution and Leakage Paths

"normal" in Figure 2-2. If an external force tends to reduce the clearance, the pressure distribution in the fluid film will change to that marked by "closing clearance", which is in the direction to increase the overall pressure within the interface. This is a result of the increased resistance to flow in the interface allowing the fluid pressure at the outlet of the restrictor to rise toward the reservoir supply pressure. The magnitude of the opening force generated to counteract the closure force is equal to the difference in the areas under the two pressure distribution curves. Vice versa, with an increased clearance over that of the equilibrium value, the resistance to flow in the interface is reduced and the pressure distribution tends toward that which exists when no restrictor is present. This is indicated by the curve marked "opening clearance" in Figure 2-2. In this case, the overall pressure in the interface is less than that existing under the equilibrium conditions and, hence, a closing force is generated by reservoir pressure to restore the ring segment to its equilibrium operating position. The two sets of pressure distribution curves in Figure 2-2 correspond to the two cases in which the combustion chamber is at its maximum pressure and when it is at the same pressure as present in the crank end.

As shown on Figure 2-1, the rings are fulcrumed near their upper ends and are internally sealed by circumferential seals of circular cross section. The upper fulcrum ensures a converging clearance from the high to low pressure ends of the piston from the pressure force tending to close the sector against the cylinder. This increases load capability and prevents ring contact. For purposes of static and low- temperature testing, the circumferential seals were "Tetraseals" made of elastomeric materials. For actual high-temperature conditions, these seals would be of high-temperature metallic ring construction. In addition to being able to adjust radially, the rings can accommodate tapering of the cylinder bore due to thermal distortions, because they will allow the segments to move in an angular as well as a radial mode. The joints between the sectors are sealed by inserts as shown on Figures 2-3 and 2-4. These inserts have circumferential clearance to allow radial and angular motions. Careful attention was paid to sealing all potential leakage paths with both the outside and inside joint inserts. Heavy side loads will bottom the loaded segments against the piston and simultaneously close off the interior annulus around the inlet hole to the sector to reduce the sector preload. The sectors can then accommodate full side thrust without consuming the gas-film clearance.

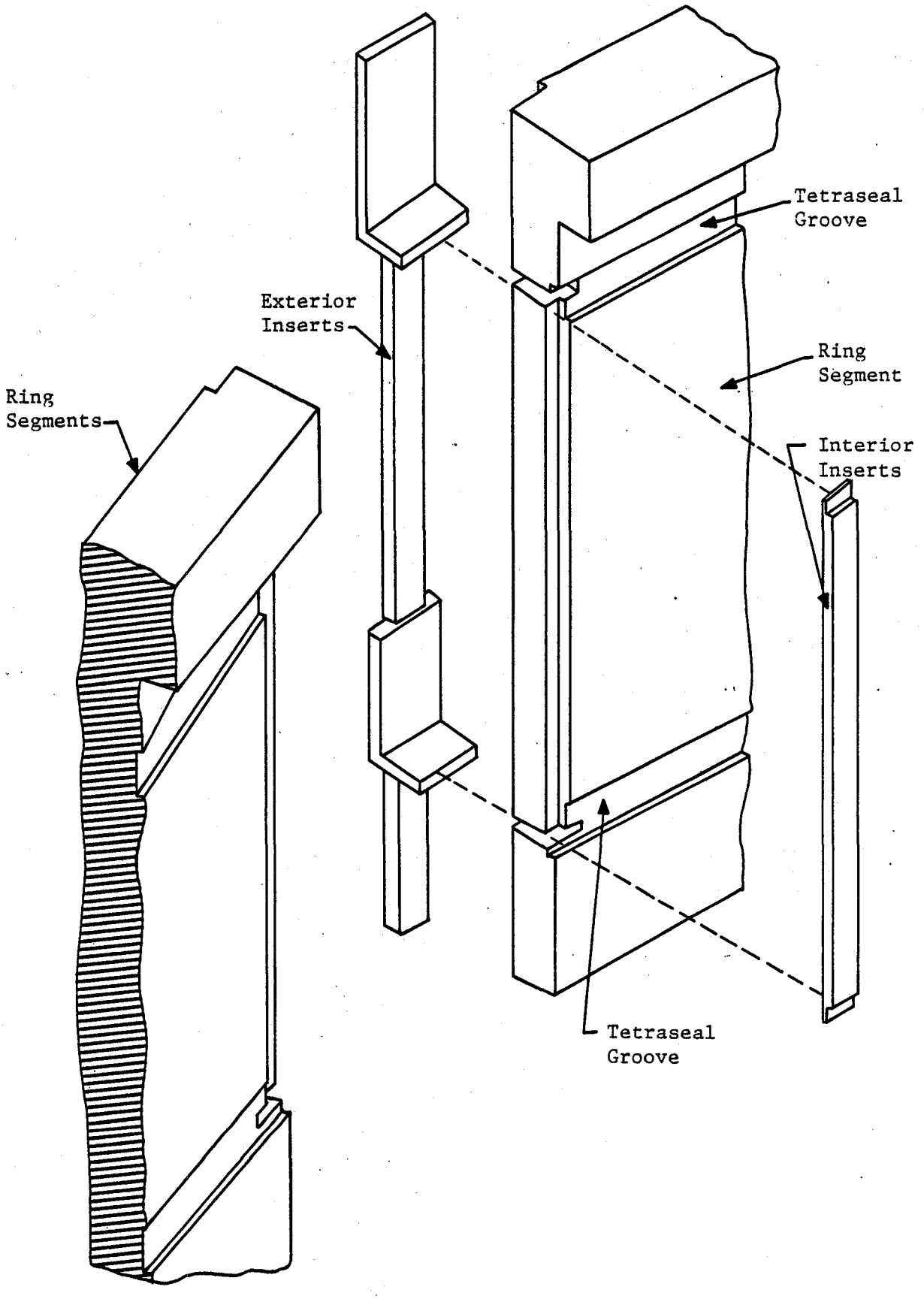

Figure 2-3 Ring Segments Joint Inserts

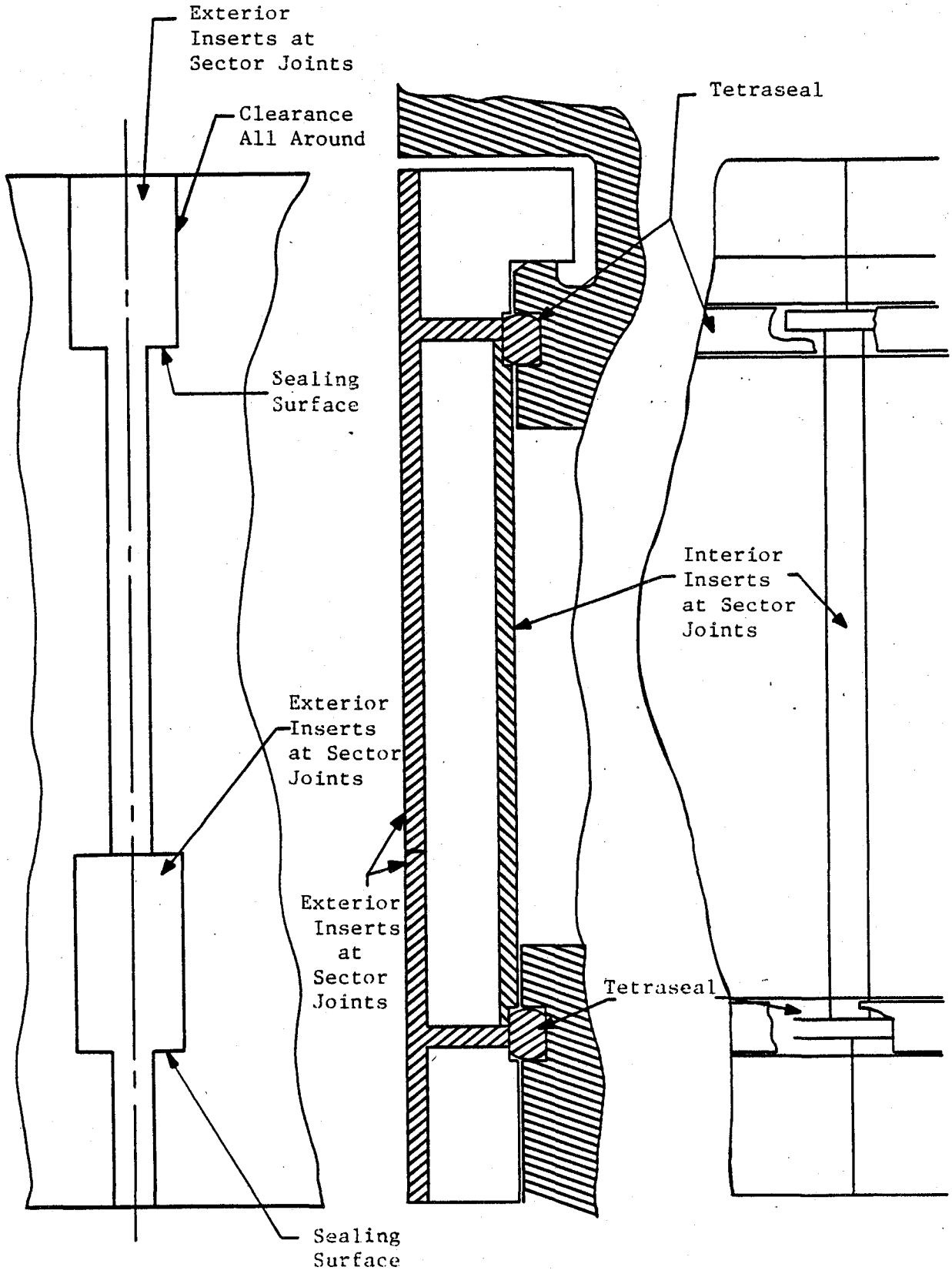

Figure 2-4 Insert, Sealing Joints

821551 -I

As shown on Figure 2-4, the exterior inserts include two sealing surfaces, one near the upper end and one near the lower end of the sectors. The upper sealing surface is intended to prevent high pressure compressed or combusted gases from leaking through the sectors. The lower sealing surface prevents through-flow leakage to provide high boundary pressures and greater load capacity.

Figure 2-5 is a photograph that shows two ring sectors with the outer inserts in place. Figure 2-6 shows the interior of two adjacent segments with the inside insert in place.

The piston-ring system incorporates an additional refinement intended to improve load capacity which has been alluded to in previous paragraphs. The total load on the gas film is the summation of the external load plus the load due to the reservoir pressure (pre-load). Before accepting external load, the segment must bottom against the piston and overcome the preload acting upon it. In the absence of external load, the segment is preloaded by the reservoir pressure acting against the annular area between the Tetraseals. As load is applied, the segment makes contact with the piston, in the annular region, and thus removes the gas pre-load and accepts greater external load. Gas supply is maintained because of the six drilled holes in the piston centrally located behind each segment. The gas supply holes in the piston are indicated on Figure 2-7. The slots that extend from each hole were intended to feed restrictor holes not covered by the main supply hole. That is also the reason for the grooved pattern on the interior of each pad as shown on Figure 2-6. The groove pattern was incorporated when the bearing compensation system consisted of multiple drilled orifices. This configuration was subsequently changed to two relatively large recesses fed by three orifices; the three orifices could be fed by the one large inlet hole behind each sector and obviated the need for the grooving patterns. Unfortunately, once the grooves were machined, they could not be removed. The grooving deleteriously affected load capacity since they prevented removal of some preload.

Figure 2-8 shows dimensions of the rings and piston in English units. Other pertinent drawings are presented in Appendix B. The recess configuration is presented in Section 4. The test ring diameter was 139.7 mm (5.5 in.) and the machined clearance between the ring and cylinder was 12.7 microns (.0005 in.).

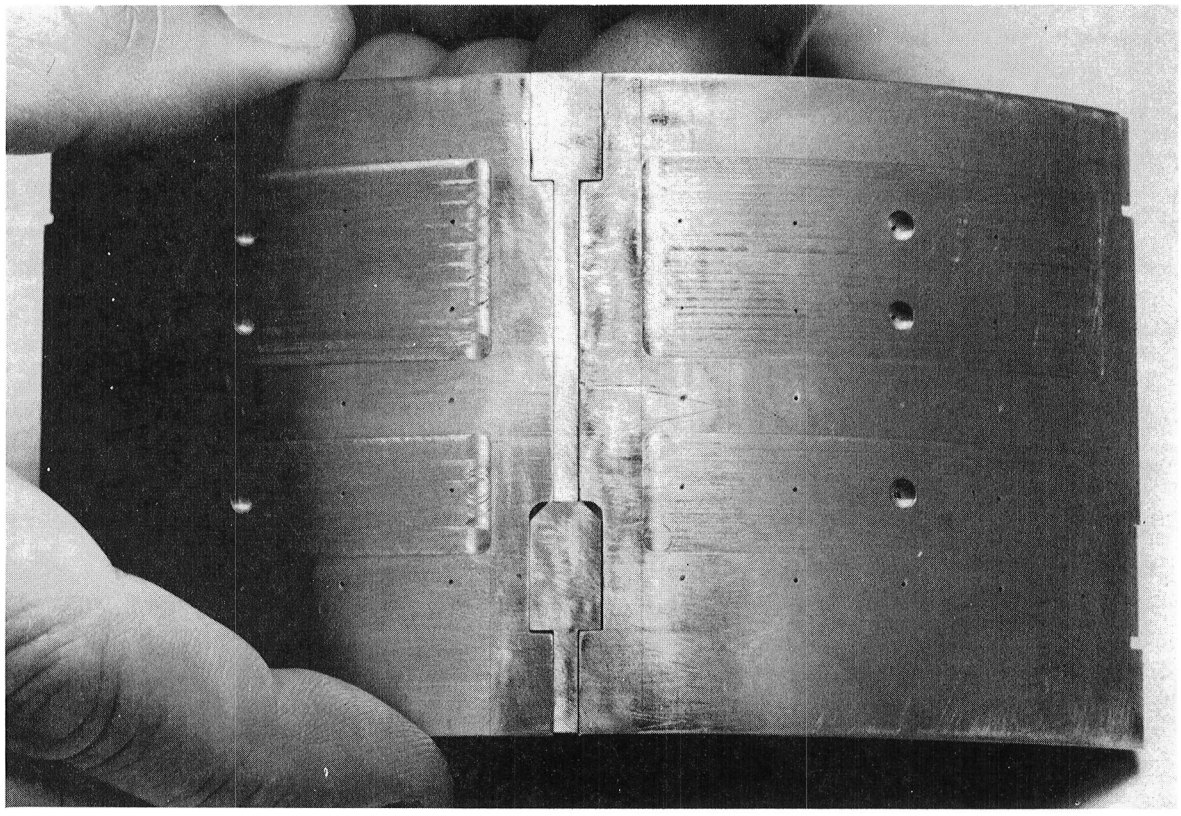

Figure 2-5 Two Adjacent Sectors with Outer Inserts Installed

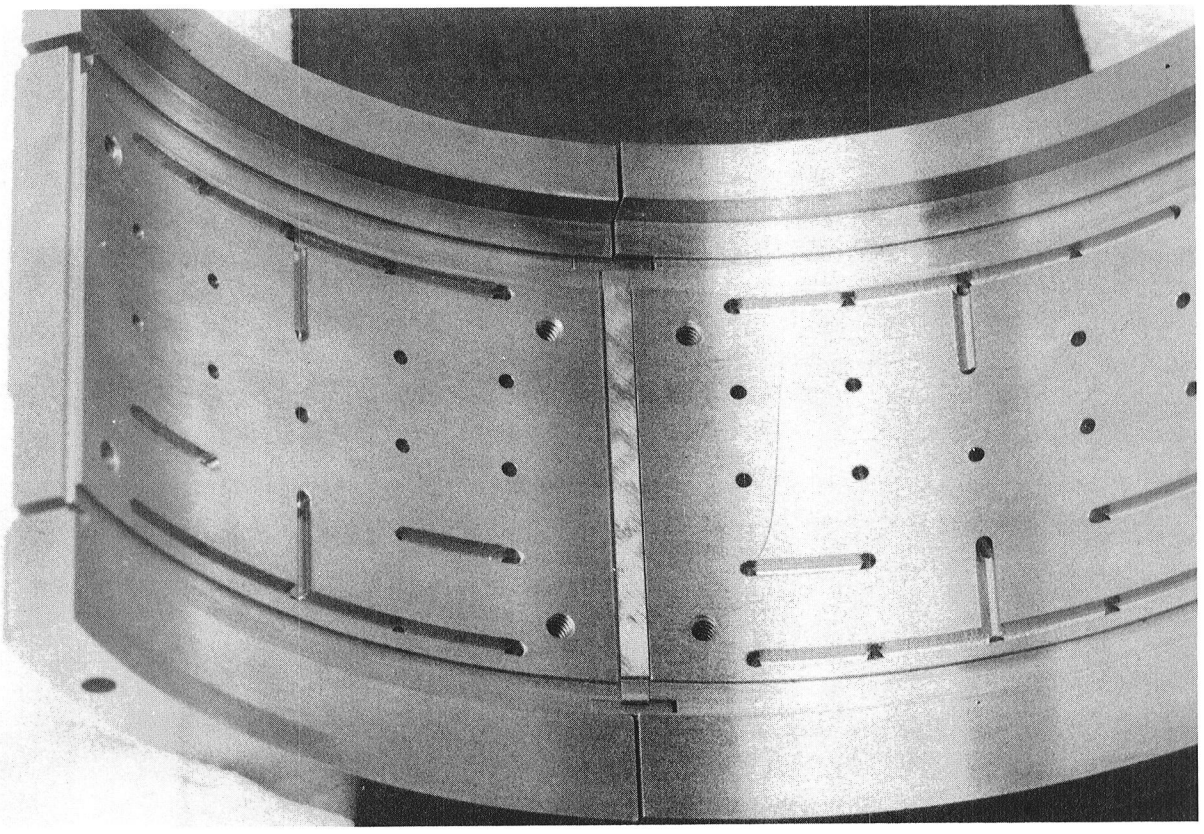

Figure 2-6 Two Adjacent Sectors with Inner Inserts Installed

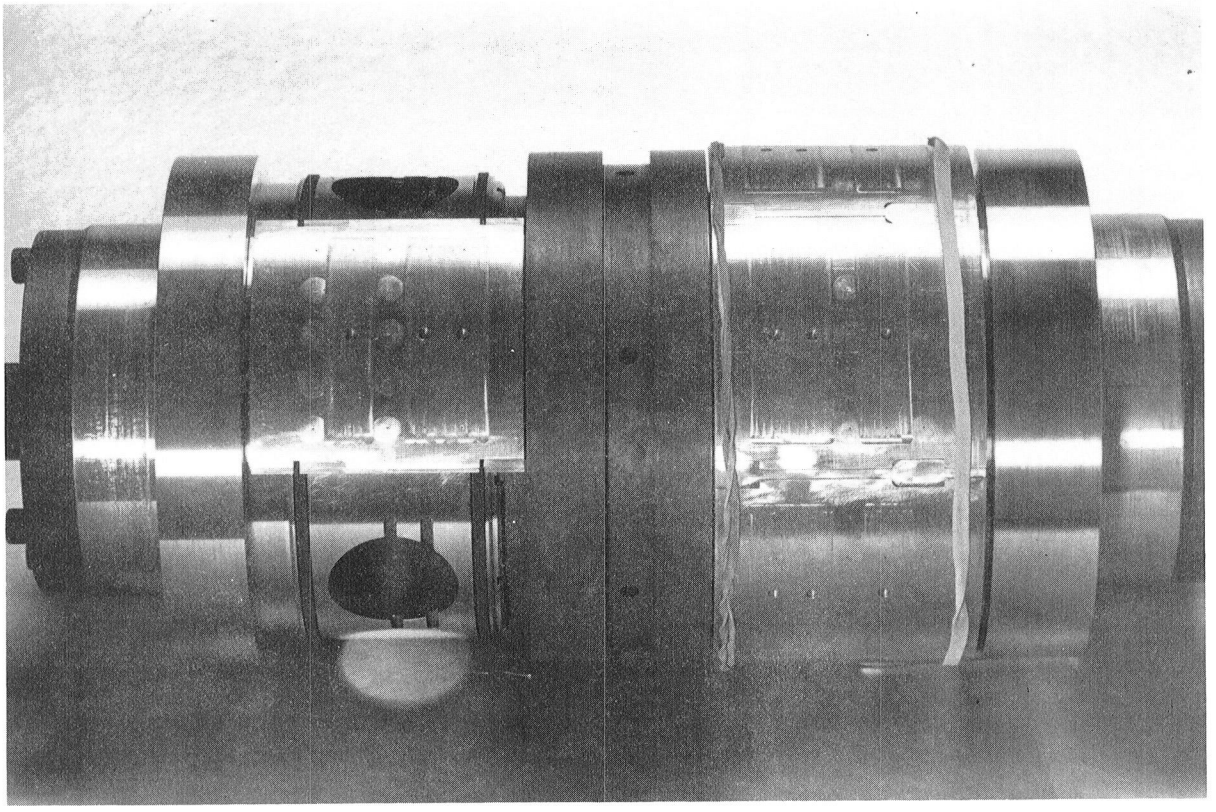

Figure 2-7 Static Test Piston with One Set of Rings Installed, and Showing Gas Supply Hole Behind Each Segment

REVISIONS		SIZE E	649E021	REV. A
SYM	DESCRIPTION		DATE	APPROVAL
A	ECN CHANGE 649-014.		7 DEC 1983	E Roark

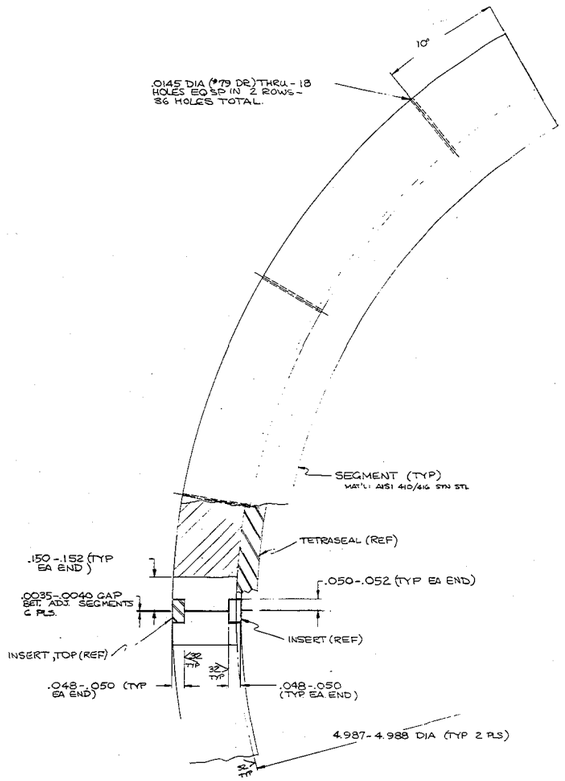

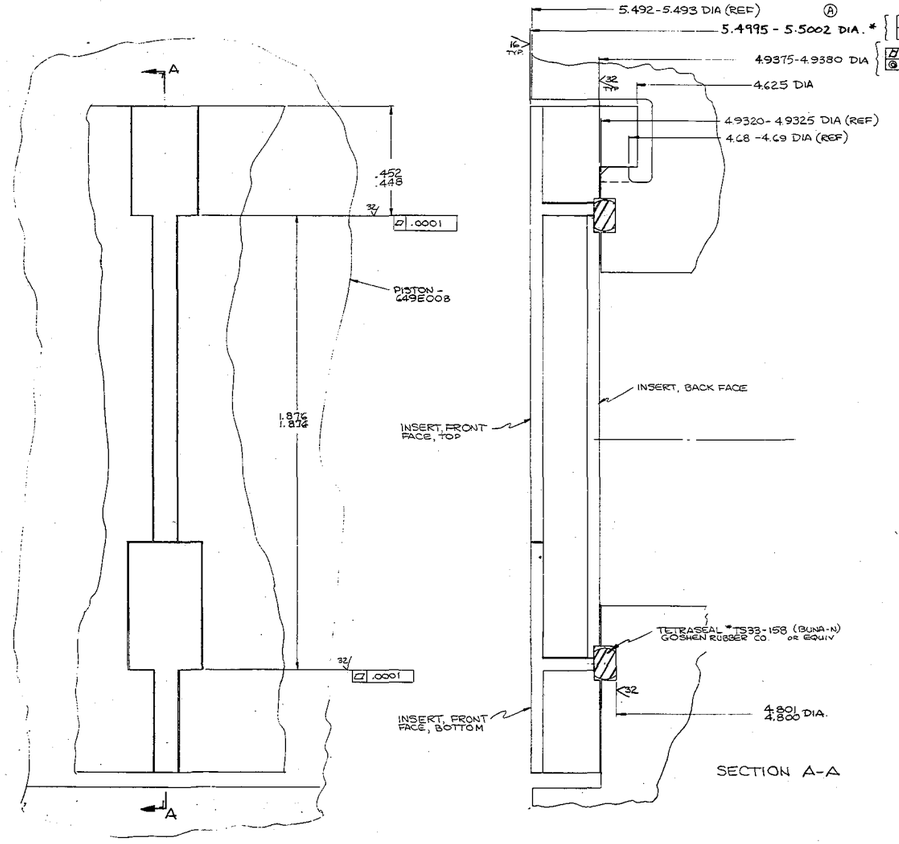

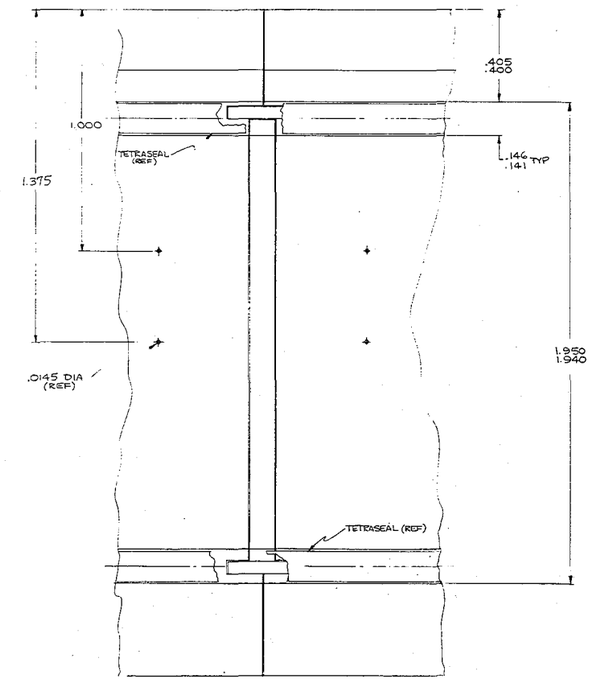

NOTES:

1) ASSEMBLY TO BE MADE OF MATCHED SETS OF SEGMENTS & FACE INSERTS.
2) INSERTS SHALL HAVE THEIR OUTSIDE SURFACES GROUND IN THE SAME OPERATION USED TO OBTAIN THE 5.5000 - 5.5005 & 4.9375 - 4.9380 DIMS.

PISTON RING SEGMENT L/O

649E021

PDE Franco 7/29/80 SCALE: 5:1

Fig. 2-8 Ring and Piston Dimensions

3.0 DESCRIPTION OF STATIC TEST RIG AND TEST FACILITY

3.1 Description of Static Test Rig

A cross section of the static test rig is shown on Figure 3-1. Two sets of rings are tested simultaneously in a back-to-back arrangement to obviate the need for high-pressure seals. Provisions were made to independently provide hydrostatic supply pressure to the rings and to provide high pressure to the combustion side of the rings. The interior piston is stationary and the cylindrical liner is floating. It can be moved relative to the piston by differential jacking screws. In between the jacking screws and cylinder are force transducers that record the force applied to the rings when the jacking screws are turned.

Six capacitance probes monitor clearance of a ring set so for the two ring assemblies there are a total of twelve capacitance probes. Longitudinally, the probes are located at either end of a segment and there are three probes in each plane. Thus, every other adjacent sector is monitored for clearance. A complete set of ring and rig drawings are included as Appendix C.

3.2 Description of Flow Loop

The flow loop is diagrammatically shown on Figure 3-2. The source of high-pressure nitrogen was from pressurized bottles located on a truck trailer outside of the bay area where the test rig was located. The nitrogen splits into two separate paths to the test rig. One path feeds the interior of the sectors (bearing supply); the other feeds the combustion chamber side of the rings. Pressure regulators control the pressure and flow to each of the independent paths. Separate flow meters and pressure transducers are incorporated in each path.

3.3 Instrumentation

All test data was recorded on a Fluke 2240C data logger with digital printout. There were 23 channels of information which are identified on Table 3-1.

All instrumentation was carefully calibrated by MTI or the supply vendor. Calibration curves were recorded in log books available at MTI. The calibration for the orifice plate flow meters is indicated on Table 3-2.

REVISIONS		SIZE E	649E017	REV B
REV.	DESCRIPTION	DATE	APPROVED	
A	ISSUED	9-24-79	E Bennett	
B	REVISED PER E.C.N. 544-001	10-31-80	E Bennett	

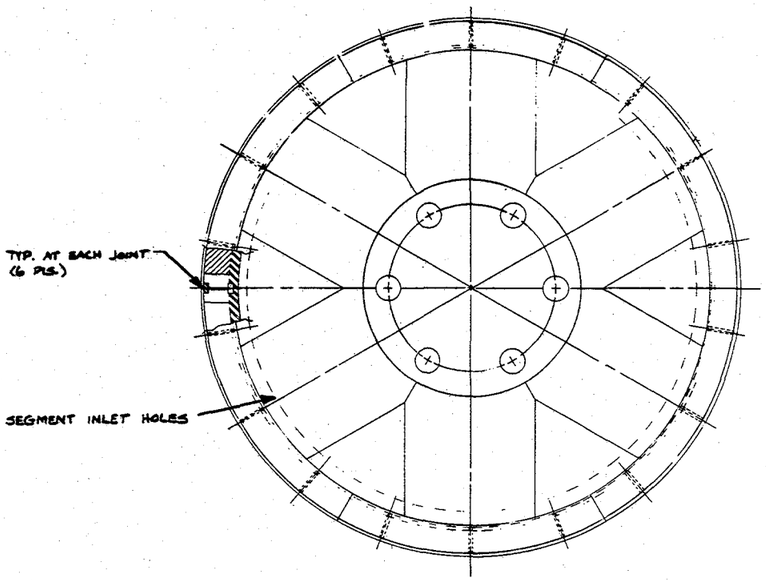

SECTION E-E
(SCALE 2/1)
TYPICAL 2 PLACES

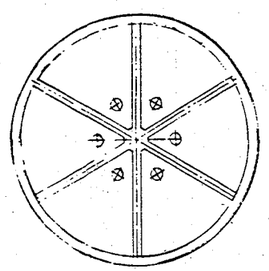

SECTION D-D

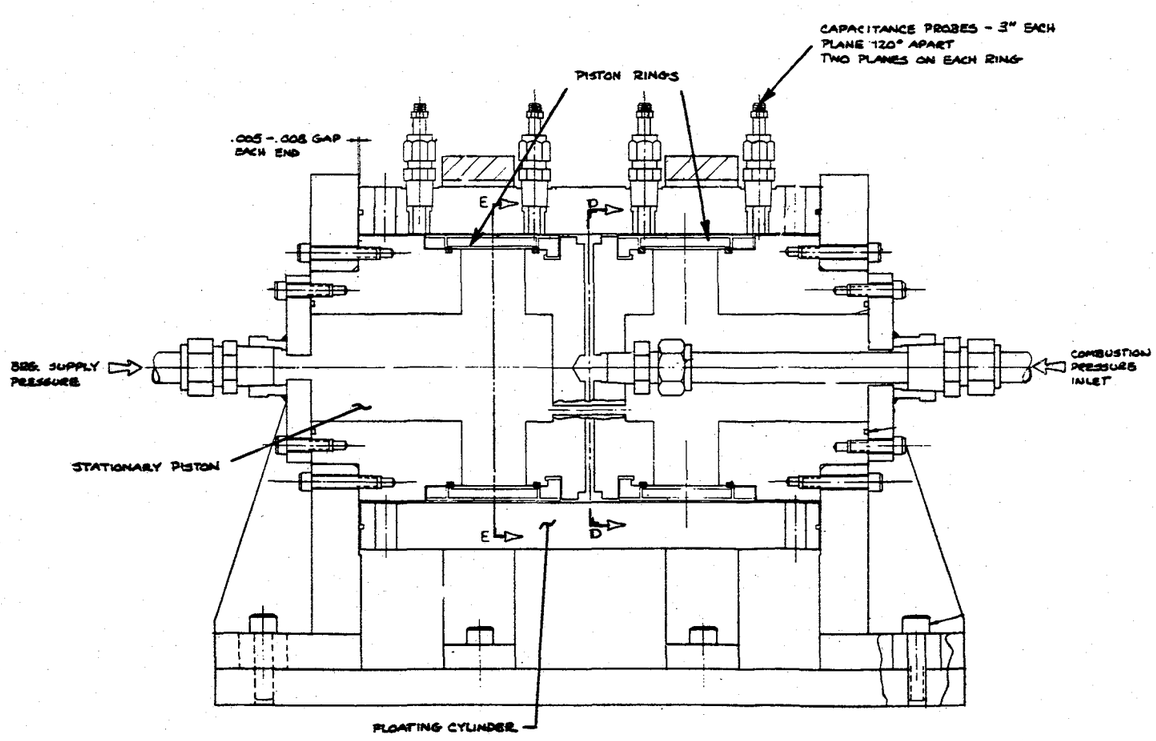

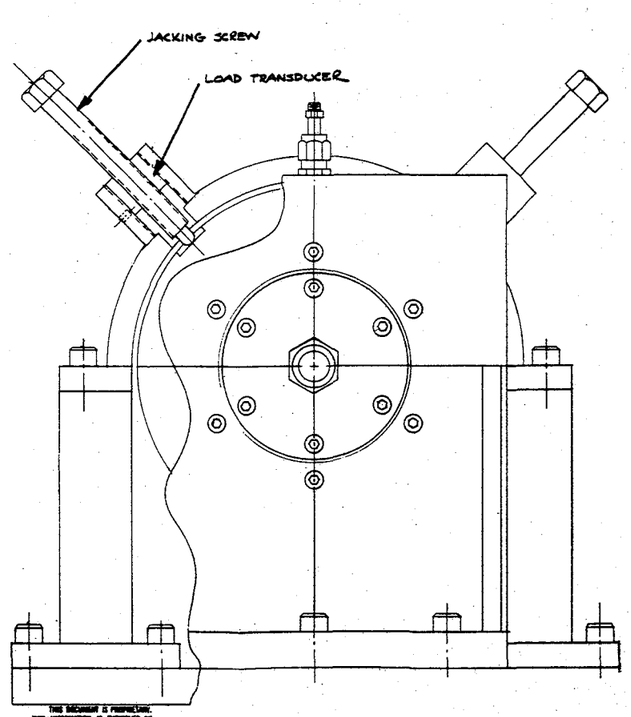

Fig. 3-1 Cross Section of Static Test Rig

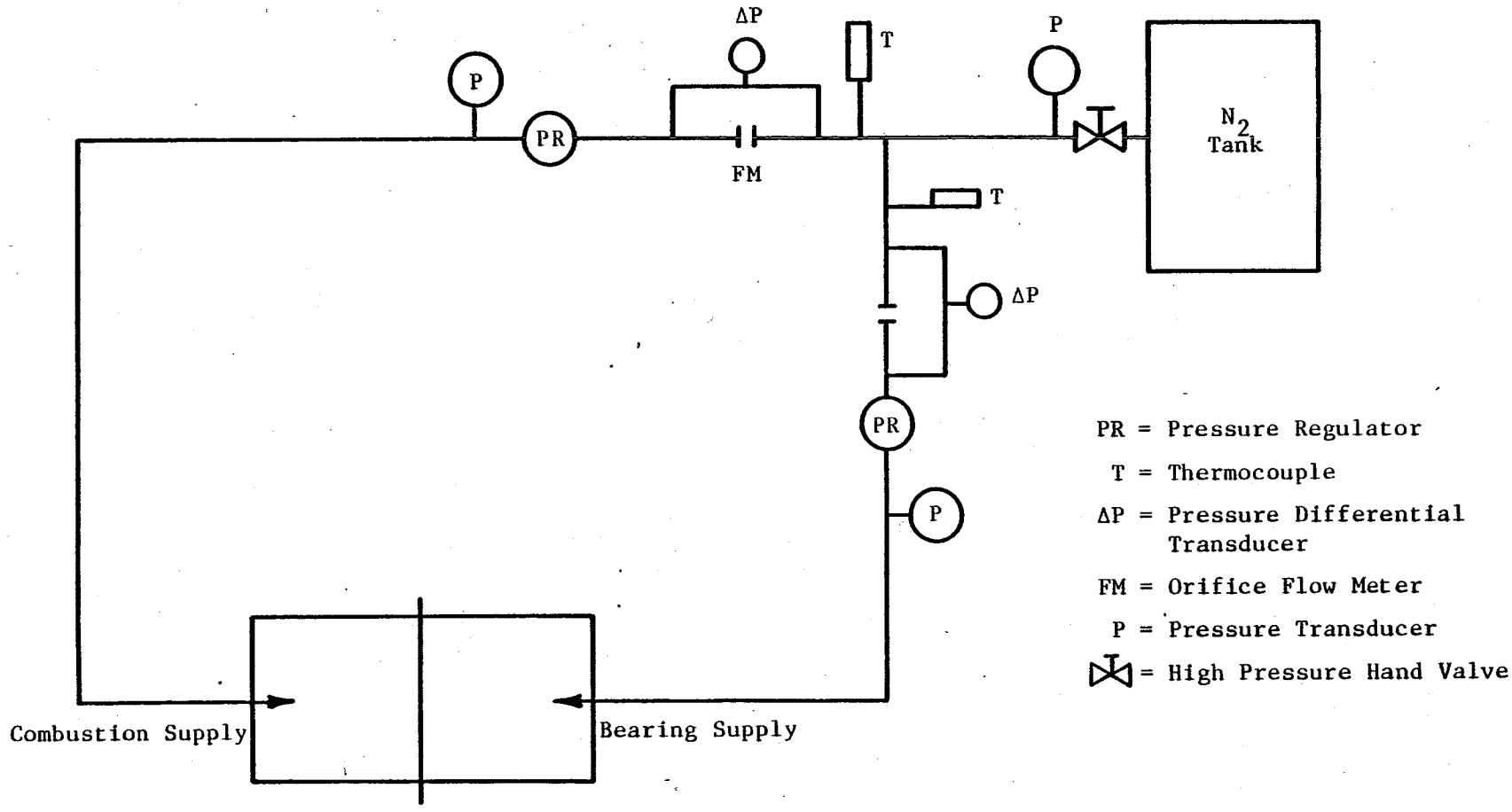

Fig. 3-2 Flow Loop Diagram

TABLE 3-1

LIST OF INSTRUMENTATION

Channel	Function	Instrument
1	N_2 Supply Pressure	Valdyne DP 15-64 Transducer with Pace Wiancko CD-25 Transducer Indicator
2	Bearing Supply, P	Celesco P 2805-3000 PSI - with Salient Electric MTI 15/15A #03 Power Supply
3	Bearing Flow, ΔP	Whittaker KP 15 Transducer, CD-10 Carrier Demodulator - 25 PSI - ΔP
4	Combustion Supply, P	Celesco P 2805-3000 PSI - with Salient Electric MTI 15/15A #03 Power Supply
5	Combustion Flow, ΔP	Whittaker KP 15 Transducer, CD-10 Carrier Demodulator - 25 PSI ΔP
6	Capacitance Probe 1	MTI ASP-5 with Wayne Kerr DM-100B Amplifier - 5 mil range
7	Capacitance Probe 2	MTI ASP-5 with Wayne Kerr DM-100 Amplifier - 5 mil range
8	Capacitance Probe 3	MTI ASP-5 with Wayne Kerr DM-100B Amplifier - 5 mil range
9	Capacitance Probe 4	MTI ASP-5 with Wayne Kerr DM-100 Amplifier - 5 mil range
10	Capacitance Probe 5	MTI ASP-5 with Wayne Kerr DM-100B Amplifier - 5 mil range
11	Capacitance Probe 6	MTI ASP-5 with Wayne Kerr DM-100 Amplifier - 5 mil range
12	Capacitance Probe 7	MTI ASP-5 with Wayne Kerr TE-600 Amplifier - 5 mil range
13	Capacitance Probe 8	MTI ASP-5 with Wayne Kerr TE-600 Amplifier - 5 mil range
14	Capacitance Probe 9	MTI ASP-5 with Wayne Kerr TE-600 Amplifier - 5 mil range
15	Capacitance Probe 10	MTI ASP-5 with Wayne Kerr TE-600 Amplifier - 5 mil range
16	Capacitance Probe 11	MTI ASP-5 with Wayne Kerr TE-600 Amplifier - 5 mil range
17	Capacitance Probe 12	MTI ASP-5 with Wayne Kerr TE-600 Amplifier - 5 mil range
18	Load Transducer 1	StrainSert Bolt Transducer - 10,000 lb. Capacity - BLH 120 C Power Supply
19	Load Transducer 2	StrainSert Bolt Transducer - 10,000 lb. Capacity - BLH 1200 B Strain Indicator
20	Load Transducer 3	StrainSert Bolt Transducer - 10,000 lb. BLH 1200 B Strain Indicator
21	Load Transducer 4	StrainSert Bolt Transducer - 10,000 lb. Ellis Bridge Amplifier
22	Bearing Supply T	Copper - Constantin Thermocouple
23	Combustion Supply T	Copper - Constantin Thermocouple

TABLE 3-2

ORIFICE BORE CALCULATIONS

Customer: PFK Company Date: 5/18/81

Order No.: 1139 S.O. 81-0688

Steam, Gas or Vapor Flow

Tag

Operating Conditions

In Line 444, S= .0651

Meter Type		Dry	
Differential Range H2O		100.00	
Meter Tube ID inches		.466	
Orifice Type		Concentric	
Meter Tap		Flange	
Tap Location			
Flowing Material	Nitrogen		
Max. Flow at Base Conditions		170.00	pounds/H
Avg. Flow at Base Conditions		120.21	pounds/H
SP. GV. (Air=1.0)		.96700	
Specific Heat Ratio		1.400	
Base Temperature Deg. F		60.00	
Flowing Temperature Deg. F		60.00	
Base Pressure PSIA		14.70	
Atmospheric Pressure PSIA		14.70	
Flowing Pressure PSIG		2000.00	
Static Pressure Tap Location		Downstream	
Operating Viscosity		.0190	
Sealing Liquid SP.GV. at 60 Deg. F		.00	
Orifice Plate Material		304 SS	

Calculations

1	WM =	170.00000
2	D*D =	.2172
3	FA =	1.0000
4	FM =	1.0000
5	SQ, ROOT SP.WT.FLOWING=	3.3517
6	SQ, ROOT HM =	10.00
7	Y =	1.0002
8	FC =	1.0034
9	359*(2 thru 8) =	2622.22
	S = (1/9E =	.0648
	BETA =	.3273
	BORE =	.153
	Reynolds Number =	85804.

Coefficient (C) based upon above given conditions

C' = 17.000 pounds/H

Reference. Principles and Practice of Flow Meter Engineering - Foxboro- 9th Edition

Equation 44, Page 332

The numerical and channel locations of the capacitance probes and force transducers are indicated on the photographs, Figures 3-3 and 3-4, respectively. Photographs of the test facility and instrumentation are shown on Figures 3-5 and 3-6.

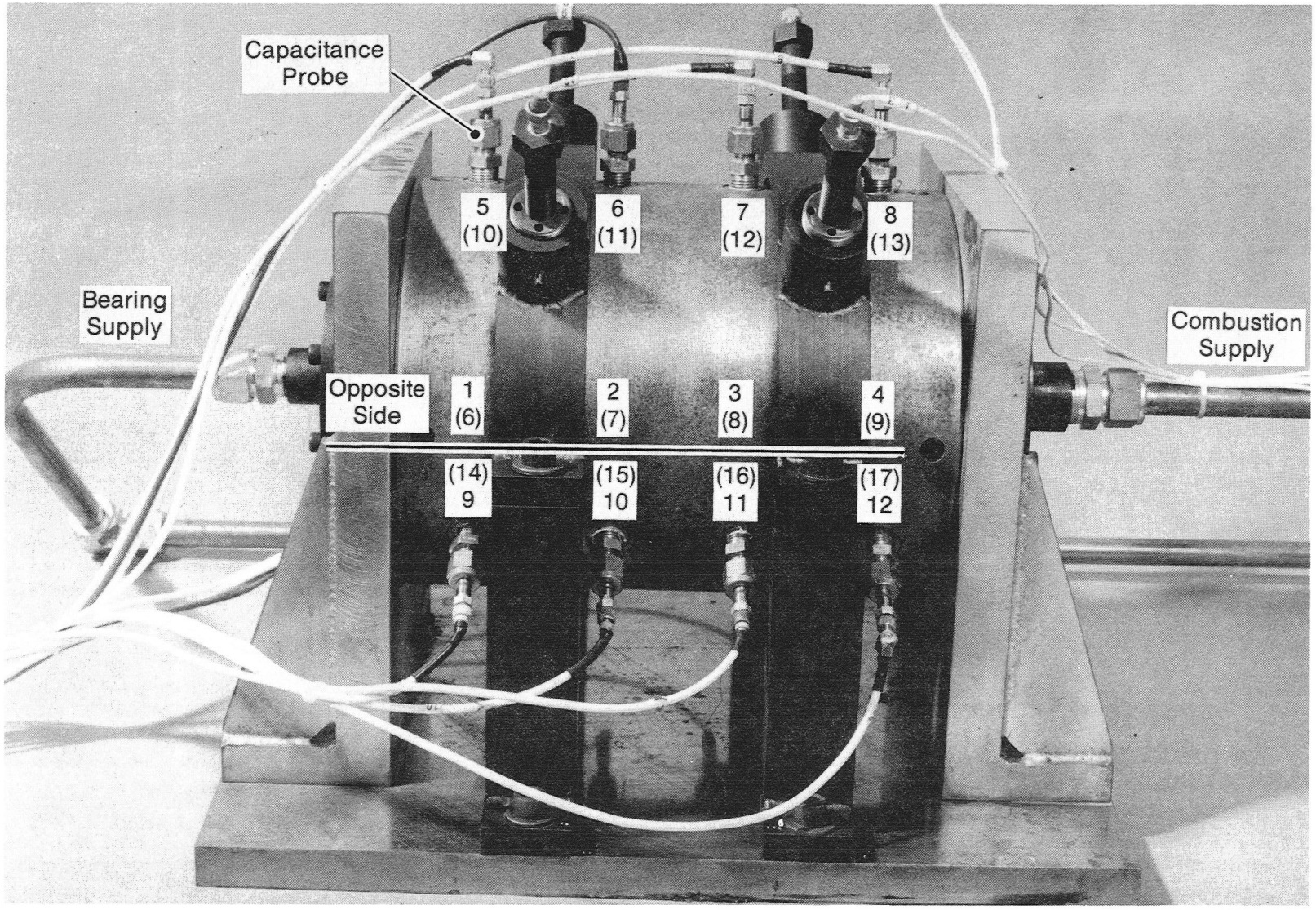

Figure 3-3 Capacitance Probe Numbers and Channels

MTI-21797

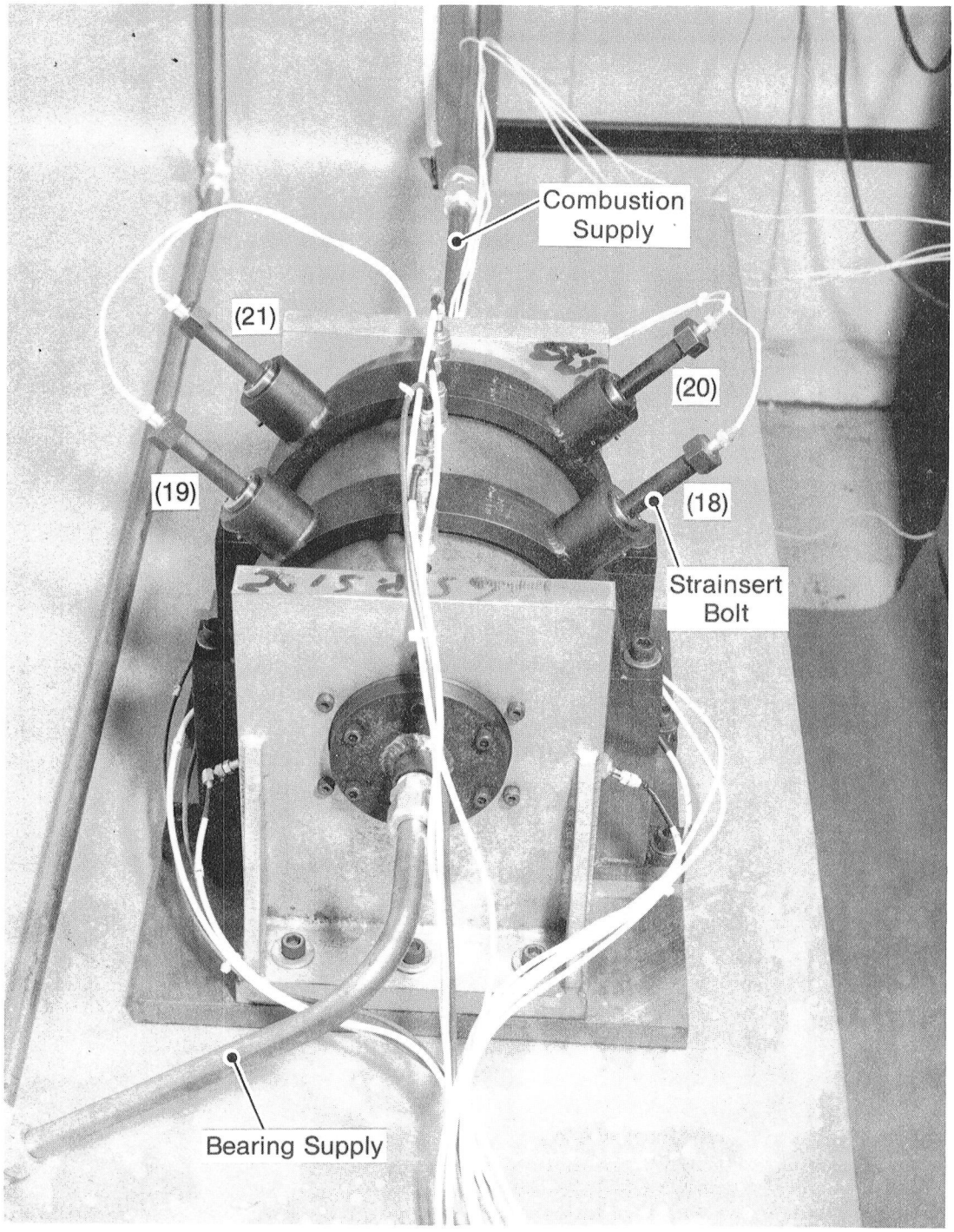

Figure 3-4 Load Cell Channels

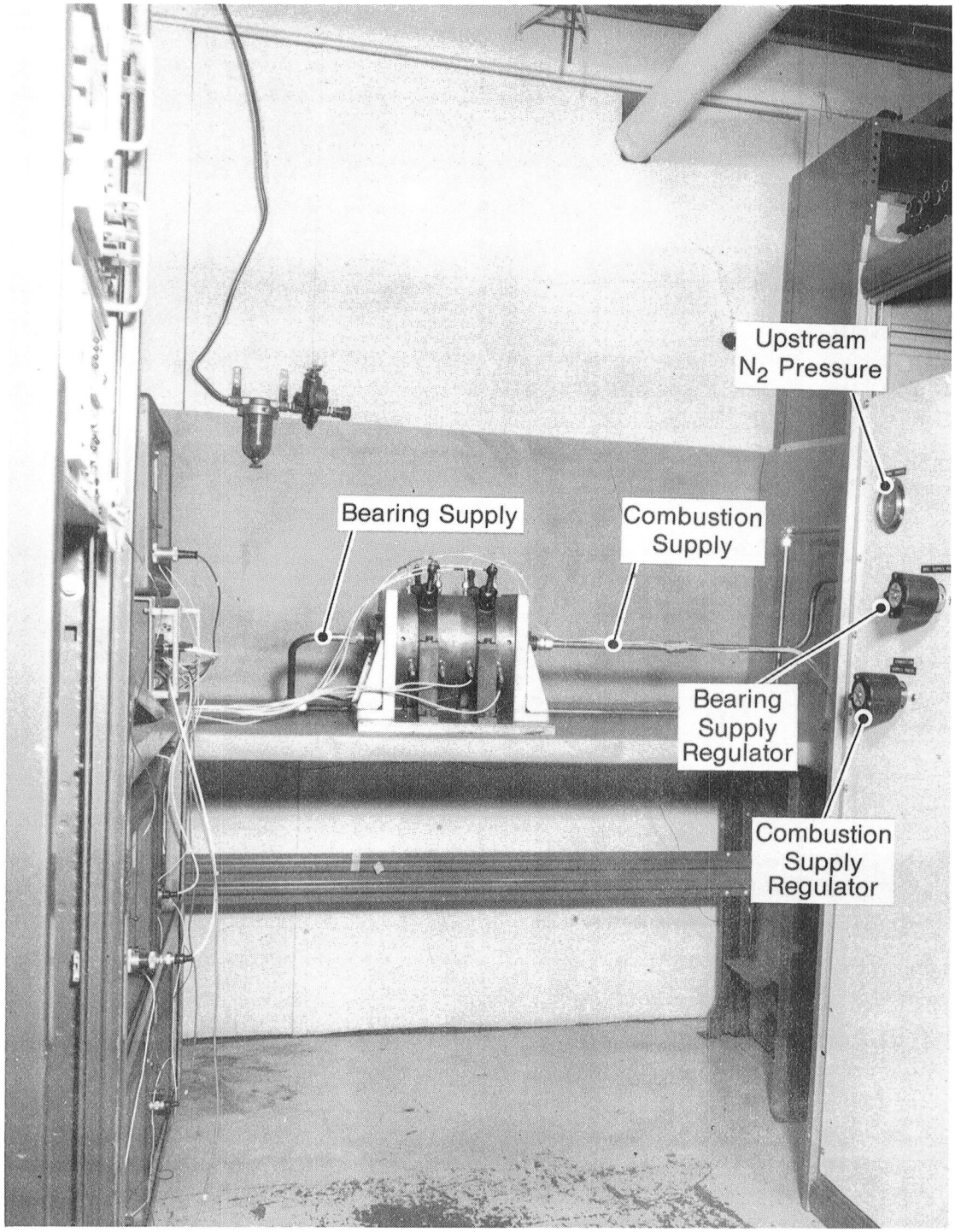

Figure 3-5 Photograph of Test Rig and Facility

MTI-21793

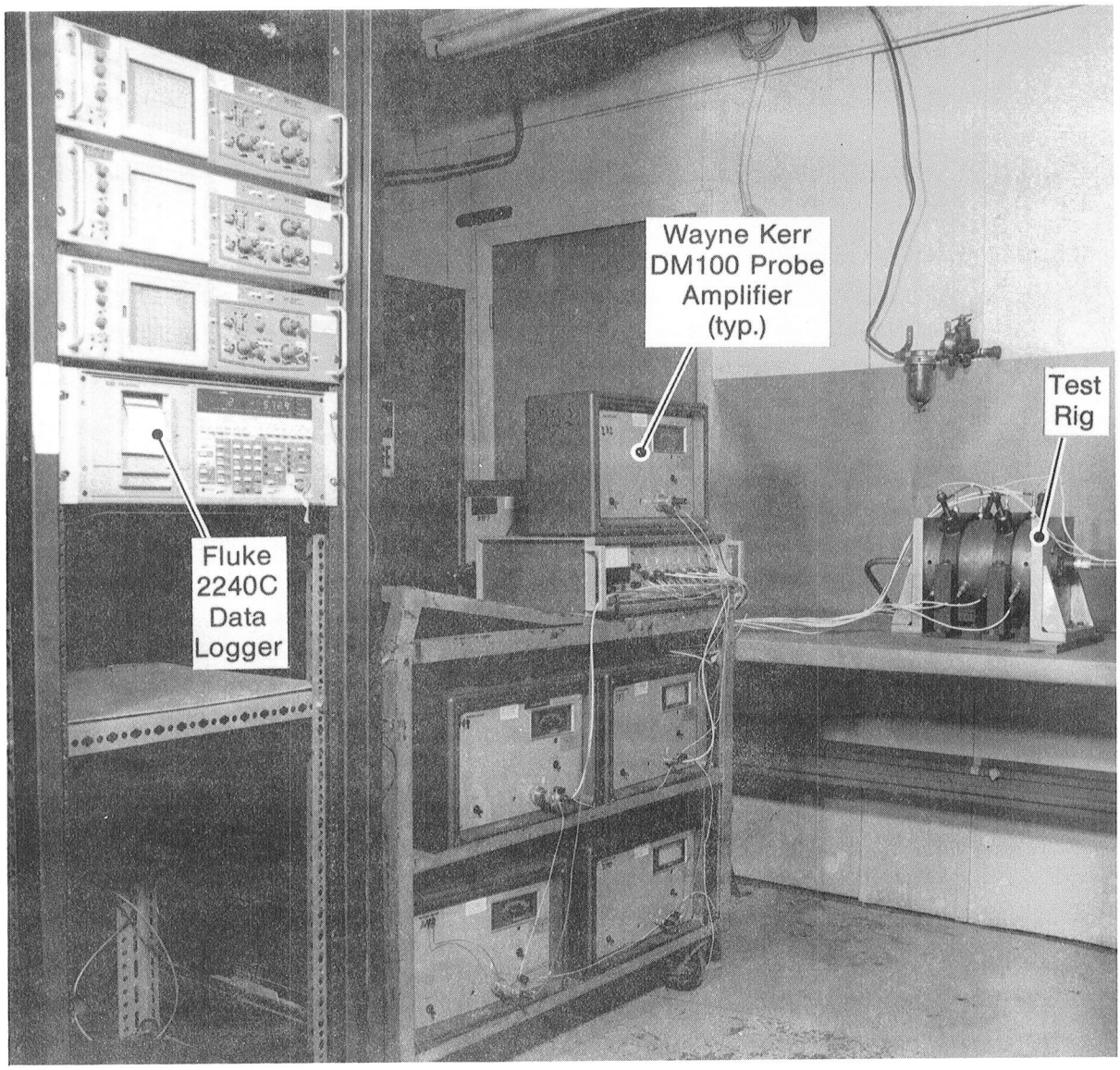

Figure 3-6 Photograph of Test Rig and Instrumentation

4.0 SUMMARY OF TEST RESULTS

4.1 Final Test Pad Configuration

The recess configuration on the outer periphery of the sector was one of the parameters that could be physically varied. Because test results indicated consistent lift-off difficulties, significant variations in the pad surface geometry occurred over the life of the program. These are documented in Section 6, which provides a chronological history of the test program.

The final pad recess configuration is shown on Figure 4-1. It consists of two recesses milled to a depth of 0.0254 mm (.001 in.). The angular extent of the recesses is approximately 47°. The recesses are not symmetrical because of the non-symmetry in boundary conditions that occur over the four-stroke cycle. The recesses are separated to provide greater righting moment when the pads are inclined due to off-setting moments about the pivot position. The original drawing of the pad is shown on Figure 4-2. When the pad is installed, it is intended to pivot about the interior surface located 6.35 mm (.25 in.) from the upper edge.

As shown on Figure 4-1, the upper recess is fed through two orifice restrictors 0.406 mm in diameter, and the lower recess is fed by one identical restrictor. The restrictors feed into a counterbored hole that is 3.18 mm in diameter and is 1.52 mm deep. This depth would have been increased to 10-12 orifice diameters if it would not have interfered with the counterbore on the inside diameter of the pad. This particular recess geometry was selected on the basis of theoretical studies which are discussed in Section 5 and single-pad test results. A photograph of the latest pad configuration is shown on Figure 4-3. In addition to the recesses and orifice feeds, the photographs indicate a number of rows of holes on the surface of the pads. These holes were employed on prior configurations but were blocked off from the inside with molten soft metal when they were no longer to be employed. A photograph of the pad interior is shown on Figure 4-4.

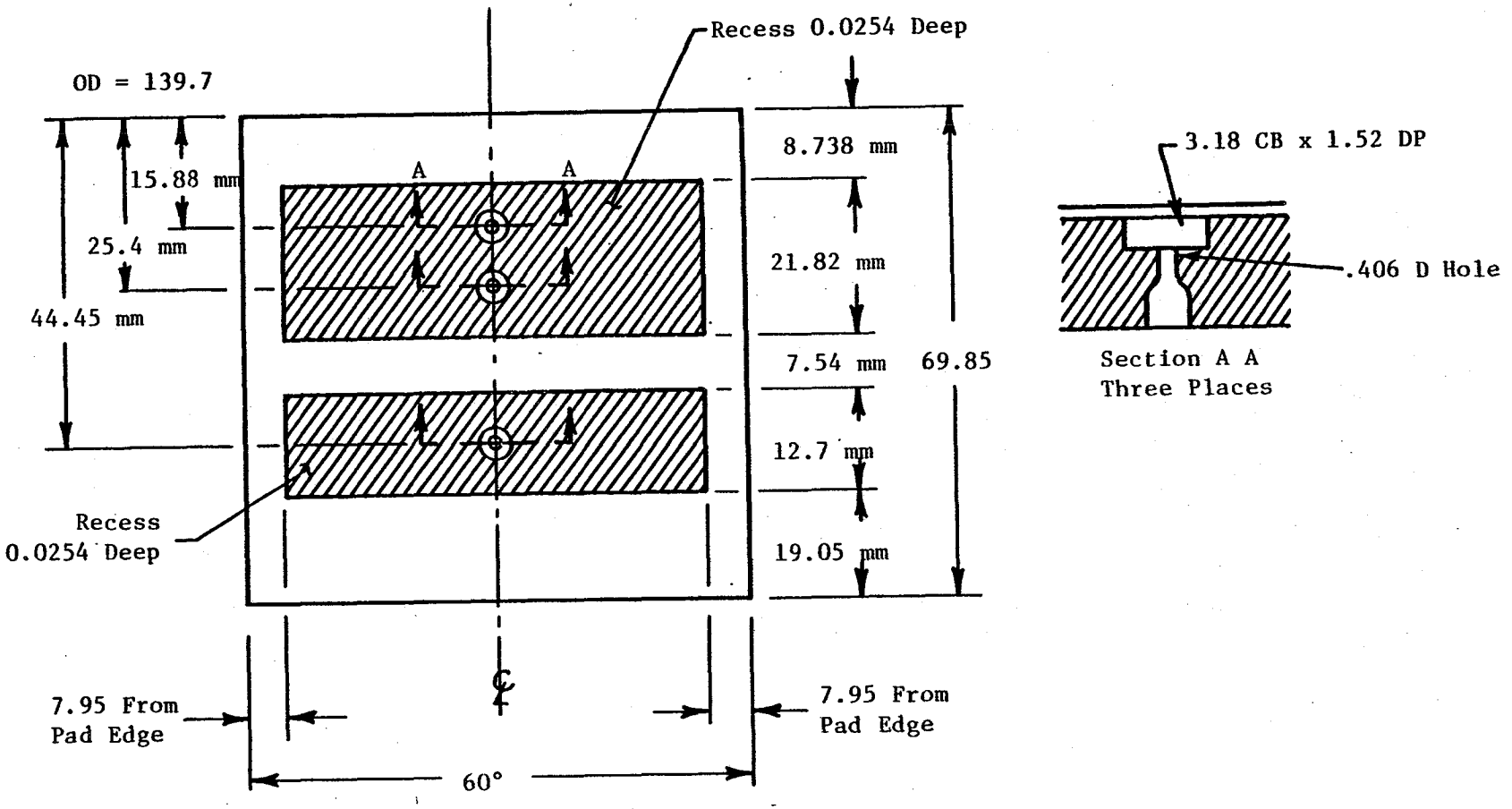

Fig. 4-1 Final Segment Recess Configuration

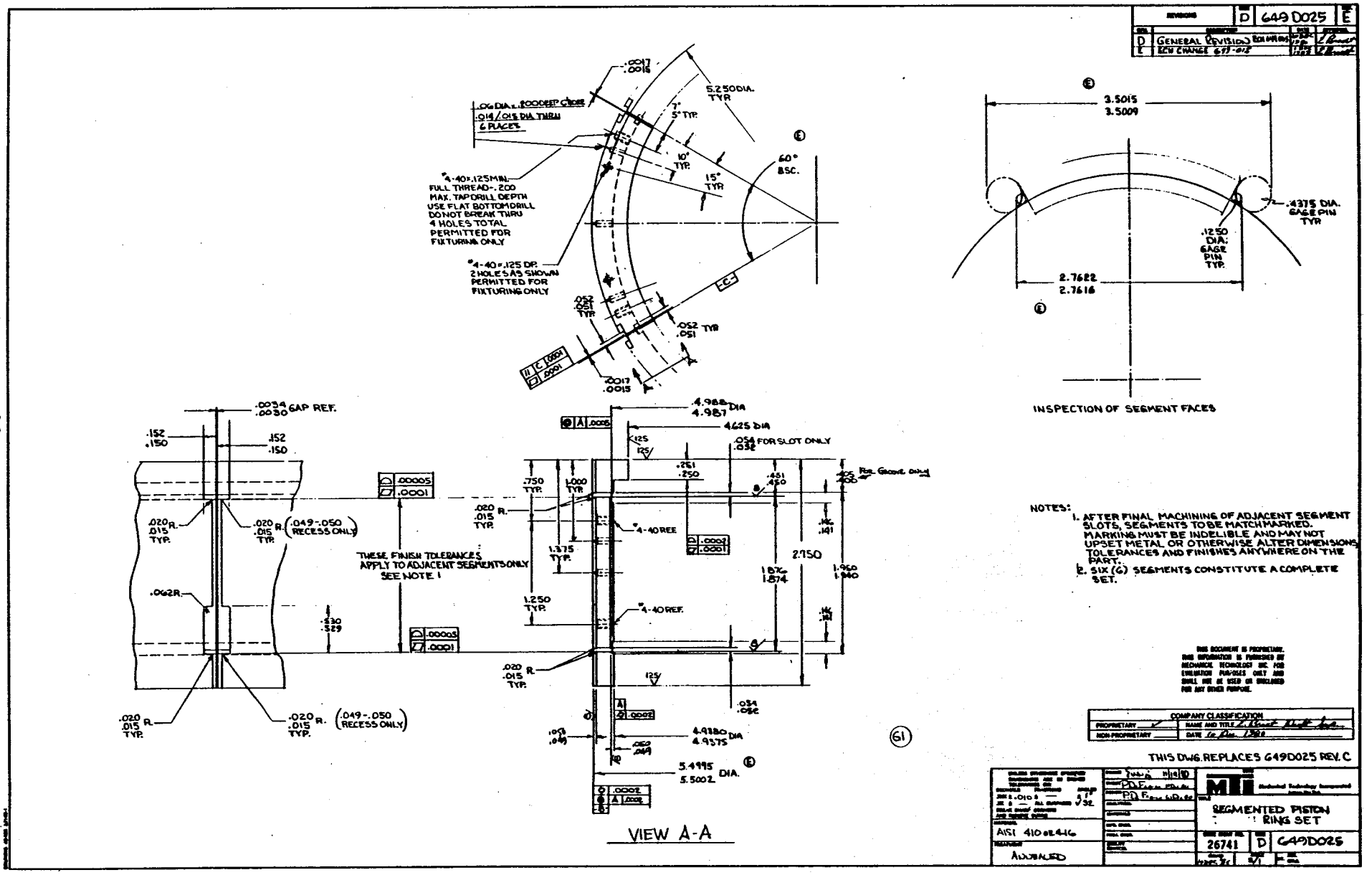

Figure 4-2 Ring Segment Drawing

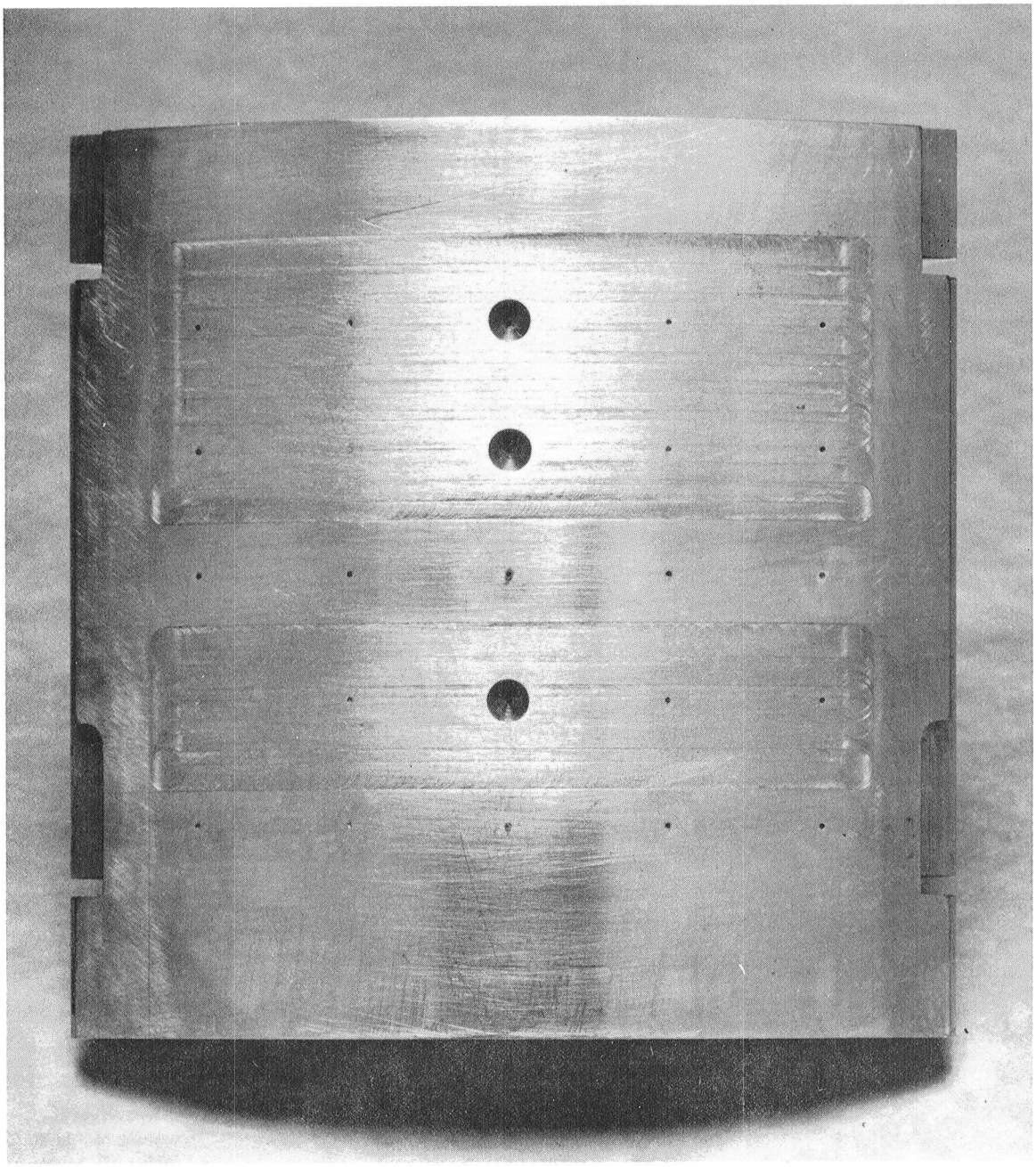

Figure 4-3 Photograph of Latest Recess Configuration

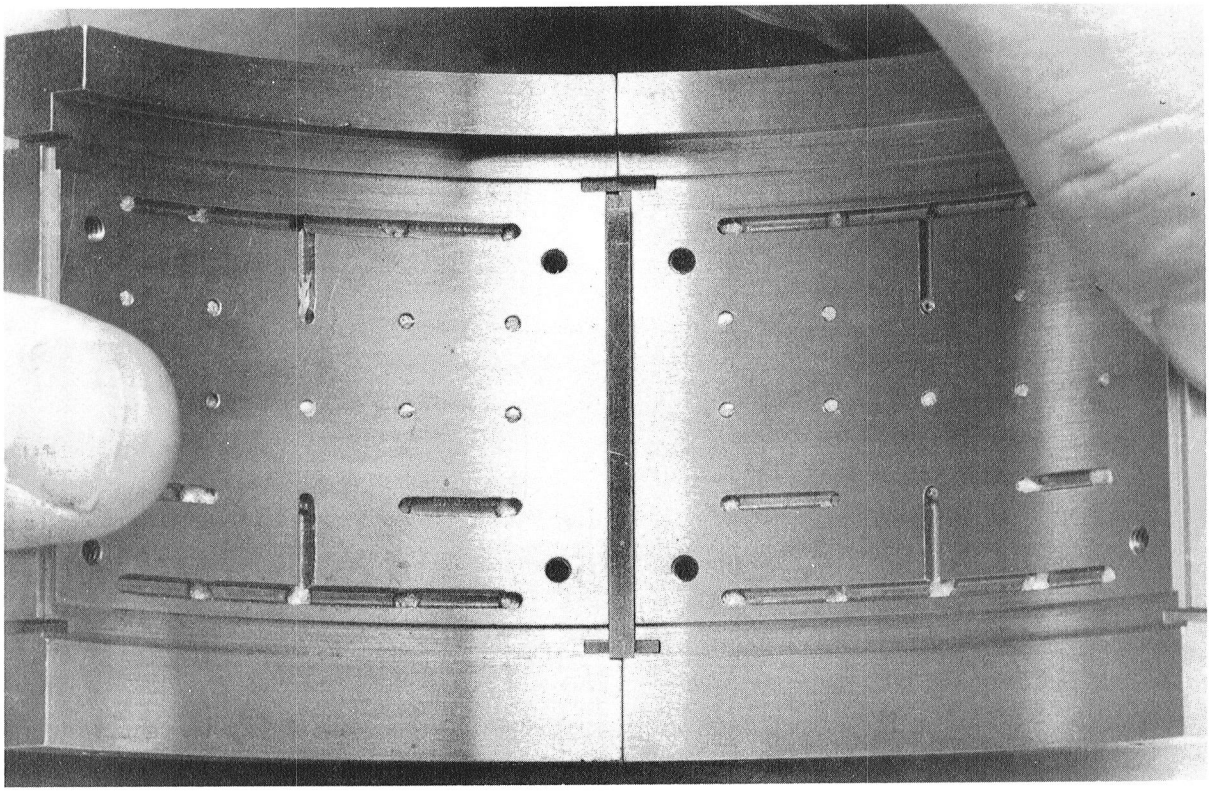

Figure 4-4 Photograph of Pad Interior Showing Plugged Orifice Holes and Inside Insert

4.2 Final Test Assembly Configuration

During final testing of the modified pads, certain variations were made to the test assembly to correct instrumentation problems. Because of prior damage that had occurred to the cylinder, it was reworked and the interior plated with electroless nickel to proper dimensions. During the plating process, the threaded connections for inserting the capacitance probes were not masked off properly and hard plating was deposited on the thread surfaces. Subsequent use of hard carbide taps removed most of the deposits, but it was still difficult to accurately set some of the probes to read consistently. Similar problems were experienced with the StrainSert load bolts. It was decided to ensure that load and probe instrumentation was working properly on one ring set and record confident data during the production testing. The ring set that was most amenable was ring set A located on the combustion supply end of the rig. Also, the cylinder was rotated from its normal position (see Figure 3-3) so that the probe channels were as indicated on Figure 4-5. Probes 11 and 12 are monitoring the top pad rather than the original probes 7 and 8. Also, load cells channels (18) and (19) were used to monitor loads on the instrumented pads as indicated on Figure 4-6. Pad Number 1A was located on the near side of Figure 4-5 and monitored by probe channels (8) and (9), and Pad Number 5A was located on the opposite side, Figure 4-5, and monitored by probe channel (12) and (13).

In addition to the variations in instrumentation, there were also variations in geometry on some of the pads. In the evolutionary process leading to the final pad configuration, modifications had been made which were not able to be rectified. (e.g., oversize recesses could not be refilled and remachined, although this was attempted). Although each of these pads had the final recesses machined, there were other variations that made them different than the final selected geometry. Figure 4-7 shows the final pad sets laid out in segmented order. The A set of segments is on the top row, and the B set is on the bottom. Pads increase numerically from left to right, pads 1A through 6A on top and 1B through 6B on the bottom. The pads containing geometrical variations are pads 6A, 6B, and 2B. Individual performance of these pads are discussed in Section 6. Insertion of the non-conforming pads had only a slight effect on overall flow measurements which were not considered serious. Film thickness of these pads were not monitored during the production running.

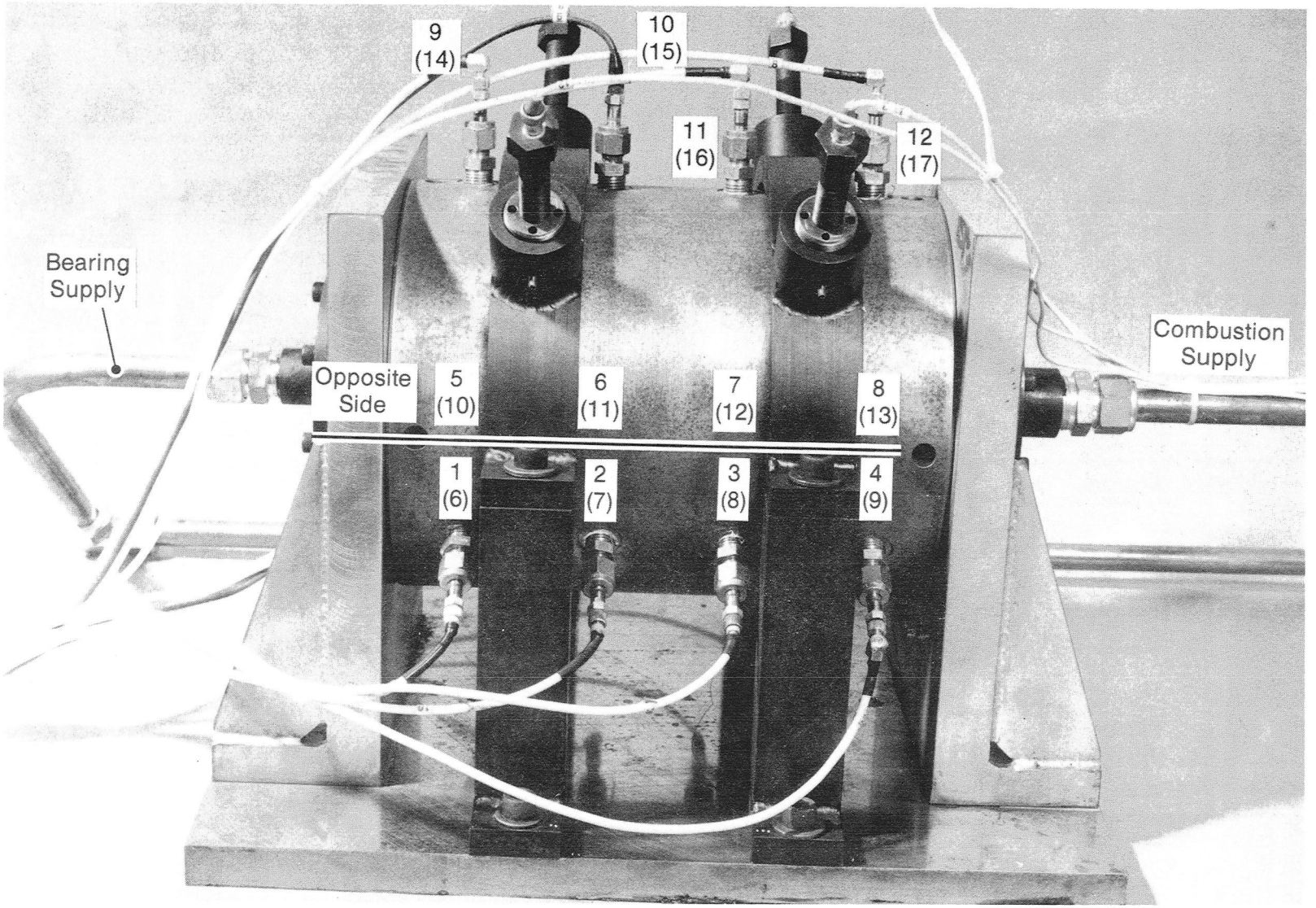

Figure 4-5 Capacitance Probe Numbers and Channel Numbers for Final Testing

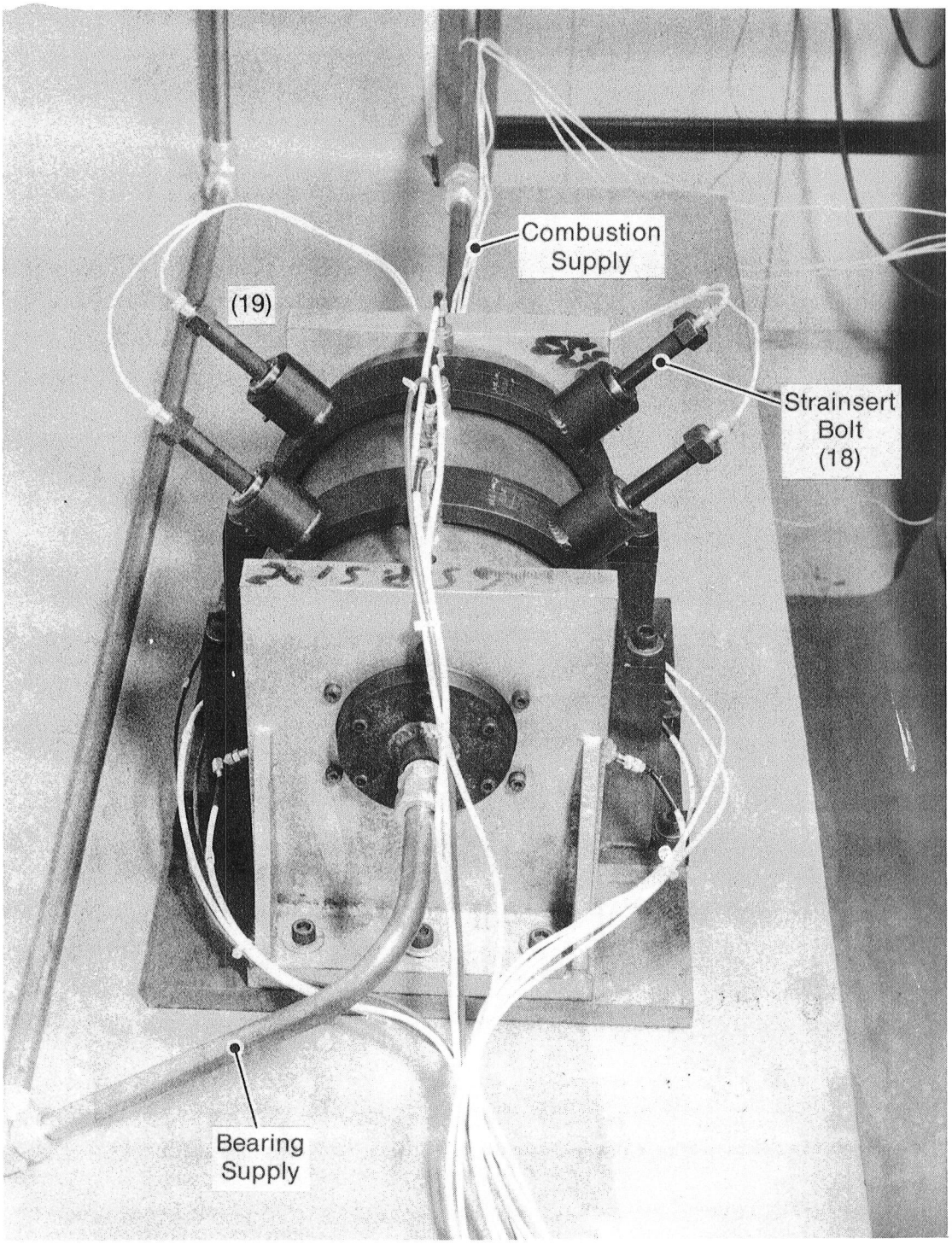

Figure 4-6 Load Cell Channels for Final Testing

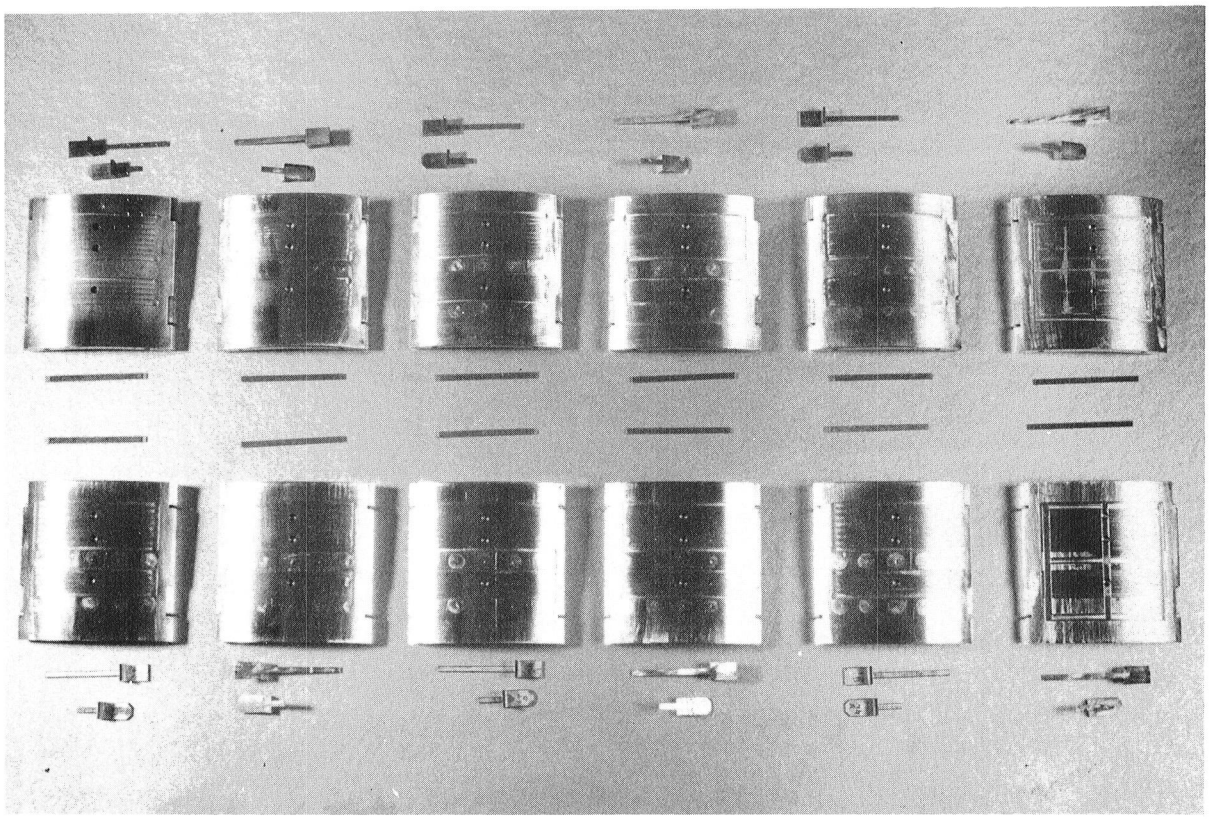

Figure 4-7 Pad Arrangement for Final Testing

4.3 Test Procedures

The usual procedure for conducting the testing was as follows:

1. All probes were set at approximately .1016 mm (4 mils) from the pad surface.

2. Pressure was applied to the pressure regulators.

3. A reference set of readings were printed out by the data logger. The reference values were used as a zero base for subsequent test points.

4. For testing in the absence of combustion pressure, the combustion side piping to the test rig was disconnected.

5. Between load applications, load was completely removed and proper pressure applied before the next load point was set.

Tabulated data from the runs are included in Appendix A.

4.4 Test Results

4.4.1 Clearance Distribution, Zero Load, Zero Combustion Pressure

The first series of tests were run to simulate intake and exhaust conditions, i.e., zero load on the ring set, and zero pressure on the combustion side of the ring. Figure 4-8 shows clearance results for pad number 3A, as a function of bearing supply pressure. The end points of the lines correspond to the probe locations at each end of the pad. Pad 3A was located at the top position of the rig and was monitored by probes 11 and 12, channels (16) and (17), respectively. The pressure levels varied from 2.7 MPa to 10.07 MPa. Under all conditions of operation, this particular pad maintained a positive clearance, i.e., the pads moved away from the cylinder wall and the probe measurement increased from that of the reference position. The magnitude of the clearances are in the approximate design range. The combustion end of the pad is on the left end of the clearance curves and the pivot position is approximately 6.35 mm from the origin. All curves form a converging clearance from the combustion end towards

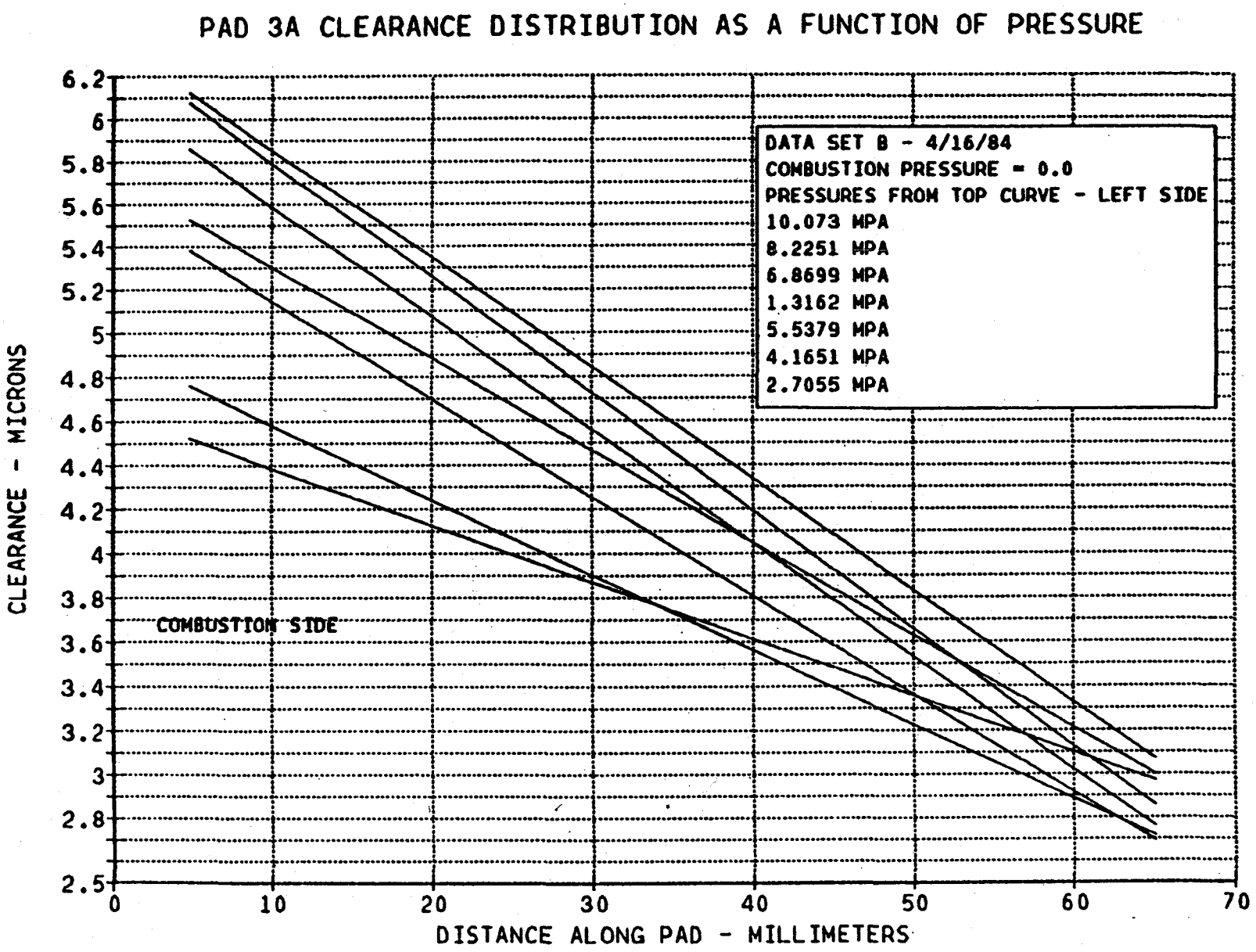
PAD 3A CLEARANCE DISTRIBUTION AS A FUNCTION OF PRESSURE
DATA SET B - 4/16/84
COMBUSTION PRESSURE = 0.0
PRESSURES FROM TOP CURVE - LEFT SIDE
10.073 MPA
8.2251 MPA
6.8699 MPA
1.3162 MPA
5.5379 MPA
4.1651 MPA
2.7055 MPA
COMBUSTION SIDE
CLEARANCE - MICRONS
DISTANCE ALONG PAD - MILLIMETERS
6.2
6
5.8
5.6
5.4
5.2
5
4.8
4.6
4.4
4.2
4
3.8
3.6
3.4
3.2
3
2.8
2.5
0
10
20
30
40
50
60
70

Figure 4-8

the crankcase end of the ring. This would be expected since the non-symmetry of the recess configuration and orifice supply system would produce a converging inclination with zero boundary pressures applied at either end. In general, the higher the supply pressure, the larger the clearance, although the test results produced some contradictions with respect to this pattern. The general trend regarding the slope of the curves is that they tend to increase with pressure.

Figure 4-9 shows similar results for Pad 1A, which was located on the near side of Figure 4-5, and monitored by probe channels (8) and (9). Notice that the clearance is negative along a substantial portion of the pad. What this implies is that the pads moved closer to the cylinder walls and measurement probes, when pressure was applied, than that measured in the reference position or under conditions of zero applied pressure. The chances are that the pads are contacting at the exhaust end, but when pressure is applied, deformations occurring in both the cylinder and pads makes it difficult to precisely establish the film thickness distribution. For purposes of definition, when negative clearances occur, the pads are not considered to have "positive lift- off". Note, that when the pads do not lift-off, higher pressures aggravate the situation and the clearances become more negative.

There is a tendency, however, for the slope to reduce as pressure increases which is beneficial to operation. The results for pad 5A are shown on Figure 4-10. This pad is located on the opposite side of Figure 4-5 and was monitored by probes 7 and 8, channels (12) and (13), respectively. This pad did not lift-off and the situation was similarly aggravated by higher pressures. Again, there is a tendency for the slope to decrease as pressure is applied.

The reason why some pads lift and others do not is not easily discernable. In the operating clearance range, minute variations produce significant differences. The problem of lift-off, however, appears to be related to the sensitivity of the pad to moment unbalance. Apparently, the pads do not have sufficient righting moment to correct themselves once they are headed in the wrong direction and increased pressure levels further deteriorate performance. On the other hand, for a pad that does lift-off well, performance improves with pressure.

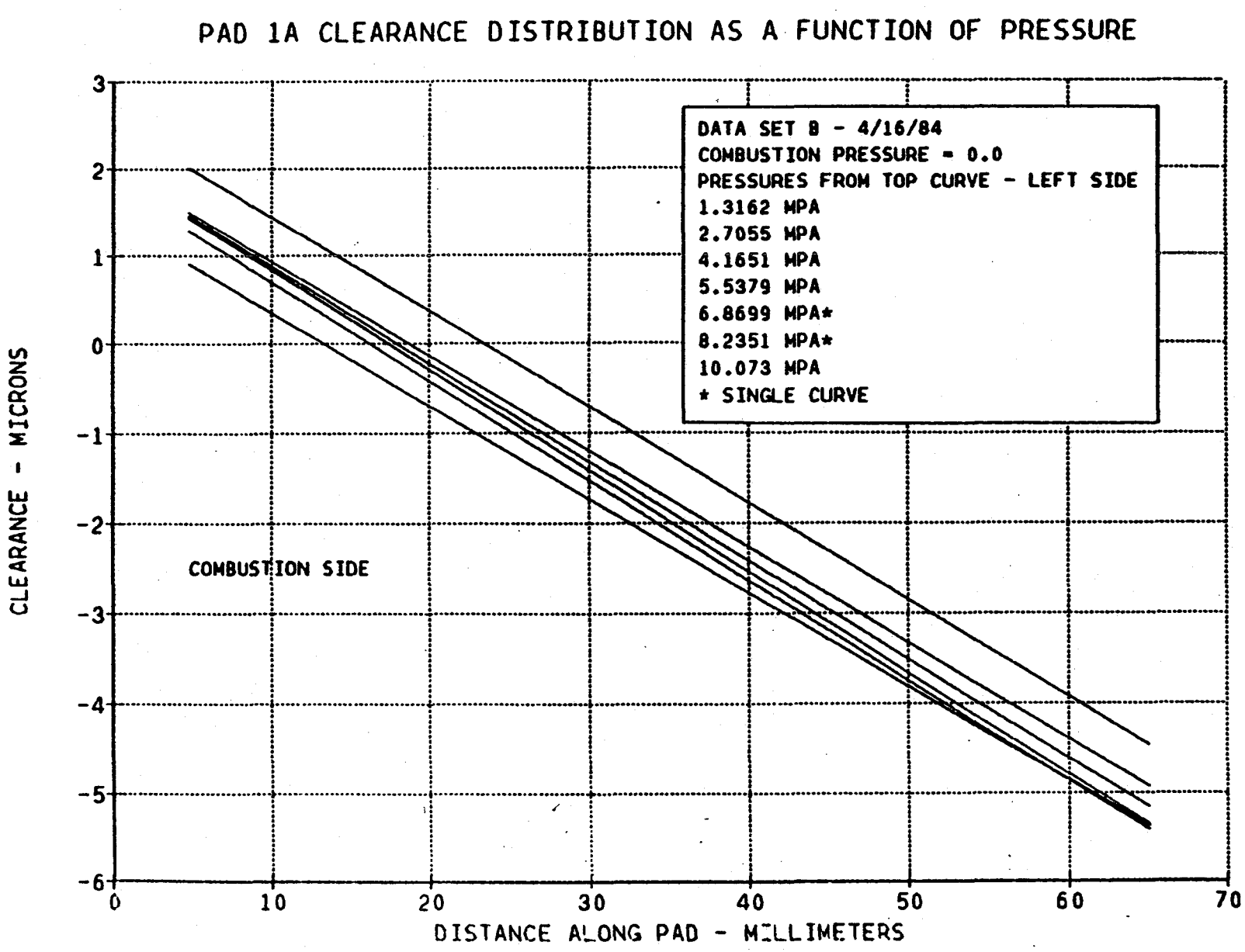
PAD 1A CLEARANCE DISTRIBUTION AS A FUNCTION OF PRESSURE
DATA SET B - 4/16/84
COMBUSTION PRESSURE = 0.0
PRESSURES FROM TOP CURVE - LEFT SIDE
1.3162 MPA
2.7055 MPA
4.1651 MPA
5.5379 MPA
6.8699 MPA*
8.2351 MPA*
10.073 MPA
* SINGLE CURVE
COMBUSTION SIDE
CLEARANCE - MICRONS
DISTANCE ALONG PAD - MILLIMETERS
3
2
1
0
-1
-2
-3
-4
-5
-6
0
10
20
30
40
50
60
70

Figure 4-9

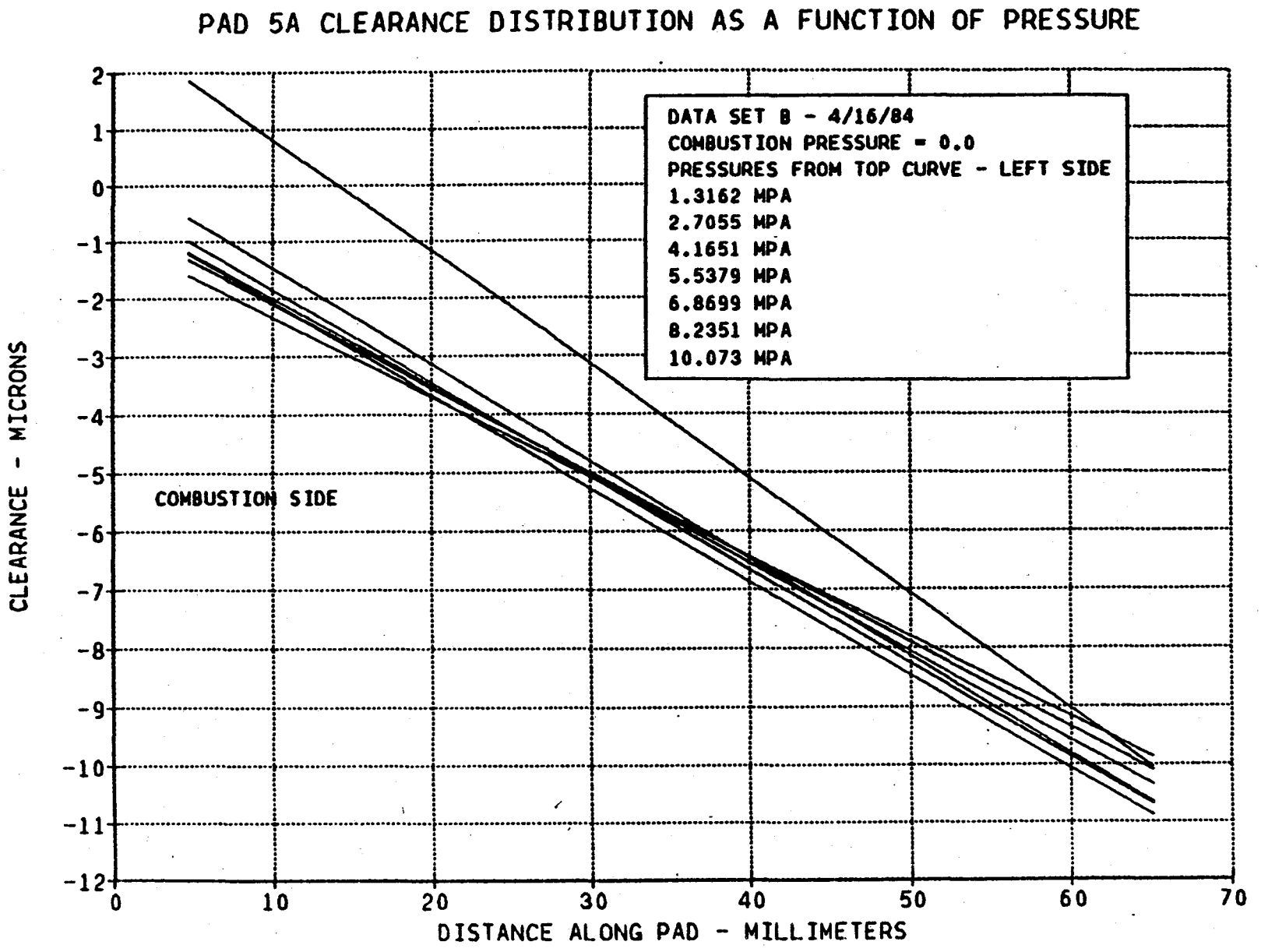
PAD 5A CLEARANCE DISTRIBUTION AS A FUNCTION OF PRESSURE
DATA SET B - 4/16/84
COMBUSTION PRESSURE = 0.0
PRESSURES FROM TOP CURVE - LEFT SIDE
1.3162 MPA
2.7055 MPA
4.1651 MPA
5.5379 MPA
6.8699 MPA
8.2351 MPA
10.073 MPA
COMBUSTION SIDE
CLEARANCE - MICRONS
DISTANCE ALONG PAD - MILLIMETERS
2
1
0
-1
-2
-3
-4
-5
-6
-7
-8
-9
-10
-11
-12
0
10
20
30
40
50
60
70

Figure 4-10

Additional clearance measurements were made on pad 3A at an earlier date. Results are shown on Figure 4-11 and are indicated to demonstrate the kind of consistency achievable with the test rig. As shown on Figure 4-11, the pad lifts off nicely and produces the same order of clearances as for the test data indicated on Figure 4-8. Considering the magnitude of clearances involved, test repeatability is very reasonable. In general, the tests indicated that trends were always repetitive. Thus, if a pad lifted off, it consistently did so and vice versa. Absolute magnitude may have varied somewhat due to variations in ambient and fluid temperatures, distortions under pressure, etc.

4.4.2 Clearance Distribution - Zero Load Combustion Pressure Equal Bearing Supply Pressure

During the compression and combustion regions of the cycle, the bearing supply pressure will approach the combustion chamber pressure. Thus, a series of tests were conducted over equalized pressure boundary conditions. Figure 4-12 shows the results for pad 3A. Several items are noteworthy. First, the slope of the curves are opposite to the zero pressure boundary conditions (intake and exhaust strokes). Hence, there is a diverging clearance from the high pressure to low pressure ends of the pad. This is contrary to theoretical predictions (see Section 5) and an undesirable characteristic. A converging clearance would provide improved stiffness and load capability and much greater assurance that contact will not occur. The obvious reason for the diverging clearance is that the center of pressure in the clearance region is below the center of pressure inside the pad, producing a net counter-clockwise moment on the pad causing a divergent tilt in the direction of the pressure gradient. An attempt was made to raise the center of pressure by relocating the lower recess towards the pad fulcrum, but this was not successful. Further description of the process leading towards an appropriate recess configuration is included in Section 6. The other significant item concerned with Figure 4-12 is that the clearance goes negative towards the combustion end. Thus, the pivoting action brings the upper edge of the pad towards the cylinder and it is quite probable that contact takes place there. This has not been a consistent phenomenon for Pad 3A. Figure 4-13 shows results of data taken at a different time, and at the higher pressure levels, clearances are positive. Positive clearances also occurred during other tests of Pad 3A. The pad inclination, however, is still in the wrong direction. It should be noted that a reversal in pad inclination takes place from the

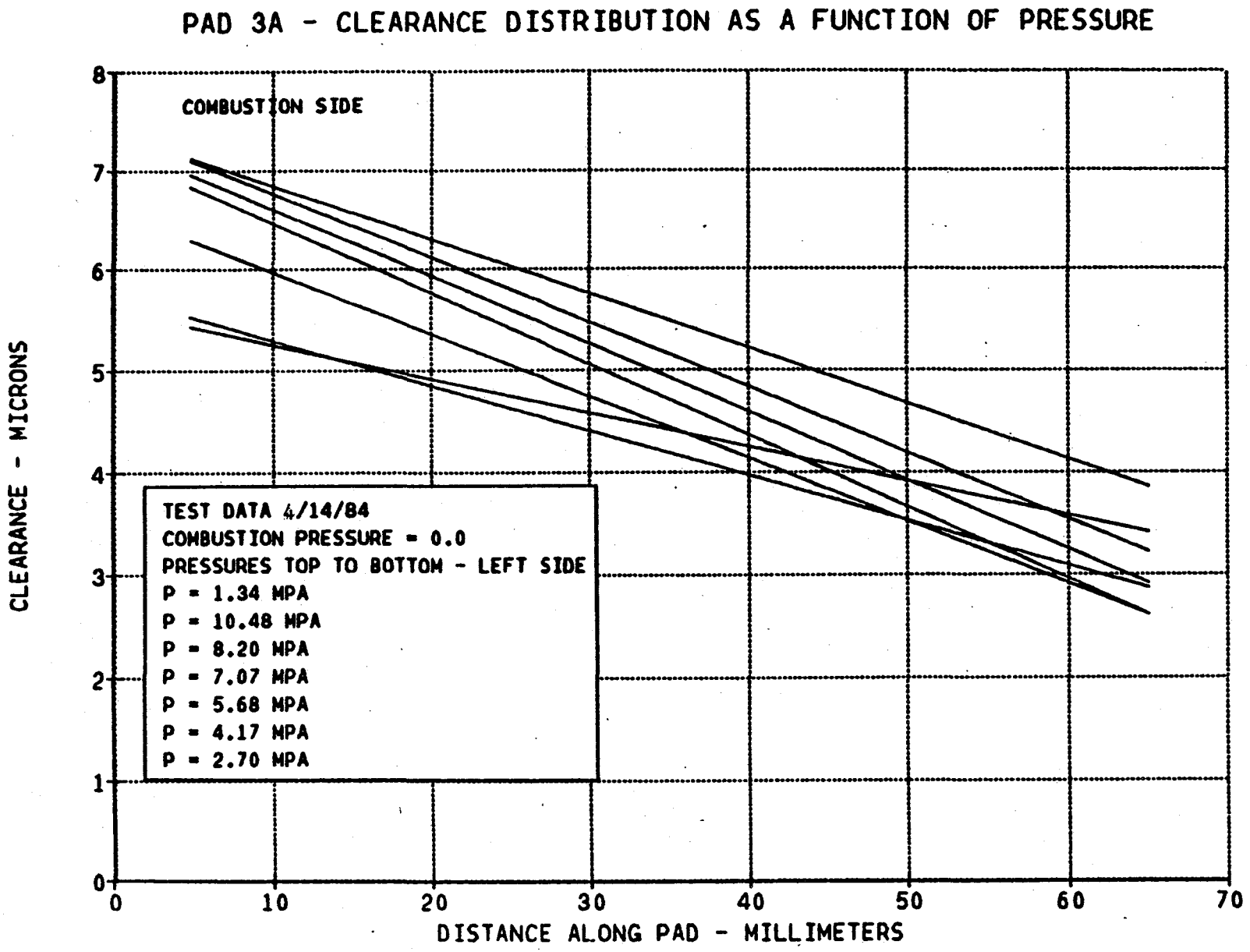
PAD 3A - CLEARANCE DISTRIBUTION AS A FUNCTION OF PRESSURE
COMBUSTION SIDE
TEST DATA 4/14/84
COMBUSTION PRESSURE = 0.0
PRESSURES TOP TO BOTTOM - LEFT SIDE
P = 1.34 MPA
P = 10.48 MPA
P = 8.20 MPA
P = 7.07 MPA
P = 5.68 MPA
P = 4.17 MPA
P = 2.70 MPA
CLEARANCE - MICRONS
DISTANCE ALONG PAD - MILLIMETERS
0
1
2
3
4
5
6
7
8
0
10
20
30
40
50
60
70

Figure 4-11

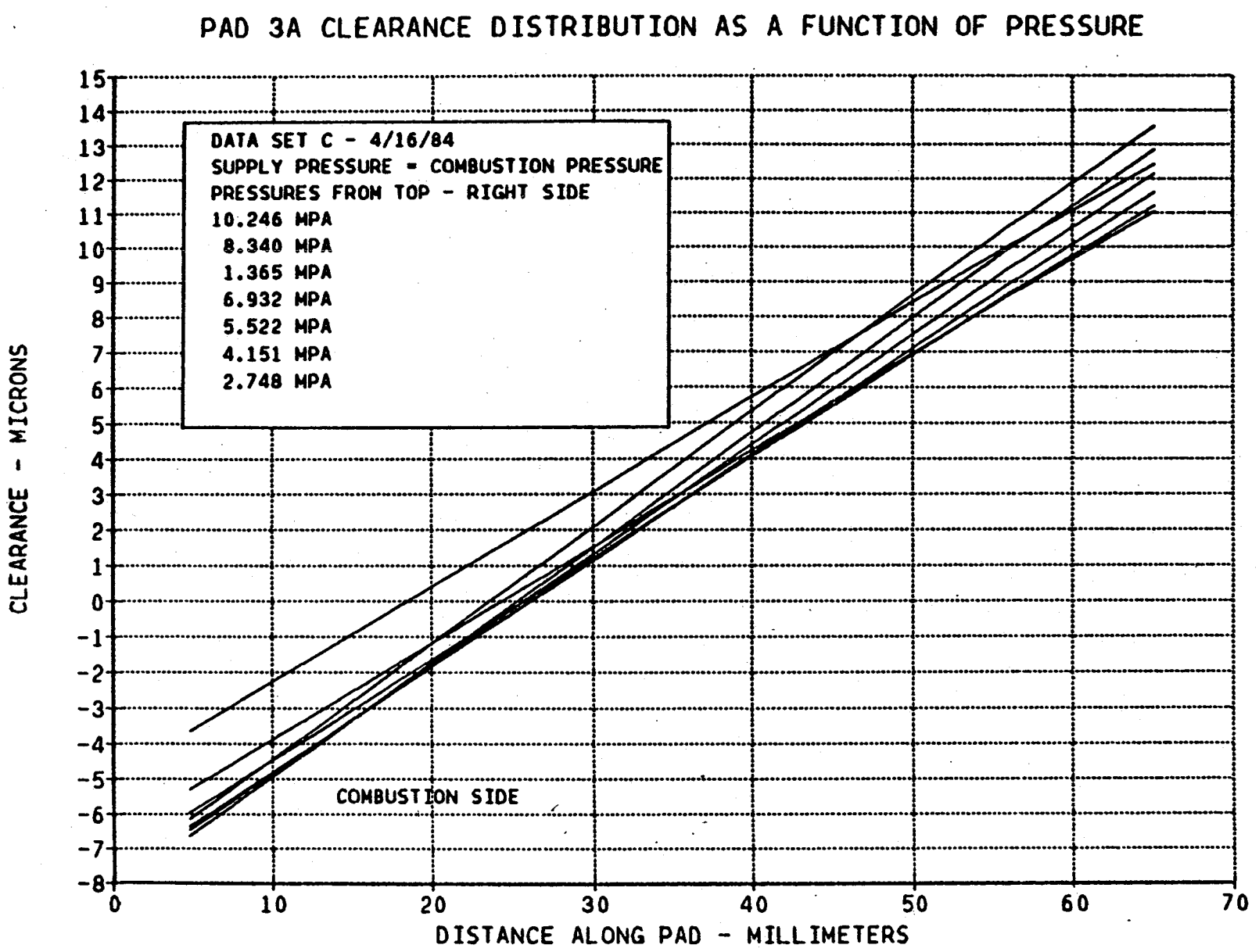
PAD 3A CLEARANCE DISTRIBUTION AS A FUNCTION OF PRESSURE
DATA SET C - 4/16/84
SUPPLY PRESSURE = COMBUSTION PRESSURE
PRESSURES FROM TOP - RIGHT SIDE
10.246 MPA
8.340 MPA
1.365 MPA
6.932 MPA
5.522 MPA
4.151 MPA
2.748 MPA
COMBUSTION SIDE
CLEARANCE - MICRONS
DISTANCE ALONG PAD - MILLIMETERS
15
14
13
12
11
10
9
8
7
6
5
4
3
2
1
0
-1
-2
-3
-4
-5
-6
-7
-8
0
10
20
30
40
50
60
70

Figure 4-12

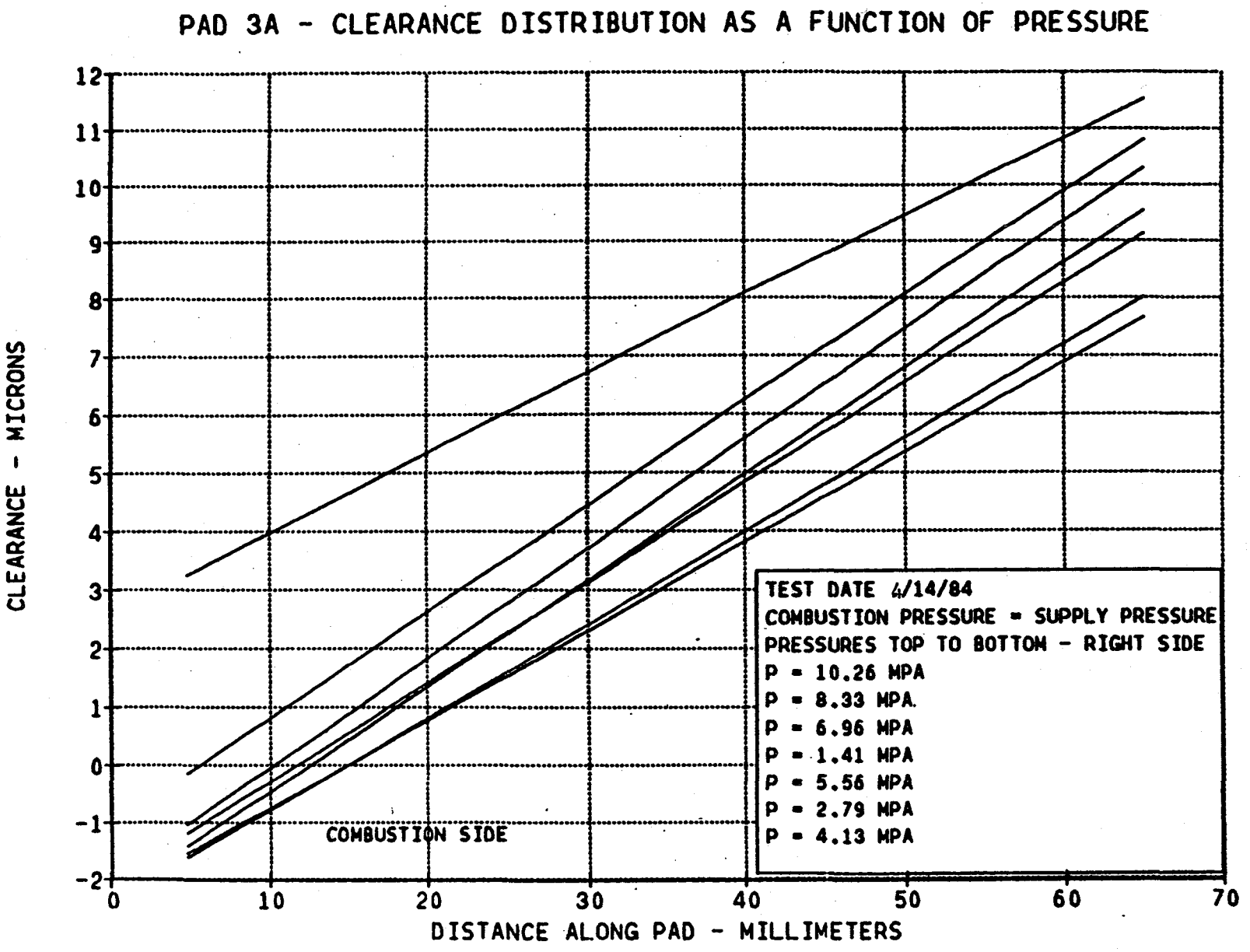
PAD 3A - CLEARANCE DISTRIBUTION AS A FUNCTION OF PRESSURE
CLEARANCE - MICRONS
DISTANCE ALONG PAD - MILLIMETERS
COMBUSTION SIDE
TEST DATE 4/14/84
COMBUSTION PRESSURE = SUPPLY PRESSURE
PRESSURES TOP TO BOTTOM - RIGHT SIDE
P = 10.26 MPA
P = 8.33 MPA.
P = 6.96 MPA
P = 1.41 MPA
P = 5.56 MPA
P = 2.79 MPA
P = 4.13 MPA
12
11
10
9
8
7
6
5
4
3
2
1
0
-1
-2
0
10
20
30
40
50
60
70

Figure 4-13

intake-exhaust conditions to the compression-combustion condition. This reversal will have some beneficial squeeze film effect, although quantitative numbers are not available. Results for Pads 1A and 5A are shown on Figures 4-14 and 4-15, respectively. Similar characteristics are produced. In general, the slope or divergence increases with pressure.

4.4.3 Ring Flow as a Function of Pressure

Flow was computed from the pressure drop across the orifice plate flow meters and the absolute temperature of the nitrogen entering the flow meter. The following formula was used in computing flows:

$$W = 77.18\sqrt{\frac{\Delta P}{3.611}\quad\frac{520}{T}} \qquad (4\text{-}1)$$

W = Flow kg/h

ΔP = Pressure drop across flow meter - psi

T = Absolute temperature - ^{o}R

Several sets of flow data were plotted because there were some significant variations. The flow is very sensitive to the clearance in the pads (to the third power) so that if, for any reason, the clearance opens slightly, high flow will result. Figure 4-16 shows flow under zero load conditions and for both boundary conditions (combustion pressure =0 and combustion pressure = supply pressure). In the case of zero combustion pressure, the flow levels off to a maximum value of 55 kg/h. When combustion pressure equals supply pressure, the flow rises to a value of approximately 97 kg/h at the highest pressure condition. This flow is excessive and is not characteristic of usual conditions. As will be subsequently demonstrated the normal condition is that high combustion pressure reduces flow from the zero combustion pressure condition. The distribution of flow under high combustion pressure conditions is indicated on Figure 4-17. The total flow has two components; one that supplies the recesses from the inside, i.e., the normal bearing flow; the other is the flow that emanates from the combustion end of the rings. As indicated on Figure 4-17, the bearing flow levels off while the combustion end flow continually rises. There are two explanations for the high combustion end flow. The first is that one or several pads hung-up with excessive clearance. The second is that nitrogen temperatures were quite low during this run. The rig had run a considerable period of time before these conditions were imposed and the temperatures had reduced to some

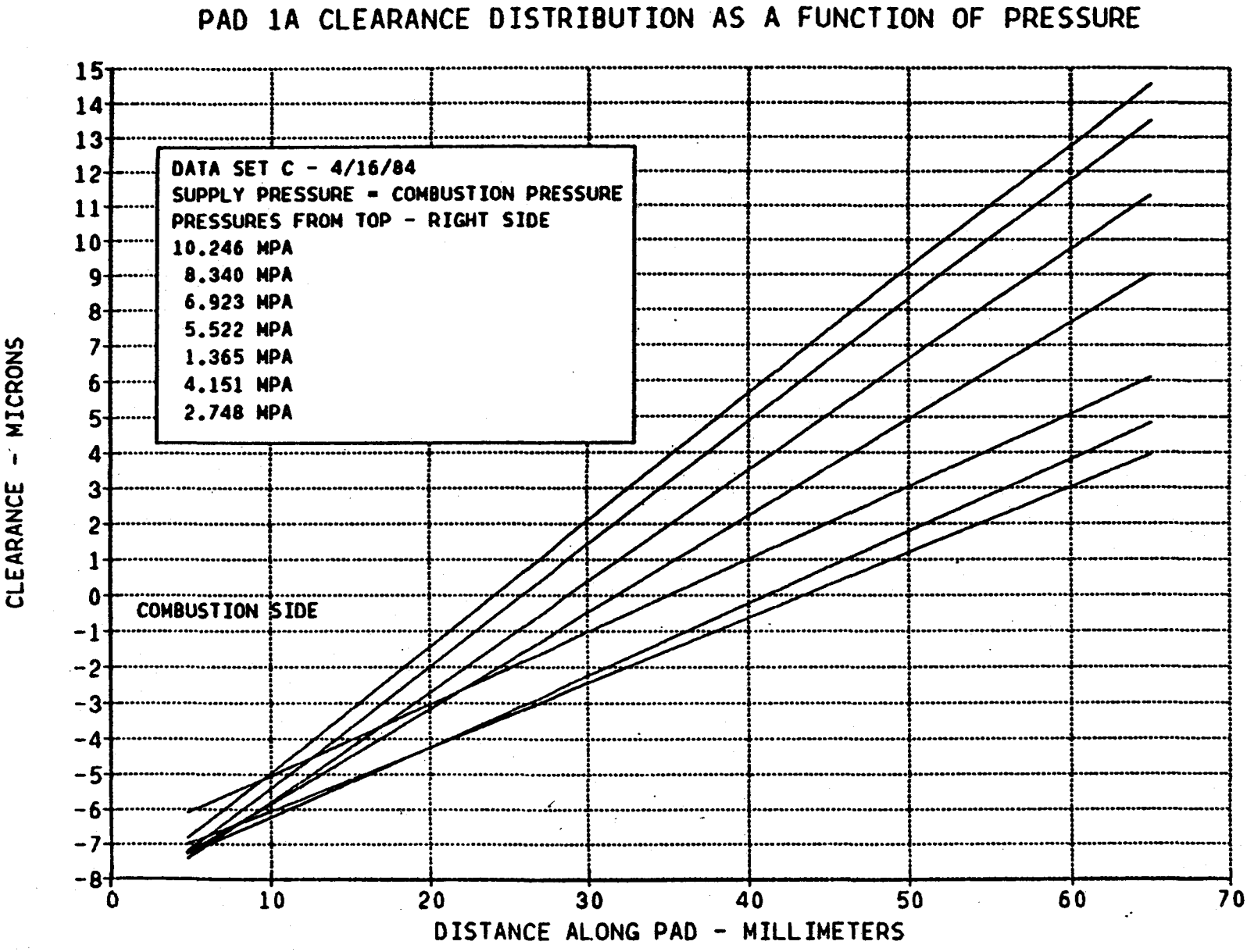
PAD 1A CLEARANCE DISTRIBUTION AS A FUNCTION OF PRESSURE
DATA SET C - 4/16/84
SUPPLY PRESSURE = COMBUSTION PRESSURE
PRESSURES FROM TOP - RIGHT SIDE
10.246 MPA
8.340 MPA
6.923 MPA
5.522 MPA
1.365 MPA
4.151 MPA
2.748 MPA
COMBUSTION SIDE
CLEARANCE - MICRONS
DISTANCE ALONG PAD - MILLIMETERS
15
14
13
12
11
10
9
8
7
6
5
4
3
2
1
0
-1
-2
-3
-4
-5
-6
-7
-8
0
10
20
30
40
50
60
70

Figure 4-14

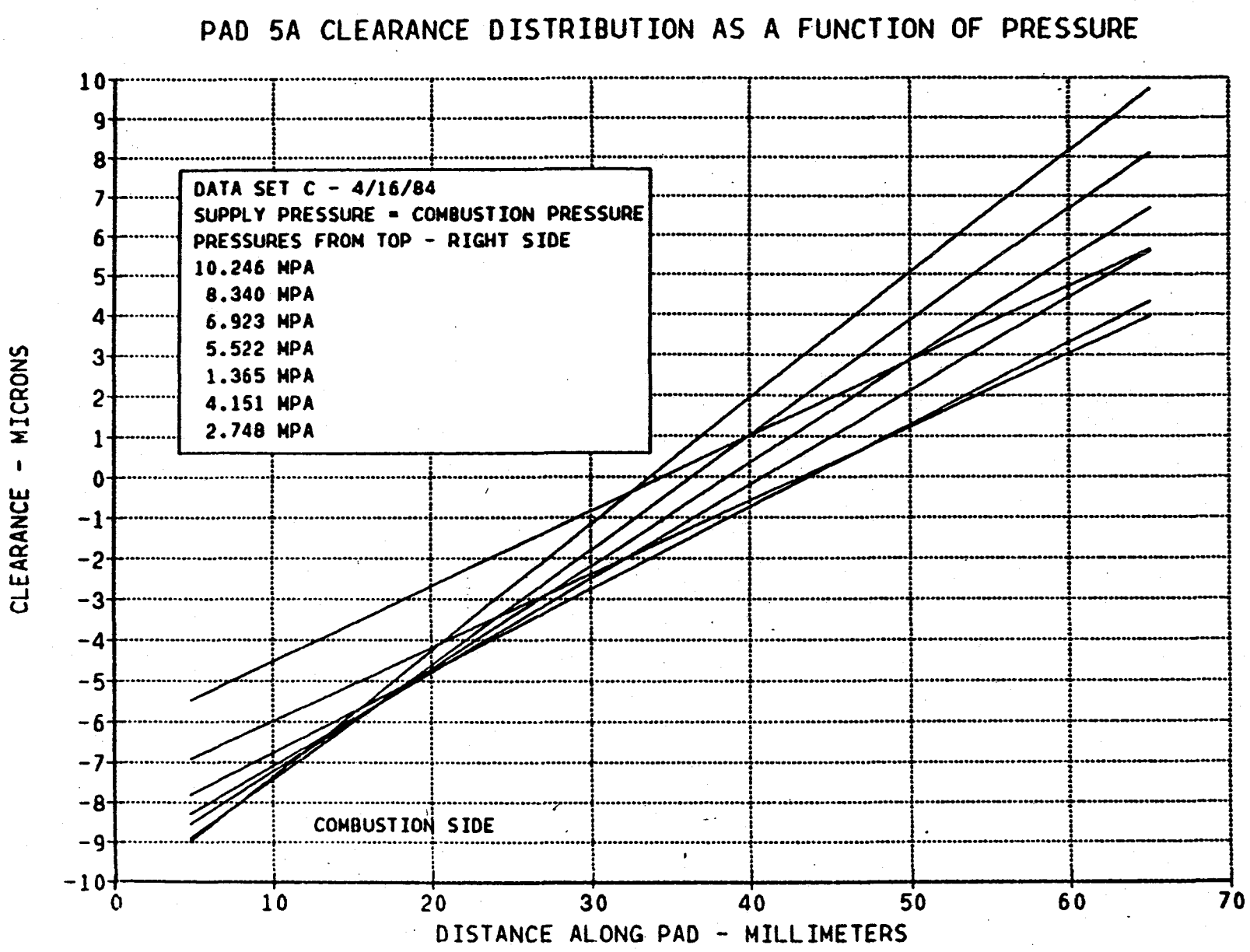
PAD 5A CLEARANCE DISTRIBUTION AS A FUNCTION OF PRESSURE
DATA SET C - 4/16/84
SUPPLY PRESSURE = COMBUSTION PRESSURE
PRESSURES FROM TOP - RIGHT SIDE
10.246 MPA
8.340 MPA
6.923 MPA
5.522 MPA
1.365 MPA
4.151 MPA
2.748 MPA
COMBUSTION SIDE
CLEARANCE - MICRONS
DISTANCE ALONG PAD - MILLIMETERS
10
9
8
7
6
5
4
3
2
1
0
-1
-2
-3
-4
-5
-6
-7
-8
-9
-10
0
10
20
30
40
50
60
70

Figure 4-15

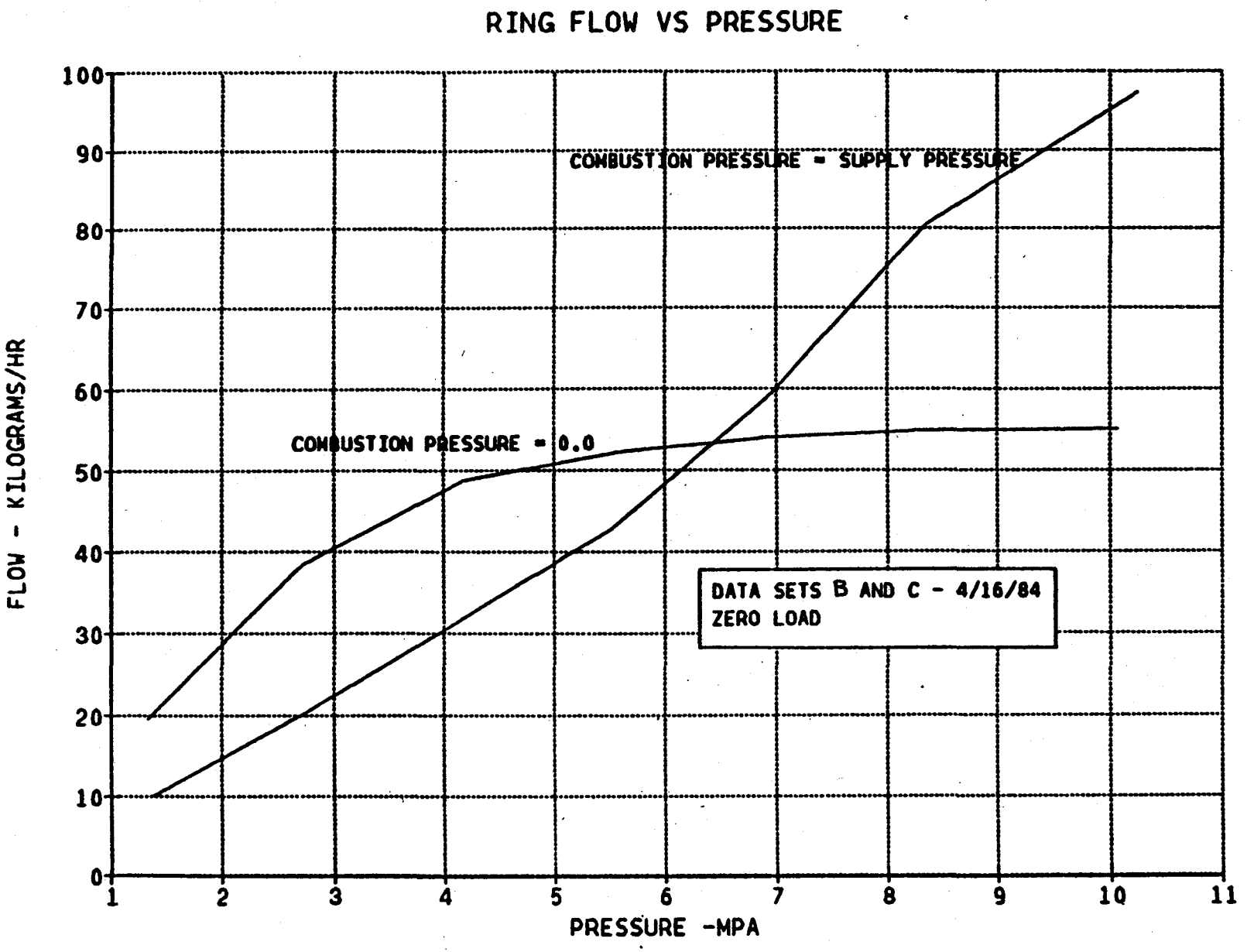
RING FLOW VS PRESSURE
FLOW - KILOGRAMS/HR
PRESSURE -MPA
COMBUSTION PRESSURE = SUPPLY PRESSURE
COMBUSTION PRESSURE = 0.0
DATA SETS B AND C - 4/16/84
ZERO LOAD
0
10
20
30
40
50
60
70
80
90
100
1
2
3
4
5
6
7
8
9
10
11

Figure 4-16

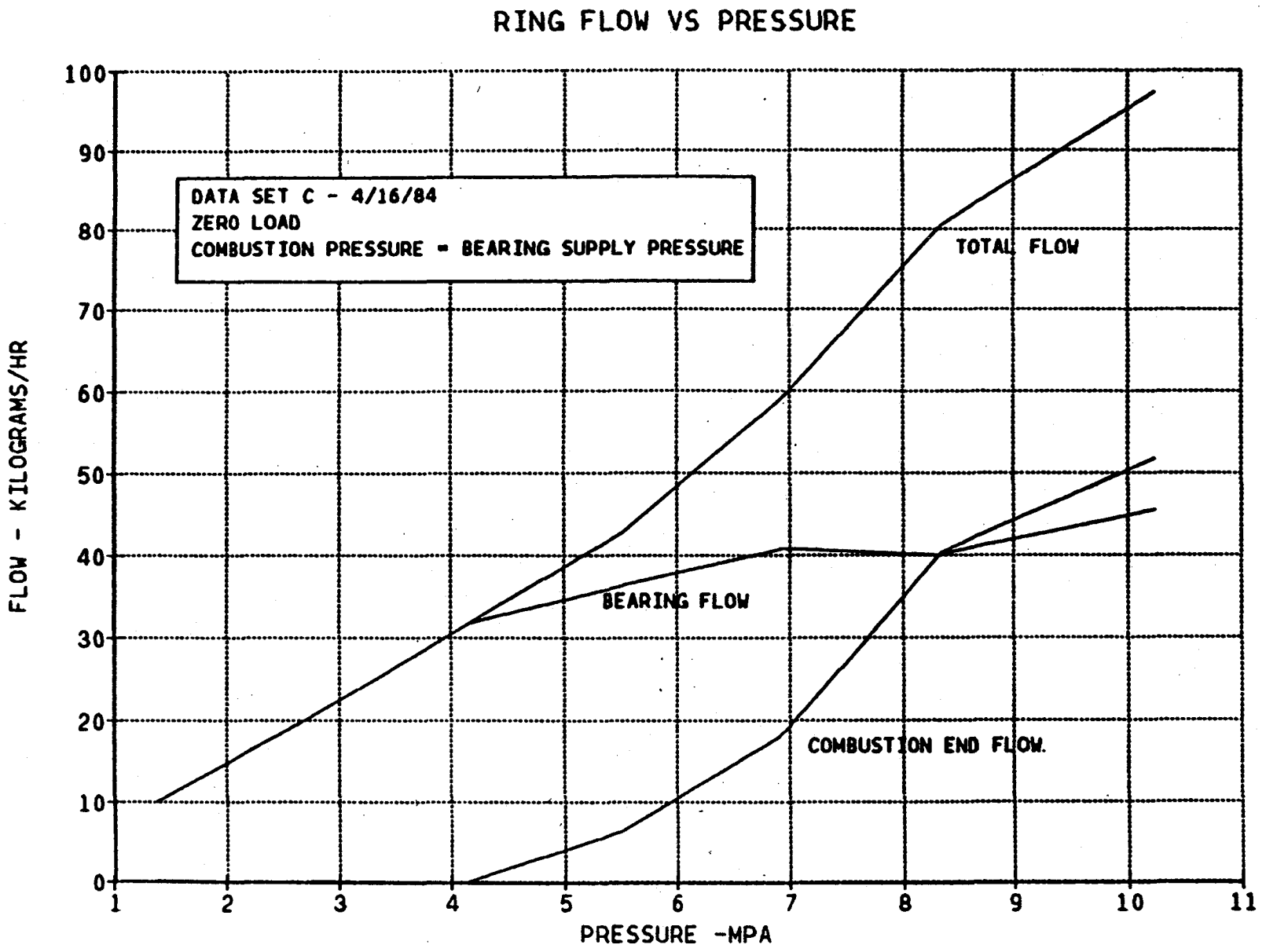
RING FLOW VS PRESSURE
DATA SET C - 4/16/84
ZERO LOAD
COMBUSTION PRESSURE = BEARING SUPPLY PRESSURE
TOTAL FLOW
BEARING FLOW
COMBUSTION END FLOW
FLOW - KILOGRAMS/HR
PRESSURE -MPA
0
10
20
30
40
50
60
70
80
90
100
1
2
3
4
5
6
7
8
9
10
11

Figure 4-17

10°C at the flow meter and probably significantly less in the rig. More representative flow values are as indicated on Figure 4-18, which is a plot of data taken several days before. Results indicate that when combustion pressure is absent, the flow is greater than when combustion pressure equals supply pressure. This occurs because when combustion pressure is applied the flow path from the recesses to the combustion end is effectively blocked off and a net reduction in flow results. The highest flow at 10 MPa bearing supply pressure is approximately 80 kg/h. The flow distribution is indicated on Figure 4-19, for the situation where combustion pressure equals supply pressure. The higher flow is the bearing flow, most of which exhausts to the low pressure end. The combustion end flow is inhibited by the upper recess pressures which maintains the combustion end pressure gradient at low levels. Further data was obtainable from some of the load test runs, where zero load flow information was extracted. This data is plotted on Figure 4-20 and substantiates the results of Figure 4-19. Table 4-1 summarizes flow values for the two primary operating conditions.

TABLE 4-1

REPRESENTATIVE FLOW VALUES
AS A FUNCTION OF
PRESSURE BOUNDARY CONDITIONS

Bearing Supply Pressure (P_s, MPa)	Combustion End Pressure (P_c, MPa)	Total Ring Flow (kg/hr.)
10	0	80
5	0	40
10	10	55

A maximum acceptable value of leakage blowby would be about 7% of the intake values or approximately 16 kg/hr. As indicated from the above numbers, this flow limit is being significantly exceeded. By appropriate design of the reservoir system, the bearing supply pressure levels during the intake and exhaust conditions can probably be reduced to half of the anticipated maximum levels without adversely affecting bearing performance. This conclusion follows from

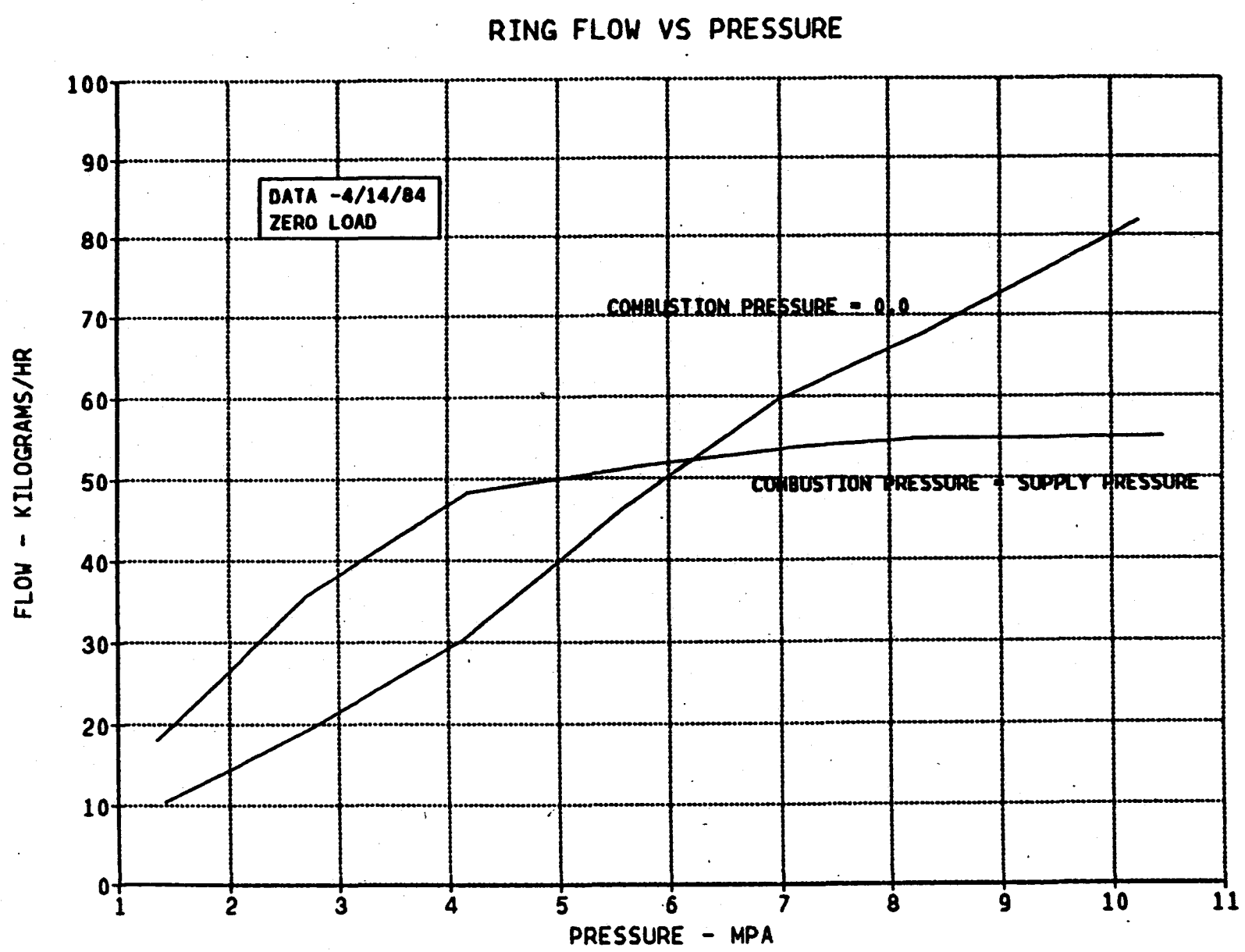
RING FLOW VS PRESSURE
DATA -4/14/84
ZERO LOAD
COMBUSTION PRESSURE = 0.0
COMBUSTION PRESSURE = SUPPLY PRESSURE
FLOW - KILOGRAMS/HR
PRESSURE - MPA
0
10
20
30
40
50
60
70
80
90
100
1
2
3
4
5
6
7
8
9
10
11

Figure 4-18

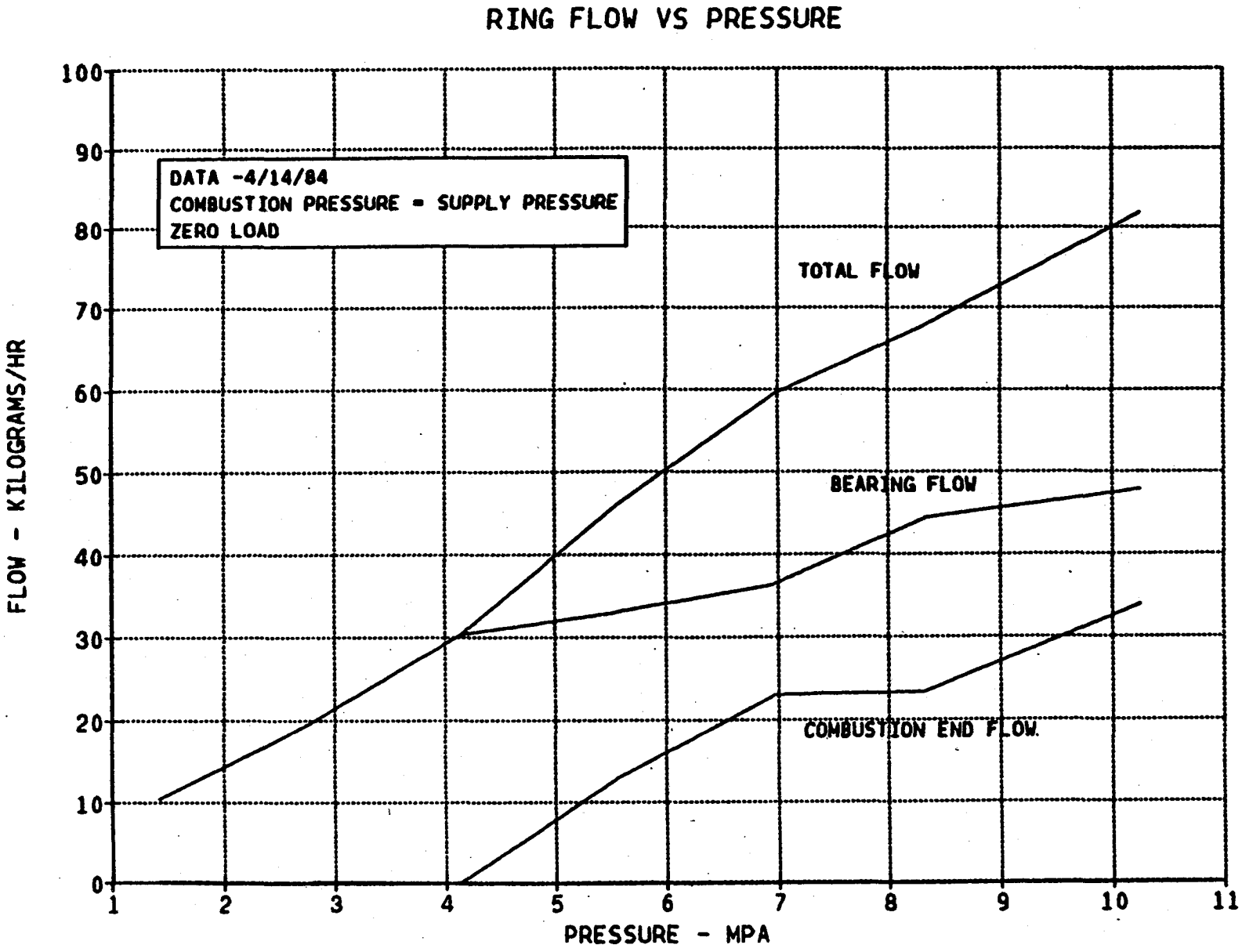
RING FLOW VS PRESSURE
DATA -4/14/84
COMBUSTION PRESSURE = SUPPLY PRESSURE
ZERO LOAD
TOTAL FLOW
BEARING FLOW
COMBUSTION END FLOW
FLOW - KILOGRAMS/HR
PRESSURE - MPA
0
10
20
30
40
50
60
70
80
90
100
1
2
3
4
5
6
7
8
9
10
11

Figure 4-19

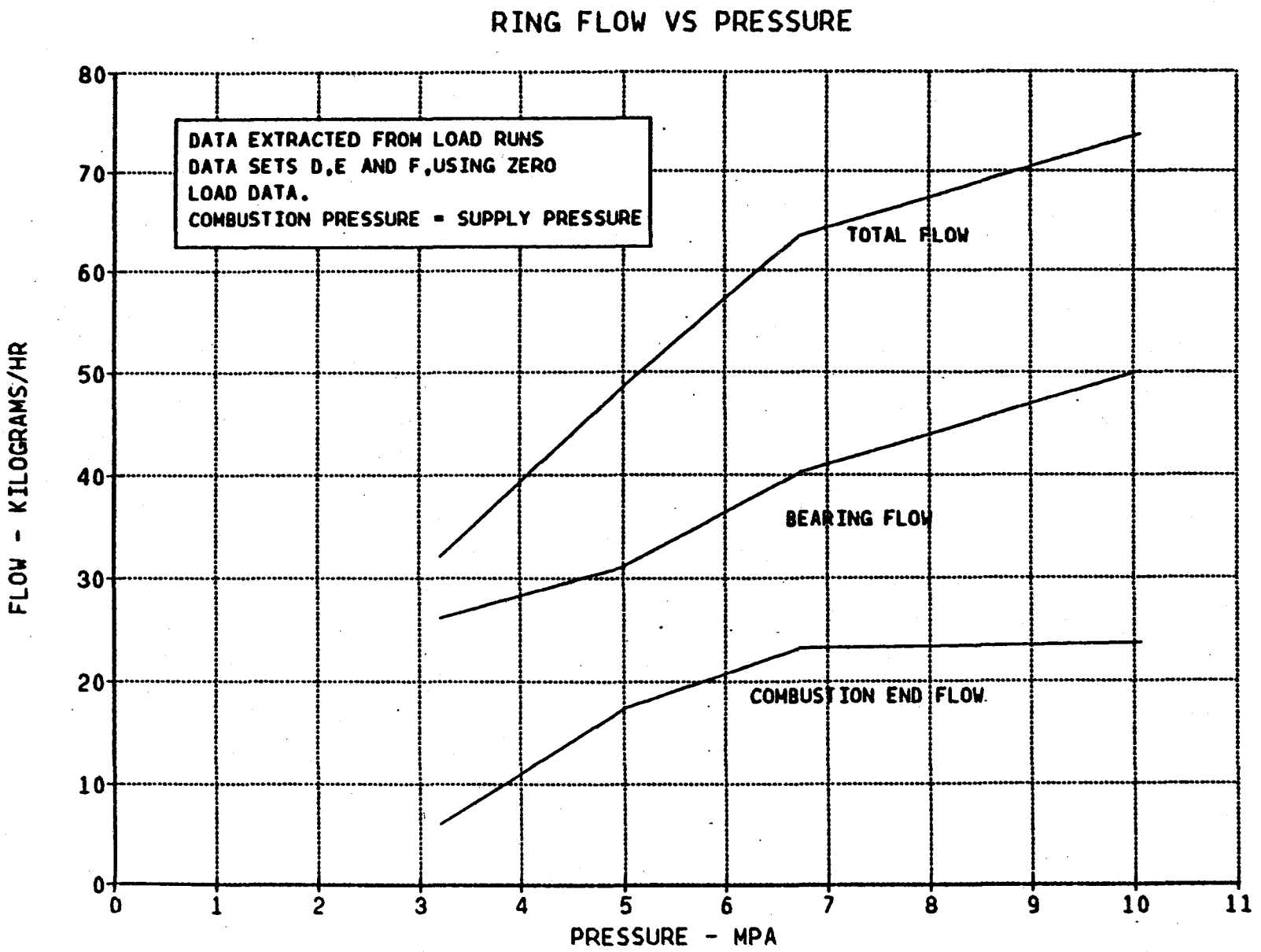
RING FLOW VS PRESSURE
DATA EXTRACTED FROM LOAD RUNS
DATA SETS D,E AND F,USING ZERO
LOAD DATA.
COMBUSTION PRESSURE = SUPPLY PRESSURE
TOTAL FLOW
BEARING FLOW
COMBUSTION END FLOW
FLOW - KILOGRAMS/HR
PRESSURE - MPA
0
10
20
30
40
50
60
70
80
0
1
2
3
4
5
6
7
8
9
10
11

Figure 4-20

the fact that side loads are absent during these strokes. Then an average flow value would be in the vicinity of 50 kg/hr.

Another factor entering into the flow levels experienced during testing is the leakage occurring between the segments. Some test work had been previously accomplished to determine sector joint leakage. This was accomplished by blocking off all orifices and measuring flow values at different supply pressure levels. An average leakage rate for a single ring is approximately 15 kg/hr. Thus, in the absence of leakage, the expected flow rate for a single ring is 35 kg/hr. Appropriate configuration changes could considerably reduce this flow rate and bring the values to acceptable levels.

4.4.4 Load Capacity vs. Pad Clearance

4.4.4.1 - Combustion Pressure equal Supply Pressure.

The most significant load data occurs when combustion pressure equals supply pressure. This is when side loads are applied to the piston. Figure 4-21 shows results of the final test run on the loaded pad (3A). The negative clearance on the combustion end remains as it did when there was zero load on the pad (see Figure 4-11). Again this implies that the pad moves towards the cylinder with respect to the reference position which is a zero load, zero supply pressure condition. The combustion and supply pressure for the test results plotted on Figure 4-21 was approximately 10 MPa, or about the maximum pressure considered during the program. When load is applied the pad inclination reduces, although it still remains divergent with respect to the combustion end pressure gradient. Since there are regions of negative clearance, even at zero load, it is difficult to accurately pinpoint the pad load capability. Fortunately, an earlier test of a pad with an identical recess and orifice configuration lifted off cleanly and an accurate measurement of load capacity could be established. These test results are shown on Figure 4-22. This pad showed positive clearance for applied loads in excess of 6,000 N. If load is applied between pads rather than directly on a pad, capacity would increase to 10,400 N. If the effects of squeeze film were included, it is possible to momentarily sustain an absolute maximum side loading of 13,344 N (see Table 1-1). Thus, load capacity results are quite promising, even though momentary contact is a distinct possibility.

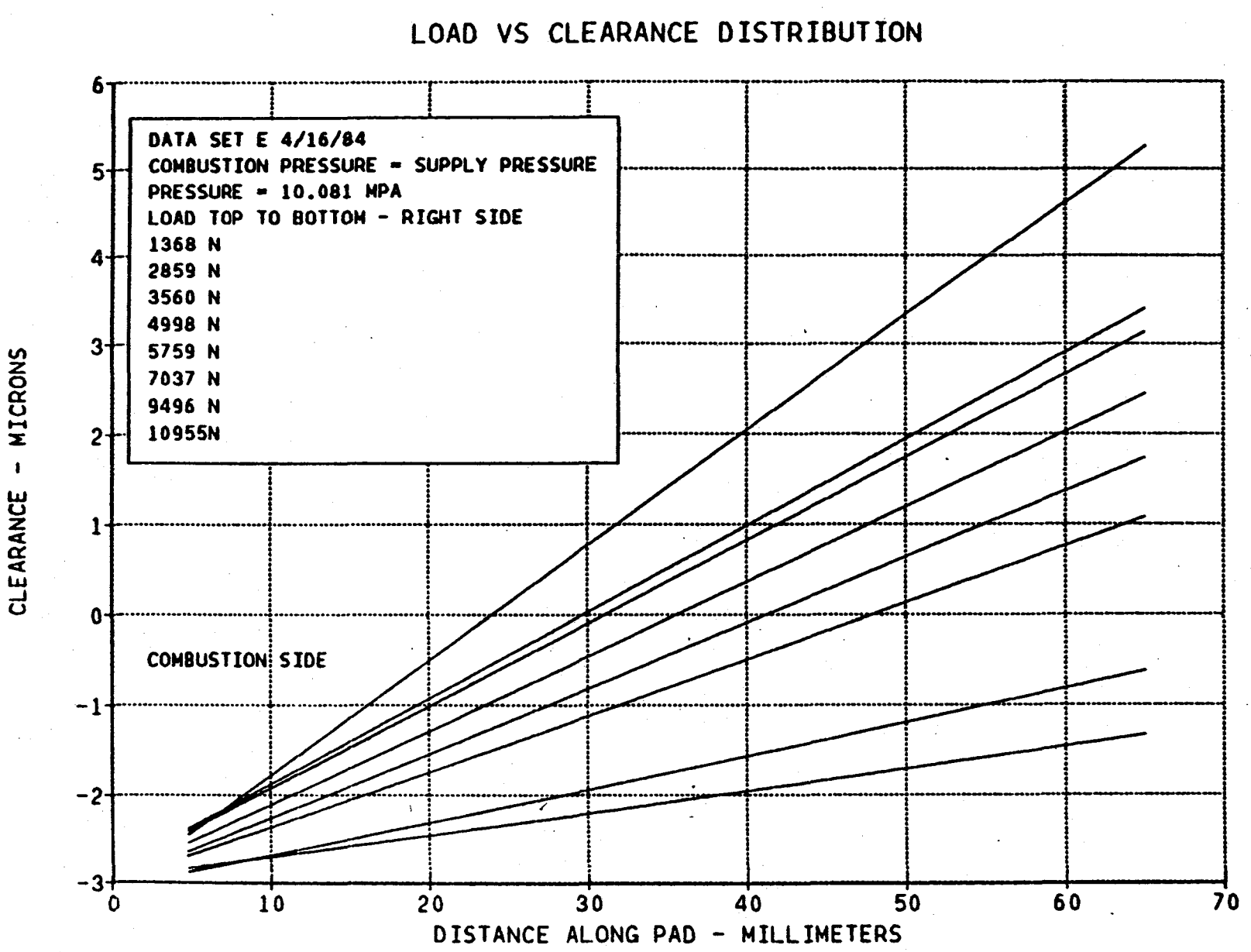
LOAD VS CLEARANCE DISTRIBUTION
DATA SET E 4/16/84
COMBUSTION PRESSURE = SUPPLY PRESSURE
PRESSURE = 10.081 MPA
LOAD TOP TO BOTTOM - RIGHT SIDE
1368 N
2859 N
3560 N
4998 N
5759 N
7037 N
9496 N
10955N
COMBUSTION SIDE
CLEARANCE - MICRONS
DISTANCE ALONG PAD - MILLIMETERS
6
5
4
3
2
1
0
-1
-2
-3
0
10
20
30
40
50
60
70

Figure 4-21

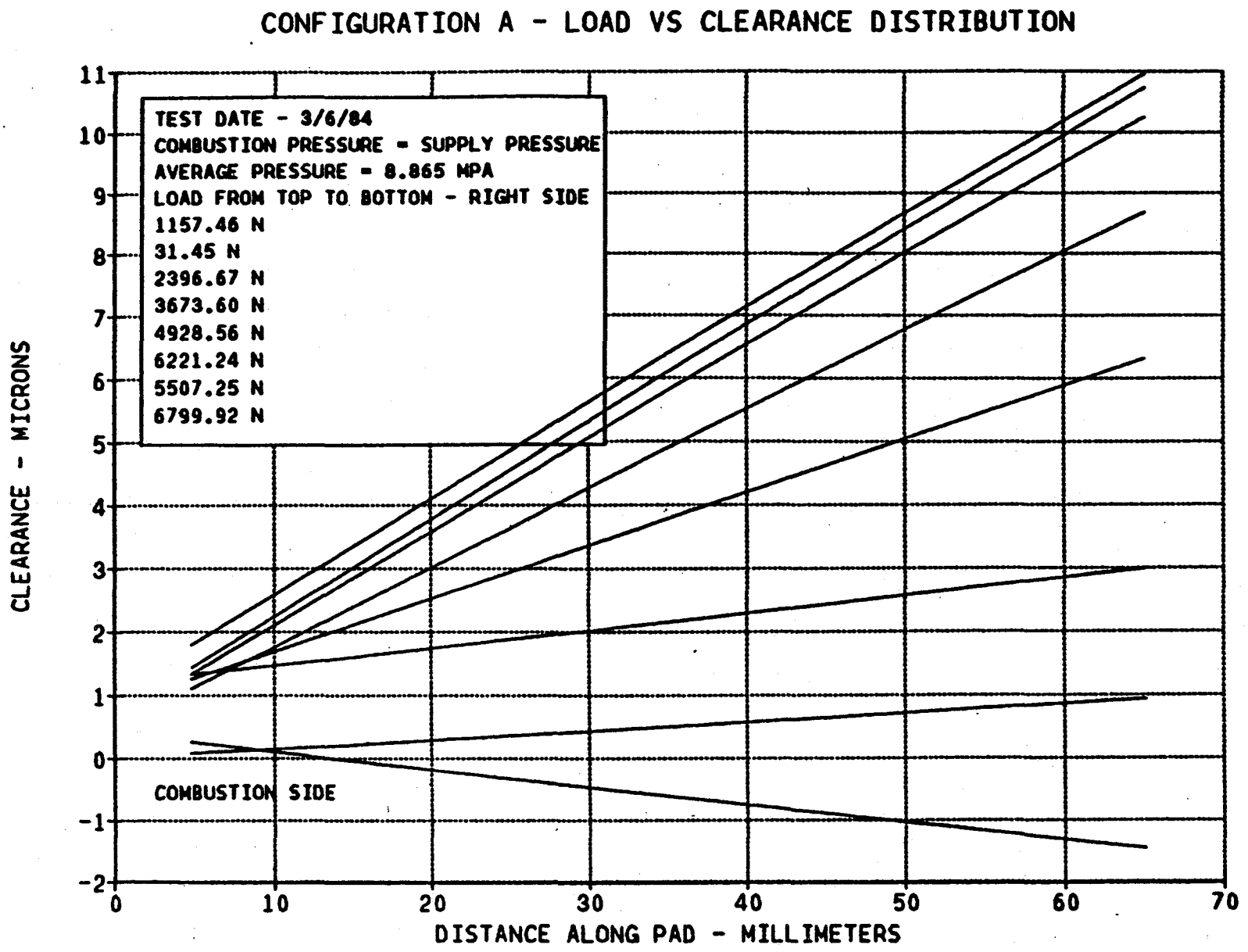
CONFIGURATION A - LOAD VS CLEARANCE DISTRIBUTION
TEST DATE - 3/6/84
COMBUSTION PRESSURE = SUPPLY PRESSURE
AVERAGE PRESSURE = 8.865 MPA
LOAD FROM TOP TO BOTTOM - RIGHT SIDE
1157.46 N
31.45 N
2396.67 N
3673.60 N
4928.56 N
6221.24 N
5507.25 N
6799.92 N
COMBUSTION SIDE
CLEARANCE - MICRONS
DISTANCE ALONG PAD - MILLIMETERS
11
10
9
8
7
6
5
4
3
2
1
0
-1
-2
0
10
20
30
40
50
60
70

Figure 4-22

For reasonable life, it would probably be necessary to apply low wear material combinations.

Load data was also taken when the combustion pressure was set to zero. Although this is not a load condition, the information is useful in establishing the capacity of the gas film. Typical results are shown on Figure 4-23. Except for the most heavily loaded case, all clearances remain positive and reasonably healthy. Maximum load capacity is in the vicinity of 5,000 to 6,000 N.

A multitude of load vs. clearance data was plotted as a function of clearance levels and is included in Appendix B for reference purposes.

4.4.5 Flow as a Function of Load

The variation of flow with load at different pressure levels is shown on Figures 4-24 and 4-25. Figure 4-24 shows flow variations when the combustion pressure equals the supply pressure and Figure 4-25 shows the variation when the combustion pressure is zero. The results indicate that flow does not vary significantly with load; the most sensitive independent parameter is pressure. The reason load is not an important variable with respect to flow variations is that the integrated clearance distribution over all pads does not vary significantly. Although there is some clearance closure on the loaded pad, it is compensated for by slight opening on adjacent and opposite pads.

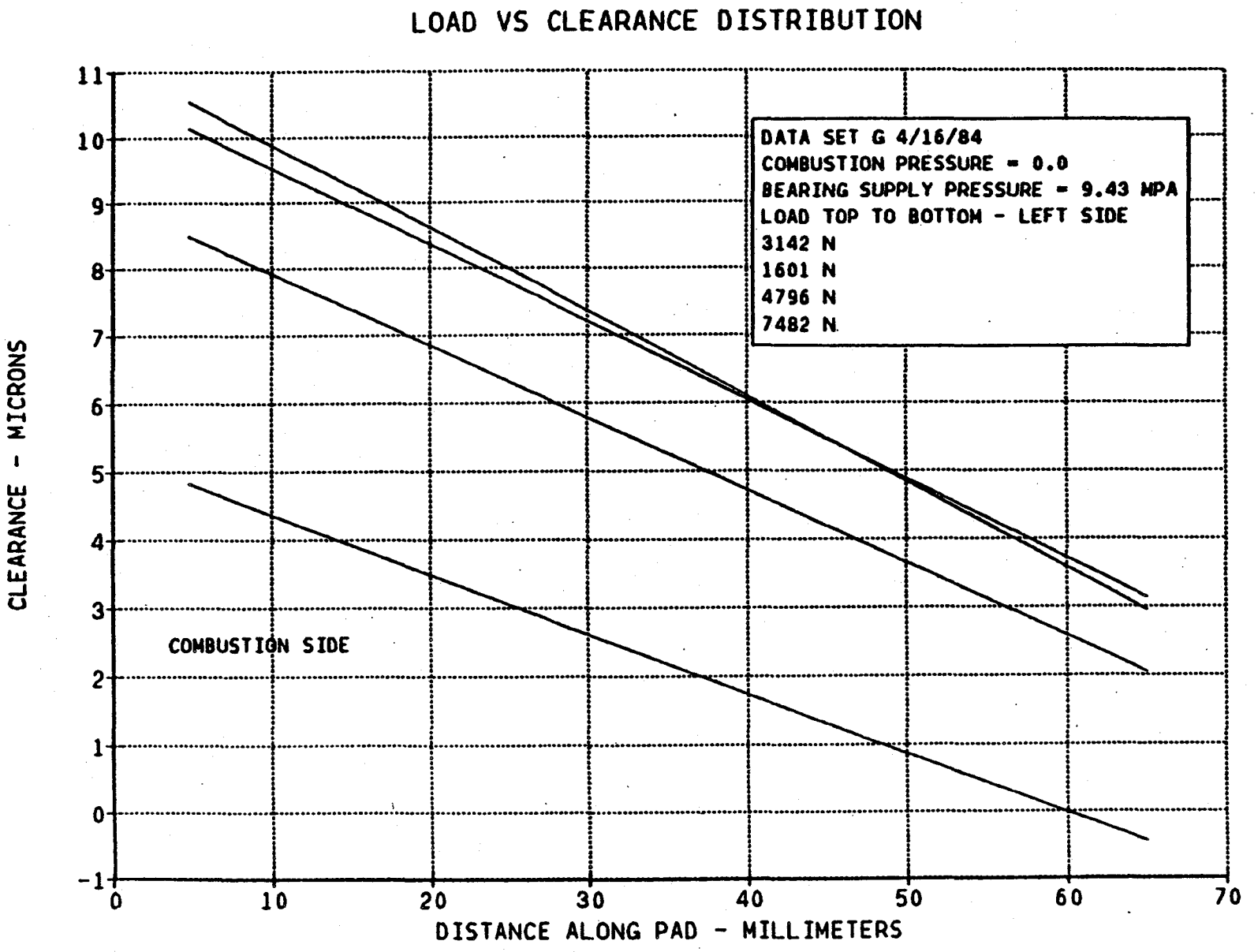
LOAD VS CLEARANCE DISTRIBUTION
DATA SET G 4/16/84
COMBUSTION PRESSURE = 0.0
BEARING SUPPLY PRESSURE = 9.43 MPA
LOAD TOP TO BOTTOM - LEFT SIDE
3142 N
1601 N
4796 N
7482 N
COMBUSTION SIDE
CLEARANCE - MICRONS
DISTANCE ALONG PAD - MILLIMETERS
11
10
9
8
7
6
5
4
3
2
1
0
-1
0
10
20
30
40
50
60
70

Figure 4-23

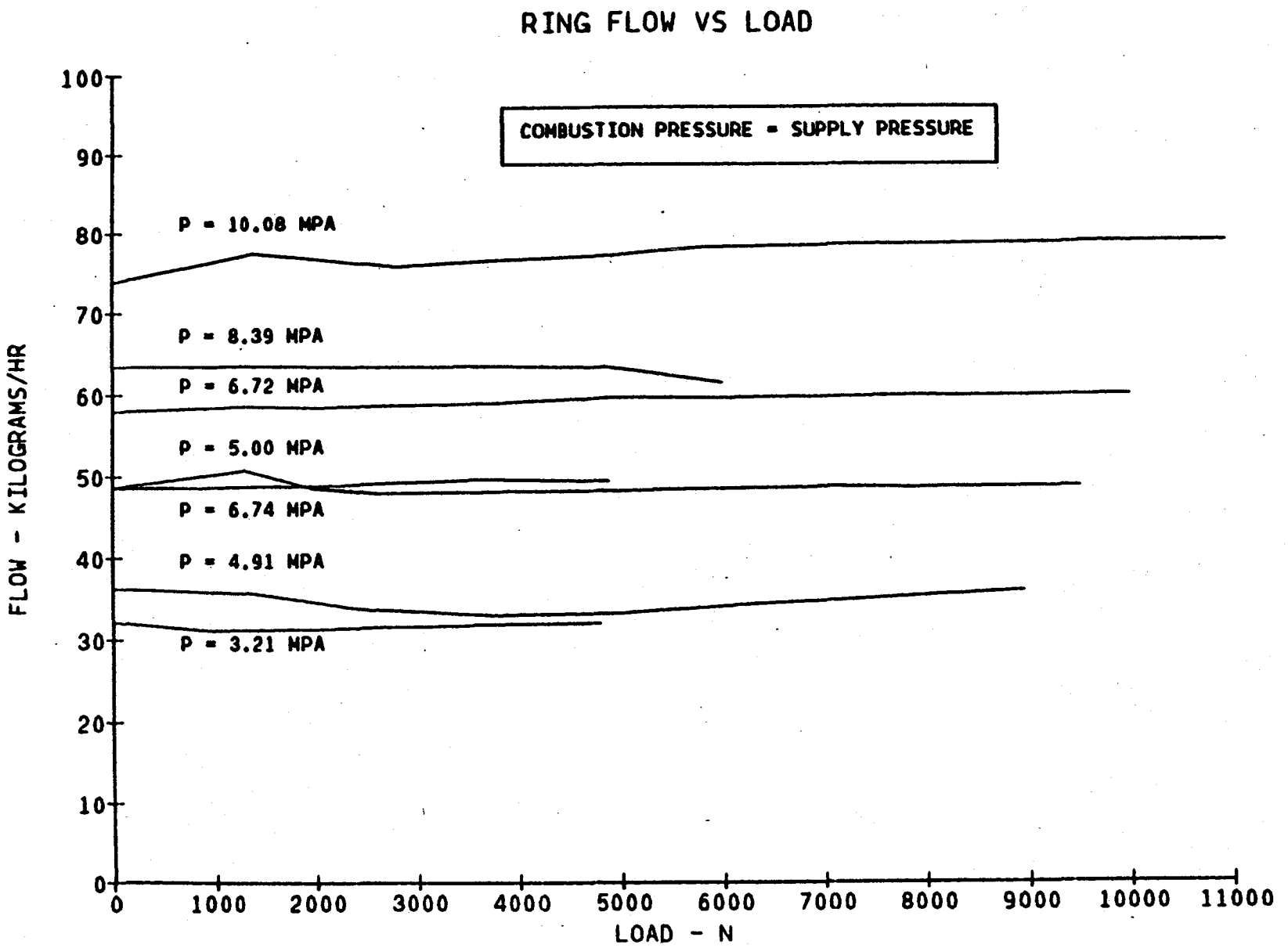
RING FLOW VS LOAD
COMBUSTION PRESSURE = SUPPLY PRESSURE
P = 10.08 MPA
P = 8.39 MPA
P = 6.72 MPA
P = 5.00 MPA
P = 6.74 MPA
P = 4.91 MPA
P = 3.21 MPA
FLOW - KILOGRAMS/HR
LOAD - N
0
10
20
30
40
50
60
70
80
90
100
0
1000
2000
3000
4000
5000
6000
7000
8000
9000
10000
11000

Figure 4-24

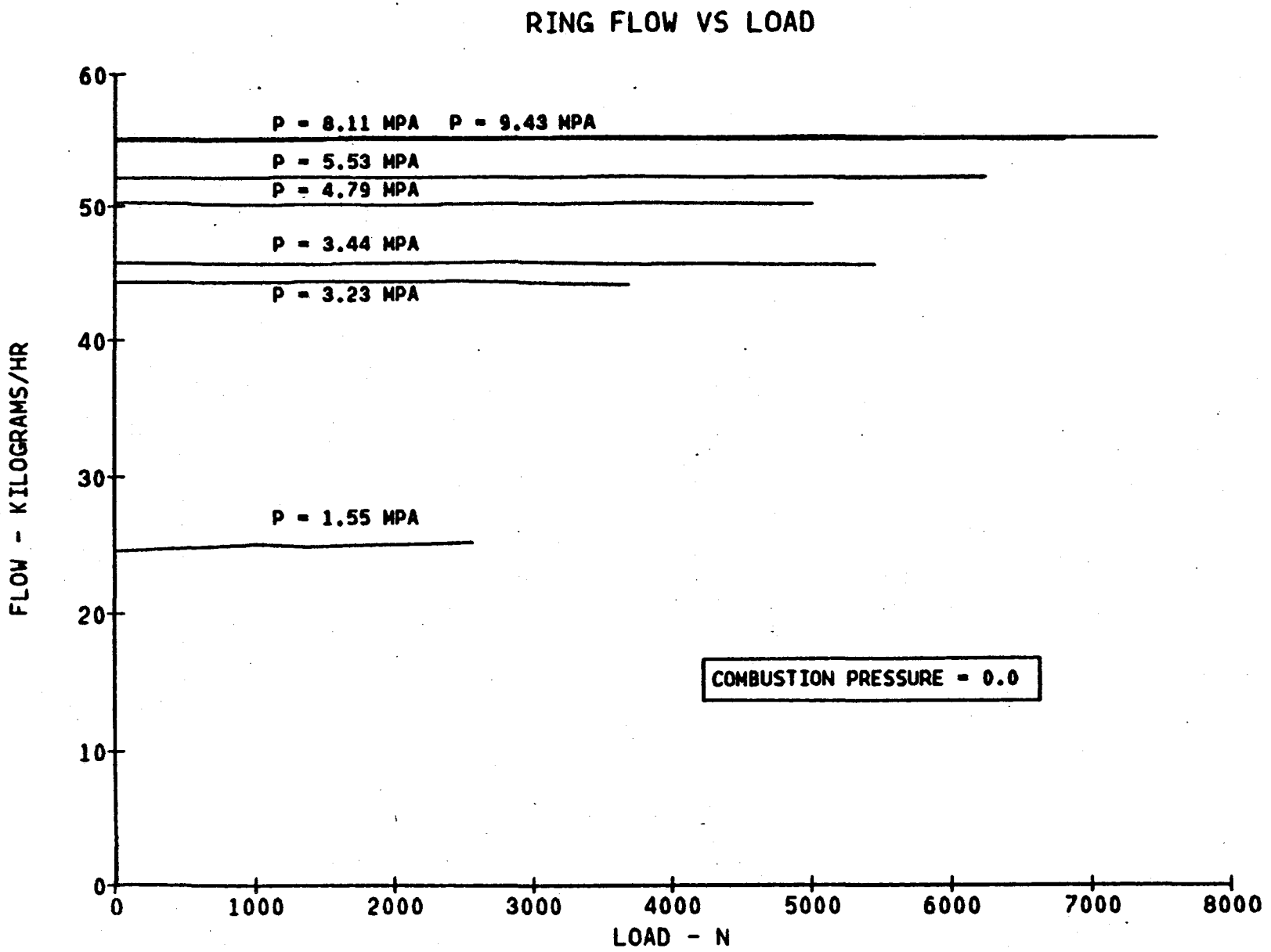
RING FLOW VS LOAD
P = 8.11 MPA
P = 9.43 MPA
P = 5.53 MPA
P = 4.79 MPA
P = 3.44 MPA
P = 3.23 MPA
P = 1.55 MPA
COMBUSTION PRESSURE = 0.0
FLOW - KILOGRAMS/HR
LOAD - N
0
10
20
30
40
50
60
0
1000
2000
3000
4000
5000
6000
7000
8000

Figure 4-25

5.0 ANALYTICAL PREDICTIONS

5.1 Computer Codes

The initial analysis of the gas-lubricated piston ring made a number of simplifying assumptions that overestimated performance and was a significant underlying factor in producing a deficient design. The major assumptions included in the analysis were as follows:

1. The ring was presumed to be solid without geometric interruption between segments.

2. Feed orifices were treated as inherently compensated line sources around the circumference of the ring.

Section 6, Chronology of Test Program, provides more details and insights into the development history. When it became apparent that initial computer codes would not be adequate to provide guidance for configuration changes, it was decided to use an available incompressible computer code that contained the required number of options necessary to conduct parametric studies. The capabilities included:

1. Single or multi-recess configuration with arbitrary locations.

2. Orifice compensation.

3. Pre-specified pressure boundary conditions.

4. Ability to determine pad position to satisfy a given radial load and moment about the known fulcrum position.

Results of the incompressible theory differs from the more accurate compressible predictions in the following areas:

1. The pressure distribution over land or sill regions (as opposed to over the recess) is more linear with incompressible theory and is somewhat parabolic for compressible theory. These distributions become

distorted with greater variation when pad inclination occurs. Although absolute comparisons between the results of compressible and incompressible theory may not produce large differences, small variations are significant. The pre-load on a pad is in the neighborhood of 35,584 N and if the center of pressure is off by only 5 to 10 mm, it could have a significant impact on righting moment and cause a diverging clearance rather than the desired converging clearance in the direction of the pressure gradient. In other words, small differences in large numbers can have appreciable effects even though percentages are small.

2. Incompressible theory does not allow for choking in the orifice, although this is not of serious consequence for the application since pressure ratios across the orifice are in the neighborhood of 0.8 or greater.

3. Flow conversion from incompressible to compressible theory is made by using the average density in the film. This can be shown to be exact for isothermal flow which is the normal assumption in compressible theory.

5.2 Applied Forces and Moments

The pressure applied to a segment by the bearing supply and the combustion chamber pressure impose radial loads and moments about the pad fulcrum. These loads and moments must be balanced by the gas-film. Figures 5-1 and 5-2 show closing forces and moments respectively as a function of pressure levels. In computing forces and moments, it was presumed that the bearing supply pressure is applied to the outboard ends of the Tetraseal grooves. When combustion pressure equals supply pressure, the normal area of the pad above the upper Tetraseal is exposed to high pressure gas and will produce an additional closing load over that of the zero pressure boundary conditions. Thus in Figure 5-1, when the combustion pressure equals supply pressure, the closing loads are greater. With respect to applied moments, when the combustion pressure equals supply pressure, there is a moment caused by pressure acting on the top surface of the pad that counterbalances that due to the additional radial pressures above the upper Tetraseal.

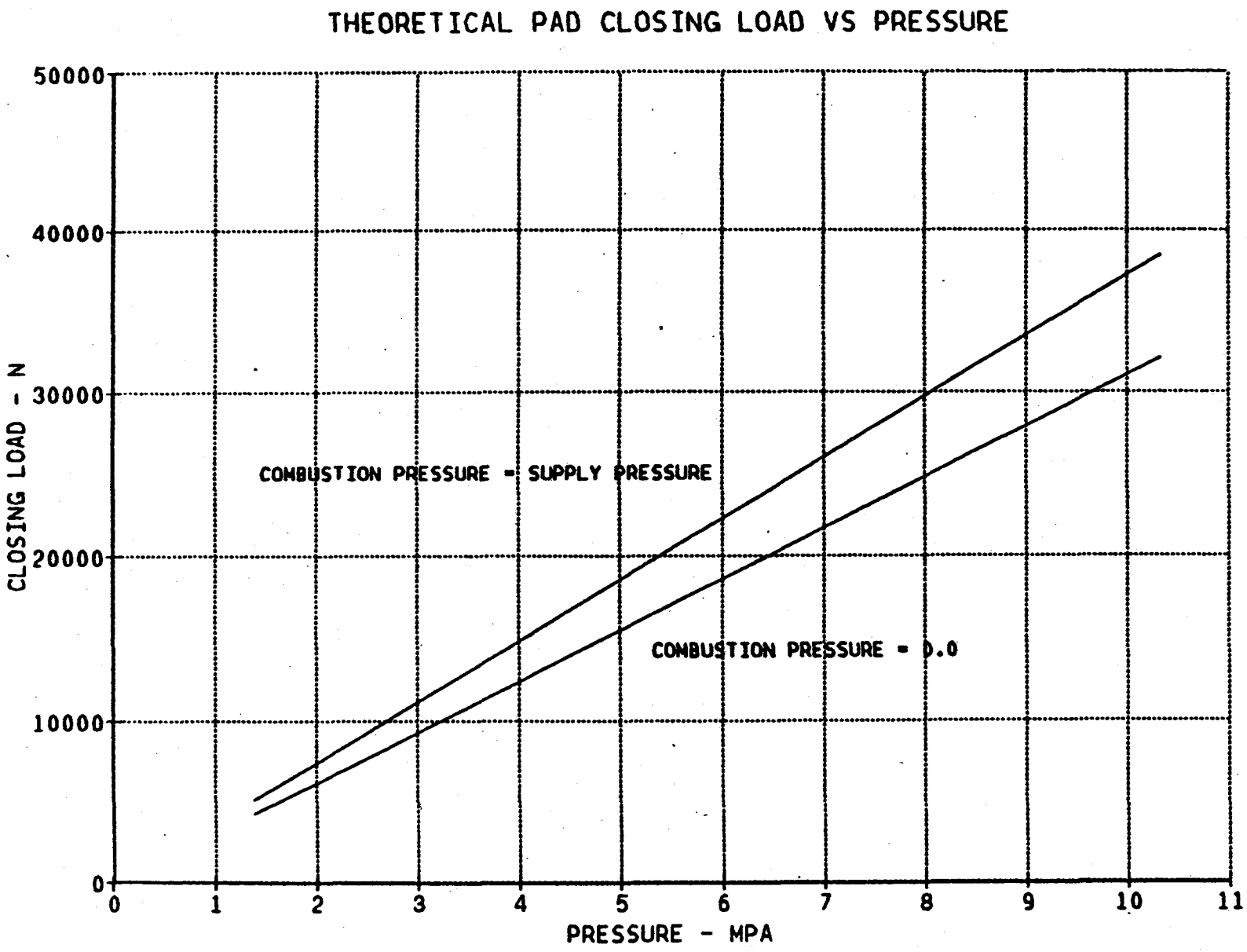
THEORETICAL PAD CLOSING LOAD VS PRESSURE
CLOSING LOAD - N
50000
40000
30000
20000
10000
0
COMBUSTION PRESSURE = SUPPLY PRESSURE
COMBUSTION PRESSURE = 0.0
0
1
2
3
4
5
6
7
8
9
10
11
PRESSURE - MPA

Figure 5-1

Thus, the moments for both sets of boundary conditions are nearly equal as indicated on Figure 5-2.

5.3 Boundary Conditions Between Sectors

In determining theoretical performance, an appropriate model for determining the pressure occurring at the joints between sectors must be decided upon. Initially, it was presumed that there would be essentially zero flow normal to the joint. However, when comparing the theoretical predictions with zero normal flow joints with actual test data, the theory seems to overestimate performance. More accurate results were produced when zero joint pressures were applied. The reason why zero pressure joints produce more correct theoretical predictions is not well understood, but to provide the greatest accuracy for determining recess configurations to be tested these were the conditions applied.

5.4 Theoretical Models

The theoretical computer models employed are depicted on Figure 5-3. The grid network is for one sector. The abscissa represents the circumferential direction and the ordinate represents the axial direction. There are 24 grid intervals (2.5° each) in the circumferential direction and 16 grid intervals (4.366 mm each) in the axial direction. The numbers at the grid points are used to identify boundary points, recesses, computation points, etc. The numbers 11 and 12 identify recesses numbers 1 and 2, respectively. The number 8 indicates a grid point at which the pressure is determined from numerical solution of the lubrication equation. The zeros imply 0 pressure. The numbers 4 and 13 are used to apply appropriate pressure boundaries to the top of the pad when combustion pressure equals supply pressure. The dimensions used in the analysis are not identical to the final dimensions physically machined into the pad. There are two reasons for the discrepancy:

1. Test results indicated a variation of dimensions to improve performance.

2. Grid intervals must be sufficiently large to avoid excessive consumption of computer time.

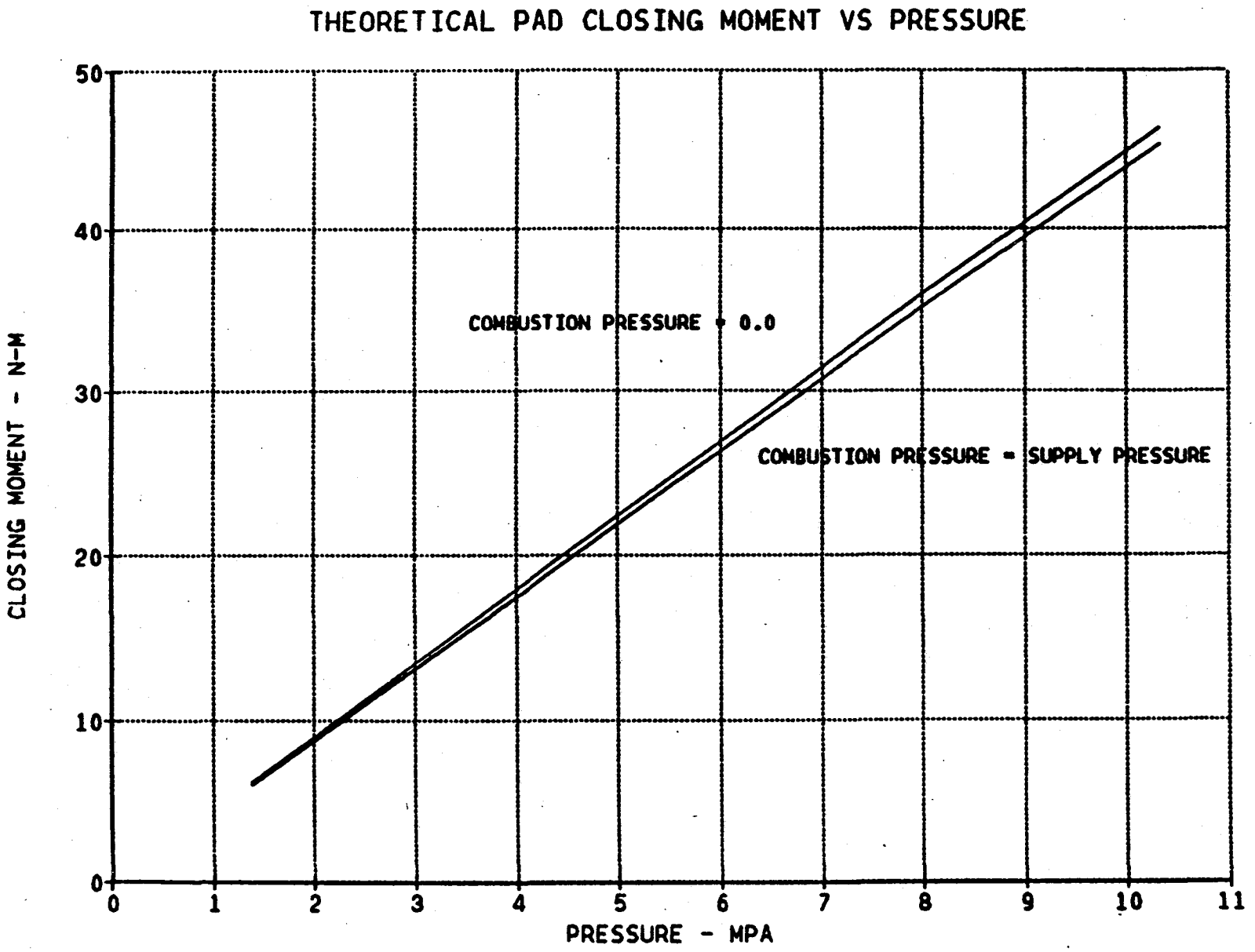
THEORETICAL PAD CLOSING MOMENT VS PRESSURE
CLOSING MOMENT - N-M
PRESSURE - MPA
COMBUSTION PRESSURE = 0.0
COMBUSTION PRESSURE = SUPPLY PRESSURE
0
10
20
30
40
50
0
1
2
3
4
5
6
7
8
9
10
11

Figure 5-2

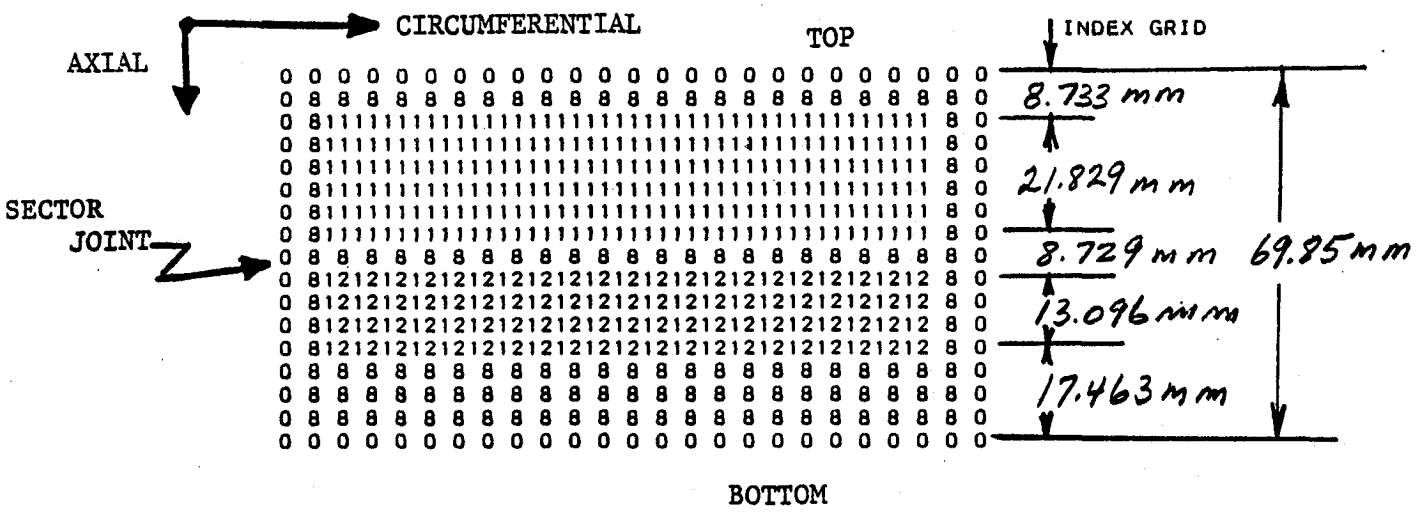

Figure 5-3A - Segment Grid - Zero Combustion End Pressure

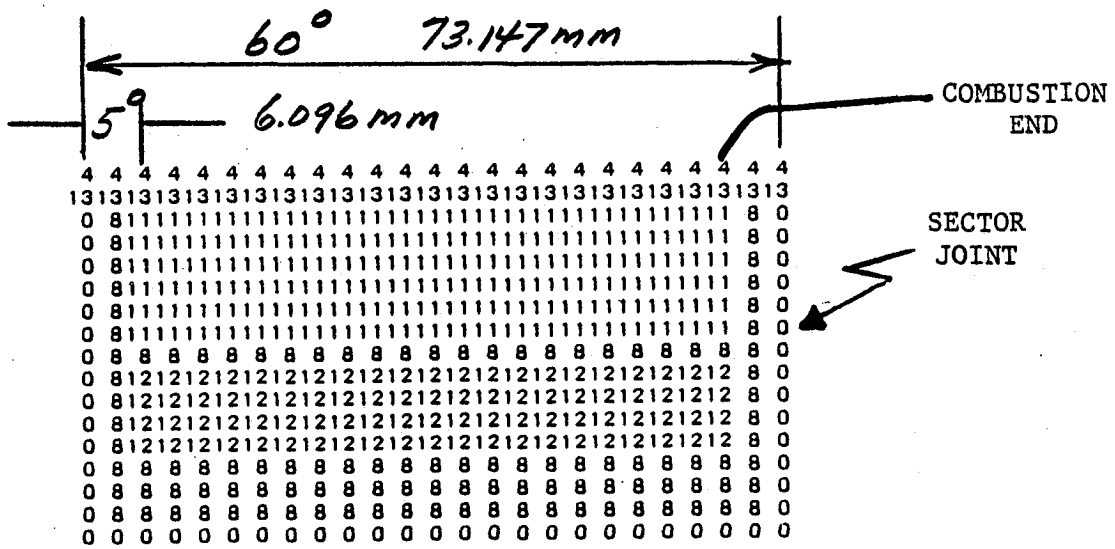

Figure 5-3B - Segment Grid - Combustion Pressure Equal Supply Pressure

5.5 Theoretical Results

Since theory is not limited by instrumentation capability, a significant amount of theoretical information can be readily produced. This section discusses theoretical results, and Section 5.6 following compares the results with experiment.

Minimum film thickness as a function of pressure is shown on Figure 5-4. The first observation is that all film thicknesses are positive. Minimum films are less for the case where combustion pressure =0. When combustion pressure equals supply pressure, the combustion pressure provides additional capacity that opens clearances. The absolute values of minimum films are in the range where achievable surface topography would not interfere, but are stretching what would be considered safe limits in bearing technology (2.5 - 5.0 microns). Figures 5-5 and 5-6 shows the clearance distribution along the length of the pad at various pressure levels for combustion pressure equal zero and equal to supply pressure respectively. These two plots can be directly compared to experimental results (see previous section). Absolute magnitude of pad inclination for the two pressure boundary conditions are shown on Figure 5-7. A negative inclination implies a converging clearance from the combustion end to the exhaust end. Theoretically converging clearances are predicted although for combustion pressure equal supply pressure, the pad inclinations are quite low. Also note, that there is not a significant variation of the inclination angle with pressure.

Ring flow as a function of pressure is shown on Figure 5-8. The higher flow occurs when the combustion pressure equal zero, because there is no pressure gradient to inhibit flow from the recess towards the combustion end. Flow levels do increase with pressure.

Figures 5-9 and 5-10 indicate the variations of both recess pressures with supply pressure for the combustion pressure equal to zero and to the supply pressure respectively. Recess 1 is the large recess at the combustion end and Recess 2 is the smaller recess closer to the exhaust end. Optimally, there should be a good separation between the recess pressure and supply pressure in a hydrostatic bearing. As the recess pressure approaches the supply pressure, stiffness is adversely affected. Unfortunately, when low flow and high loads are prerequisites, small films and high recess pressures are consequences. As

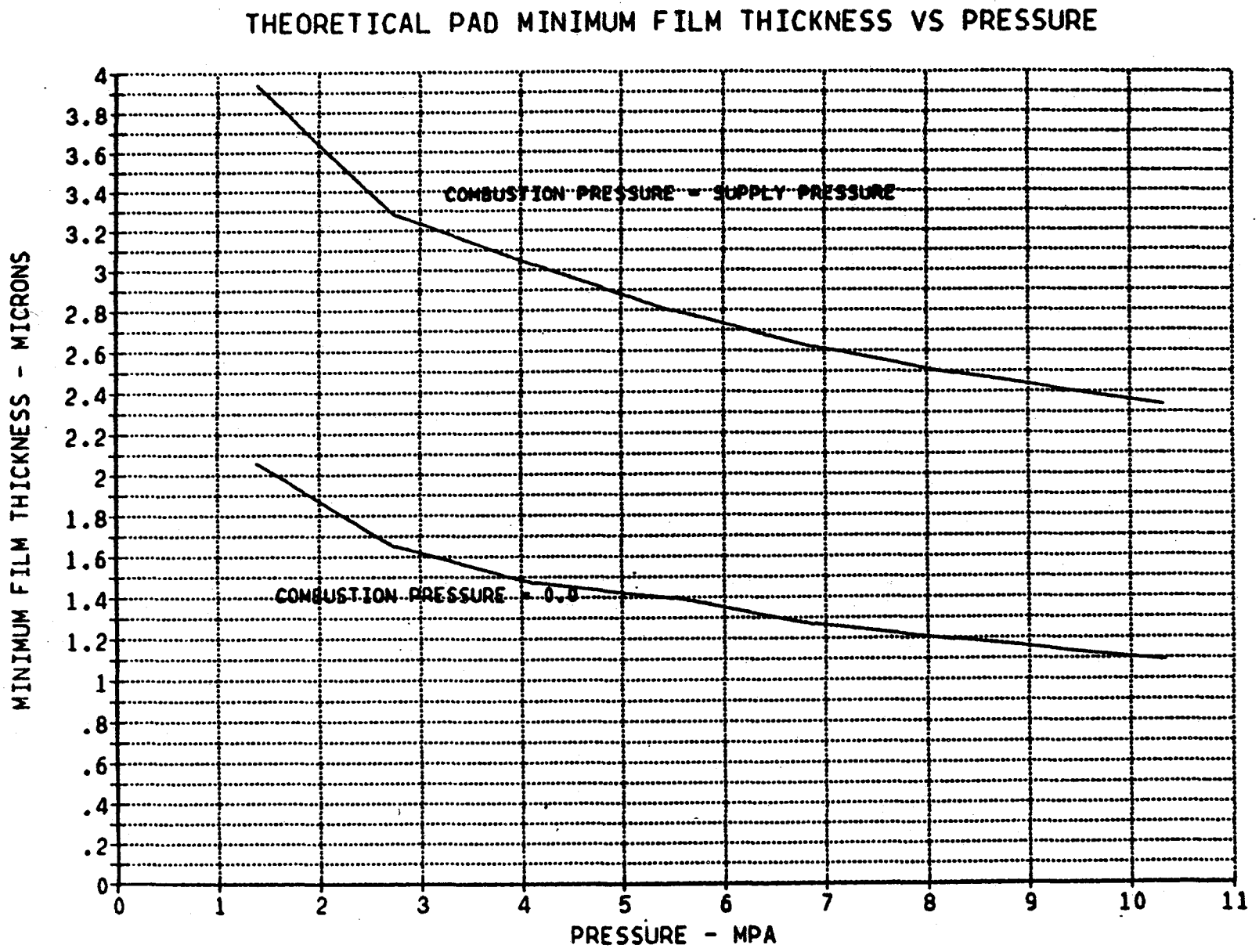
THEORETICAL PAD MINIMUM FILM THICKNESS VS PRESSURE
MINIMUM FILM THICKNESS - MICRONS
PRESSURE - MPA
COMBUSTION PRESSURE = SUPPLY PRESSURE
COMBUSTION PRESSURE = 0.0
0
.2
.4
.6
.8
1
1.2
1.4
1.6
1.8
2
2.2
2.4
2.6
2.8
3
3.2
3.4
3.6
3.8
4
0
1
2
3
4
5
6
7
8
9
10
11

Figure 5-4

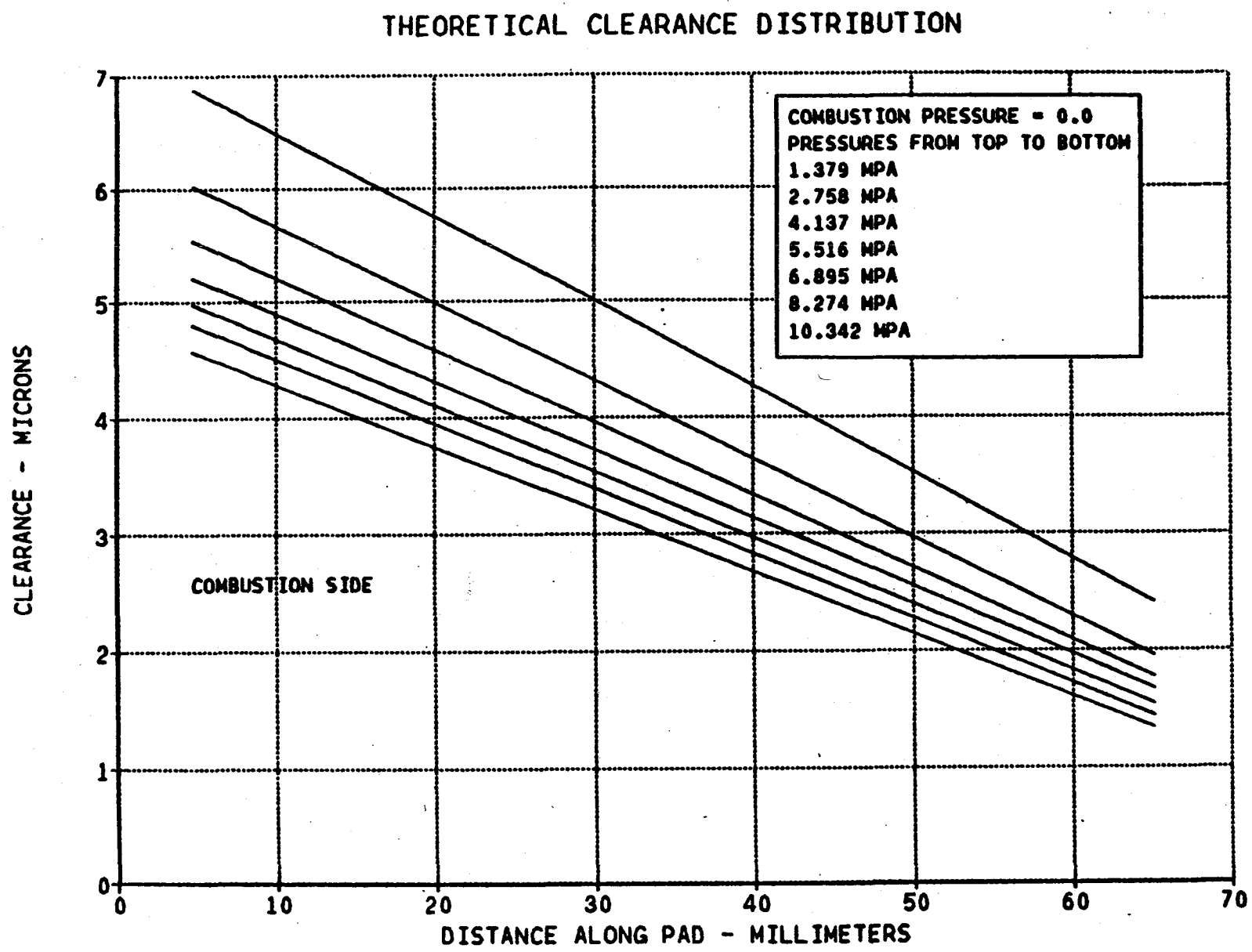
THEORETICAL CLEARANCE DISTRIBUTION
COMBUSTION PRESSURE = 0.0
PRESSURES FROM TOP TO BOTTOM
1.379 MPA
2.758 MPA
4.137 MPA
5.516 MPA
6.895 MPA
8.274 MPA
10.342 MPA
COMBUSTION SIDE
CLEARANCE - MICRONS
DISTANCE ALONG PAD - MILLIMETERS
0
1
2
3
4
5
6
7
0
10
20
30
40
50
60
70

Figure 5-5

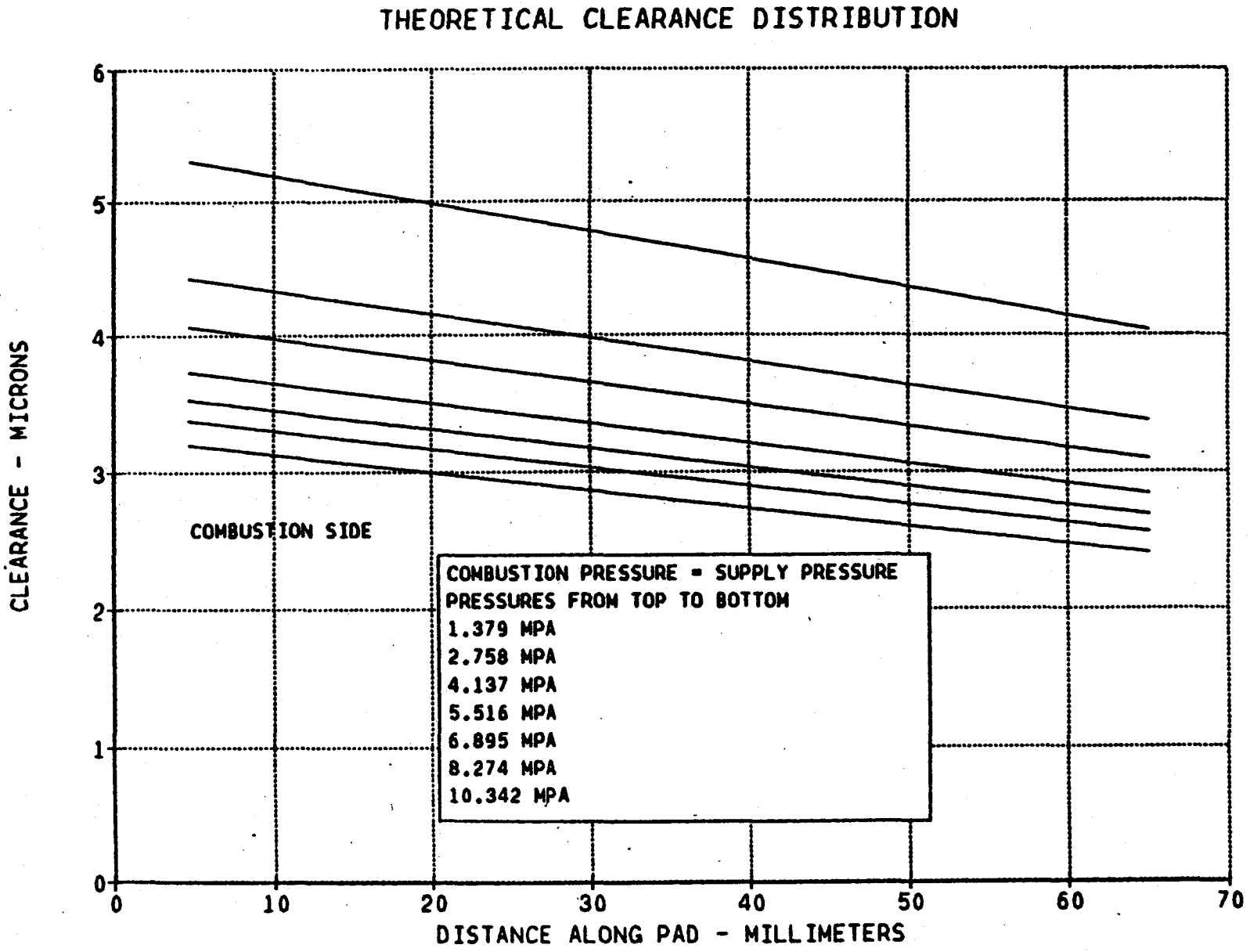
THEORETICAL CLEARANCE DISTRIBUTION
CLEARANCE - MICRONS
DISTANCE ALONG PAD - MILLIMETERS
COMBUSTION SIDE
COMBUSTION PRESSURE = SUPPLY PRESSURE
PRESSURES FROM TOP TO BOTTOM
1.379 MPA
2.758 MPA
4.137 MPA
5.516 MPA
6.895 MPA
8.274 MPA
10.342 MPA
0
1
2
3
4
5
6
0
10
20
30
40
50
60
70

Figure 5-6

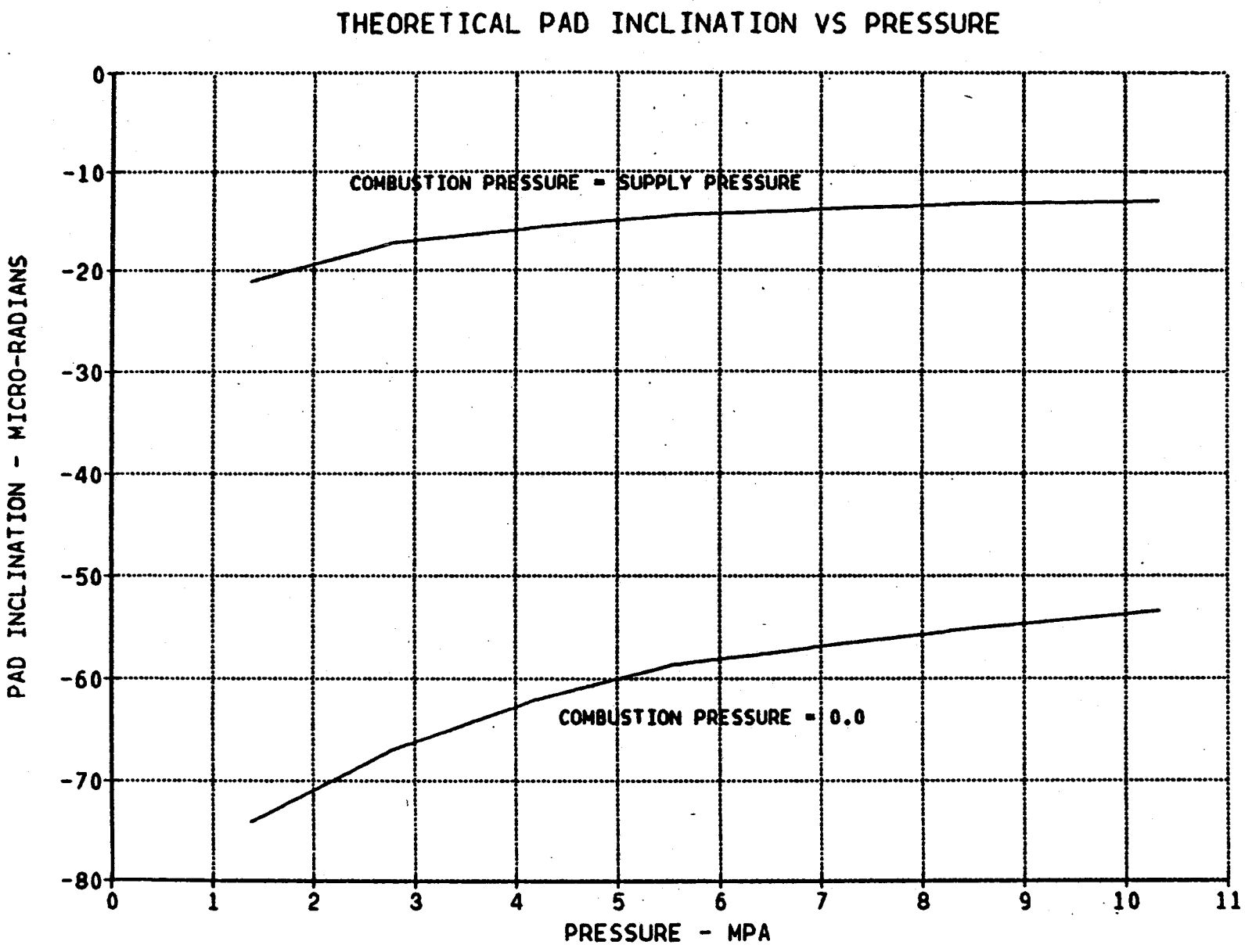
THEORETICAL PAD INCLINATION VS PRESSURE
PAD INCLINATION - MICRO-RADIANS
0
-10
-20
-30
-40
-50
-60
-70
-80
COMBUSTION PRESSURE = SUPPLY PRESSURE
COMBUSTION PRESSURE = 0.0
0
1
2
3
4
5
6
7
8
9
10
11
PRESSURE - MPA

Figure 5-7

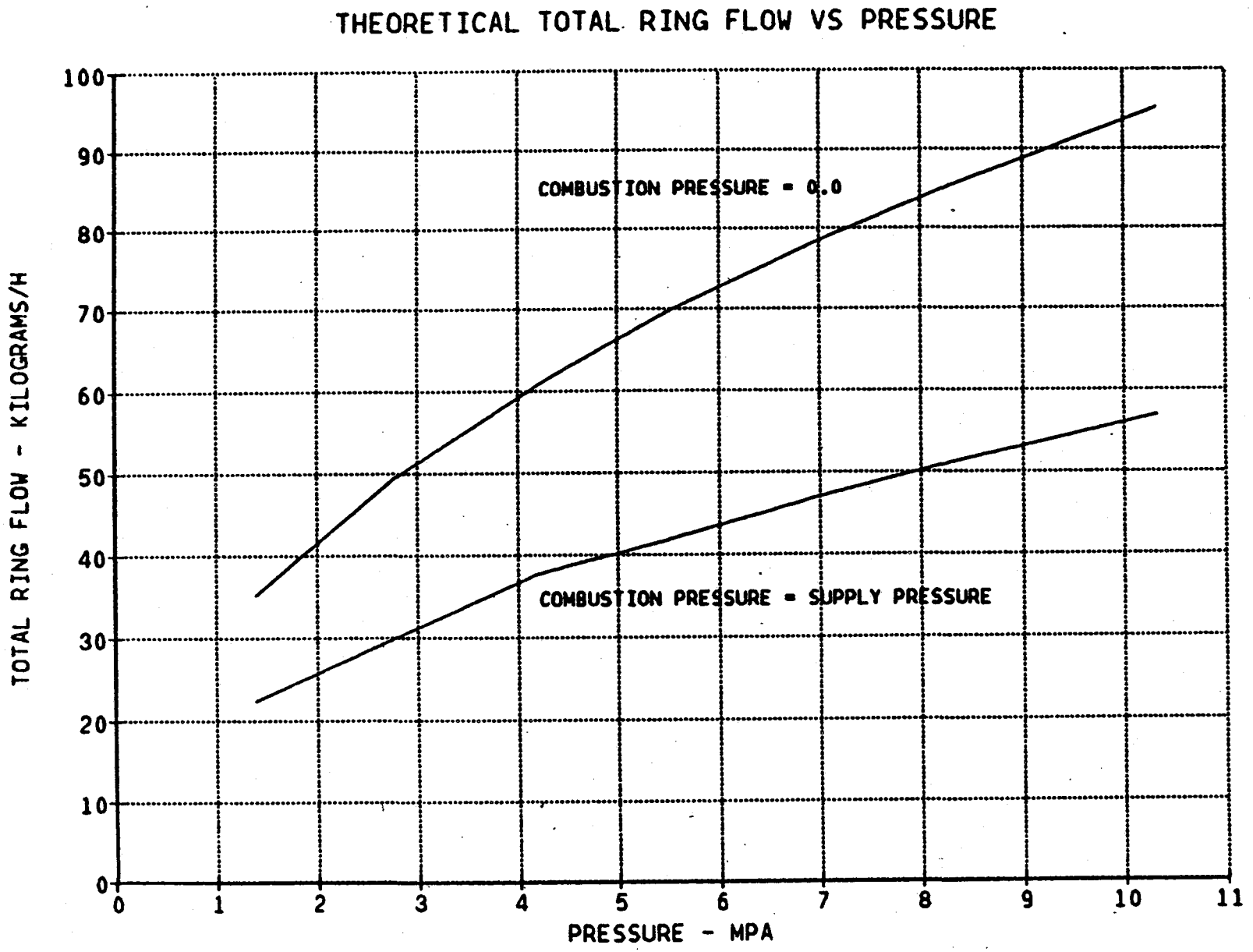
THEORETICAL TOTAL RING FLOW VS PRESSURE
TOTAL RING FLOW - KILOGRAMS/H
PRESSURE - MPA
COMBUSTION PRESSURE = 0.0
COMBUSTION PRESSURE = SUPPLY PRESSURE
0
10
20
30
40
50
60
70
80
90
100
0
1
2
3
4
5
6
7
8
9
10
11

Figure 5-8

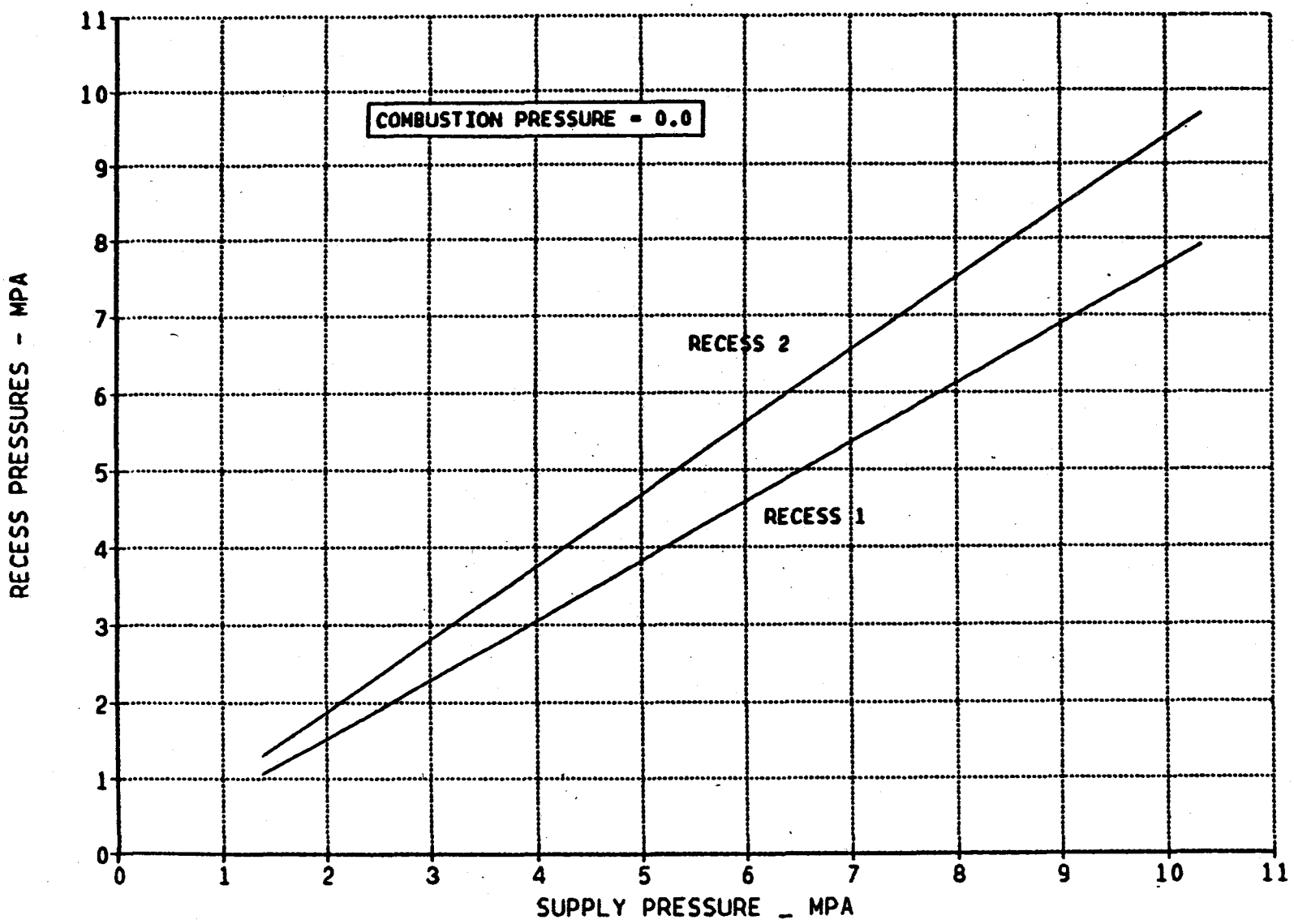
THEORETICAL RECESS PRESSURES VS SUPPLY PRESSURE
COMBUSTION PRESSURE = 0.0
RECESS 2
RECESS 1
RECESS PRESSURES - MPA
SUPPLY PRESSURE _ MPA
0
1
2
3
4
5
6
7
8
9
10
11

Figure 5-9

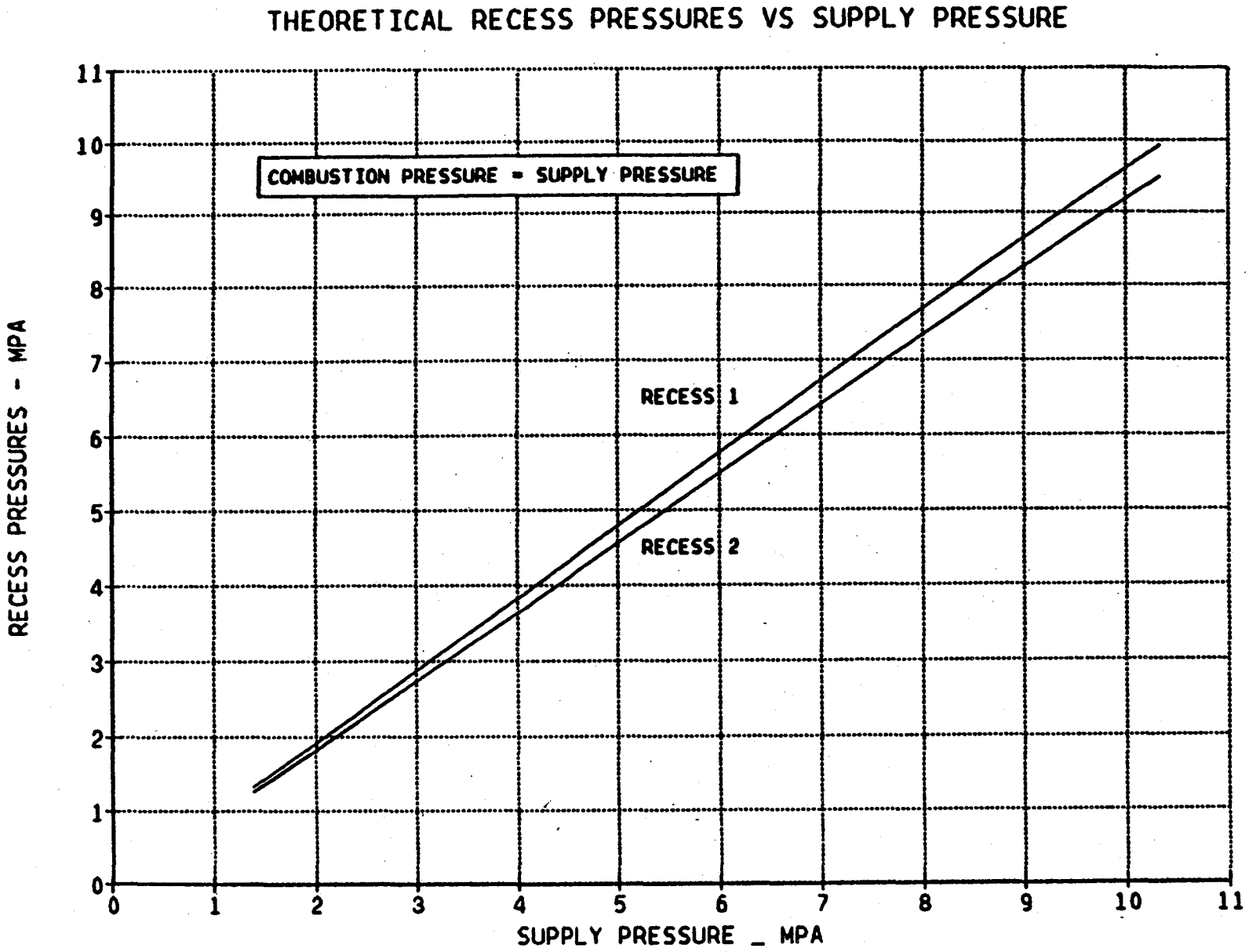
THEORETICAL RECESS PRESSURES VS SUPPLY PRESSURE
COMBUSTION PRESSURE = SUPPLY PRESSURE
RECESS 1
RECESS 2
RECESS PRESSURES - MPA
SUPPLY PRESSURE _ MPA
0
1
2
3
4
5
6
7
8
9
10
11

Figure 5-10

indicated on Figure 5-9, for combustion pressure equal zero, pressures in Recess 2 are quite high, while those in Recess 1 maintain an adequate separation with the supply pressure. The reason that high pressures occur in Recess 2 is that moment unbalance tends to close off the clearance on the downstream end where Recess 2 is located, increasing flow resistance in that region with consequent high recess pressures. For the case of combustion pressure equal to supply pressure, Recess 1 has slightly higher pressures than Recess 2, but both pressures are relatively high because of the close clearances and boundary conditions.

Figure 5-11 shows the radial stiffness of the sector as a function of bearing supply pressure. At a pressure of 10 MPa, the stiffness when the combustion pressure is zero is more than twice the value when combustion pressure equals supply pressure. Although the stiffness values appear to be large, they are deceiving because of the low operating film thickness. Figure 5-12 shows the pad tilt stiffness as a function of pressure. It is significant to note that the pad stiffness values continue to increase with pressure and have not leveled off. In theory, the predicted stiffness values are adequate enough to prevent segment contact. The final theoretical performance curve is the pad eccentricity ratio as a function of supply pressure, shown on Figure 5-13. The eccentricity ratio is defined as the radial displacement at the pad pivot position divided by the machined clearance of the pad (.0127 mm). An eccentricity ratio of 1 would mean that pad contact had occurred. For the general operating conditions the pad eccentricity ratios are very acceptable, but the more meaningful parameter is the minimum film thickness since this accounts for tilt about the pivot points.

5.6 Comparison Between Theory and Experiment

Direct comparisons can be made between theory and experiment for the clearance distribution and flow. Consider first the clearance distribution when the combustion end pressure is zero. If Figures 4-8 and 5-5 are compared, the following conclusions can be made:

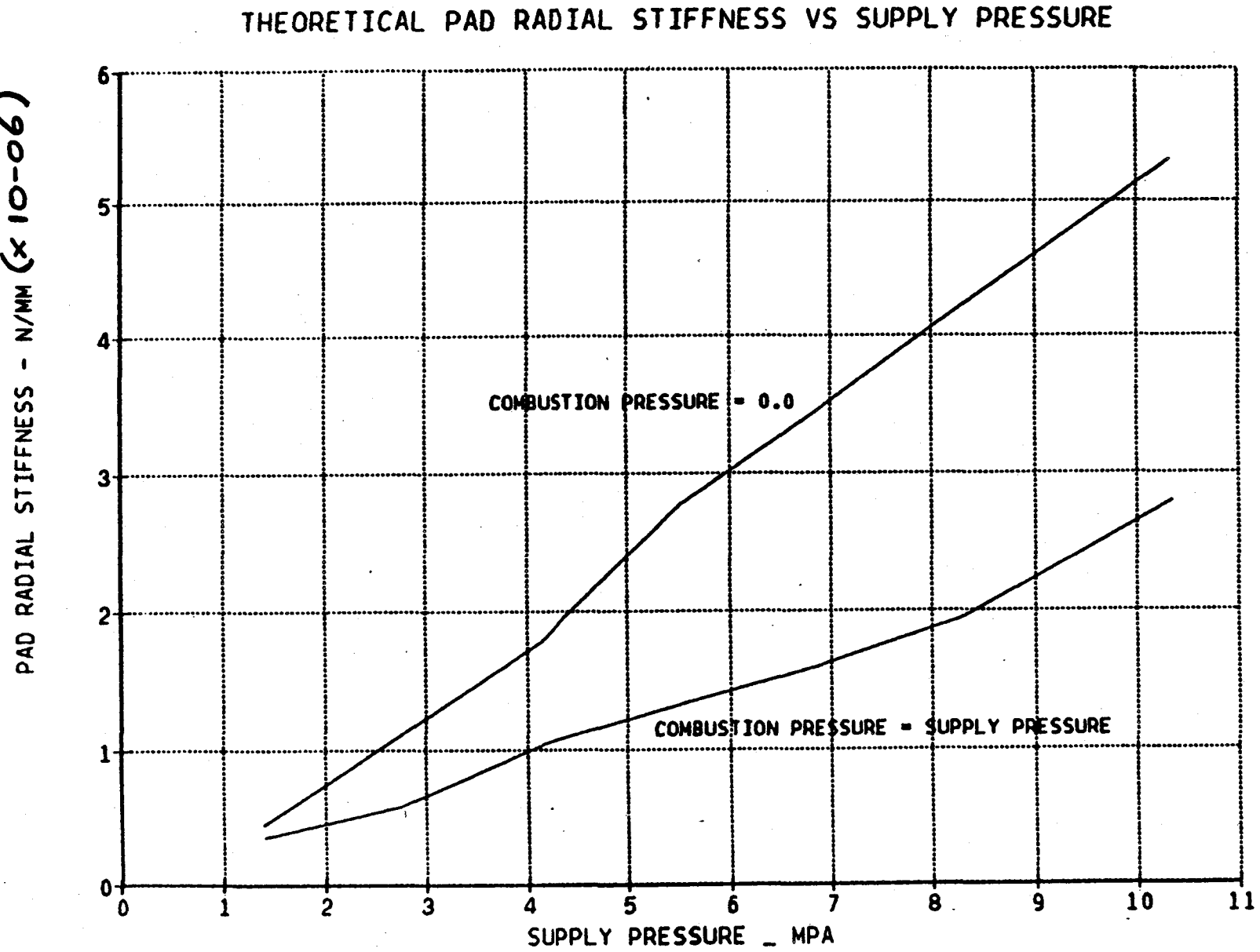
THEORETICAL PAD RADIAL STIFFNESS VS SUPPLY PRESSURE
PAD RADIAL STIFFNESS - N/MM (x 10-06)
SUPPLY PRESSURE _ MPA
COMBUSTION PRESSURE = 0.0
COMBUSTION PRESSURE = SUPPLY PRESSURE
0
1
2
3
4
5
6
7
8
9
10
11

Figure 5-11

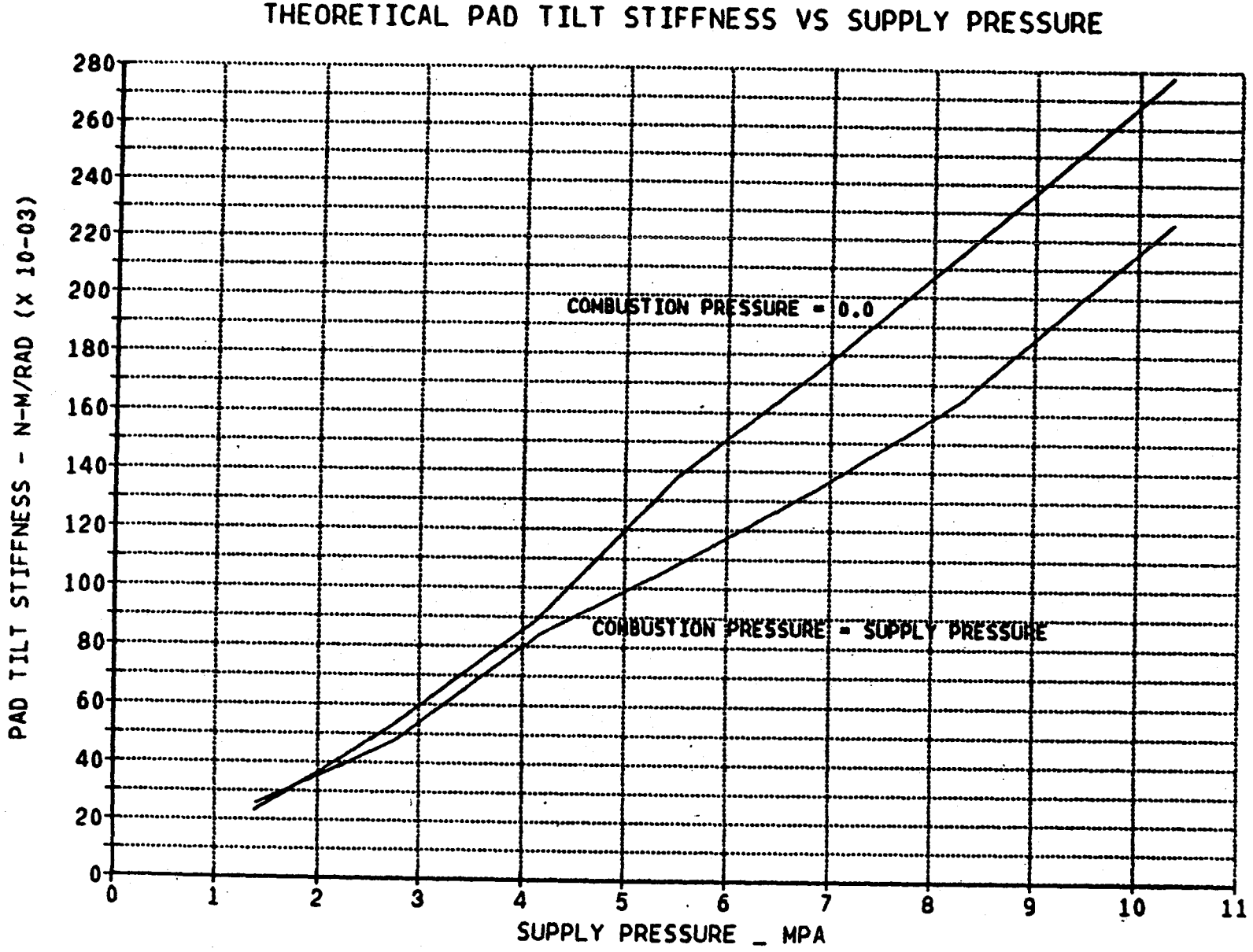
THEORETICAL PAD TILT STIFFNESS VS SUPPLY PRESSURE
PAD TILT STIFFNESS - N-M/RAD (X 10-03)
SUPPLY PRESSURE _ MPA
COMBUSTION PRESSURE = 0.0
COMBUSTION PRESSURE = SUPPLY PRESSURE
0
20
40
60
80
100
120
140
160
180
200
220
240
260
280
0
1
2
3
4
5
6
7
8
9
10
11

Figure 5-12

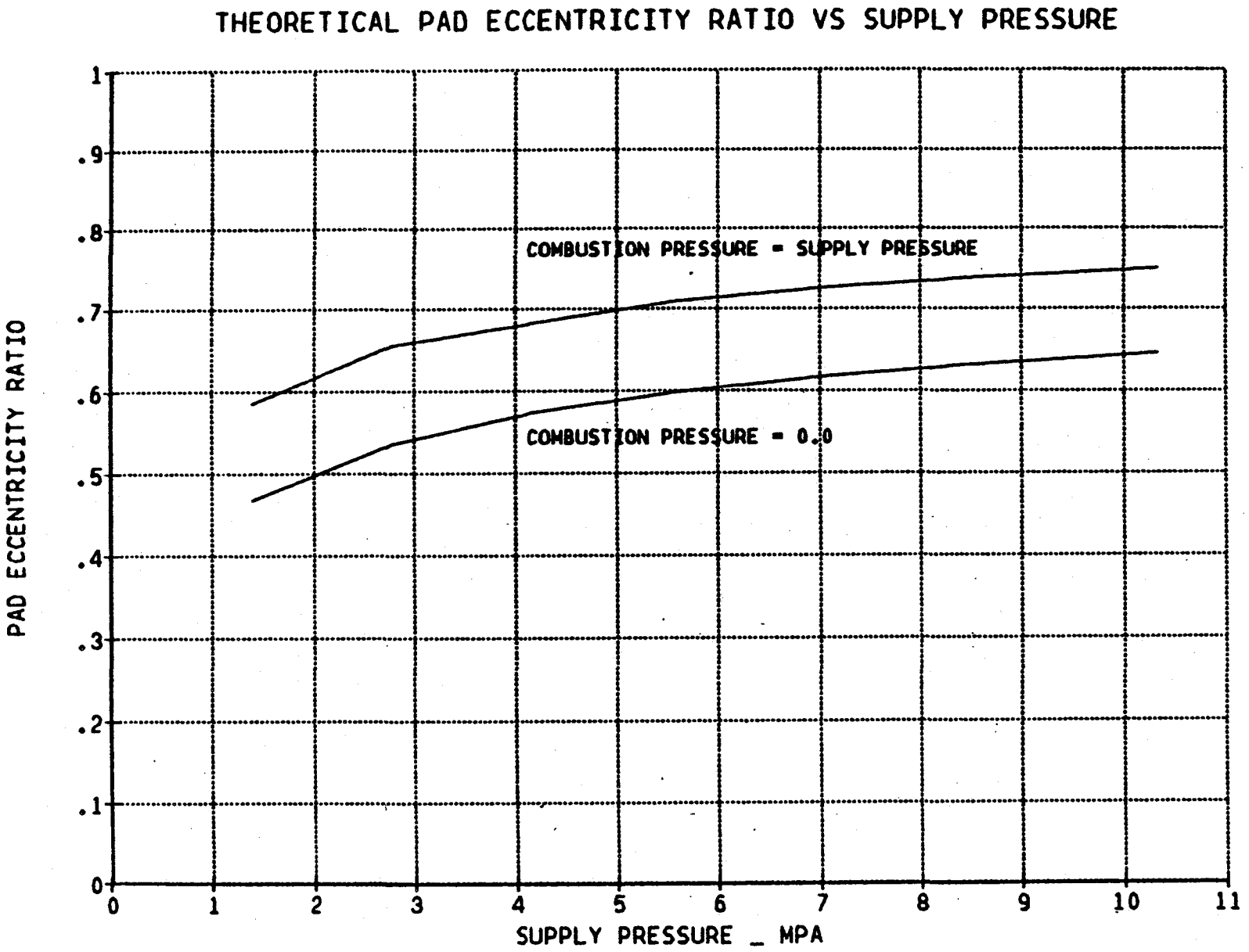
THEORETICAL PAD ECCENTRICITY RATIO VS SUPPLY PRESSURE
PAD ECCENTRICITY RATIO
1
.9
.8
.7
.6
.5
.4
.3
.2
.1
0
COMBUSTION PRESSURE = SUPPLY PRESSURE
COMBUSTION PRESSURE = 0.0
0
1
2
3
4
5
6
7
8
9
10
11
SUPPLY PRESSURE _ MPA

Figure 5-13

Clearance Distribution, Combustion Pressure =0 (Figures 4-8 and 5-5).

- The theory indicates decreasing clearances with pressures. Experiments provide mixed results but, in general, clearances are greater at higher pressures.
- The pad inclination for both experiment and theory provides a converging clearance from the combustion end to the exhaust end.
- Figure 4-9 shows clearance results for pad 1A. Although this pad experiences negative clearances, note the general trend towards reduced clearances as pressures increase. This is in conformance with the general theoretical results of Figure 5-5. Similar results apply to pad 5A, as can be seen by comparing Figures 4-10 and 5-5.
- Clearance distribution comparisons between theory and experiment for the case where combustion pressure equals supply pressure can be made by examining Figures 5-6 and 4-12 (pad 3A). The theoretical results shown on Figure 5-6 indicate a good converging clearance in the direction of the combustion end pressure gradient and reasonable values of operating clearance. Also, the clearance decreases as the pressure increases. The experimental results, Figure 4-12, on the other hand, show a diverging clearance in the direction of the pressure gradient. Also, the higher pressures produce higher clearances, which is again contrary to theory. Positive clearances at the higher pressures were produced experimentally for pad 3A, at a different test date (see Figure 4-13) indicating some inconsistency in pad performance. Figures 4-14 and 4-15 show that pads 1A and 5A maintained similar performance characteristics.
- Flow data comparisons can be made by examining Figures 4-18 and 5-8. Theoretical values shown on Figure 5-8 indicate that when the combustion pressure equals zero, the flow is always higher than when combustion pressure equals supply pressure. The test results indicate that the curves cross each other and at lower pressure levels, the flow is higher for the combustion pressure equal to supply pressure. This is due to the diverging clearance distribution as opposed to theory. At the higher pressure levels, the absolute magnitude of the flows compare reasonably well. Also, the general trend in flow are correct; the flow gradient with pressure is greater for zero combustion end pressure.
- In general, the computer code proved very useful in evolving a final configuration and predicted general trends (e.g. improved performance)

very well. The theory was lacking, however, in predicting final clearance distributions.

5.7 Pneumatic Hammer Instability

Hydrostatic gas bearings are prone to a phenomenon known as "pneumatic hammer", a self-excited, and often destructive, vibration of the opposed surfaces.

Pneumatic hammer comes about because of compressibility in the film and is aggravated by trapped fluid regions within the clearance volume. References 1, 2 and 3 indicate theoretical methods for determining criteria for avoiding pneumatic hammer problems. Theoretical development is outlined on the following pages.

NOMENCLATURE

A = Bearing area

A_o = Orifice area

A_r = Surface area of recess

A_s = Surface area of bearing

C_D = Coefficient of discharge

g = Gravity constant

h = Film thickness

h' = Film thickness perturbation

K = Flow constant of bearing

K_o = Orifice constant = $N_o C_D A_o \sqrt{\frac{2\gamma g}{(\gamma-1)R_g T}}$

m = Mass of bearing

$\dot{M}$ = Rate of change of fluid mass inside bearing region

N_o = Number of orifices

p = Pressure

p' = Pressure perturbation

p_a = Ambient pressure

p_r = Recess pressure

p_s = Orifice supply pressure

q_i = Incompressible flow through bearing

q_{in} = Mass flow into bearing

q_{out} = Mass flow out of bearing

R_g = Universal gas constant

T = Absolute gas temperature

V_r = Recess volume = $Ar\delta$

β = $\left(p_r/p_s\right)^{\frac{\gamma-1}{\gamma}}$

γ = Ratio of specific heats

δ = Depth of recess

ρ_a = Density of fluid at ambient pressure

ρ_r = Density of fluid at recess pressure

The equation of motion (neglecting tetraseal stiffness and damping and coulomb friction) for the bearing is

$$m\ddot{h} = p'A \tag{5-1}$$

The conservation of mass states that the time rate of change of the bearing gas content equals the difference between inflow and outflow. Corresponding to the time rates of small deviations from the equilibrium position the following equations are obtained:

$$Q_{in} = \left(\frac{\partial Q_{in}}{\partial p}\right) p' + \left(\frac{\partial Q_{in}}{\partial h}\right) h' \tag{5-2}$$

Similarly,

$$Q_{out} = \left(\frac{\partial Q_{out}}{\partial p}\right) p' + \left(\frac{\partial Q_{out}}{\partial h}\right) h' \tag{5-3}$$

$$Q_{in} - Q_{out} = \left(\frac{\partial Q_{in}}{\partial p} - \frac{\partial Q_{out}}{\partial p}\right) p' + \left(\frac{\partial Q_{in}}{\partial h} - \frac{\partial Q_{out}}{\partial h}\right) h' \tag{5-4}$$

The rate of change of mass within the bearing is:

$$\dot{M} = \left(\frac{\partial M}{\partial p}\right) \dot{p}' + \left(\frac{\partial M}{\partial h}\right) \dot{h}' \tag{5-5}$$

Equating (5-4) to (5-5) we obtain

$$\left(\frac{\partial Q_{in}}{\partial p} - \frac{\partial Q_{out}}{\partial p}\right) p' + \left(\frac{\partial Q_{in}}{\partial h} - \frac{\partial Q_{out}}{\partial h}\right) h' = \left(\frac{\partial M}{\partial p}\right) \dot{p}' + \left(\frac{\partial M}{\partial p}\right) \ddot{h}' \tag{5-6}$$

From (5-1)

$$p' = \frac{m\ddot{h}'}{A} \tag{5-7}$$

$$\dot{p}' = \frac{m\dddot{h}'}{A} \tag{5-8}$$

Eliminating p' and $\dot{p}'$ from (5-6) by substitution of (5-7) and (5-8) we obtain

$$\dddot{h}' + \frac{\left(\frac{\partial Q_{out}}{\partial p} - \frac{\partial Q_{in}}{\partial p}\right)}{\frac{\partial M}{\partial p}} \ddot{h}' + \frac{\left(\frac{\partial M}{\partial h}\right)\frac{A}{m}}{\frac{\partial M}{\partial p}} \dot{h}' + \frac{\frac{A}{m}\left(\frac{\partial Q_{out}}{\partial h} - \frac{\partial Q_{in}}{\partial h}\right)}{\frac{\partial M}{\partial p}} h' = 0 \qquad (5\text{-}9)$$

let

C_2 = ceofficient of $\ddot{h}'$

C_1 = coefficient of $\dot{h}'$

C_0 = ceofficient of h'

Equation (5-9) thus becomes

$$\dddot{h}' + C_2 \ddot{h}' + C_1 \dot{h}' + C_0 h' = 0 \qquad (5\text{-}10)$$

In accordance with Routh's criteria, the condition for stability is that all coefficients are positive and that

$$C_2 C_1 > C_0 \qquad (5\text{-}11)$$

Substitution of the values of the coefficients leads to the inequality

$$\frac{\frac{\partial M}{\partial p}}{\frac{\partial M}{\partial h}} \leq \frac{\frac{\partial Q_{out}}{\partial p} - \frac{Q_{in}}{\partial p}}{\frac{\partial Q_{out}}{\partial h} - \frac{\partial Q_{in}}{\partial h}} \qquad (5\text{-}12)$$

The mass content within the clearance is equal to the clearance volume multiplied by the average density

$$M = \left[A_s h + A_r \delta\right] \quad \frac{\rho_r + \rho_a}{2} \qquad (5\text{-}13)$$

but since isothermal conditions are presumed to exist in the clearance region

$$\rho = \frac{p}{R_g T} \qquad \text{and}$$

$$M = \frac{1}{R_g T} \left[A_s h + A_r \delta\right] \frac{\left(p_r + p_a\right)}{2} \qquad (5\text{-}14)$$

Then

$$\boxed{\frac{\partial M}{\partial p} = \frac{1}{2R_g T} \left(A_s h + A_r \delta\right)} \qquad (5\text{-}15)$$

$$\boxed{\frac{\partial M}{\partial h} = \frac{(p_r + p_a) A_s}{2 R_g T}} \qquad (5\text{-}16)$$

$$Q_{out} = q_i \left(\frac{\rho_r + \rho_a}{2} \right) = \frac{q_i (p_r + p_a)}{2 R_g T} \tag{5-17}$$

$$q_i = Kh^3 (p_r - p_a) \tag{5-18}$$

$$Q_{out} = \frac{Kh^3}{2R_gT} \left(p_r^2 - p_a^2 \right) \tag{5-19}$$

$$\boxed{\frac{\partial Q_{out}}{\partial p} = \frac{Kh^3 p_r}{R_g T}} \tag{5-20}$$

$$\boxed{\frac{\partial Q_{out}}{\partial h} = \frac{3Kh^2}{2 R_g T} (p_r^2 - p_a^2)} \tag{5-21}$$

$$Q_{in} = N_o C_D A_o \sqrt{\frac{2\gamma g}{(\gamma-1) R_g T}} \; p_s \left\{ \left(\frac{p_r}{p_s} \right)^{2/\gamma} \left[1 - \left(\frac{p_r}{p_s} \right)^{\frac{\gamma-1}{\gamma}} \right] \right\}^{1/2} \tag{5-22}$$

For orifice compensation $\frac{\partial Q_{in}}{\partial h} = 0$, since A_o is not a function of h

$$\boxed{\frac{\partial Q_{in}}{\partial p} = \frac{K_o \frac{1}{\gamma} \left[\left(\frac{1}{\beta} - 1 \right) + \frac{1}{2} \left(1 - \gamma \right) \right]}{(1-\beta)^{1/2}}} \tag{5-23}$$

The equation (5-12) was applied to one sector of the bearing.

For one sector of the bearing

$K\ (p_s = 1500,\ p_c = 0) = 1.392 \times 10^9$ (from previously developed theory)

$A_s = 7.9194\ in^2$ $\qquad\qquad$ $\gamma - 1.5814$

$P_r = 1300$ psig $\qquad\qquad$ $\beta = .9493$

$P_s = 1500$ psig

$h = 130 \times 10^{-6}$ in

$R_g = 662\ \frac{in}{^oR}$

$T = 530\ ^oR$

$$\frac{\partial M}{\partial p} = \frac{1}{2R_gT}\left[A_s h + A_r \delta\right] = \frac{1}{2(662)(530)}\left[7.9194(130 \times 10^{-6}) + V_r\right]$$

$$= 1.4671 \times 10^{-9} + 1.425 \times 10^{-6}\ V_r$$

$$\frac{\partial M}{\partial h} = \frac{(p_r + p_a)}{2\,R_gT}\ A_s = \frac{(1315 + 15)(7.9194)}{2(662)(530)} = 1.501 \times 10^{-2}$$

$$\frac{\partial Q_{out}}{\partial p} = \frac{Kh^2 p_r}{R_gT} = \frac{1.392 \times 10^9 \times (130 \times 10^{-6})^3\ (1315)}{(662)(530)} = 1.1462 \times 10^{-5}$$

$$\frac{\partial Q_{out}}{\partial h} = \frac{3Kh^2}{2R_gT}\left(p_r^2 - p_a^2\right) = \frac{3(1.392 \times 10^9)(130 \times 10^{-6})^2}{2(662)(530)}\left[1315^2 - 15^2\right]$$

$$= 173.89$$

$$K_o = N_o C_D A_o \sqrt{\frac{2\gamma g}{(\gamma-1)R_g T}} = 3(.85)\ \frac{\pi(.016)^2}{4}\ \sqrt{\frac{2(1.5814)(386.4)}{(.5815)(662)(530)}}$$

$$= 3.9684 \times 10^{-5}$$

$$\frac{\partial Q_{in}}{\partial p} = \frac{K_o}{\gamma}\ \frac{\left[\left(\frac{1}{\beta-1}\right) + \frac{1}{2}\left(1-\gamma\right)\right]}{(1-\beta)^{\frac{1}{2}}} = \frac{3.9684 \times 10^{-5}}{1.5814}\ \frac{\left[\left(\frac{1}{.9493-1}\right) + \frac{1}{2}\left(1-1.5814\right)\right]}{(1-.9493)^{1/2}}$$

$$= -2.6446 \times 10^{-5}$$

$$\frac{\frac{\partial M}{\partial p}}{\frac{\partial M}{\partial h}} = \frac{\frac{\partial Q_{out}}{\partial p} - \frac{\partial Q_{in}}{\partial p}}{\frac{\partial Q_{out}}{\partial h}}$$

$$\frac{1.4671 \times 10^{-9} + 1.425 \times 10^{-6}\ V_r}{1.501 \times 10^{-2}} = \frac{1.1462 \times 10^{-5} - (-2.6446 \times 10^{-5})}{173.89}$$

$$V_r = .0013$$

$$A_r = \frac{5.5\pi}{6}\ \frac{46.96}{60}\ (.5 + .859) = 3.0629$$

$$\delta_r = \frac{.0013}{3.0629} = 4.14 \times 10^{-4} \text{ in.}$$

The theory states that the depth of the recess should be limited to 0.0105 mm (0.414 mils). This theory, however, is conservative because sector damping and coulomb friction have not been accounted for. The actual manufactured pad was limited to a recess depth of .0254 mm (1 mil), and pneumatic hammer was not a problem during the test program.

6.0 CHRONOLOGY OF TEST PROGRAM

This section is intended to document the history of the test program and outline the evolutionary process that led to the final sector configuration.

Prior to the inception of the program, all hardware had been designed and manufactured, through prior contracts between the Cummins Engine Company of Columbus, Indiana and MTI. Reference (4) is a report issued by MTI that covered the initial portion of the Cummins contract. The analytical effort covered by this report, and subsequent analysis used in the hardware design treated the rings as complete circular bearings with line sources of pressure introduced into the film via inherently compensated inlet holes. The predicted performance of the rings are indicated on Tables 6-1 and 6-2.

Table 6-1 indicates performance at intake and exhaust conditions. The orifice rows were located at 25.4 mm (1 in) and 34.925 mm (1.375 in) from the upper end of the pad. There were 18 orifices located around the circumference of each row. The orifice diameter was 0.3683 mm (.0145 in). The 18 orifices divide into 3 orifices per sector per row, and that was the original construction of the pads. The line source pressures were predicted to be 7.64 MPa (1108.65 psia) and 8.398 MPa (1218.08 psia) respectively with supply pressure of 10.34 MPa (1500 psia). The total flow was computed to be 13.02 kg/h (28.68 lb/h). The clearance varied from 5.31 microns (209 μ) at the top of the pad to 2.26 microns (89 μin) at the bottom. Stiffnesses in the radial and angular direction are also indicated on the tabulations. Principal stiffness values of 4.7×10^9 N/m (2.682×10^7 lbs/in) and 3.07×10^5 N-m/rad (5.38×10^7 in-lbs/rad) were considered very adequate.

Table 6-2 shows similar performance during compression and combustion conditions. Here again performance appears to be adequate. The clearance distribution is almost constant, but there is a slight convergence in the direction of flow.

Rig checkout commenced in May, 1983. Capacitance probes were changed from one mil range to five mil range to reduce the sensitivity of the probes to the tightening process at installation. The one mil probes could not be set easily because of their sensitivity to installation tightening. Some probes that could

TABLE 6-1

PREDICTED PERFORMANCE AT INTAKE AND EXHAUST CONDITIONS

RADIUS OF PISTON	2.750	IN	TEMPERATURE	530.000	DEG R
LENGTH OF PISTON	2.750	IN	ABS. VISCOSITY	.26400D-08	PSI-S
PROJECTED WIDTH	2.750	IN	DENSITY	.44239D-02	LBM/IN3
SUPPLY PRESSURE	1500.00	PSI	GAS CONSTANT	.24720D+06	IN2/S2.R
CYL. HEAD PRESS.	14.70	PSI	GAMA	1.400	
AMBIENT PRESS.	14.70	PSI			
PIVOT LOCATION	0.250	IN	NO. OF SEGMT	6.	
CLOSING FORCE	6430.00	LB	CLOSING MOMENT	-7550.00	IN-LB
OPENING FORCE	6437.68	LB	OPENING MOMENT		IN-LB

ORIFICES - - (CD = 1.00)

	LOCATION (IN)	DIAMETER (IN)	NUMBER	PRESSURE (PSI)	FLOW LBM/HR
ROW #1	1.000	0.0145	18	1108.65	15.64
ROW #2	1.375	0.0145	18	1218.08	13.04

CHARACTERISTICS WHEN PARALLEL

C = 0.000154 IN

KRR = .24463D+08 LB/IN KAR = .26538D+08

KRA = .27457D+08 KAA = .43313D+08 IN-LB /RAD

MOMENT UNBALANCE = -553.236 IN-LB

WHEN REACH EQUILIBRIUM POSITION

CP = 0.000198 IN ER1 = 0.0012

ALFA= -0.000039 RAD ER2 = 0.0022

C1= 0.000209 C2= 0.000165 C3= 0.000149 C4= 0.000089

TOTAL FLOW = 28.68 LBM/HR

KRR = .26828D+08 LB/IN KAR = .34619D+08

KRA = .30899D+08 KAA = .53839D+08 IN-LB /RAD

MOMENT UNBALANCE = -16.655 IN-LB

PLENUM VOL REQ"D 1.08 IN3 AT 2000.00 RPM

IRL	IRK	IRA	IRED
0	0	0	0

TABLE 6-2

PREDICTED PERFORMANCE COMPRESSION STROKE

RADIUS OF PISTON	2.750	IN	TEMPERATURE	530.000	DEG R
LENGTH OF PISTON	2.750	IN	ABS. VISCOSITY	.26400D-08	PSI-S
PROJECTED WIDTH	2.750	IN	DENSITY	.44239D-02	LBM/IN3
SUPPLY PRESSURE	1500.00	PSI	GAS CONSTANT	.24720D+06	IN2/S2 R
CYL. HEAD PRESS.	1500.00	PSI	GAMA	1.400	
AMBIENT PRESS.	14.70	PSI			
PIVOT LOCATION	0.250	IN	NO. OF SEGMT	6.	
CLOSING FORCE	8155.00	LB	CLOSING MOMENT	-7200.00	IN-LB
OPENING FORCE	8162.91	LB	OPENING MOMENT		IN-LB

ORIFICES - - (CD = 1.00)

	LOCATION (IN)	DIAMETER (IN)	NUMBER	PRESSURE (PSI)	FLOW LBM/HR
ROW #1	1.000	0.0145	18	1311.21	27.33
ROW #2	1.375	0.0145	18	1200.15	32.31

CHARACTERISTICS WHEN PARALLEL

C = 0.000332 IN

KRR = .28906D+07 LB/IN KAR = .35316D+07

KRA = .18438D+08 KAA = .24944D+08 IN-LB /RAD

MOMENT UNBALANCE = -45.140 IN-LB

WHEN REACH EQUILIBRIUM POSITION

CP = 0.000389 IN ER1 = 0.0010

ALFA= -0.000009 RAD ER2 = 0.0022

C1= 0.000393 C2= 0.000379 C3= 0.000374 C4= 0.000354

TOTAL FLOW = 76.86 LBM/HR

KRR = .23587D+07 LB/IN KAR = .29542D+07

KRA = .16430D+08 KAA = .22415D+08 IN-LB /RAD

MOMENT UNBALANCE = -16.186 IN-LB

PLENUM VOL REQ"D 2.25 IN3 AT 2000.00 RPM

IRL	IRK	IRA	IRED
0	0	0	0

not be adequately tightened would be blown out of the rig when pressure got underneath the probes. Installation of the five mil probes corrected this situation; they are accurate to within .025 microns (1 μ in) which is satisfactory.

Checkout runs indicated that the piston ring sectors did not lift off and form a film between the cylinder wall and sector. The initial assumption of 360° circumferential line sources for each of the two rows of orifices over-estimated the load capability of the sectors because there are pressure depressions between sectors. Additional computer studies were made using an incompressible code that could handle appropriate boundary conditions existing in the sectors. Approximate correction factors were applied to account for compressibility. A single pad was modified as follows:

- The number of rows of orifices was increased from two to five, with five orifices in each row (originally there were three). One row was added above the original two rows, and three rows were added below. The spacing between rows was 9.525 mm (0.375 in), and between columns was 10 degrees.
- The orifice diameter was increased from .3683 mm (0.0145 in) to .4064 mm (0.0160 in).
- Shallow recesses of approximately 9.525 mm (.375 in) in diameter and 0.0127 mm (.0005 in) to .0254 mm (0.001 in) deep were lapped around each hole to promote the introduction of gas between the cylinder wall and sectors. The recesses were shallow to avoid pneumatic hammer instability problems.

Testing of a revised single pad proved satisfactory. Lift-off was achieved for both extremes of operation (zero and full combustion chamber pressure). A photograph of the revised pad is shown on Figure 6-1. The 25 holes and surrounding recesses are clearly indicated. The interior of the pad is shown on Figure 6-2. Grooves were milled along some rows and columns to assure gas supply to the orifices. The piston also incorporated grooving to feed those orifices that did not contain grooves in the pad themselves.

Results of single pad data taken on July 5, 1983 is shown on Table 6-3. Good lift-off was achieved on the single test pad. Actual clearances are quite high, exceeding 25 microns (1 mil) for many of the data points. Also note that when

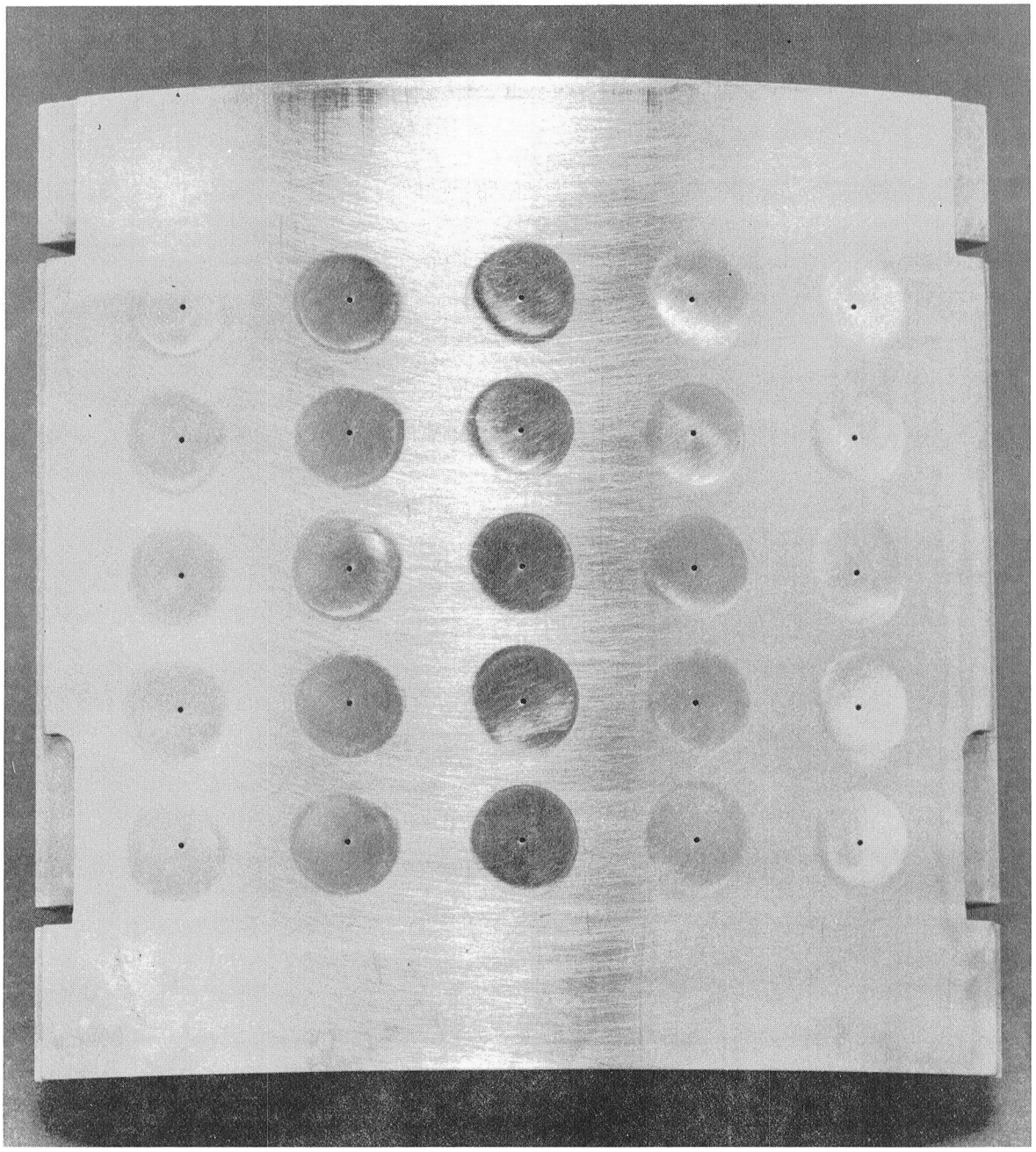

Figure 6-1 Pad Modified with 25 Holes and Surrounding Shallow Recesses

MTI-21821

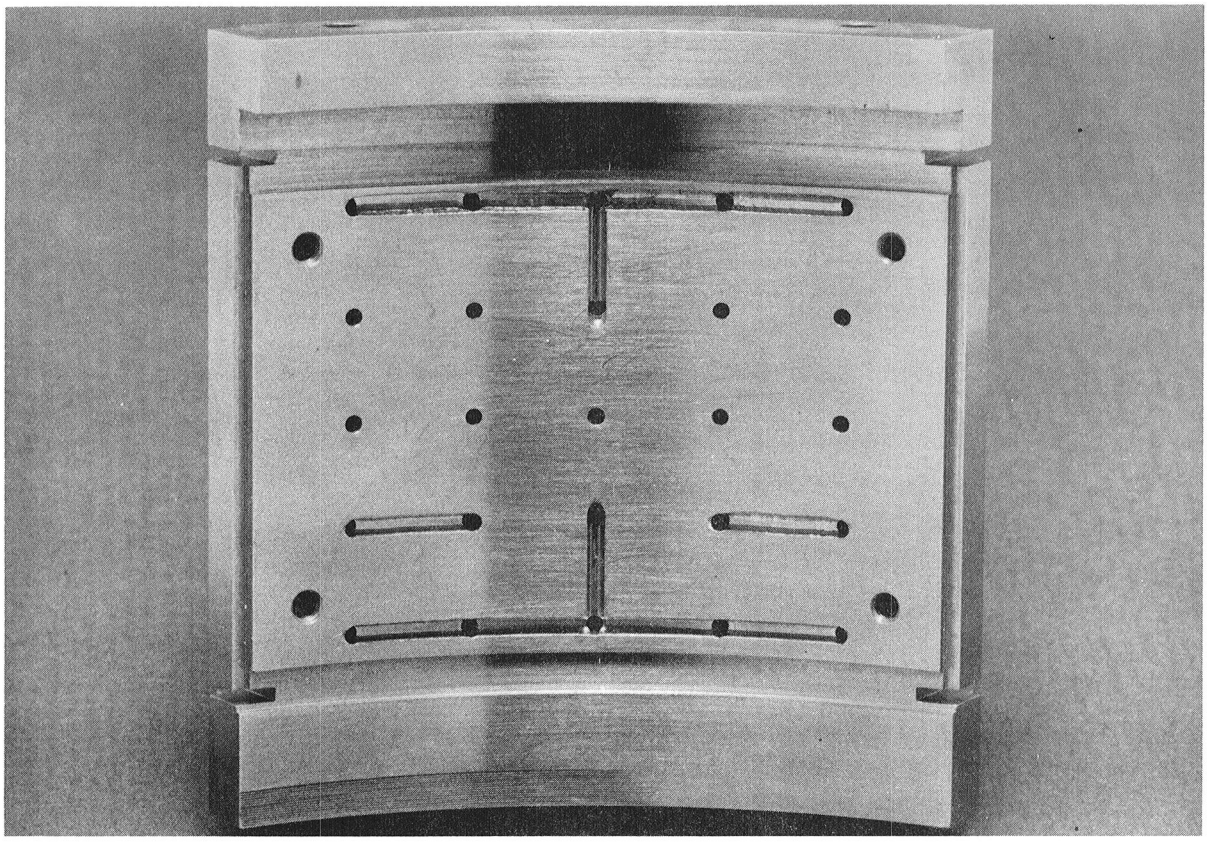

Figure 6-2 Interior of 25 Hole Pad Modified with Inlet Feed Grooves

Table 6-3

SINGLE PAD DATA - JULY 5, 1983

25 Orifices 0.4064 mm (.016 in), with shallow recesses to assist liftoff

P_s MPa (psi)	P_c MPa (psi)	h_5 μ-m (mils)	h_6 μ-m (mils)
3.45 (500)	0 (0)	18.86 (.7427)	29.13 (1.147)
5.17 (750)	0 (0)	18.21 (.717)	29.87 (1.176)
6.89 (1000)	0 (0)	15.88 (.625)	27.58 (1.086)
8.62 (1250)	0 (0)	13.89 (.547)	25.91 (1.020)
10.34 (1500)	0 (0)	12.65 (.498)	25.02 (.985)
3.45 (500)	3.45 (500)	16.0 (.63)	.94 (.037)
5.17 (750)	5.17 (750)	21.69 (.854)	1.98 (.078)
6.89 (1000)	6.89 (1000)	25.45 (1.002)	3.00 (.118)
8.62 (1250)	8.62 (1250)	27.13 (1.068)	4.11 (.162)
10.34 (1500)	10.34 (1500)	27.69 (1.090)	3.76 (.148)

h_5 = clearance at exhaust end of pad

h_6 = clearance at combustion end of pad

the combustion pressure was zero the pads assumed a converging clearance from combustion to exhaust end; when combustion pressure equaled supply pressure the clearance rotated to a diverging distribution from the combustion to exhaust end.

Attempts were made to reduce the number of active orifices by plugging on the backside. Blanking off rows and individual orifices to improve moment balance did not work. Any reduction in the number of orifices resulted in negative clearances, or inability to achieve proper lift-off. It was then decided to modify all pads with 25 orifices consisting of 5 rows and 5 columns with shallow recesses around each hole. These recesses were produced by a hard electrical eraser and lapping compound. Figures 6-3, 6-4, 6-5 and 6-6 show various views of the pads and pistons assembly.

A series of production test runs were made with all twelve modified pads on September 19, 1983. Results indicated the following:

- Lift-off was not being achieved on all pads. At the zero load condition and combustion pressure $P_c = 0$, lift-off was completely achieved on one ring set, and only one monitored pad on the second ring set did not lift properly. Clearances were fairly high and similar to those experienced during single pad testing.
- At $P_s = P_c$ (supply pressure = combustion pressure), the lift-off situation was not as good. At least one pad on each ring set did not lift-off. As had been typical of this situation the clearance diverged from the combustion to exhaust end.
- In either case load capacity (and stiffness) was not very good, being in the neighborhood of 300-400 lbs.
- The most disturbing aspect of this test was the flow data. The flow was beyond the range of the differential pressure transducer. A plate with approximately 5 times the range also bottomed, which indicated flow ranges well beyond those considered to be acceptable.

The excessive clearances and flows experienced were contrary to predictions from prior approximate analysis. Further study revealed the reasons for the anomalies occurring. To achieve liftoff, it was necessary to machine shallow recesses on the bearing surface around each of the orifice holes. This altered

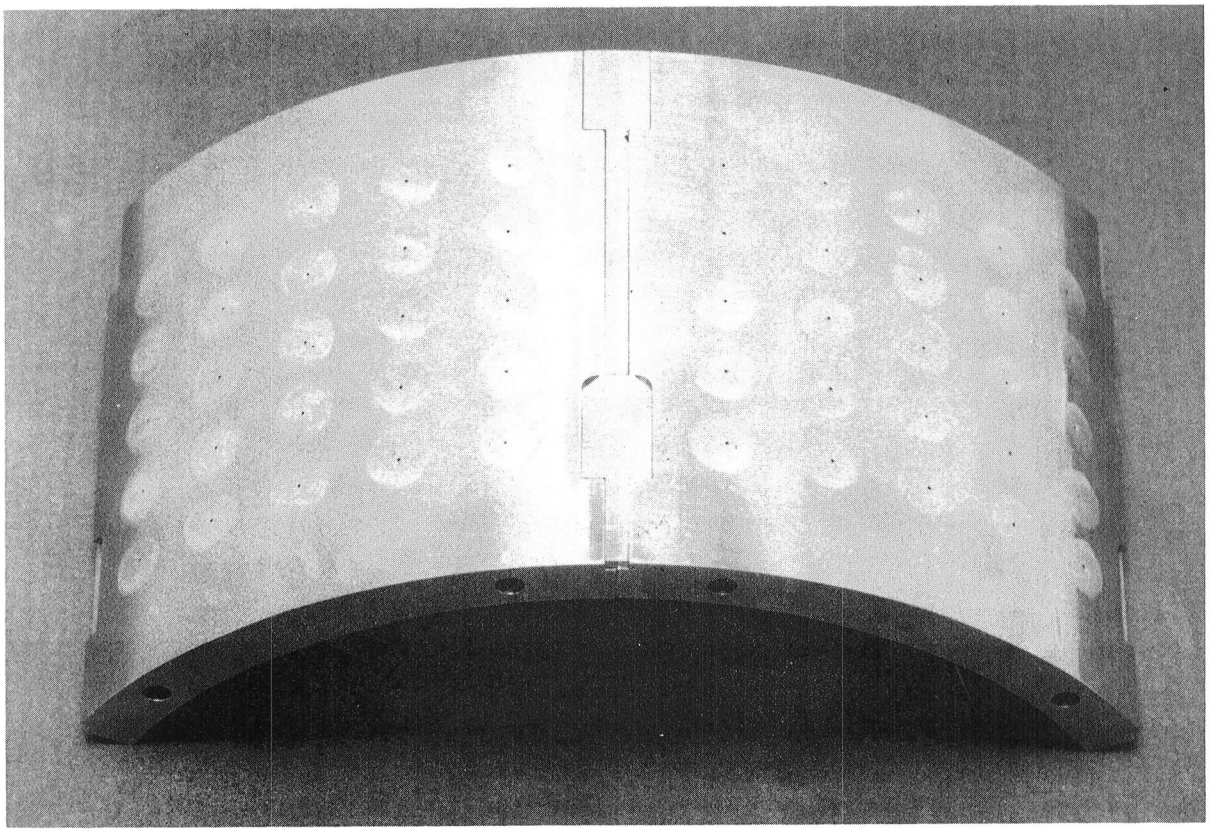

Figure 6-3 Two 25 Hole Pads Showing Exterior Inserts

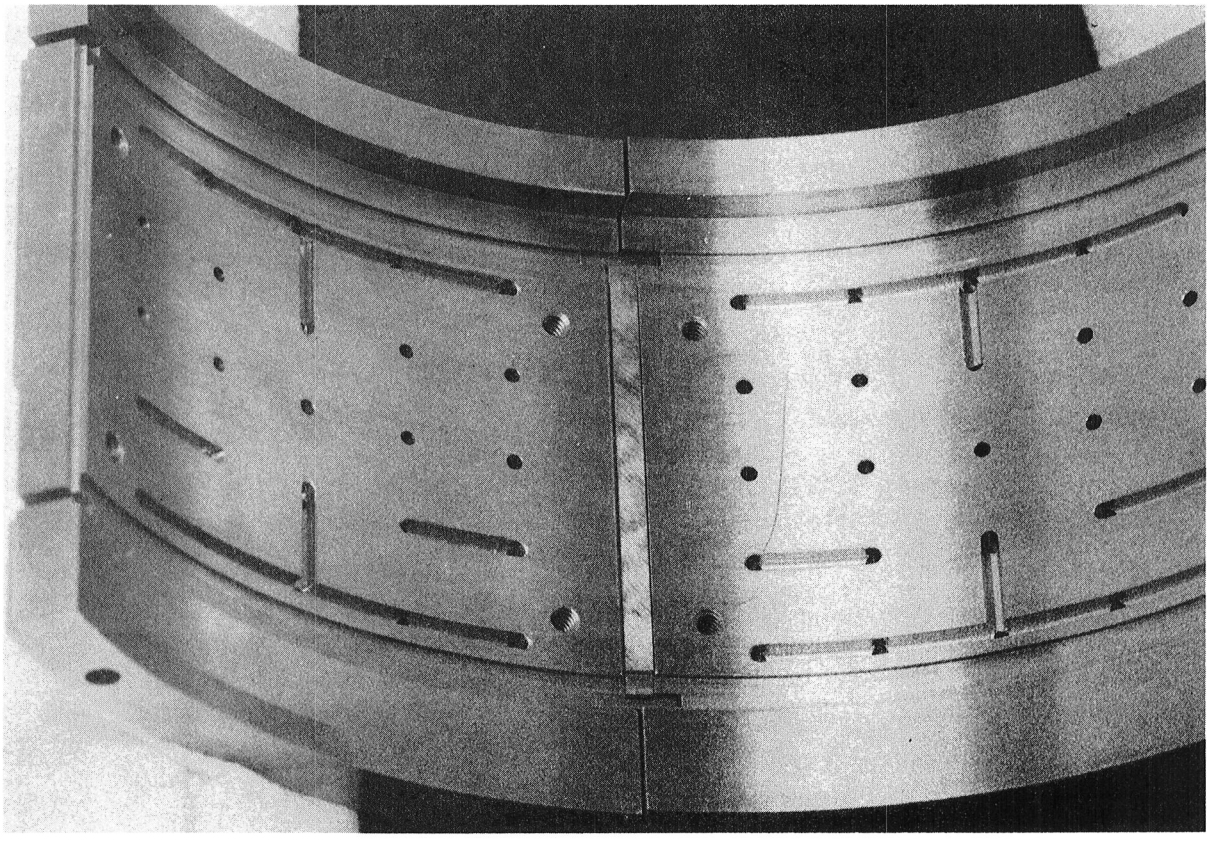

Figure 6-4 Two 25 Hole Pads Showing Interior Insert

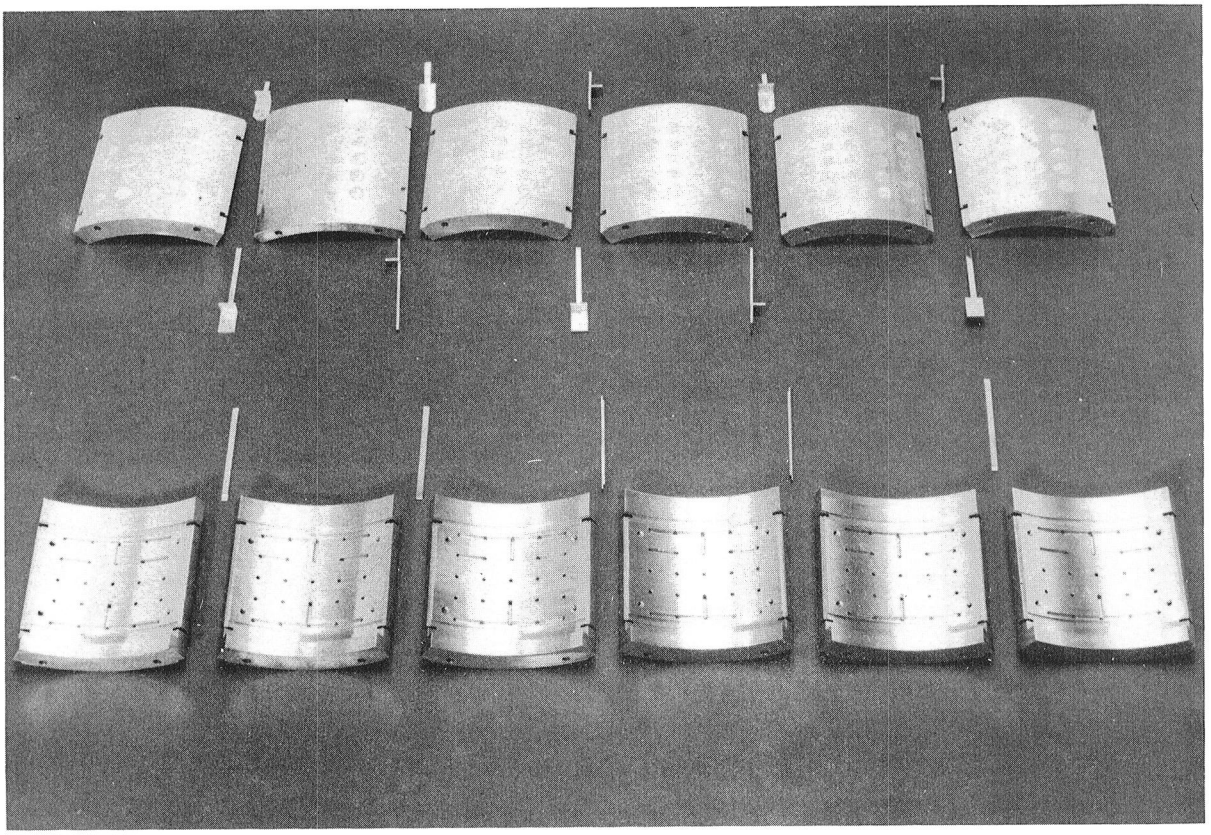

Figure 6-5 View of Two 25 Hole Pad Ring Sets

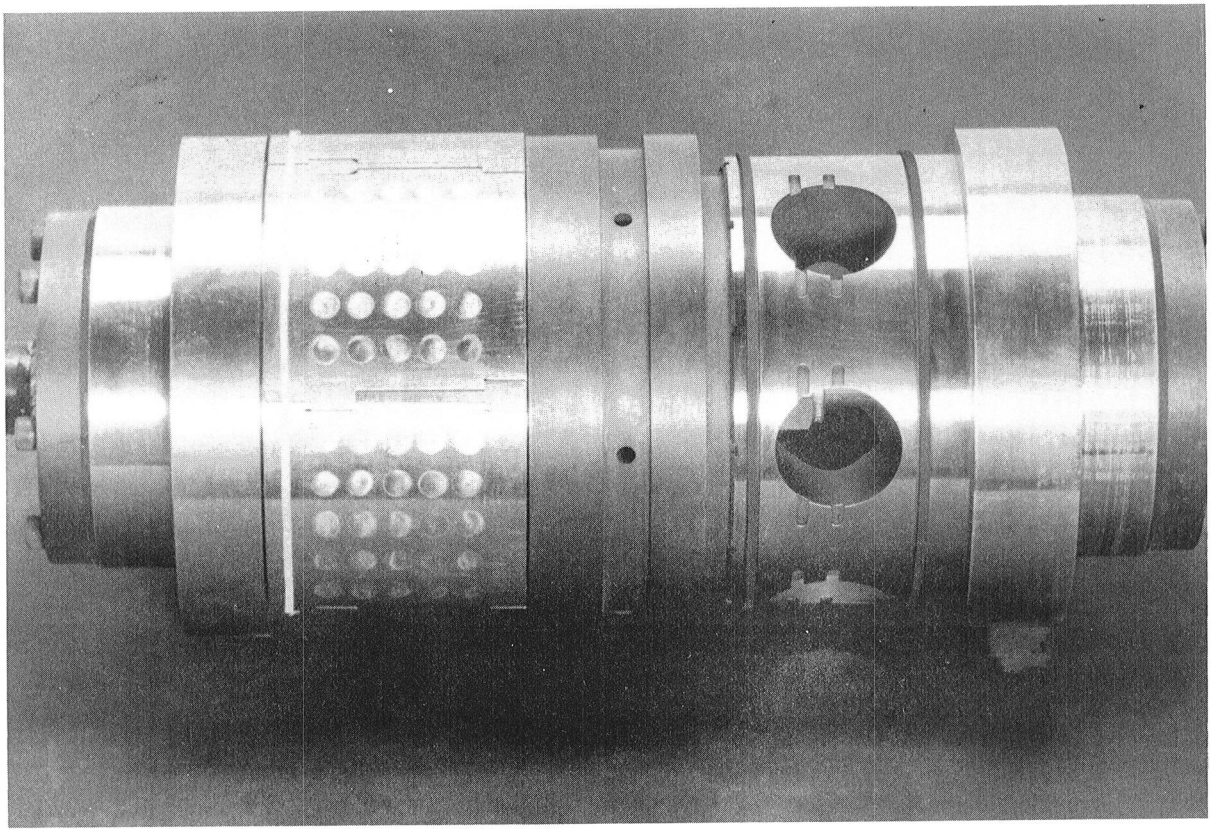

Figure 6-6 25 Hole Pads Assembled on Piston

the type of restriction or compensation of the hydrostatic bearing from the originally intended inherent compensation to recess compensation. The differences are significant. The restrictor area for inherent compensation is πdh, where d is the orifice diameter and h is the film thickness. For recess compensation the restrictor area is the area of the hole which is $\pi d^2/4$. Considering an operating clearance of 5.08 microns (200 μ-in), and an orifice diameter of .4064 mm (.016 in), the ratio of hole area to inherent compensation area is approximately 20:1. Thus, if inherent compensation is assumed, and in reality, recess compensation is occurring, performance characteristics will be dramatically different. This would be especially true of the flow which would be orders of magnitude greater if recess compensation rather than inherent compensation was occurring. It is believed that near recess compensation was happening.

The initial reason for designing for inherent compensation was to avoid "pneumatic hammer" which is a common malady of recessed gas bearings. However, there had been no evidence to this time of pneumatic hammer occurring, because the recesses were made shallow and the O-ring support of the sectors introduces damping into the system.

Since the primary objection to a recessed configuration had been pneumatic hammer which was not evident, it was logical to pursue recessed configurations because they provided decided advantages. These were:

- Greater stiffness and load capacity than inherent compensation.
- Providing a passage for inlet fluid so that pressure could get into the film and lift-off could occur.
- Enabling a large area to be supplied by a small number of restrictors, thereby reducing flow consumption to manageable proportions.

A series of configurations were tried that consisted of peripheral grooves fed by one or multiple orifices, such as shown on Figure 6-7. The peripheral groove maintained recess pressure over a large area, while simultaneously keeping trapped volume to a minimum to inhibit the onset of pneumatic hammer. Most of the grooved configurations were done on a single pad. After one of the tests, the rig did not come apart as easily as usual, and some gouging of the cylinder walls occurred. Locations of the gouging coincided with locations of the

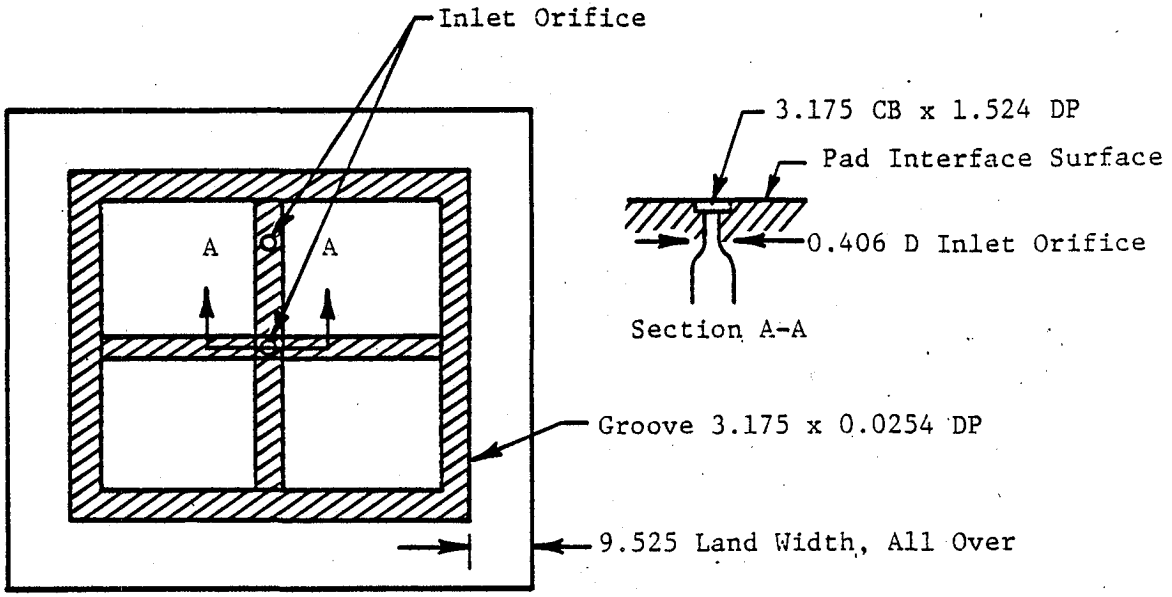

Fig. 6-7 Peripherel Groove Recess Configuration

inserts, and this was verified by gouging of the inserts themselves. Manufacturing fixtures used for producing the sectors were obtained from the subcontractor who produced the sectors. When the sectors were assembled on the fixture and measured with a micrometer, they were within print dimensions and tolerances.

When the inserts were inserted into the fixture to produce a complete ring assembly, diametral measurements were taken across the inserts. The inserts were found to be 50-100 microns too large in diameter. In operation, the inserts were contacting the inner walls of the cylinder, preventing further inward radial motion of the sectors. Some sectors were kept too far away from the cylinder walls to allow the necessary pressure buildup for lift-off to take place.

Measurements also indicated that the inside diameter of the cylinder was undersize which compounded the liftoff problem. Machining fixtures were obtained from the vendor who manufactured the pads, and a special fixture for machining the inserts was received from Cummins Engine Company. The pads and inserts were subsequently machined to the correct dimensions by the MTI Model Shop. The cylinder was re-bored and sent out for electroless nickel plating and grinding to final dimensions.

For the configuration shown on Figure 6-7, liftoff was achieved for zero combustion chamber pressure and bearing supply pressures from 1.38 MPa to 10.34 MPa (200 to 1500 psi). The magnitude of the indicated liftoff was 1.52 - 1.78 microns (60 - 70 μ-in). However, when combustion chamber pressure was applied, the sector became moment unbalanced resulting in contact at one end (combustion side end). The results, however, were encouraging in that they were significantly better than the test results of prior configurations. Flow levels appeared reasonable, although total flow included not only the flow through the test pad, but the leakage flow through the other pads and sectors as well.

The most persistent problem had been the inability of the sectors to appropriately liftoff and form a small and stiff gas film. Modifications made to the sector inserts obviated prior problems associated with pad hangup from oversize inserts and modifications made to the piston eliminated any possibility of excessive closing loads on the sectors. Thus, the liftoff problem was associ-

ated with insufficient opening force due to excessive restriction of inlet flow. Flow restrictions that do not ordinarily occur in usual clearance hydrostatic bearings are present in very close micro-inch clearance bearings that in effect restrict the flow into the pad to a prohibitive degree. The additional restrictions include the curtain area of the inlet orifice and the cross-sectional area of the recess grooves. Corrective action included counterboring the interface surface at the inlet hole and increasing the cross-sectional area of the recess grooves to the maximum extent possible without introducing a geometry prone to pneumatic hammer.

A significant change was made to the computer code used for analyzing the sector. It was modified to determine the sector position in both radial and angular degrees of freedom to balance a given radial force and a given moment about the pad pivot position. Prior to this addition it was necessary to input the radial eccentricity and pad inclination and load and moment was produced as output. Manual iterations were required and the procedure was quite awkward to implement.

Analytical studies led to a two recess configuration that could balance the loads and moments over both sets of boundary conditions and perform satisfactorily in all other respects. The mathematical model is shown on Figures 5-3a and 5-3b.

For improved righting-moment capability, two segregated recesses were employed. The recesses were non-symmetrical to accommodate the non-symmetry existing under the high pressure boundary conditions. With this basic recess configuration a series of computer runs were made, where the number of orifices feeding each recess was varied. The principal objective was to obtain a configuration that provided a converging clearance distribution from the combustion to exhaust end during the high pressure boundary condition, and simultaneously perform acceptably during intake and exhaust boundary conditions. The results of the studies are indicated on Table 6-4. The nomenclature for this table is indicated with the table. The loads and moments, W_o and M_o, are input quantities for each set of boundary conditions, and they are tabulated to indicate the convergence achieved from the Newton-Raphson iterative process employed. The principal variables were the number of orifices, N_1 and N_2, of diameter, d_o = .4064 mm (.016 in) feeding each recess. The best theoretical performance was obtained

for $N_1 = 2$ and $N_2 = 1$, where N_1 is the number of orifices feeding the large recess on the combustion end and N_2 is the number of orifices feeding the smaller recess on the exhaust end. The inclination angle α, is convergent from combustion to exhaust end, when it is a negative number. For $P_s = P_c$, and the above number of orifices, theory predicts a converging clearance which is the desirable condition. For the boundary condition of $P_c = 0$, the flow is relatively high, but this assumes a high bearing supply pressure, P_s. By allowing P_s to drop during the intake and exhaust strokes, the flow will also drop (see Section 5.0).

Table 6-4

RESULTS OF SEGREGATED RECESS COMPUTER STUDIES

P_s = 10.34 MPa (1500 psi) P_c = 0

W_o	M_o	h_m	M_t	$\alpha \times 10^{+4}$	Pr_1	Pr_2	$K_{yy} \times 10^{-6}$	$K_{y\alpha} \times 10^{-6}$	$K_{\alpha\alpha} \times 10^{-6}$	$K_{\alpha y} \times 10^{-6}$	ε	N_1	N_2
31,968 (7187)	45.4 (7950)	1.47 (58)	94.4 (208)	-.44	8115 (1177)	9542 (1384)	-6479 (-37)	160 (36)	-.360 (-63)	200 (45)	.66	2	1
32,083 (7213)	46.4 (8117)	1.04 (41)	134.4 (296)	-.66	7998 (1160)	9453 (1371)	-6304 (-36)	169 (38)	-.411 (-72)	205 (46)	.59	3	1
32,088 (7214)	46.4 (8131)	1.12 (44)	52.7 (116)	-.35	7839 (1137)	9991 (1449)	-5429 (-31)	102 (23)	-.226 (-39.6)	122.3 (27.5)	.74	1	1
32,092 (7215)	46.4 (8123)	1.75 (69)	148.9 (328)	-.56	7867 (1141)	9832 (1426)	-4378 (-25)	93 (21)	-.211 (-37)	114.8 (25.8)	.58	3	2

$P_s = P_c$ = 10.34 MPa (1500 psi)

38,457 (8646)	45.4 (7948)	2.36 (93)	56.8 (125)	-.13	9935 (1441)	9494 (1377)	-2627 (-15)	111 (25)	-.217 (-38)	87.2 (19.6)	.75	2	1
38,351 (8622)	45.2 (7918)	2.26 (89)	76.3 (168)	-.26	9956 (1444)	9280 (1346)	-3257 (-18.6)	128 (28.8)	-.259 (-45.3)	111.6 (25.1)	.69	3	1
38,422 (8638)	45.4 (7943)	2.03 (80)	37.2 (82)	.06	9860 (1430)	9894 (1435)	-3047 (-17.4)	111 (25)	-.206 (-36)	84.5 (19)	.84	1	1
38,413 (8636)	45.3 (7934)	3.45 (136)	97.2 (214)	.058	9901 (1436)	9542 (1384)	-2242 (-12.8)	90 (20.2)	-.175 (-30.6)	71.2 (16)	.70	3	2

Table 6-4 (Cont.)

NOMENCLATURE

h_M	=	Minimum film thickness, microns (μ-in)
K_{yy}	=	Radial stiffness, due to radial displacement, N/m (lbs/in)
$K_{y\alpha}$	=	Radial stiffness, due to angular displacement, N/rad (lbs/rad)
$K_{\alpha\alpha}$	=	Angular stiffness, due to angular displacement, N-m/rad (in-lb/rad)
$K_{\alpha y}$	=	Angular stiffness due to radial displacment, N-m/m (in-lb/in)
M_o	=	Fluid film moment, N-m (in-lbs)
M_T	=	Total ring flow, kg/h (lbs/h)
N_1	=	Number of orifices feeding large or upper recess
N_2	=	Number of orifices feeding small or lower recess
P_c	=	Combustion end pressure, MPa (psi)
Pr_1	=	Top or large recess pressure, MPa (psi)
Pr_2	=	Bottom or small recess pressure, MPa (psi)
P_s	=	Supply pressure, MPa (psi)
W_o	=	Fluid film opening load, N (lbs)
α	=	Inclination, about pivot position, radians
ε	=	Radial eccentricity at pivot position

Three pads of dual recess construction were tested. Each had the required number of orifices per recess. The test pads were tested singly, and the test results were to form the basis for modification of the remaining pads and final full ring testing.

Configuration B is shown on Fig. 6-8. It incorporated a land length of 15.88 mm (.625 in) at the bottom on the exhaust end of the piston. Test results for Configuration B are indicated on Figs. 6-9, 6-10, and 6-11. Figure 6-9 shows the clearance distribution as a function of pressure when combustion pressure equals zero. For most of the pressure range the clearance is positive and there is the usual converging distribution from the combustion side to the exhaust side. Figure 6-10 shows the clearance distribution of Configuration B when the combustion pressure equals the bearing supply pressure. The clearance goes negative on the combustion end, and also the clearance diverges from the combustion to the crankcase end. This was contrary to theory which predicted a converging distribution. Figure 6-11 shows the effect of load on Configuration B when combustion pressure equals supply pressure. Except for very high loading, the clearance distribution is slightly improved when load is applied. Although clearances becomes positive on the combustion end, when load is applied, values are very small in magnitude (0.5 microns).

In an effort to improve the clearance distribution, and in particular to produce a converging clearance when $P_s = P_c$, the bottom land was increased to 19.05 mm (0.75 in); this configuration was designated as configuration A, and was the finally selected configuration (see Fig. 4-1).

Clearance as a function of pressure for $P_c = 0$ is shown on Fig. 6-12. The clearance is positive for all values of supply pressure and has the predicted converging distribution from combustion to exhaust end. Figure 6-13 shows results for $P_c = P_s$. Clearances are positive except for the lower values of supply pressure. Clearances appeared to increase with pressure. Again, this configuration did not produce the desired converging clearance distribution. As shown on Fig. 6-14, performance when loaded was acceptable, but slightly erratic.

In a final attempt to produce a converging clearance from combustion to crankcase end, when $P_s = P_c$, configuration C as shown on Fig. 6-15 was made and test-

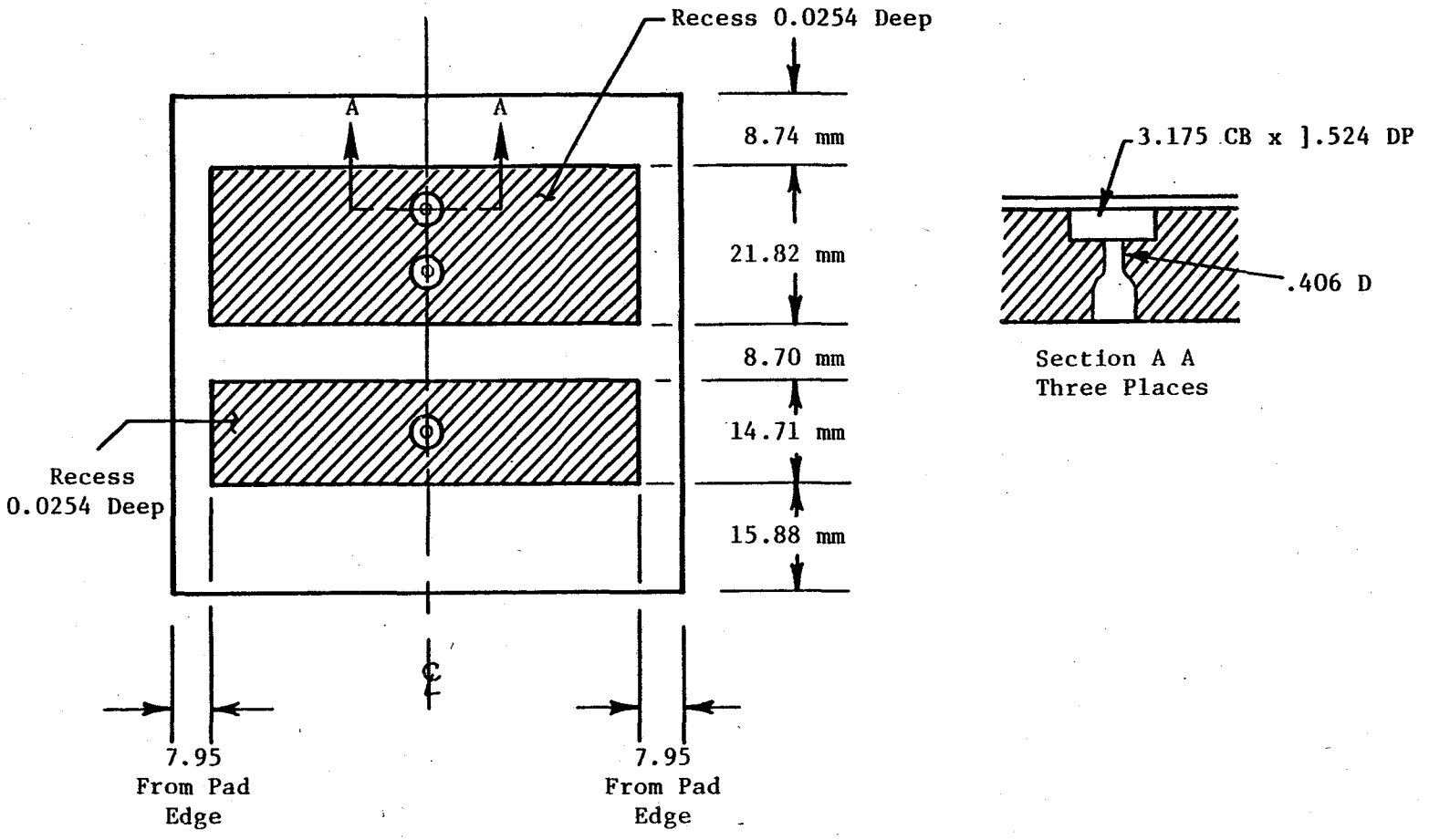

Fig. 6-8 Recess Configuration B

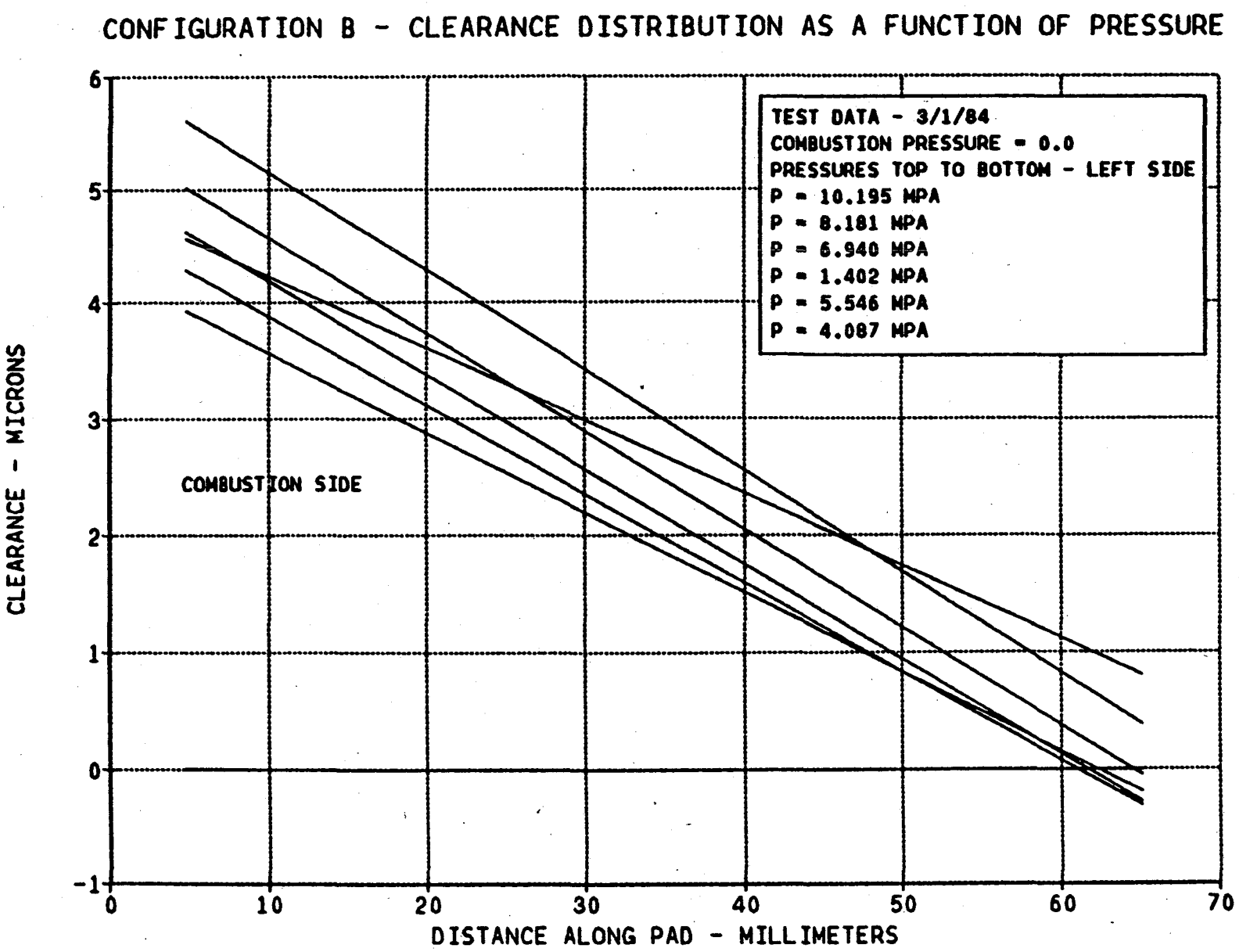
CONFIGURATION B - CLEARANCE DISTRIBUTION AS A FUNCTION OF PRESSURE
TEST DATA - 3/1/84
COMBUSTION PRESSURE = 0.0
PRESSURES TOP TO BOTTOM - LEFT SIDE
P = 10.195 MPA
P = 8.181 MPA
P = 6.940 MPA
P = 1.402 MPA
P = 5.546 MPA
P = 4.087 MPA
COMBUSTION SIDE
CLEARANCE - MICRONS
DISTANCE ALONG PAD - MILLIMETERS
6
5
4
3
2
1
0
-1
0
10
20
30
40
50
60
70

Figure 6-9

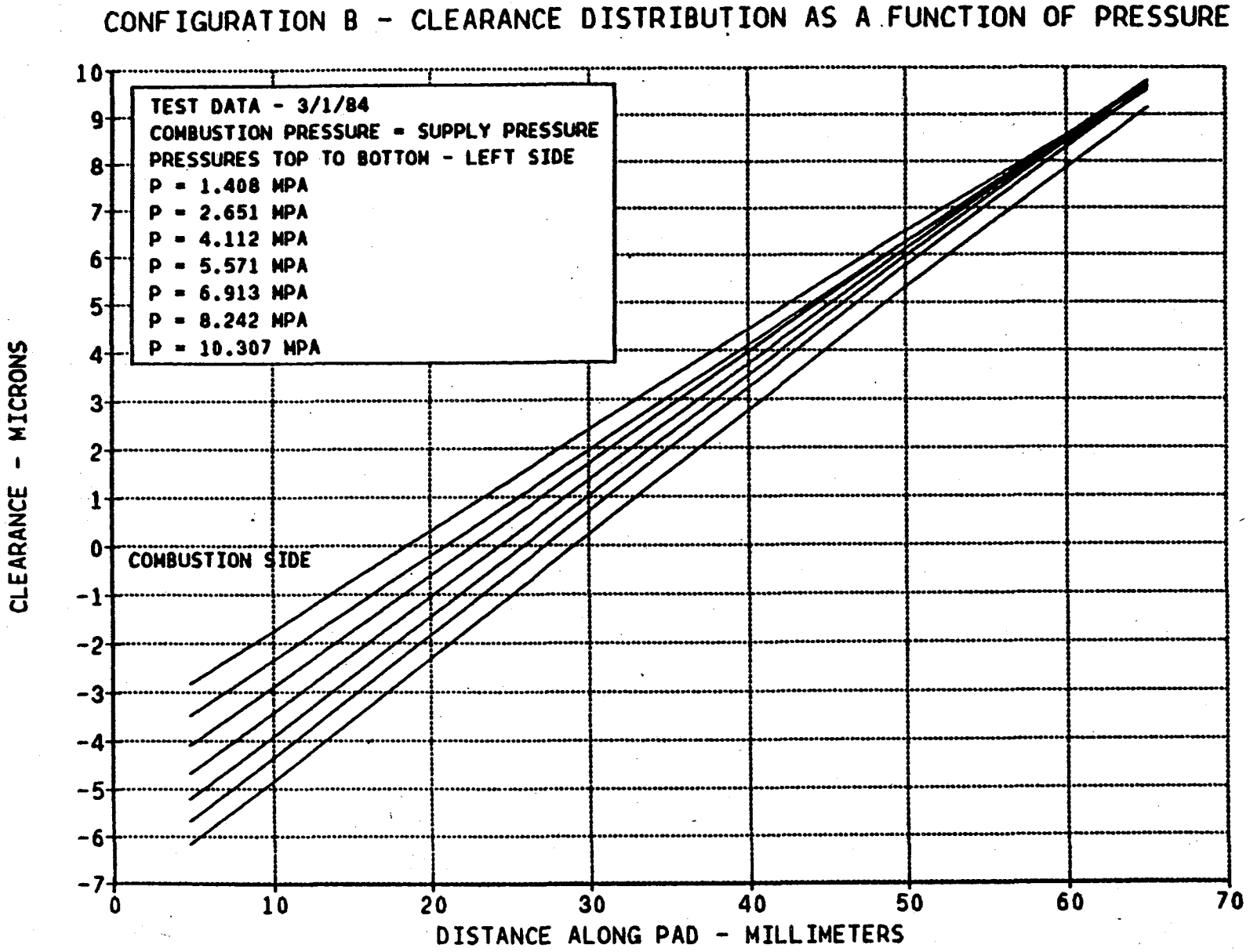
CONFIGURATION B - CLEARANCE DISTRIBUTION AS A FUNCTION OF PRESSURE
TEST DATA - 3/1/84
COMBUSTION PRESSURE = SUPPLY PRESSURE
PRESSURES TOP TO BOTTOM - LEFT SIDE
P = 1.408 MPA
P = 2.651 MPA
P = 4.112 MPA
P = 5.571 MPA
P = 6.913 MPA
P = 8.242 MPA
P = 10.307 MPA
COMBUSTION SIDE
CLEARANCE - MICRONS
10
9
8
7
6
5
4
3
2
1
0
-1
-2
-3
-4
-5
-6
-7
0
10
20
30
40
50
60
70
DISTANCE ALONG PAD - MILLIMETERS

Figure 6-10

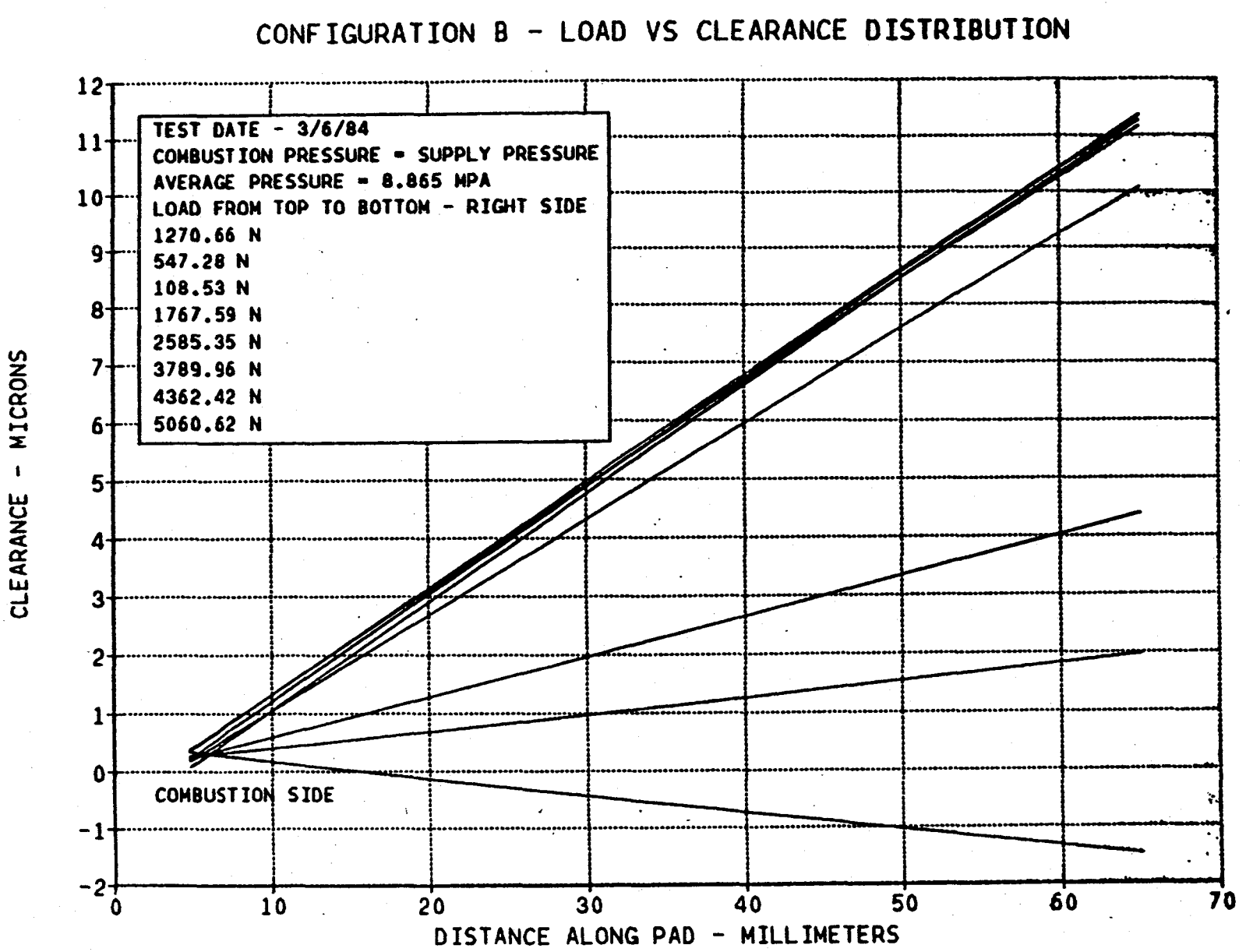
CONFIGURATION B - LOAD VS CLEARANCE DISTRIBUTION
TEST DATE - 3/6/84
COMBUSTION PRESSURE = SUPPLY PRESSURE
AVERAGE PRESSURE = 8.865 MPA
LOAD FROM TOP TO BOTTOM - RIGHT SIDE
1270.66 N
547.28 N
108.53 N
1767.59 N
2585.35 N
3789.96 N
4362.42 N
5060.62 N
COMBUSTION SIDE
CLEARANCE - MICRONS
DISTANCE ALONG PAD - MILLIMETERS
12
11
10
9
8
7
6
5
4
3
2
1
0
-1
-2
0
10
20
30
40
50
60
70

Figure 6-11

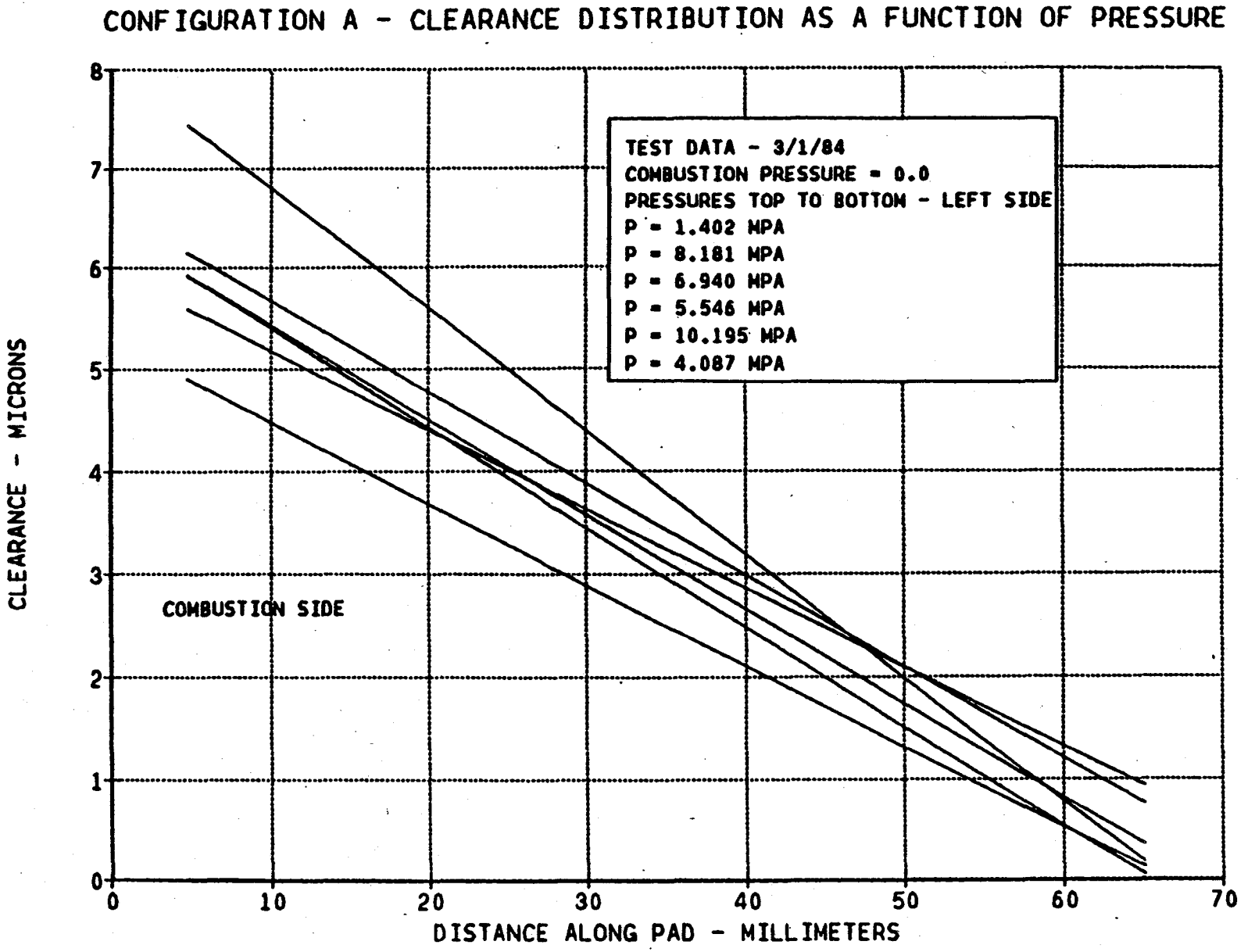
CONFIGURATION A - CLEARANCE DISTRIBUTION AS A FUNCTION OF PRESSURE
TEST DATA - 3/1/84
COMBUSTION PRESSURE = 0.0
PRESSURES TOP TO BOTTOM - LEFT SIDE
P = 1.402 MPA
P = 8.181 MPA
P = 6.940 MPA
P = 5.546 MPA
P = 10.195 MPA
P = 4.087 MPA
COMBUSTION SIDE
CLEARANCE - MICRONS
DISTANCE ALONG PAD - MILLIMETERS
0
1
2
3
4
5
6
7
8
0
10
20
30
40
50
60
70

Figure 6-12

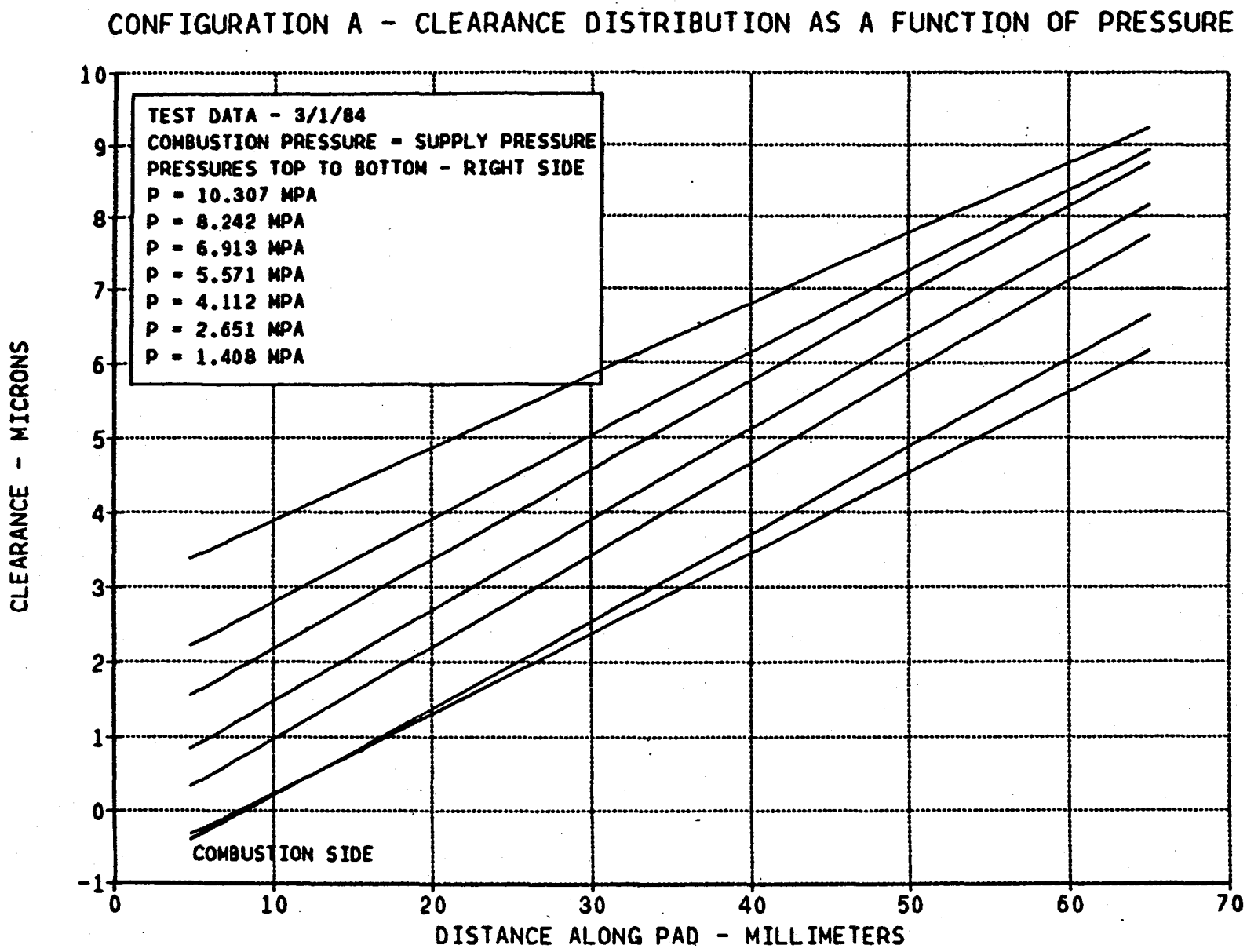
CONFIGURATION A - CLEARANCE DISTRIBUTION AS A FUNCTION OF PRESSURE
TEST DATA - 3/1/84
COMBUSTION PRESSURE = SUPPLY PRESSURE
PRESSURES TOP TO BOTTOM - RIGHT SIDE
P = 10.307 MPA
P = 8.242 MPA
P = 6.913 MPA
P = 5.571 MPA
P = 4.112 MPA
P = 2.651 MPA
P = 1.408 MPA
COMBUSTION SIDE
CLEARANCE - MICRONS
DISTANCE ALONG PAD - MILLIMETERS
10
9
8
7
6
5
4
3
2
1
0
-1
0
10
20
30
40
50
60
70

Figure 6-13

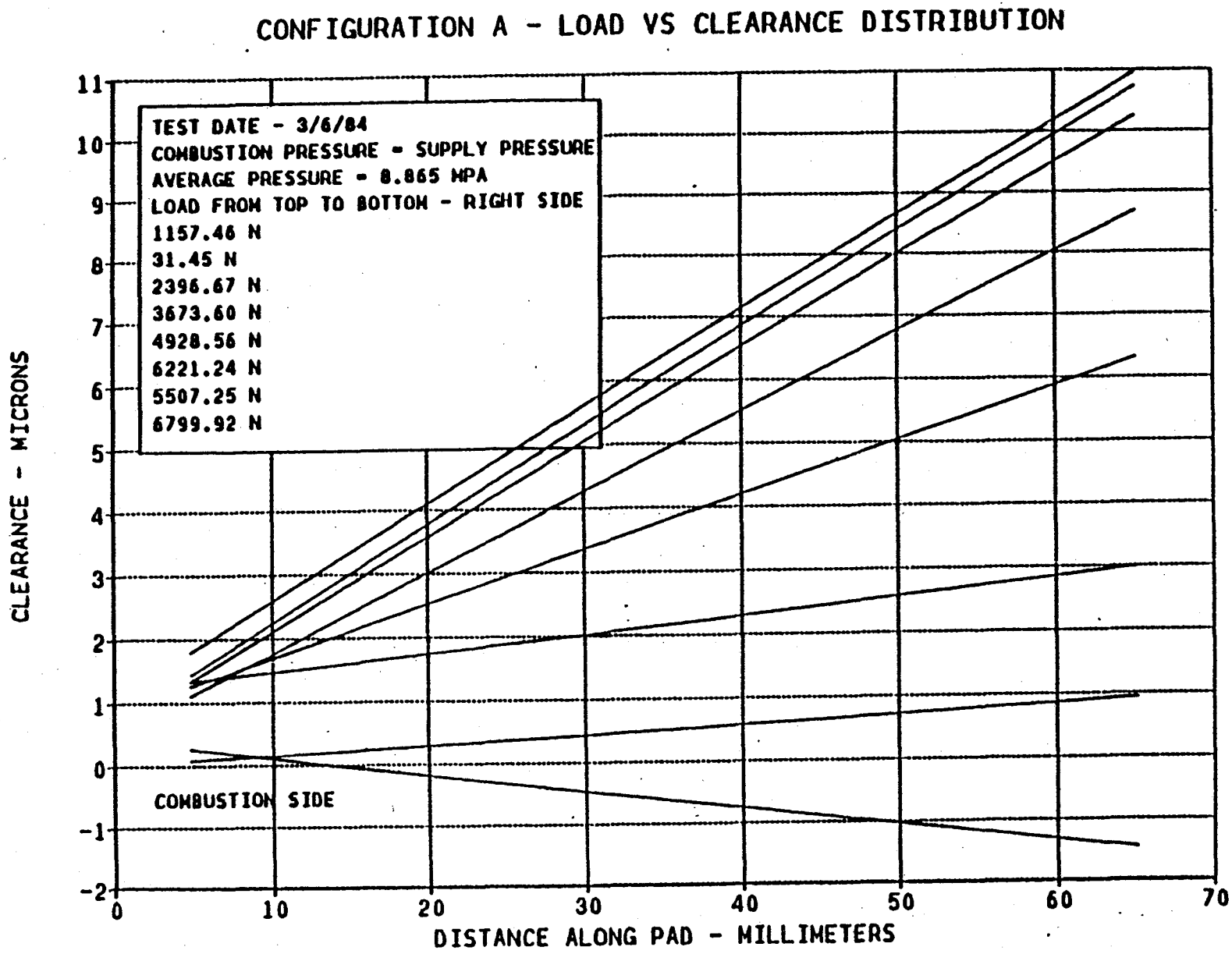
CONFIGURATION A - LOAD VS CLEARANCE DISTRIBUTION
TEST DATE - 3/6/84
COMBUSTION PRESSURE = SUPPLY PRESSURE
AVERAGE PRESSURE = 8.865 MPA
LOAD FROM TOP TO BOTTOM - RIGHT SIDE
1157.46 N
31.45 N
2396.67 N
3673.60 N
4928.56 N
6221.24 N
5507.25 N
6799.92 N
COMBUSTION SIDE
CLEARANCE - MICRONS
DISTANCE ALONG PAD - MILLIMETERS
11
10
9
8
7
6
5
4
3
2
1
0
-1
-2
0
10
20
30
40
50
60
70

Figure 6-14

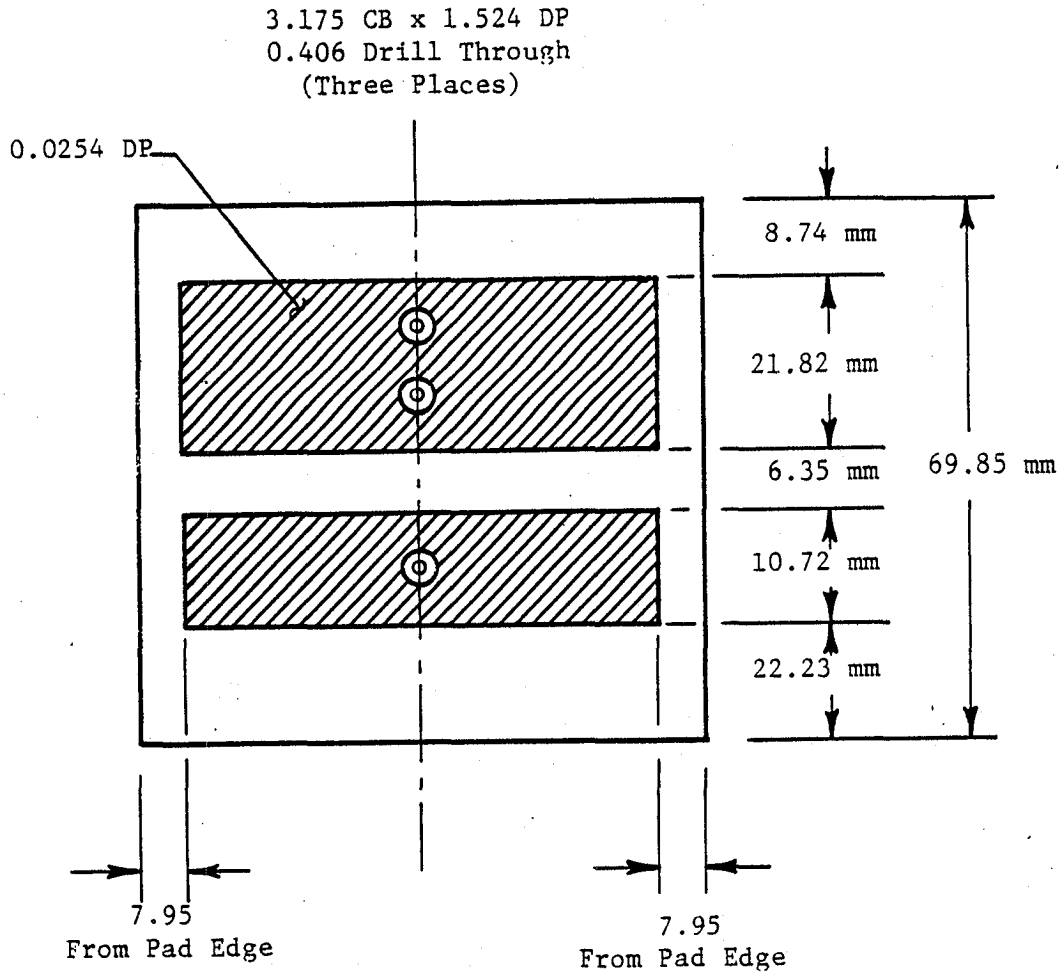

Fig. 6-15 Recess Configuration C

ed. The bottom land was increased to 22.23 mm (.875 in). Clearance as a function of supply pressure for $P_c = 0$ is shown on Fig. 6-16. The clearance was negative throughout the operating range. Ability to support moment unbalance and preload were unacceptable. Results for $P_s = P_c$ are shown on Fig. 6-17. Again, the clearance diverges from the combustion to exhaust end and the clearance goes negative on the combustion end.

Since configuration A showed superior performance, it was the selected configuration. Some general conclusions are as follows:

- Producing the desirable converging clearance from the combustion to crankcase end, when $P_c = P_s$, was not accomplished by continuously increasing the length of the bottom land. A point is reached where excessive moment unbalance occurs for the boundary condition of $P_c = 0$.

- Theory and experiment do not agree with respect to the shape of the clearance distribution for the boundary condition $P_c = P_s$.

- Configuration A was superior in all respects to configuration B and C, and therefore was selected for the remaining pads (see Section 4).

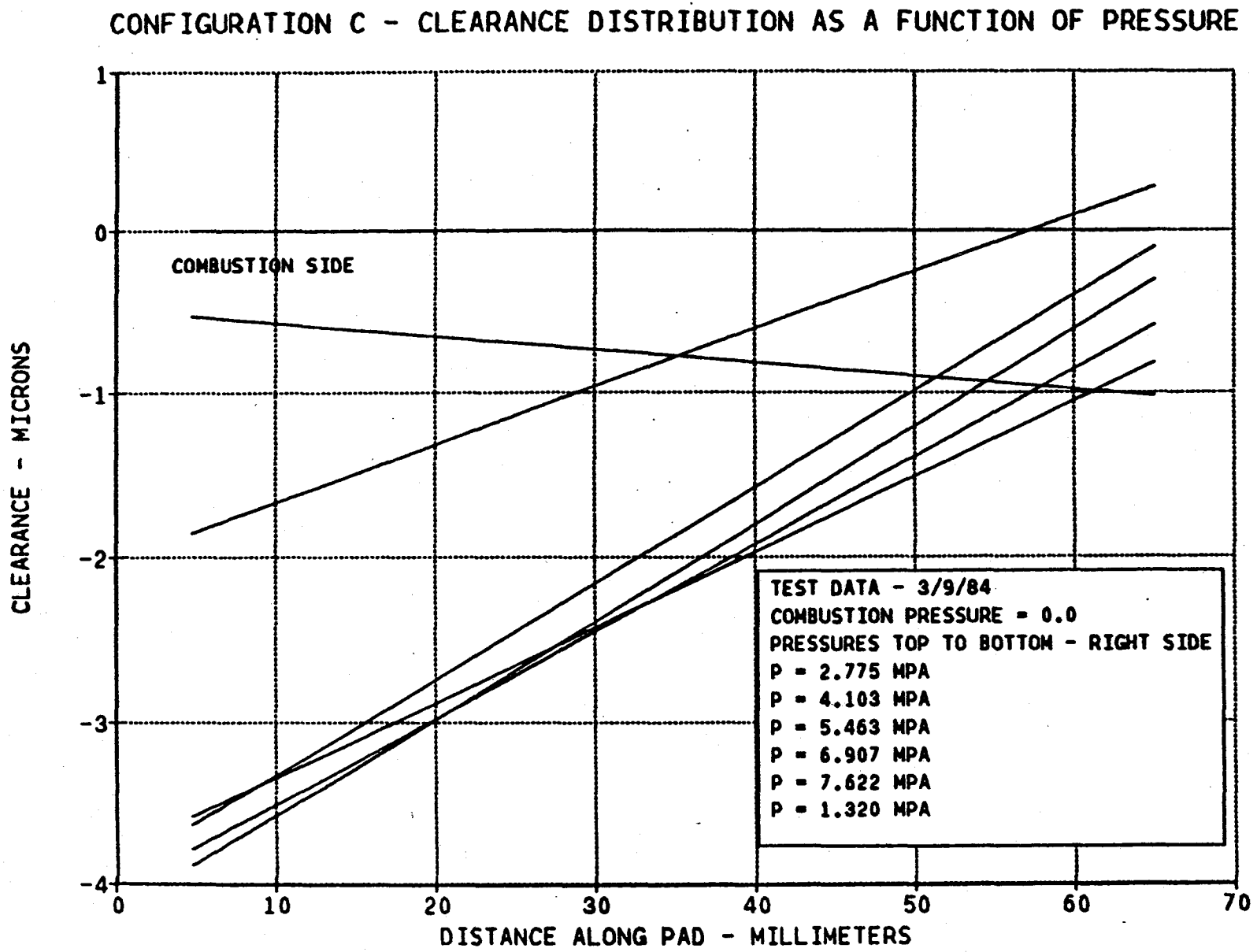
CONFIGURATION C - CLEARANCE DISTRIBUTION AS A FUNCTION OF PRESSURE
COMBUSTION SIDE
TEST DATA - 3/9/84
COMBUSTION PRESSURE = 0.0
PRESSURES TOP TO BOTTOM - RIGHT SIDE
P = 2.775 MPA
P = 4.103 MPA
P = 5.463 MPA
P = 6.907 MPA
P = 7.622 MPA
P = 1.320 MPA
CLEARANCE - MICRONS
1
0
-1
-2
-3
-4
0
10
20
30
40
50
60
70
DISTANCE ALONG PAD - MILLIMETERS

Figure 6-16

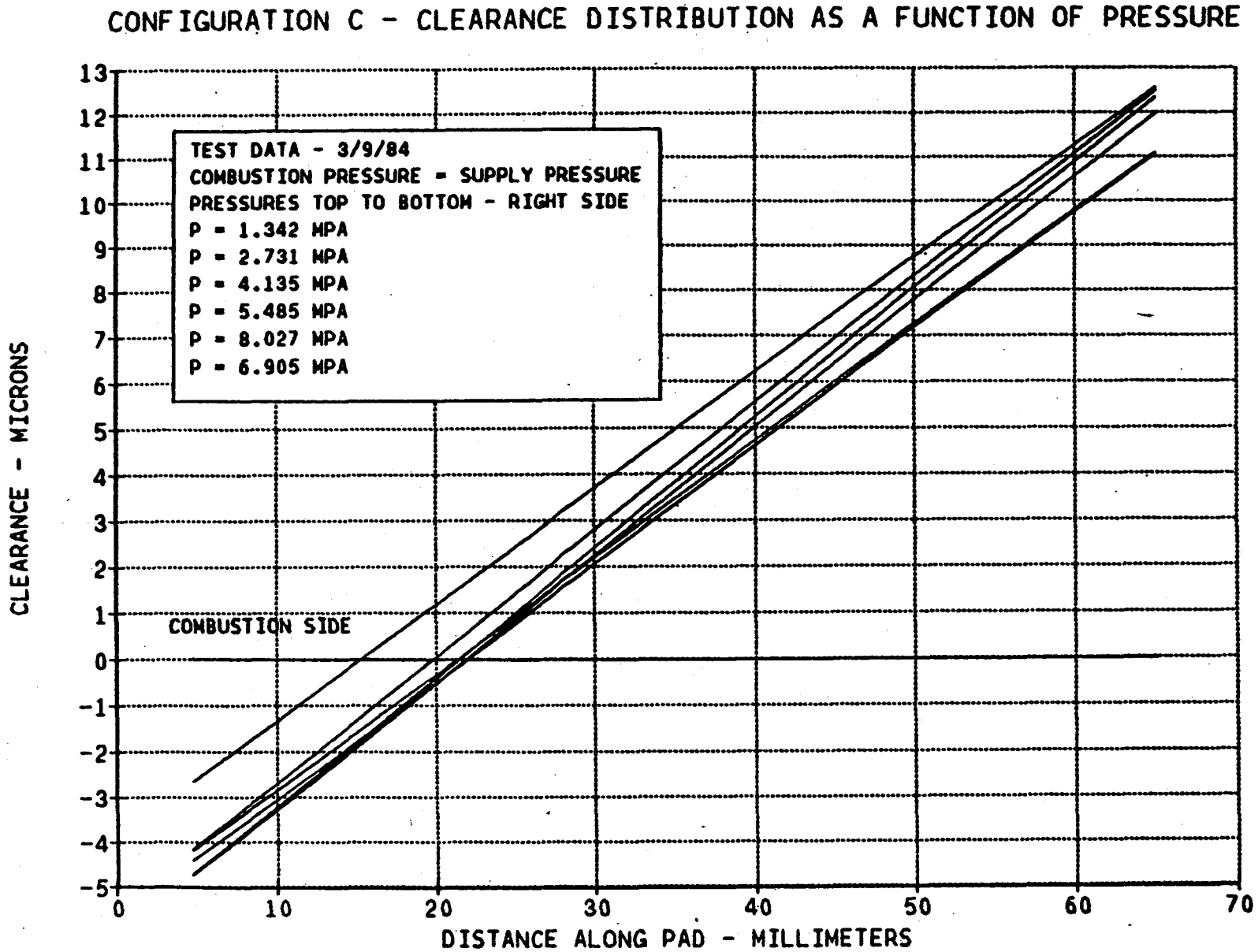
CONFIGURATION C - CLEARANCE DISTRIBUTION AS A FUNCTION OF PRESSURE
TEST DATA - 3/9/84
COMBUSTION PRESSURE = SUPPLY PRESSURE
PRESSURES TOP TO BOTTOM - RIGHT SIDE
P = 1.342 MPA
P = 2.731 MPA
P = 4.135 MPA
P = 5.485 MPA
P = 8.027 MPA
P = 6.905 MPA
COMBUSTION SIDE
CLEARANCE - MICRONS
DISTANCE ALONG PAD - MILLIMETERS
13
12
11
10
9
8
7
6
5
4
3
2
1
0
-1
-2
-3
-4
-5
0
10
20
30
40
50
60
70

Figure 6-17

7.0 BREATHABLE LINER CONSIDERATIONS

As mentioned at the outset maintaining the necessary small clearances involved is not practical with a system of rigid pistons and liners. Clearances could not be easily manufactured nor could they be maintained during operation with the large temperature and pressure gradients involved. Therefore, the system of piston and liners must be designed to have clearances that would be self-adjusting in response to the pressures in the film clearances.

The sectored hydrostatic piston-ring in which the individual sectors can move radially and angularly is one approach to the formation of a self-adjusting clearance. The other incorporates a solid hydrostatic piston with a resiliently mounted liner that can "breath" and form the necessary clearance with the piston under the stimulus of hydrostatic pressurization.

Figure 7-1 schematically depicts the breathable liner concept. In this case, the liner consists of radial split segments, supported by a compliant material that will permit each segment to move independently. The splits between segments are sealed radially by the compliant or resilient backing support. Axial leakage at the splits is inhibited by forming axially layered liner rings, with the seams staggered in the axial direction.

The material for the compliant or resilient support depends both upon the application and on whether cooling is available. For non-high-temperature applications, elastomers can be used (Fig. 7-1); for high-temperature application, some form of metal springs must be applied (Fig. 7-2). Since high spring stiffness is required, a beam spring in combination with a seal plate is one approach for sealing the joints.

Because the segmented ring design required considerably more effort than originally contemplated, it was not possible to complete a comprehensive design and analysis of a breathable liner concept. However, there were some cursory examinations conducted which demonstrates the feasibility of the concept and provides encouragement for future evaluations.

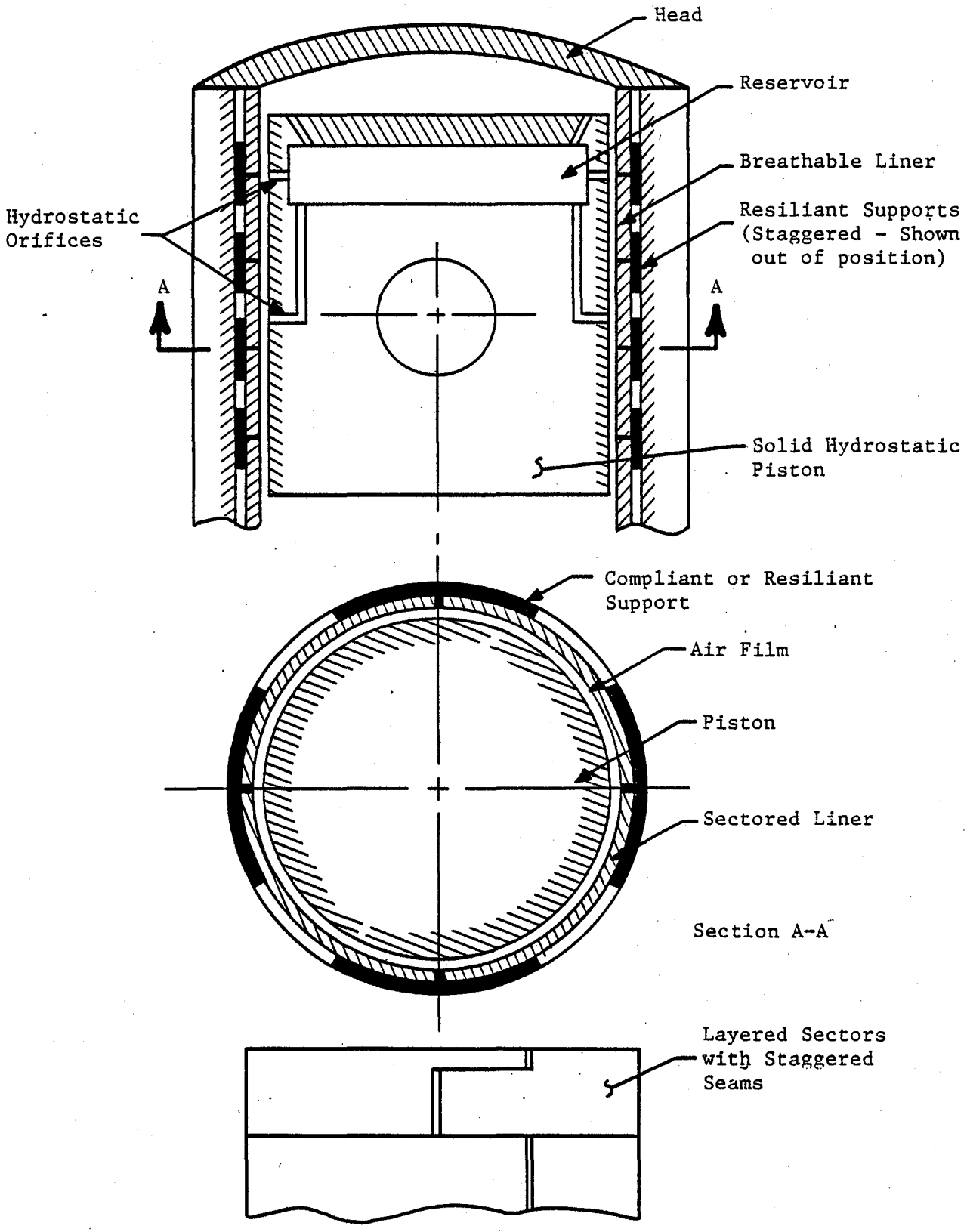

Figure 7-1 Breathable Liner Concept

821553

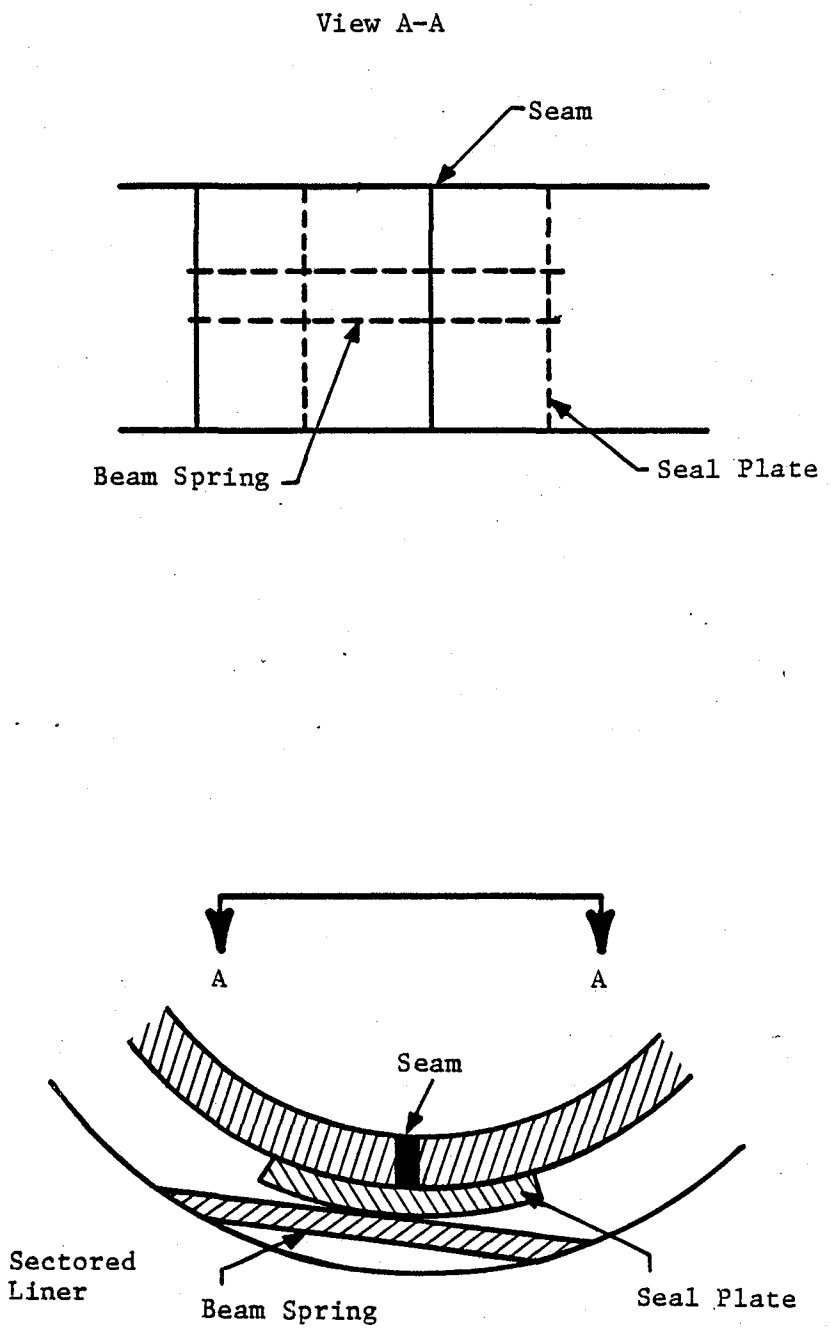

Figure 7-2 Breathable Liner Concept with Metallic Seal Plates

7.1 Solid Breathable Liner

Consideration of the elastic deformation properties of a solid cylindrical liner subjected to pressure over a portion of its length led to some very interesting results. As indicated in Ref. (5), the following formulas apply.

$$\delta_r = \frac{-pR^2}{Et}\left(1 - e^{-b\lambda}\cos b\lambda\right) \tag{7-1}$$

$$S_H = \frac{-pR\lambda}{2t} \tag{7-2}$$

$$M_x = \frac{p}{2\lambda^2}\, e^{-b\lambda} \sin b\lambda \tag{7-3}$$

where

$$\lambda = \sqrt[4]{\frac{3\left(1 - \nu^2\right)}{R^2 t^2}} \tag{7-4}$$

and p = pressure on circumferential width of 2b
R = outside radius
t = wall thickness
E = modulus of elasticity
b = half length to which pressure is applied
δ_r = radial displacement
S_H = hoop stress
M_x = maximum bending moment

Results of applying these equations are shown on Figures 7-3, 7-4 and 7-5. Figure 7-3 shows radial displacement as a function of liner thickness, t. The nominal range of clearances are in the range of .002 to .005 mm. Initially,

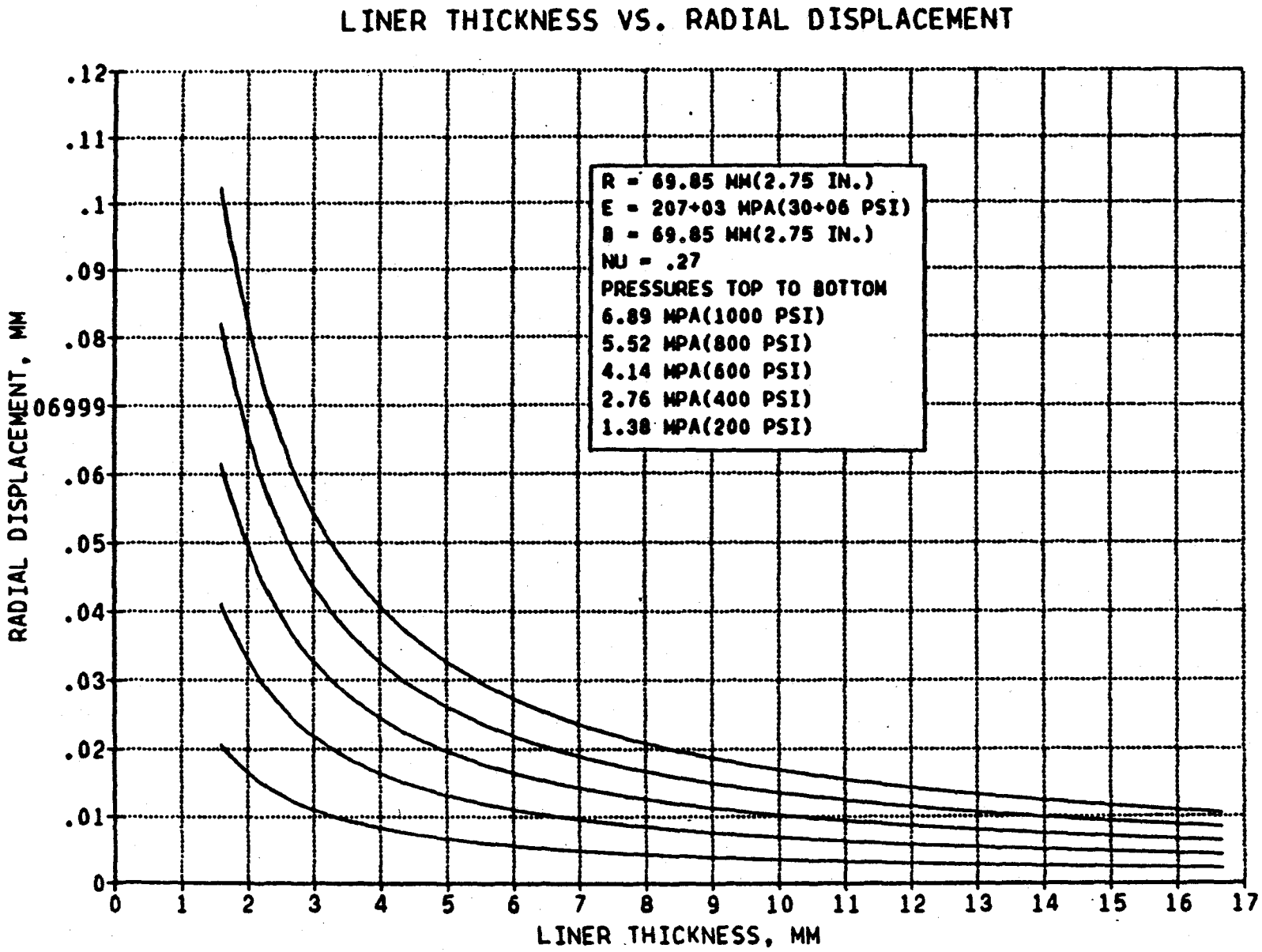
LINER THICKNESS VS. RADIAL DISPLACEMENT
R = 69.85 MM(2.75 IN.)
E = 207+03 MPA(30+06 PSI)
B = 69.85 MM(2.75 IN.)
NU = .27
PRESSURES TOP TO BOTTOM
6.89 MPA(1000 PSI)
5.52 MPA(800 PSI)
4.14 MPA(600 PSI)
2.76 MPA(400 PSI)
1.38 MPA(200 PSI)
RADIAL DISPLACEMENT, MM
.12
.11
.1
.09
.08
06999
.06
.05
.04
.03
.02
.01
0
0 1 2 3 4 5 6 7 8 9 10 11 12 13 14 15 16 17
LINER THICKNESS, MM

Figure 7-3

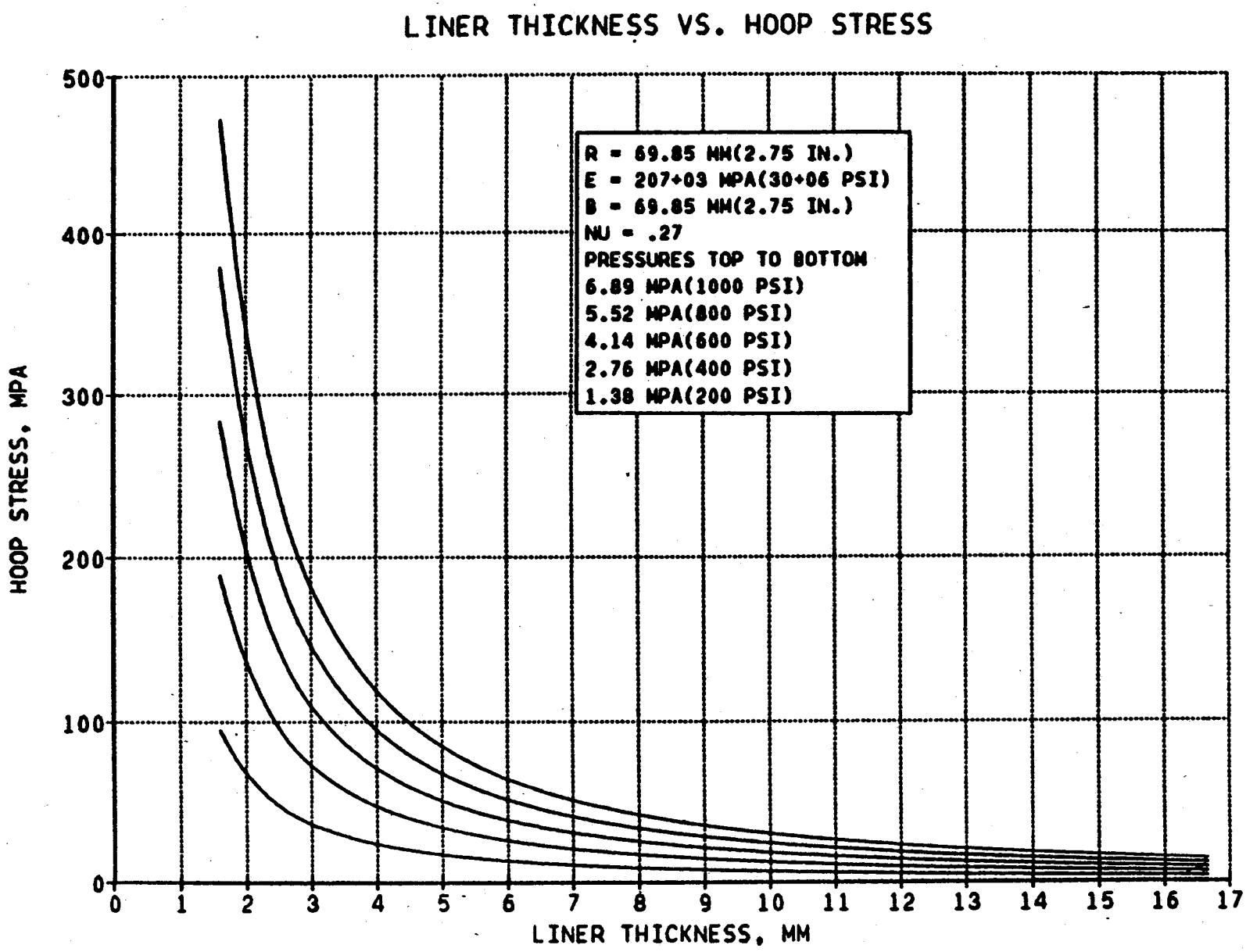
LINER THICKNESS VS. HOOP STRESS
R = 69.85 MM(2.75 IN.)
E = 207+03 MPA(30+06 PSI)
B = 69.85 MM(2.75 IN.)
NU = .27
PRESSURES TOP TO BOTTOM
6.89 MPA(1000 PSI)
5.52 MPA(800 PSI)
4.14 MPA(600 PSI)
2.76 MPA(400 PSI)
1.38 MPA(200 PSI)
HOOP STRESS, MPA
0
100
200
300
400
500
0 1 2 3 4 5 6 7 8 9 10 11 12 13 14 15 16 17
LINER THICKNESS, MM

Figure 7-4

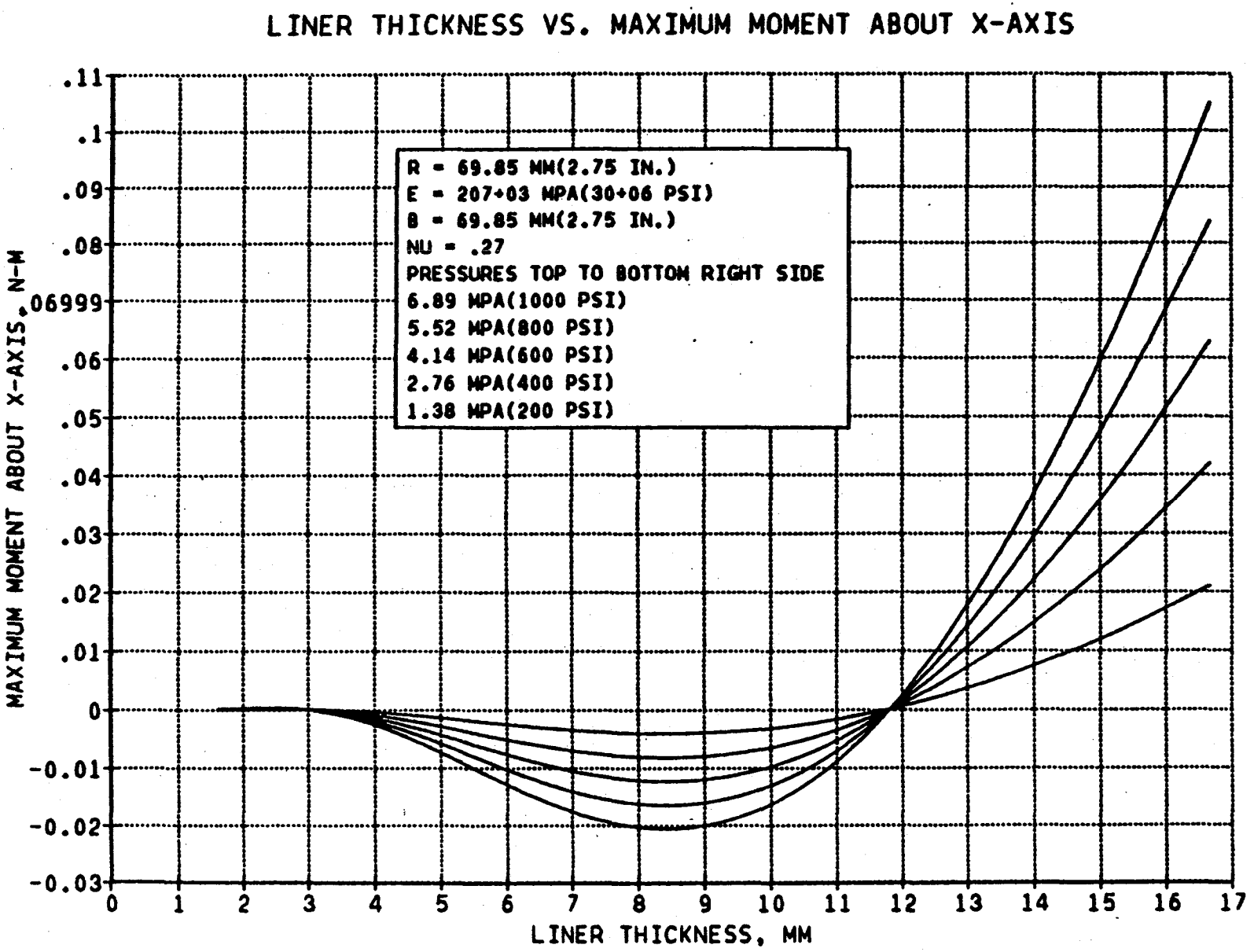
LINER THICKNESS VS. MAXIMUM MOMENT ABOUT X-AXIS
R = 69.85 MM(2.75 IN.)
E = 207+03 MPA(30+06 PSI)
B = 69.85 MM(2.75 IN.)
NU = .27
PRESSURES TOP TO BOTTOM RIGHT SIDE
6.89 MPA(1000 PSI)
5.52 MPA(800 PSI)
4.14 MPA(600 PSI)
2.76 MPA(400 PSI)
1.38 MPA(200 PSI)
MAXIMUM MOMENT ABOUT X-AXIS, N-M
.11
.1
.09
.08
.06999
.06
.05
.04
.03
.02
.01
0
-0.01
-0.02
-0.03
0 1 2 3 4 5 6 7 8 9 10 11 12 13 14 15 16 17
LINER THICKNESS, MM

Figure 7-5

there will be some preload or interference between the piston and liner. Additional deformations above the nominal clearance are required to produce load. Thus, maximum radial deformations might be approximately .010 - .025 mm. From Fig. 7-3, for average pressure levels of 2.76 - 6.89 MPa, the wall thickness would be in the range of 7 mm (0.28 in) which is quite reasonable. Neither hoop stress or applied moments would be excessive for a 7 mm wall thickness, as indicated on Figures 7-4 and 7-5 respectively. The net result is that a solid liner and solid piston appear to be feasible, which improves the practicality of gas-pistons tremendously because of manufacturing simplicity, reduced number of parts, etc.

Some preliminary analytical evaluations were made of the film characteristics a solid piston with machined recesses on either side. No attempt was made at optimization, since the present scope would not allow extensive studies or analyses to be made. A total of 4 recesses were incorporated, two in each of the oppositely loaded zones. Geometric specifications are indicated on Table 7-1 below and the computer model is indicated on Figure 7-6.

Table 7-1

GEOMETRY SOLID HYDROSTATIC PISTON

Piston diameter	=	139.7 mm (5.5 in)
Piston ring length	=	69.85 mm (2.75 in)
No. of recesses	=	4
Angle of each recess	=	90°
Length of each recess	=	13.08 mm (.515 in)
Upper land length	=	13.08 mm (.515 in)
Lower land length	=	13.08 mm (.515 in)
Land length between upper and lower recesses	=	17.53 mm (.69 in)

Theoretical performance under varying conditions of operation is indicated on Table 7-2. As mentioned above no attempt was made at optimization; thus the flows for this configuration are high. Load capability, however, is very good. Flow can be reduced by using smaller recesses without seriously compromising the required load capability. Also, a smaller designed film thickness can be

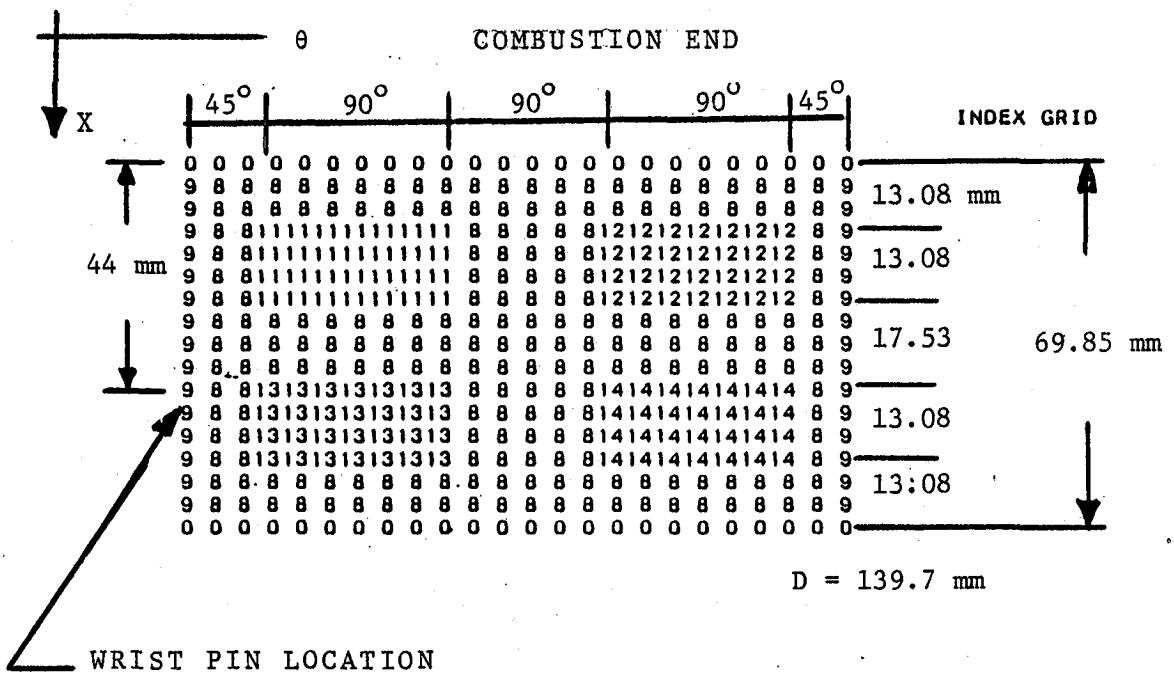

Figure 7-6 Solid Piston Computer Model

Table 7-2

FULL 360° - 4 RECESS BEARING

P_s	P_c	ε	h_M	W	M_t
3.45 (500)	0	0	7.62 (.3)	0	46.67 (102.8)
3.45 (500)	0	.292	3.00 (.118)	13415 (3016)	43.7 (96.3)
10.34 (1500)	0	0	7.62 (.3)	0	108.96 (240)
10.34 (1500)	10.34 (1500)	.4	4.57 (.18)	15879 (3570)	66.61 (146.7)
10.34 (1500)	10.34 (1500)	.6	3.05 (.12)	20252 (4553)	70.28 (154.8)

- Assumed bearing clearance = 7.62 microns (0.3 mils)
- Orifice diameter to each recess = .7366 mm (.029 in.)
- Pivot position 63% from top = 44 mm (1.7325 in.)

P_s = Supply pressure MPa (psi)

P_c = Combustion pressure MPa (psi)

ε = Eccentricity ratio

h_M = Minimum film thickness, microns (mils)

W = Load, Newtons, (lbs)

M_t = Ring flow, kg/h (lbs/h)

applied. The average flow level for the geometry indicated on Table 7-1 is approximately 55 Kg/hr. By reducing the clearance to 5.08 microns (0.2 mils), the flow is reduced to 16 Kg/hr. or at the target level. Further reductions are achieved by reducing recess size. A final compromise would consist of a combination of reduced recess size and clearance.

In conducting the theoretical analysis, it became apparent that the solid piston configuration is sensitive to the unbalance moment just as was the sectored configuration. The wrist pin (pivot position) should be located near the center of pressure of the fluid film, when combustion pressure is applied, to avoid problems with overturning moments. The theoretical center of pressure was 63% from the combustion end when the piston is loaded.

Consideration was given to one other type of breathable liner concept. It is labelled the offset radius concept and is depicted on Fig. 7-7. It consists of two offset semicircles which provide clearance between the cylinder bore and liner in the two loaded regions. This will permit the liner to deflect and provide clearance with the piston in these regions. At 90 degrees to the offset regions the liners are rigidly attached to the cylinder, with small clearance between the piston and liner.

Some preliminary analysis was conducted with the configuration indicated on Fig. 7-7. Note that the inside diameter of the liner is circular and equal to the diameter of the piston. The radius of the outside of the liner is offset to provide clearance between the liner and cylinder load in the loaded region. The net result is that the liner thickness varies around the circumference, being thinnest in the load direction and thickest 90° from the load.

Approximate computations were made using a uniform liner thickness of 3.175 mm (.125 in) indicated deformation of 11.43 mm (.45 in) opposite the load. This deformation is excessive but exaggerated by the approximations imposed, and could be reduced to desirable levels by greater wall thickness or spring supports as indicated on Figure 7-7.

Since the breathable liner operates with preload at start-up, a means to develop a fluid-film before engine start would be desirable. This can be accomplished by a separate reservoir supply of high pressure gas, that is charged during

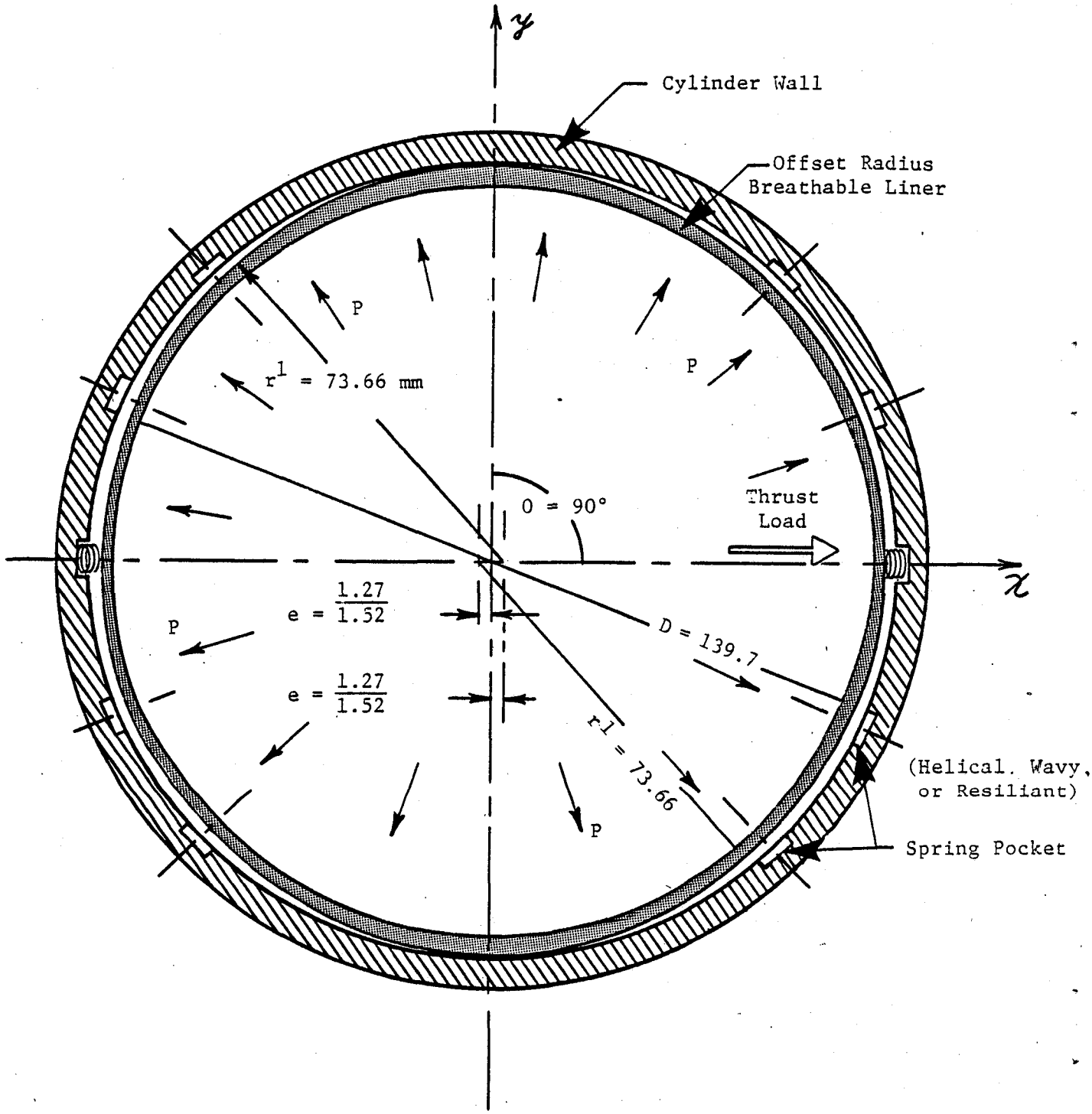

Fig. 7-7 Offset Radius Breathable Liner Concept

normal operation of the engine and energizes the hydrostatic rings immediately preceding crank rotation.

In summary, the breathable liner offers a practical alternative for a gas-lubricated hydrostatic piston. Necessary deformations are achievable. It will be necessary to conduct extensive finite element elasticity analysis of the liner coupled with gas bearing theory before a final configuration can be established. The piston wrist pin must be located so that piston overturning moments from the fluid-film pressure distribution are minimized. In general the breathable liner is the most promising concept for gas pistons.

8.0 CONCLUSIONS AND RECOMMENDATIONS

The program described by this report led to the following conclusions and recommendations:

- The segmented ring configuration demonstrated some positive results, but did not provide sufficiently adequate overall performance for use as a gas-lubricated piston ring. In addition to deficient performance, the segments and inserts are difficult to manufacture to the tolerances required and are considered too complex for mass produced engines.
- The major difficulty was the inability of all segments of a ring set to lift off and form a full film. The problem is due to the delicate moment balance required to prevent the segments from overtuning combined with the small operating films required.
- Some individual sectors did lift-off and those that did seem to perform well. Load capacity was excellent (6000 N/pad). The performance of these individual pads provide substantiation of the ultimate feasibility of gas-lubricated pistons.
- Flow levels were high (50-60 Kg/hr) but could be reduced by more advanced configurations. Approximately 30% of the flow is attributable to leakage between sectors. Substantial flow reductions can be achieved by using a solid breathable liner with solid pistons. As indicated in Section 7, an optimally designed solid breathable liner configuration can operate satisfactorily in the 15 Kg/hr flow range which is the desired level.
- Approximate gas bearing theories that were applied to the design of the segmented rings are not sufficiently accurate. Comprehensive gas-bearing computer codes that model the geometry accurately are required.
- Although more accurate theoretical predictions are necessary, extensive experimentation will still be required to consummate a successful design. Experimentation is essential because the close clearances and high pressures involved extend the present state of the art of conventional gas bearing theory.
- Recessed configurations were proven to be better for the application than inherently compensated geometries. The advantages of recesses include:

  1. Improved liftoff, especially against pre-load because the incoming gas can enter the film more easily.

2. Superior load capacity and stiffness as compared to inherently compensated geometries.

Recesses may produce slightly greater flow requirements and are more prone to pneumatic hammer. However, flow differences can be small and pneumatic hammer is mitigated by friction and damping in the support structure.

- Care must be exercised in the design process to ensure that inlet flow restrictions in the pad geometry are minimized to assure the fluid can adequately enter the film. Also, provision for adequate orifice discharge length is important to assure proper operation of the orifice restrictor element.
- The breathable liner configuration that permits solid pistons coupled with solid liners is the recommended future direction for continued development of gas-lubricated piston rings.
- The work presented here concentrated on the formation of the fluid-film. It is clear that some contact between piston and liner will occur and that engine combustion gases may present contamination problems. Thus, appropriate low wear material combinations will still be required as will filtration of the compensating restrictors.
- Finally, it is concluded that gas-lubricated piston rings are feasible for engines such as the adiabatic engine, but considerable development and investment are required.

9.0 REFERENCES

1. "Self-Excited Vibrations of an Air-Lubricated Thrust Bearing", L. Licht, D.D. Fuller, B. Sternlicht, ASME Transactions, Vol. 80, No. 2, 1958.

2. "Air-Hammer Instability of Pressurized-Journal Gas Bearings", L. Licht, Journal of Basic Engineering, June, 1961.

3. "Extension of the Conducting Sheet Analogy to Externally Pressurized Gas Bearings", L. Licht, Journal of Basic Engineering, June 1961.

4. "Analytical Feasibility Study of a Hydrostatically Supported Piston Ring for Application of Adiabatic Diesel Engines," by Sargit S. Bupara, MTI Report 79TR3, Oct. 1979.

5. "Formulas for Stress and Strain," Raymond J. Roark, fourth edition, McGraw-Hill Book Company, p. 301.

APPENDIX A

PRODUCTION TEST DATA

SAMPLE DATA LOGGER SHEET

NOMENCLATURE

PRODUCTION RUN DATA

CHANNEL	SYMBOL	DESCRIPTION
2	P_s	Bearing supply pressure, psi
3	ΔP_s	ΔP across bearing supply flowmeter, psi
4	P_c	Combustion chamber pressure, psi
5	ΔP_c	ΔP across combustion chamber flowmeter, psi
8	h_3	Clearance combustion end, pad 1A, mils
9	h_4	Clearance exhaust end, pad 1A, mils
12	h_7	Clearance combustion end, pad 5A, mils
13	h_8	Clearance exhaust end, pad 5A, mils
16	h_{11}	Clearance combustion end, pad 3A, mils
17	h_{12}	Clearance exhaust end, pad 3A, mils
18	W_1	Load cell 1, lbs
19	W_2	Load cell 2, lbs
22	T_s	Flowmeter temperature, bearing supply, ^{o}F
23	T_c	Flowmeter temperature, combustion supply, ^{o}F

READINGS CORRECTED FROM REFERENCE DATA POINT

F_2 = Computed flow - bearing supply, lbs/hr

F_3 = Computed flow - combustion supply, lbs/hr

W = Computed load, lbs

PRODUCTION TEST DATA - 4/16/84

No Load Data

Channel	2	3	4	5	1A 8	9	5A 12	13	3A 16	17	22	23	F_2/ring
							DATA SET A						
	203.3	.8387	--	--	.1769	-.0086	.1230	-.076	.3597	.0734	50		41.36
	404.2	3.1099	--	--	.1240	-.0546	.0420	-.095	.3173	.0139	50		79.651
	605.8	5.5126	--	--	.1176	-.0743	.0380	-.097	.3211	-.00075	50		106.05
	803.7	6.2211	--	--	.1181	-.0835	.0510	-.091	.3524	-.0196	50		112.65
	998.1	6.7656	--	--	.1255	-.0931	.0560	-.072	.3757	-.0224	50		117.48
	1204.4	7.2169	--	--	.1284	*	.0560	-.049	.3898	.0344	50		121.34
	1398.2	7.2906	--	--	.1169	*	.0380	-.031	.3917	.0483	49.4	67.1	121.95
							DATA SET B						
	190.9	.9153	--	--	.1453	-.1559	.0730	-.3950	.2175	.1181	53.3	54.6	43
	392.4	3.5505	--	--	.0791	-.1756	-.023	-.4190	.1780	.1107	55.6	55.1	84.64
	604.1	5.7182	--	--	.0588	-.1939	-.0480	-.4280	.1874	.1069	52.6	55.4	107.73
	803.2	6.4801	--	--	.0573	-.2030	-.0390	-.4200	.2119	.1060	50.4		114.93
	996.4	6.9225	--	--	.0564	-.2106	-.0470	-.4070	.2307	.1087	49.4	55.7	118.91
	1194.4	7.1317	--	--	.0504	-.2131	-.0520	-.3970	.2392	.1125	48.4	55.9	120.81
	1460.9	7.1935	--	--	.0356	-.2116	-.0630	-.3880	.2411	.1209	47.1	56.2	121.49

* Lost Probe 9

** Computed values

PRODUCTION TEST DATA - 4/16/84

No Load Data

Channel 2	3	4	5	8	9	12	13	16	17	22	23	F_2	F_3	$\Sigma F/2$
							DATA SET C							
199.1	.2354	196.7	--	-.2411	.2409	-.2160	.2230	-.1440	.4901	50	50	43.83	--	21.92
398.9	.9951	398.1	--	-.2762	.1564	-.2730	.1560	-.2090	.4352	50	50	90.11	--	45.05
603.4	2.3952	600.7	--	-.2870	.1908	-.3080	.1710	-.2354	.4418	50	50	139.8	--	69.9
799.0	3.1569	802.7	.100	-.2865	.3553	-.3270	.2210	-.2514	.4575	50	50	160.5	28.6	94.55
1001.0	3.9578	1007.1	.7820	-.2930	.4458	-.3370	.2640	-.2551	.4789	50	50	179.71	79.88	129.8
1185.9	3.8228	1233.4	3.865	-.2846	.5319	-.3510	.3200	-.2617	.5068	50	50	176.62	177.6	177.1
1452.5	4.9358	1519.8	6.393	-.2693	.5734	-.3540	.3840	-.2429	.5338	50	50	200.69	228.40	214.54

PRODUCTION TEST DATA - 4/16/84

$W = (W_1 + W_2) \cos 45 = .7071 (W_1 + W_2)$

Channel 2	3	4	5	8	9	12	13	Loaded 16	Loaded 17	18	21	Load W	22	23	F_2	F_3	$\Sigma F/2$
									DATA SET D								
496.1	1.3434	492.6	.002	-.1699	.0041	-.241	-.016	-.0998	.4389	5	6		67	67.4	103	3.97	53.5
493.7	1.3808	492.0	.006	-.162	.0445	-.215	.009	-.130	.2176	204	168	263	53.9	67.2	105.7	6.88	56.29
710.1	2.9406	707.1	.001	-.163	.1382	-.245	-.022	-.1148	.3404	-13	--		49.7	66.7	154.95	2.8109	78.88
712.5	3.0093	713.0	.001	-.166	.1195	-.259	-.022	-.1139	.3822	-5			50.9	66.2	156.62	2.812	79.71
717.9	2.8388	716.6	.003	-.159	.1888	-.230	.009	-.1167	.1730	256	162	296	49.4	66.2	152.28	4.871	78.58
677.1	2.6716	718.3	--	-.163	.1412	-.183	.059	-.1130	-.0902	463	355	578	49.4	66.1	147.74	--	73.87
723.8	2.5657	720.7	--	-.173	.1068	-.159	.073	-.1101	-.1134	673	552	866	49.4	66.0	144.78	--	72.39
723.8	2.5101	719.5	.001	-.181	.1028	-.147	.104	-.1111	-.1311	869	748	1143	49.4	65.8	143.2	2.813	73.01
713.7	2.5391	712.4	.004	-.187	.0739	-.111	.233	-.1073	-.1423	1030	916	1376	48.8	65.6	144.1	5.628	74.86
698.2	2.7369	694.6	.008	-.190	.0284	.073	.464	-.0988	-.1423	1502	1349	2016	48.7	65.4	149.63	7.960	78.80
									DATA SET E								
984.4	5.1386	976.8	.010	-.176	.122	-.173	.382	-.0819	.2033	0	--		48.3	65.1	205.11	8.903	107
986.8	4.9500	978	.017	-.170	.1483	-.175	.368	-.0932	.0577	236	174	289.9	48.3	65.0	211.62	11.609	111.6
988.0	4.7860	982.7	.019	-.174	.1134	-.141	.382	-.1054	.0623	435	400	590.4	48.4	64.8	197.93	12.275	105.10
987.4	4.7490	982.1	.023	-.184	.0861	-.124	.400	-.1017	-.0614	567	597	823.1	48.3	64.6	197.18	13.508	105.34
982.0	4.7662	973.2	.025	-.199	.0521	-.077	.453	-.0988	-.0437	832	860	1196.4	48.3	--	197.54	14.08	105.81
973.1	4.8054	966.7	.026	-.206	.0243	-.043	.513	-.0819	.1172	240	398	451.0	48.3	64.4	198.35	14.36	106.36
977.9	4.7885	972.0	.029	-.208	.0157	-.083	.473	-.0847	.1014	1105	1101	1559.9	48.3	--	198.00	15.17	106.59
979	4.7557	973.2	.030	-.1996	.0415	-.103	.462	-.0885	.0409	1275	1255	1789	48.4	64.4	197.30	15.43	106.37
976.7	4.7843	968.5	.031	-.199	.0491	-.097	.461	-.0875	.0205	1541	1484	2139	48.4	63.7	197.89	15.7	106.8
1215.8	5.6604	1216.8	.200	-.182	.168	-.238	.393	-.0857	.2697	--	--		48.2	58.3	215.3	40.07	127.6
1218.2	5.5398	1221.6	.243	-.189	.1873	-.242	.386	-.0932	.2213	228	138	258.8	47.8	54.5	213.07	44.33	128.7
1216.4	5.4455	1221.0	.255	-.194	.1377	-.207	.427	-.097	.1302	315	354	473.1	47.7	51.6	211.27	45.54	128.41

PRODUCTION TEST DATA - 4/16/84

Channel 2	3	4	5	8	9	12	13	Loaded 16	Loaded 17	18	21	Load W	22	23	F_2	F_3	$\Sigma F/2$
								DATA SET E (CONT'D)									
1215.2	5.4100	1220.4	0.285	-.199	0.1265	-.205	.435	-.1045	.106	606	628	873	47.6	51.0	210.61	48.18	129.40
1214.0	5.4301	1219.2	0.307	-.199	0.1286	-.206	.431	-.1054	.093	814	732	1093	47.6	50.5	211.	50.03	130.52
1212.8	5.4008	1218.6	0.314	-.196	0.1432	-.206	.430	-.1045	.0726	1011	939	1379	47.6	50.2	210.43	50.61	130.52
1212.8	5.3976	1218.6	0.327	-.193	0.1539	-.197	.421	-.1064	.0484	1260	1120	1683	47.6	50.0	210.36	51.66	131.0
1215.3	5.3971	1218.6	0.337	-.184	0.1888	-.213	.410	-.1092	-.0372	1708	1476	2251	47.3	49.6	210.42	52.46	131.44
1466.8	5.9392	1471.7	1.331	-.189	0.2439	-.285	.368	-.097	.2613	--	--		47.0	48.8	220.8	104.34	162.57
1463.8	5.8276	1472.3	1.81	-.184	0.250	-.283	.393	-.097	.2074	231	204	307.6	46.6	48.1	218.8	121.8	170.3
1460.8	5.7231	1470.5	1.644	-.189	0.2126	-.252	.430	-.0941	.1339	446	463	642.8	46.1	47.2	216.9	116.1	166.5
1459.6	5.7187	1469.3	1.708	-.188	0.2115	-.244	.422	-.0951	.1237	598	534	800.4	46.2	47.1	216.8	118.4	167.6
1457.3	5.7080	1464	1.816	-.1842	0.2171	-.241	.428	-.1007	.0967	812	777	1123.6	46.1	47.1	216.65	122.1	169.38
1456.1	5.7229	1466.4	1.922	-.1788	0.2212	-.242	.427	-.1045	.0688	988	843	1294.7	46.2	47.0	216.91	125.6	171.26
1454.9	5.6916	1465.2	1.988	-.1758	0.2288	-.242	.423	-.1064	.0428	1250	987	1582	--	--	216.34	127.76	172.1
1454.3	5.6973	1462.2	2.033	-.1729	0.2449	-.243	.418	-.1139	-.0242	1668	1352	2135	46.1	46.9	216.44	129.19	172.8
1454.3	5.6534	1462.2	2.087	-.1768	0.2449	-.236	.424	-.112	-.0521	1840	1643	2463	46.0	46.8	215.63	130.91	173.27

PRODUCTION TEST DATA - 4/16/84

Channel 2	3	4	5	8	9	12	13	Loaded 16	Loaded 17	18	21	Load W	22	23	F_2	F_3	$\Sigma F/2$
DATA SET F (EXTRA DATA)																	
470.4	1.6380	470	0.086	-.2194	-.0248	-.222	-.047	-.0649	.3199	--	--	201	56.1	59.5	114.93	26.25	70.59
468.0	1.4971	467.6	0.088	-.2381	-.042	-.218	-.003	-.0904	-.0576	201	114	223	51.8	59.5	110.33	26.55	68.44
467.4	1.5102	467.6	0.090	-.2386	-.0551	-.235	-.0008	-.0932	.0084	391	305	492	51.4	59.4	110.86	26.85	68.86
462.7	1.5536	462.9	0.091	-.2415	-.0718	-.199	.122	-.0913	.0642	601	530	799.7	51.3	59.5	112.45	27.0	69.73
461.5	1.5727	461.7	0.094	-.2351	-.0658	-.156	.232	-.0904	.1014	803	725	1080.5	51.0	59.4	113.17	27.44	70.31
719.1	2.3071	730.8	0.722	-.2312	.0633	-.225	.265	-.0838	.1823	179	114	207.2	49.9	52.1	137.22	76.6	106.91
719.1	2.2647	729.6	0.763	-.2292	.0678	-.221	.273	-.0941	.1535	406	324	516.2	49.4	50.8	136.02	78.8	107.41
718.5	2.2920	731.4	0.790	-.2183	.1043	-.214	.263	-.096	.1153	632	485	789.8	49.3	50.5	136.9	80.3	108.6
717.3	2.2761	730.8	0.790	-.2243	.0896	-.198	.289	-.0922	.1088	822	738	1103.1	49.2	50.2	136.4	80.3	108.35
966.5	3.8328	981.5	1.278	-.2178	.1807	-.258	.276	-.0951	.2083	211	124	236.9	48.3	49.5	177.1	102.2	139.65
965.3	3.8355	982.1	1.253	-.2223	.1721	-.230	.310	-.0951	.1553	610	463	758.7	48.3	49.1	177.2	101.2	139.2
967.1	3.7824	983.3	1.261	-.2228	.1873	-.226	.319	-.0951	.1125	816	724	1089	48.0	48.8	176.03	101.6	138.82
962.5	3.5574	981.5	1.186	-.2331	.1503	-.206	.346	-.096	.1144	1003	906	1350	48.2	48.8	170.7	98.5	134.6
1216.4	5.6214	1223.4	0.549	-.2173	.2374	-.292	.282	-.1045	.2204	201	128	232.6	47.5	48.7	214.7	67	140.85
1214	5.5832	1221	0.553	-.2132	.2207	-.275	.291	-.1111	.1758	448	325	546.6	47.2	48.4	214.	67.3	140.65

PRODUCTION TEST DATA - 4/16/84

Channel	2	3	8	9	12	13	Loaded 16	Loaded 17	18	21	Load W	22	23	F_2	$\Sigma F/2$
							DATA SET G								
	466.9	4.653	.0232	-.1017	-.144	-.278	.1629	.1256	240	167	287.8	49.7	54.4	194.9	97.45
	466.9	4.6508	.0316	-.1012	-.145	-.274	.1611	.1070	381	375	534.6	49.4	54.6	194.9	97.45
	471.7	4.5912	.0356	-.1022	-.139	-.272	.1611	.0958	579	597	831.6	49.0	55.0	193.7	96.85
	700.7	5.9913	.0272	-.080	-.151	-.259	.1658	.1191			831.6	47.9	55.5	221.6	110.80
	698.3	5.9739	.0247	-.0734	-.142	-.264	.1498	.1181	10	- 1	6.36	48.6	55.6	221.1	110.55
	694.1	5.9375	.0217	-.0779	-.140	-.263	.1366	.0837	213	166	268	47.7	55.9	220.6	110.3
	694.1	5.9285	.0262	-.0795	-.149	-.261	.1290	.0921	380	364	526	47.4	56.0	220.5	110.25
	693.5	5.9370	.0247	-.0785	-.149	-.260	.1253	.0772	587	555	807.5	47.2	56.1	220.7	110.35
	694.7	5.9221	.0227	-.07784	-.151	-.258	.2988	.0586	858	736	1127.1	47.0	56.1	220.5	110.25
	1387.6	7.1398	-.003	-.08544	-.166	-.231	.1902	-.0176	1403	976	1682.2	44.3	56.3	242.7	121.35
	1369.7	7.1378	-.0025	-.08344	-.172	-.231	.3343	.0809	793	732	1078.3	43.3	56.4	242.9	121.45
	1361.3	7.1373	-.6729	-.08244	-.167	-.233	.4153	.1163	489	510	706.4	43.1	56.4	242.98	121.49
	1351.2	7.1366	.0015	-.07894	-.166	-.234	.3993	.1237	247	262	359.9	42.7	56.5	243.06	121.53
	1177.7	7.0919	.0064	-.08244	-.159	-.236	.3758	-.0204	1341	826	1532.3	43.0	56.4	242.2	121.10
	1177.1	7.0939	.0054	-.08094	-.166	-.231	.6507	.0400	1042	764	1277	42.7	56.5	242.3	121.15
	1174.7	7.0957	0	-.08244	-.154	-.231	.5820	.1070	362	555	648.4	42.7	56.5	242.4	121.20
	1172.3	7.0964	.0054	-.07684	-.167	-.231	.5123	.1107	237	238	335.9	42.7	56.4	242.4	121.20
	804.4	6.3811	.0094	-.0784	-.168	-.254	.5095	.1107				43.0	56.4	229.8	114.9
	806.8	6.3811	.0118	-.07734	-.155	-.251	.5029	.1051	170	183	249.6	43.3	56.4	229.7	114.85
	806.2	6.3799	.0109	-.07684	-.146	-.251	.4888	.0484	606	478	766.5	43.8	56.4	229.6	114.8
	803.8	6.3754	.0084	-.07944	-.153	-.250	.4445	.0223	1031	956	1405.0	44.2	58.4	229.4	114.7
	805.0	6.3637	.0079	-.07894	-.149	-.250	.1846	.0419	863	781	1162.5	44.1	56.4	229.2	114.6
	497.3	4.9165	.0178	-.06924	-.160	-.267	.5038	.1060				44.8	56.5	201.33	100.67

PRODUCTION TEST DATA - 4/16/84

Channel	2	3	8	9	12	13	16 (Loaded)	17 (Loaded)	18	21	Load W	22	23	F_2	$\Sigma F/2$
DATA SET G (CONT'D)															
	500.3	4.8932	.0178	-.06924	-.151	-.267	.5198	.1051	289	206	350.0	45.1	56.4	200.79	100.40
	499.7	4.8612	.0193	-.07034	-.154	-.266	.5179	.0809	488	363	601.7	40.0	45.3	201.15	100.58
	498.5	4.8808	.0183	-.07284	-.146	-.266	.5321	.0716	667	561	868.3	45.7	56.3	200.41	100.21
	499.1	4.8766	.0222	-.07134	-.152	-.265	.5151	.0540	892	846	1229	46.0	56.3	200.27	100.135
	223.0	1.4221	.079	-.04554	-.071	-.263	.4332	.0530				46.5	56.3	108.1	54.05
	225.4	1.4757	.084	-.03284	-.055	-.266	.3607	.0010	244	63	217	47.1	56.4	100.05	55.03
	225.4	1.4591	.0761	-.04094	-.057	-.254	.2439	.1042	279	168	316.1	47.5	56.4	109.38	54.70
	225.4	1.4993	.0706	-.03484	-.054	-.259	.3475	.0614	484	335	579.1	47.9	56.3	110.84	55.42

APPENDIX B

ADDITIONAL LOAD VS. CLEARANCE PLOTS FOR VARYING PRESSURE LEVELS AND BOUNDARY CONDITIONS

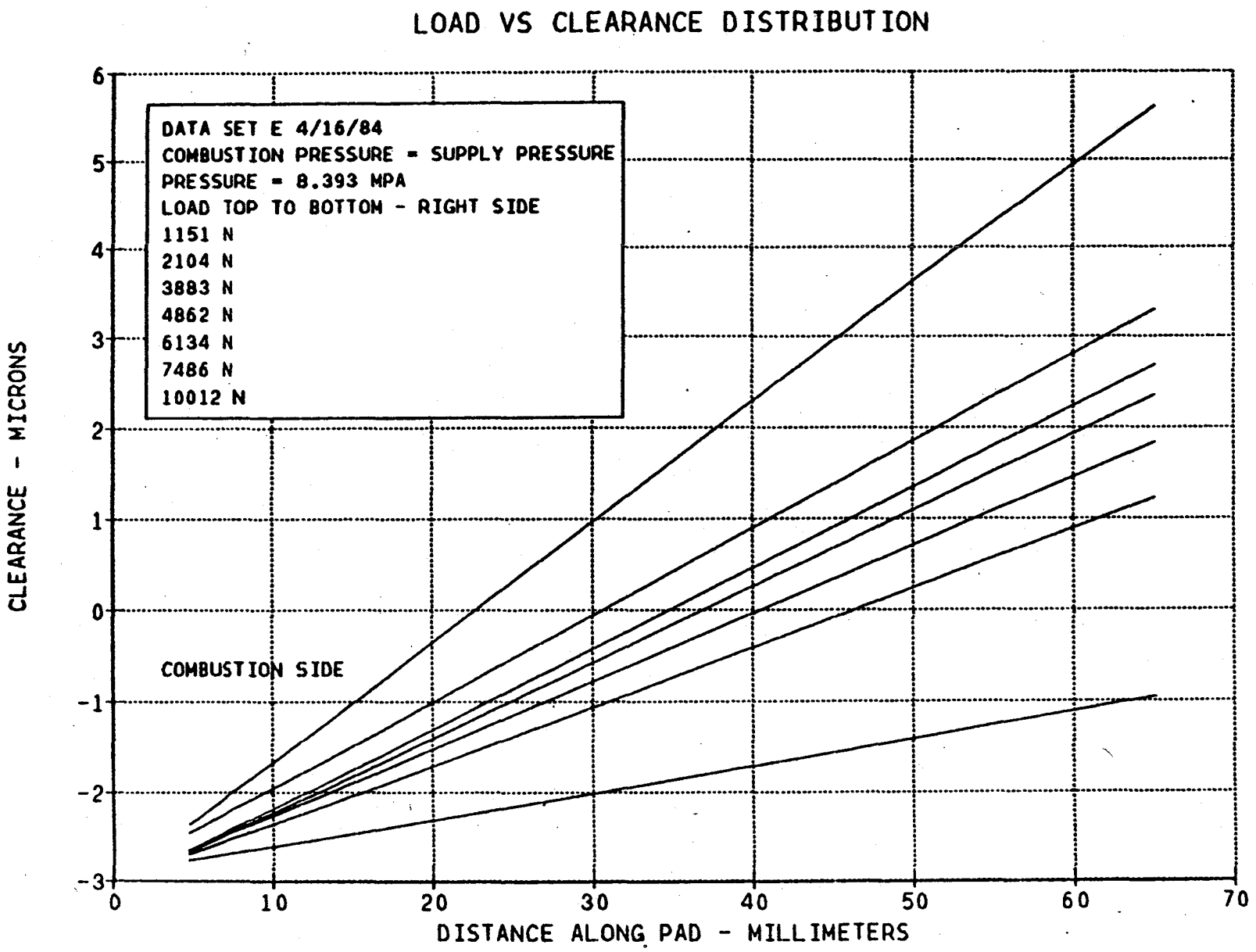
LOAD VS CLEARANCE DISTRIBUTION
DATA SET E 4/16/84
COMBUSTION PRESSURE = SUPPLY PRESSURE
PRESSURE = 8.393 MPA
LOAD TOP TO BOTTOM - RIGHT SIDE
1151 N
2104 N
3883 N
4862 N
6134 N
7486 N
10012 N
COMBUSTION SIDE
CLEARANCE - MICRONS
DISTANCE ALONG PAD - MILLIMETERS
6
5
4
3
2
1
0
-1
-2
-3
0
10
20
30
40
50
60
70

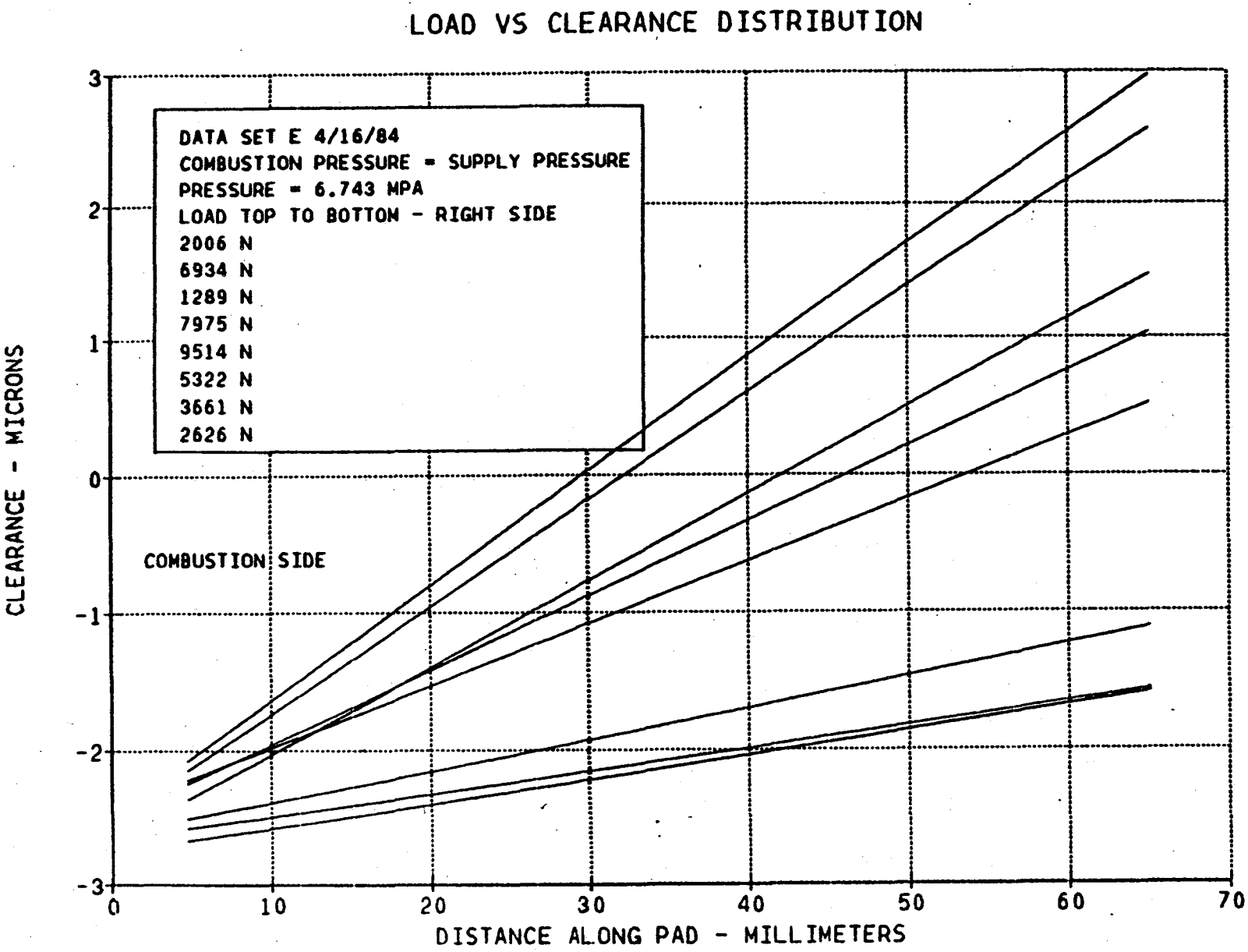
LOAD VS CLEARANCE DISTRIBUTION
DATA SET E 4/16/84
COMBUSTION PRESSURE = SUPPLY PRESSURE
PRESSURE = 6.743 MPA
LOAD TOP TO BOTTON - RIGHT SIDE
2006 N
6934 N
1289 N
7975 N
9514 N
5322 N
3661 N
2626 N
COMBUSTION SIDE
CLEARANCE - MICRONS
DISTANCE ALONG PAD - MILLIMETERS
3
2
1
0
-1
-2
-3
0
10
20
30
40
50
60
70

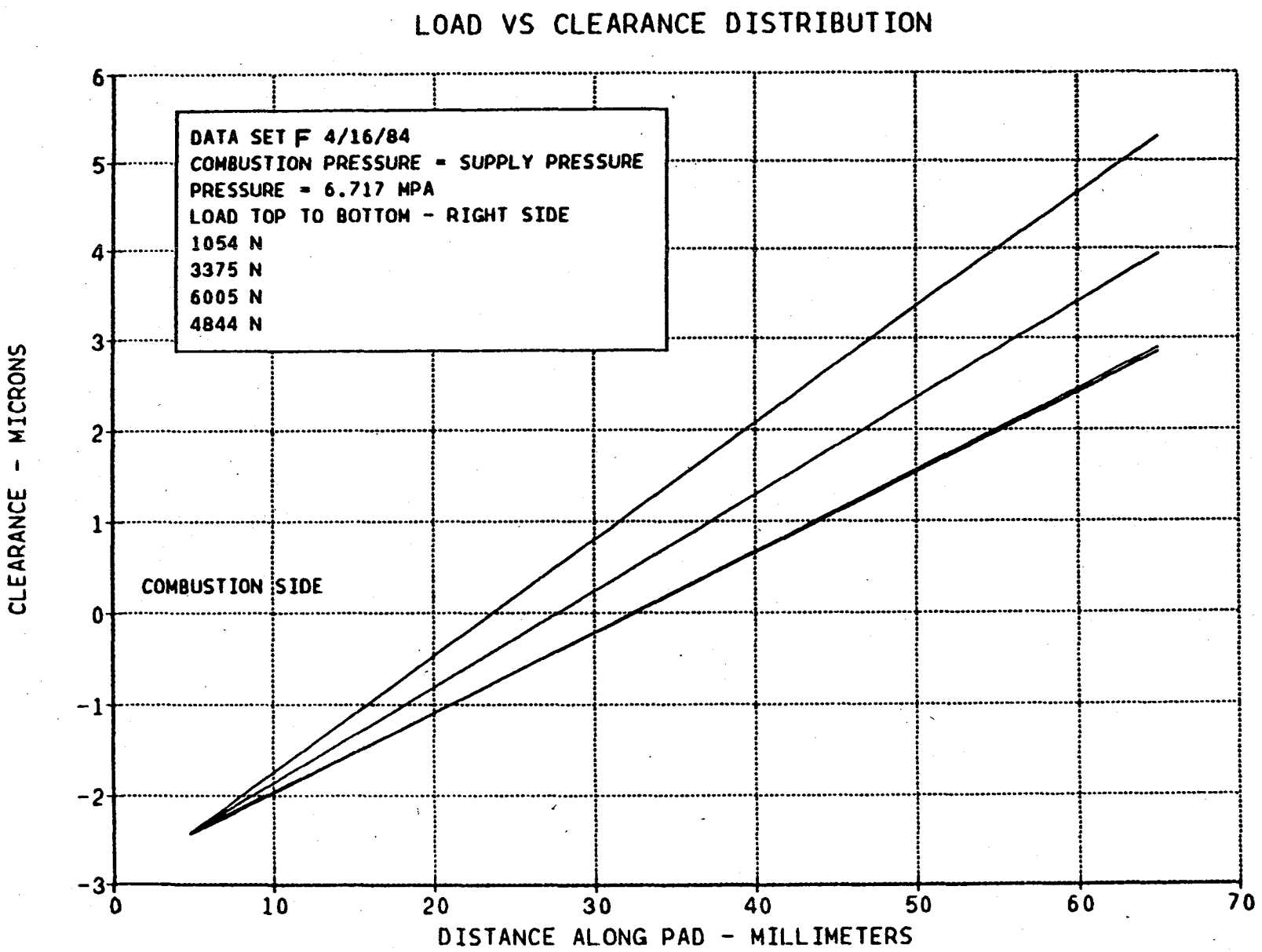
LOAD VS CLEARANCE DISTRIBUTION
DATA SET F 4/16/84
COMBUSTION PRESSURE = SUPPLY PRESSURE
PRESSURE = 6.717 MPA
LOAD TOP TO BOTTOM - RIGHT SIDE
1054 N
3375 N
6005 N
4844 N
COMBUSTION SIDE
CLEARANCE - MICRONS
DISTANCE ALONG PAD - MILLIMETERS
6
5
4
3
2
1
0
-1
-2
-3
0
10
20
30
40
50
60
70

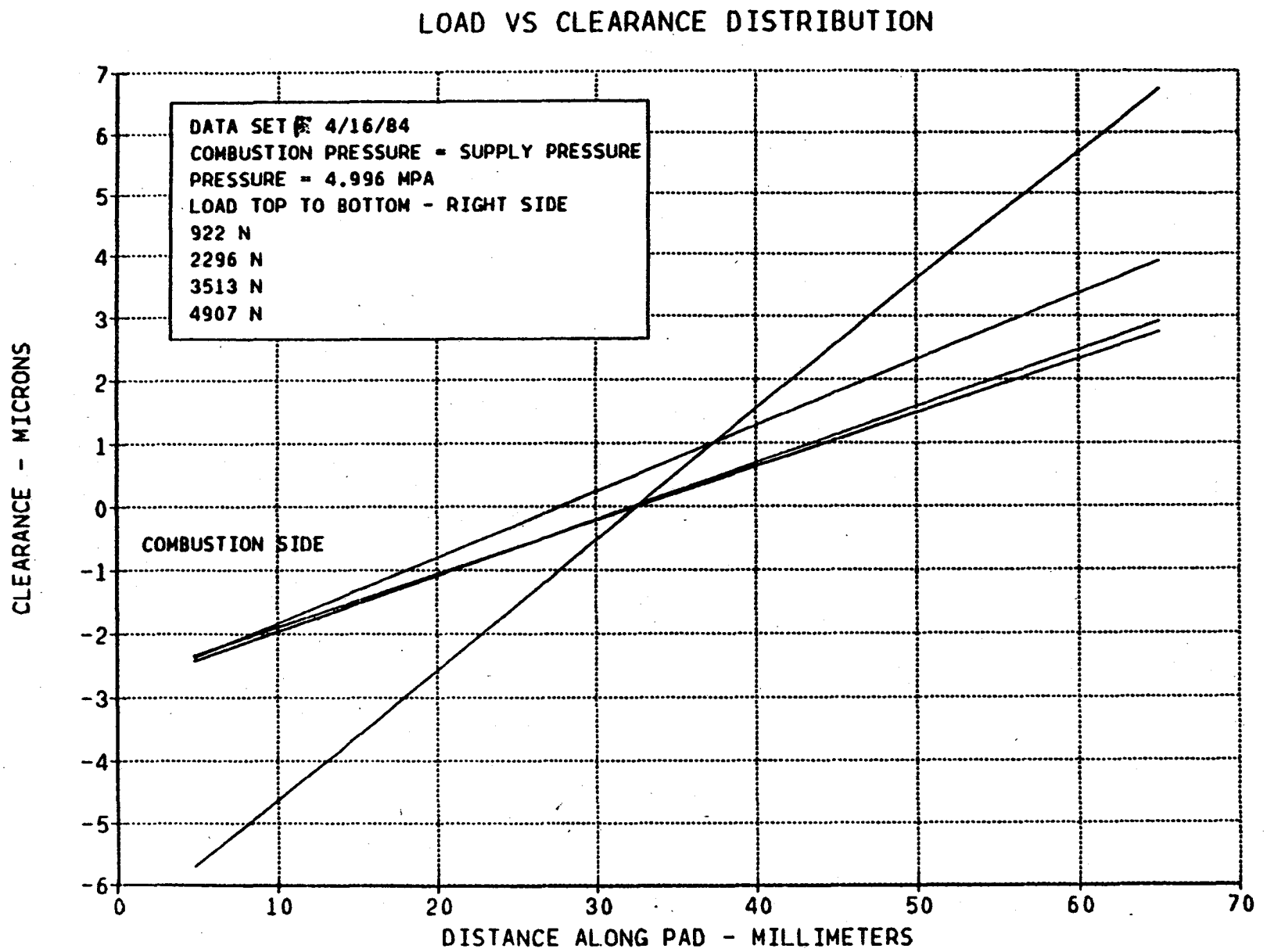
LOAD VS CLEARANCE DISTRIBUTION
DATA SET: 4/16/84
COMBUSTION PRESSURE = SUPPLY PRESSURE
PRESSURE = 4.996 MPA
LOAD TOP TO BOTTOM - RIGHT SIDE
922 N
2296 N
3513 N
4907 N
COMBUSTION SIDE
CLEARANCE - MICRONS
DISTANCE ALONG PAD - MILLIMETERS
7
6
5
4
3
2
1
0
-1
-2
-3
-4
-5
-6
0
10
20
30
40
50
60
70

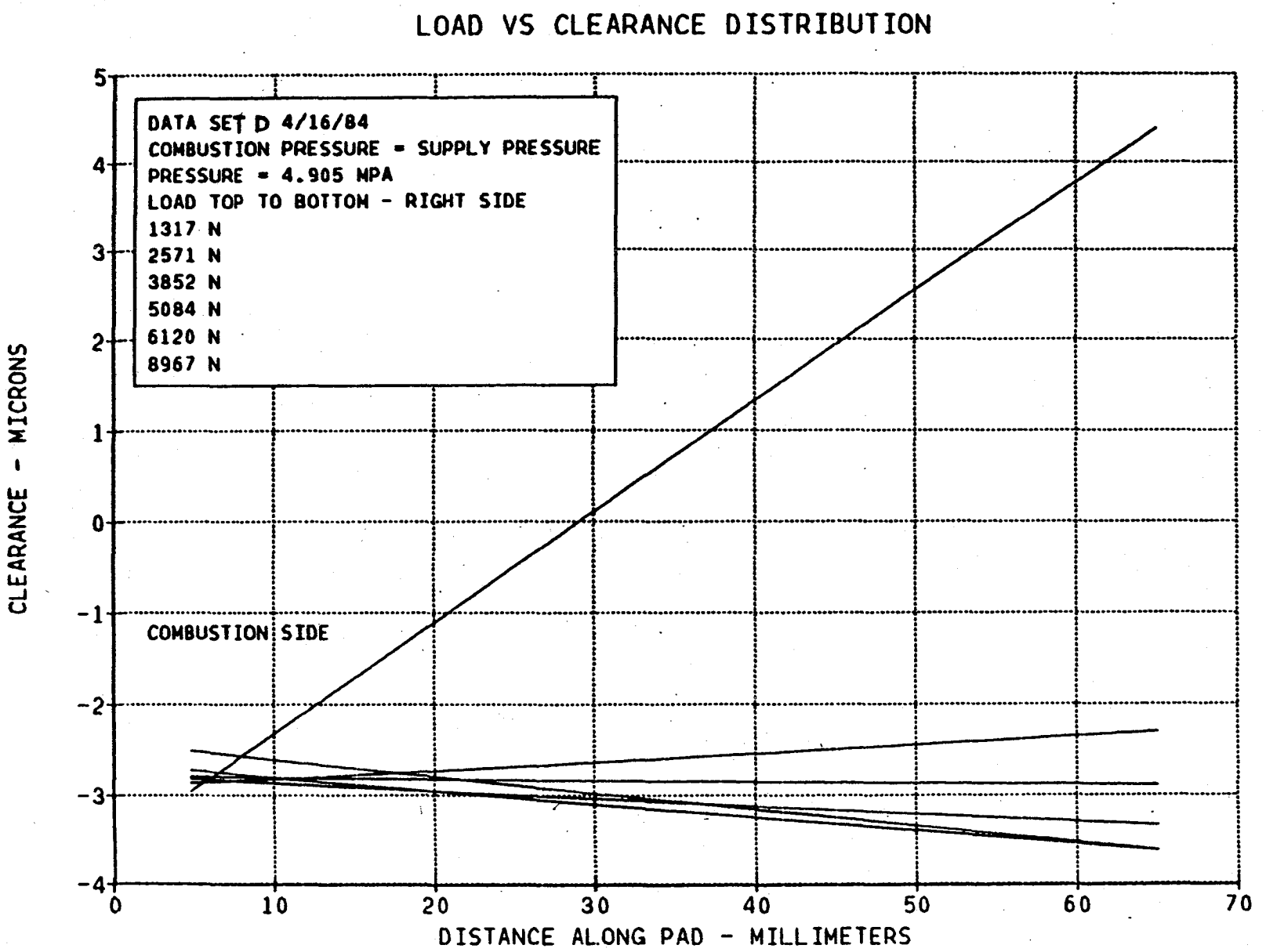
LOAD VS CLEARANCE DISTRIBUTION
DATA SET D 4/16/84
COMBUSTION PRESSURE = SUPPLY PRESSURE
PRESSURE = 4.905 MPA
LOAD TOP TO BOTTOM - RIGHT SIDE
1317 N
2571 N
3852 N
5084 N
6120 N
8967 N
COMBUSTION SIDE
CLEARANCE - MICRONS
DISTANCE ALONG PAD - MILLIMETERS
5
4
3
2
1
0
-1
-2
-3
-4
0
10
20
30
40
50
60
70

LOAD VS CLEARANCE DISTRIBUTION

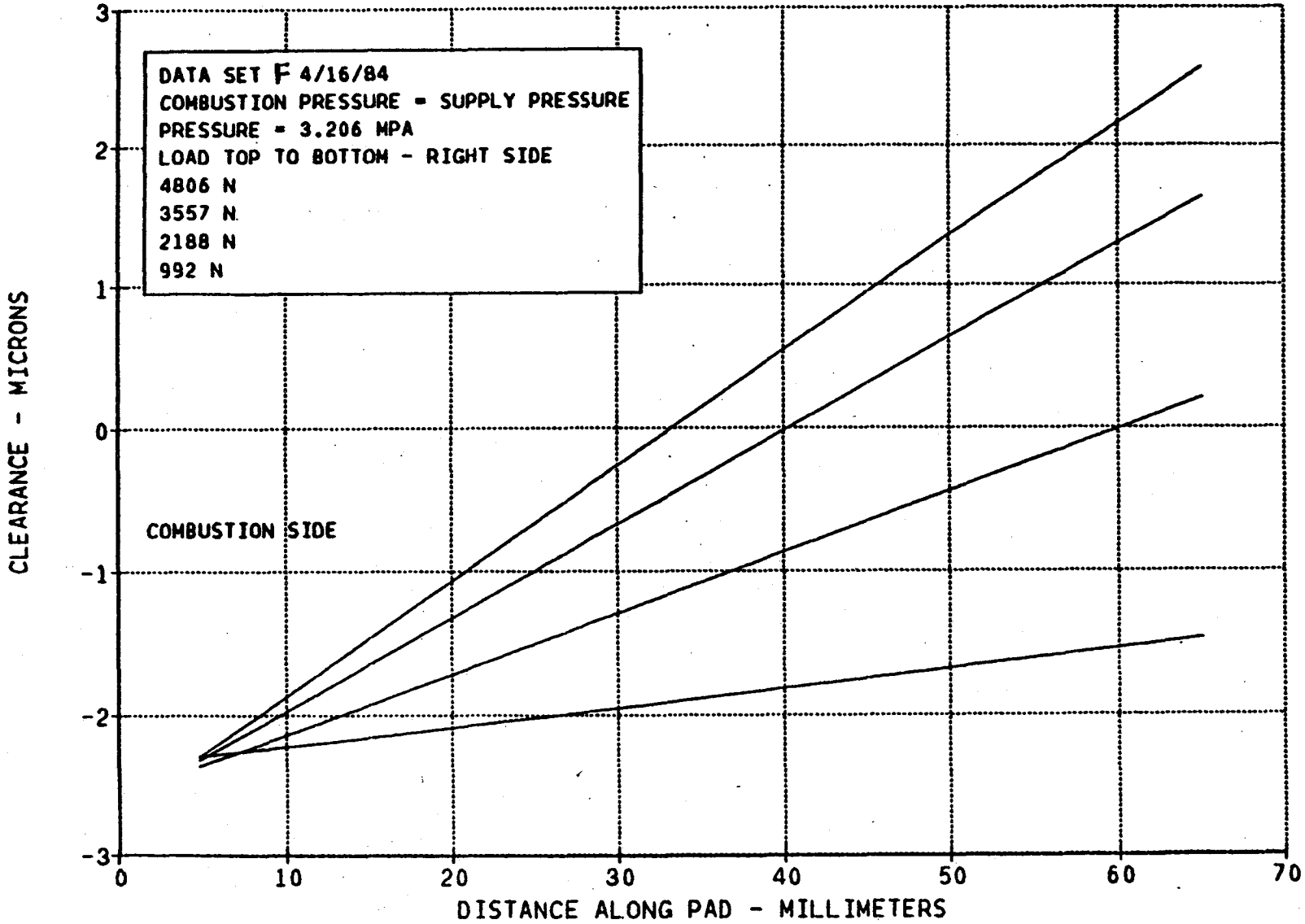

LOAD VS CLEARANCE DISTRIBUTION

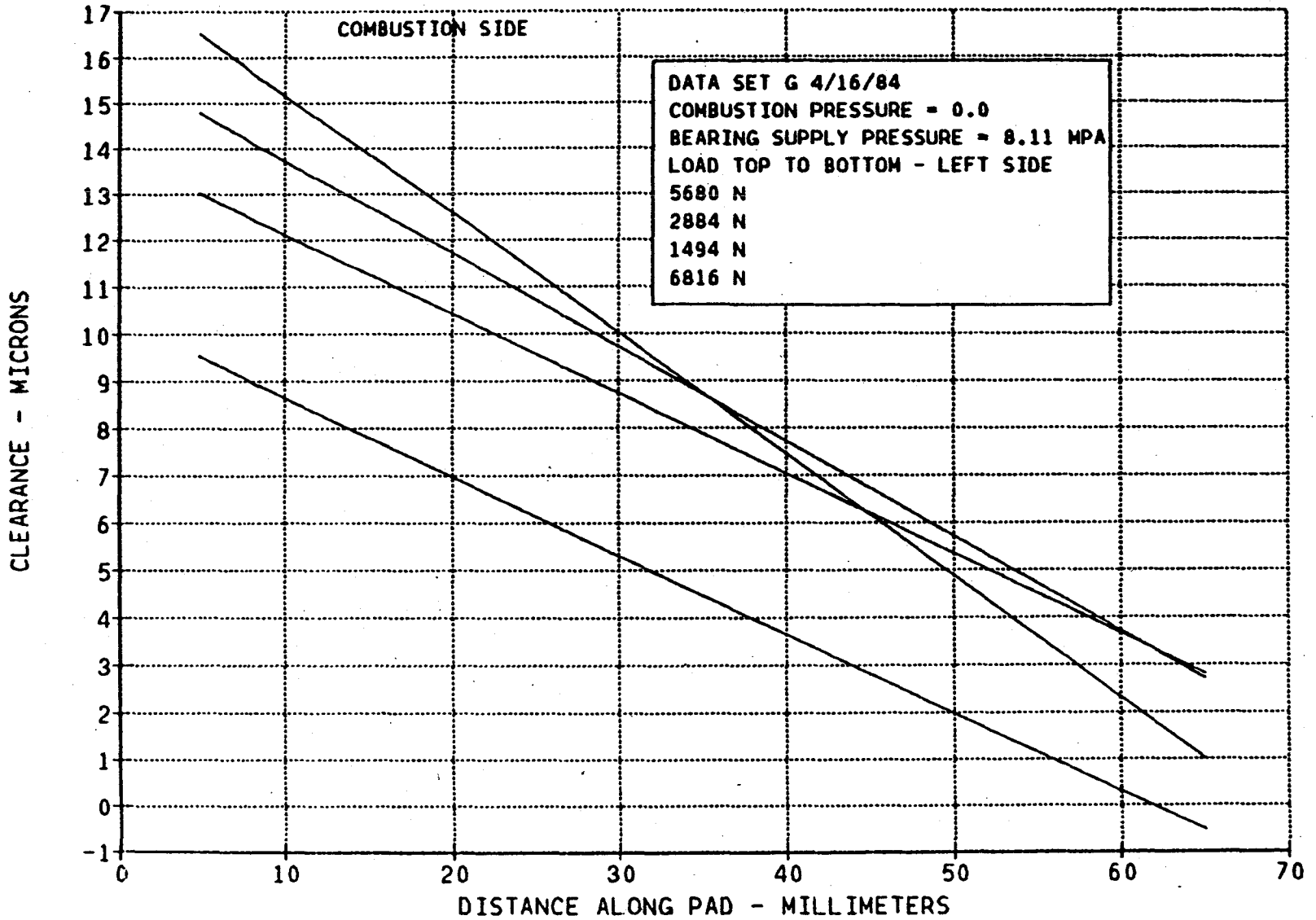

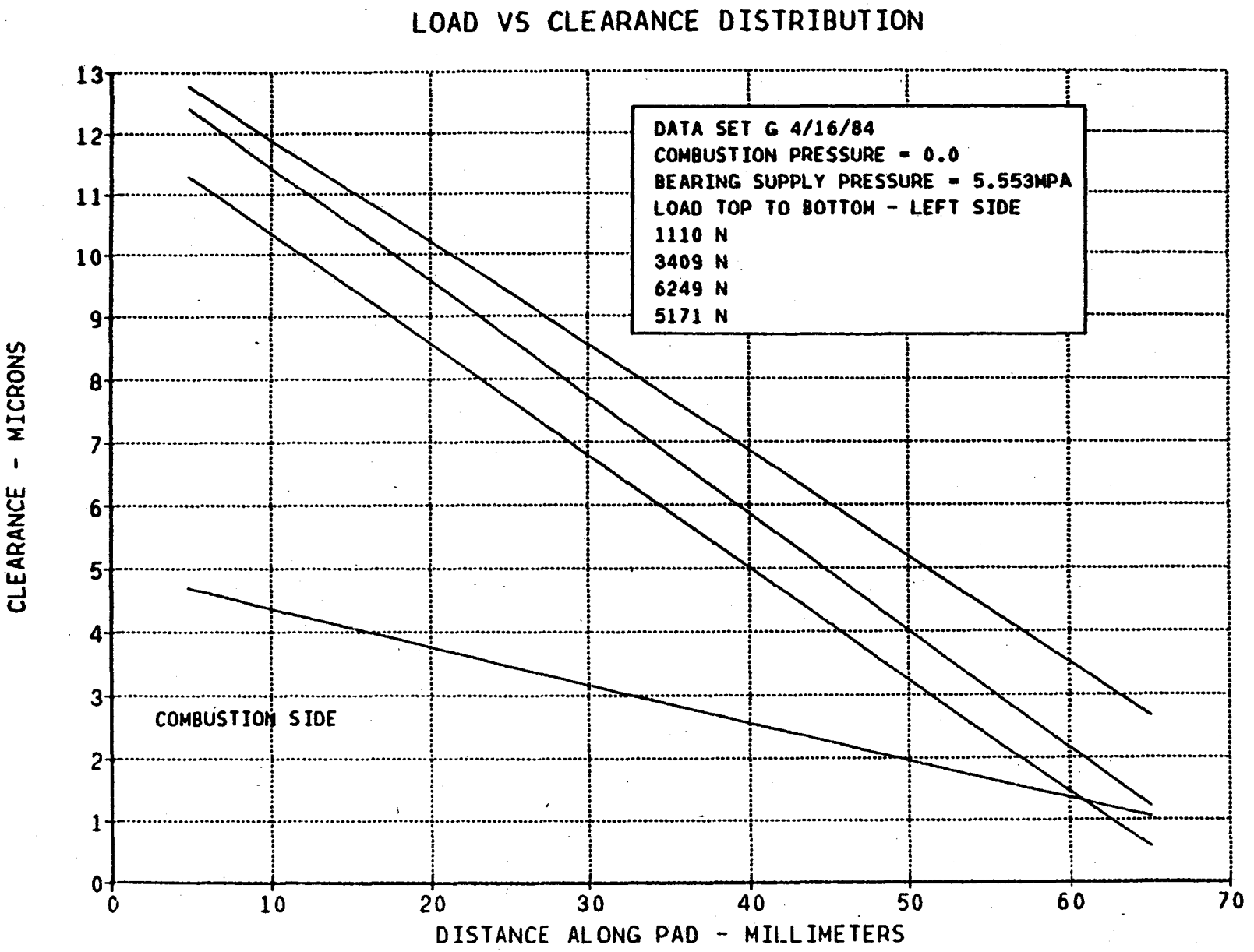
LOAD VS CLEARANCE DISTRIBUTION
DATA SET G 4/16/84
COMBUSTION PRESSURE = 0.0
BEARING SUPPLY PRESSURE = 5.553MPA
LOAD TOP TO BOTTOM - LEFT SIDE
1110 N
3409 N
6249 N
5171 N
COMBUSTION SIDE
CLEARANCE - MICRONS
DISTANCE ALONG PAD - MILLIMETERS
0
1
2
3
4
5
6
7
8
9
10
11
12
13
0
10
20
30
40
50
60
70

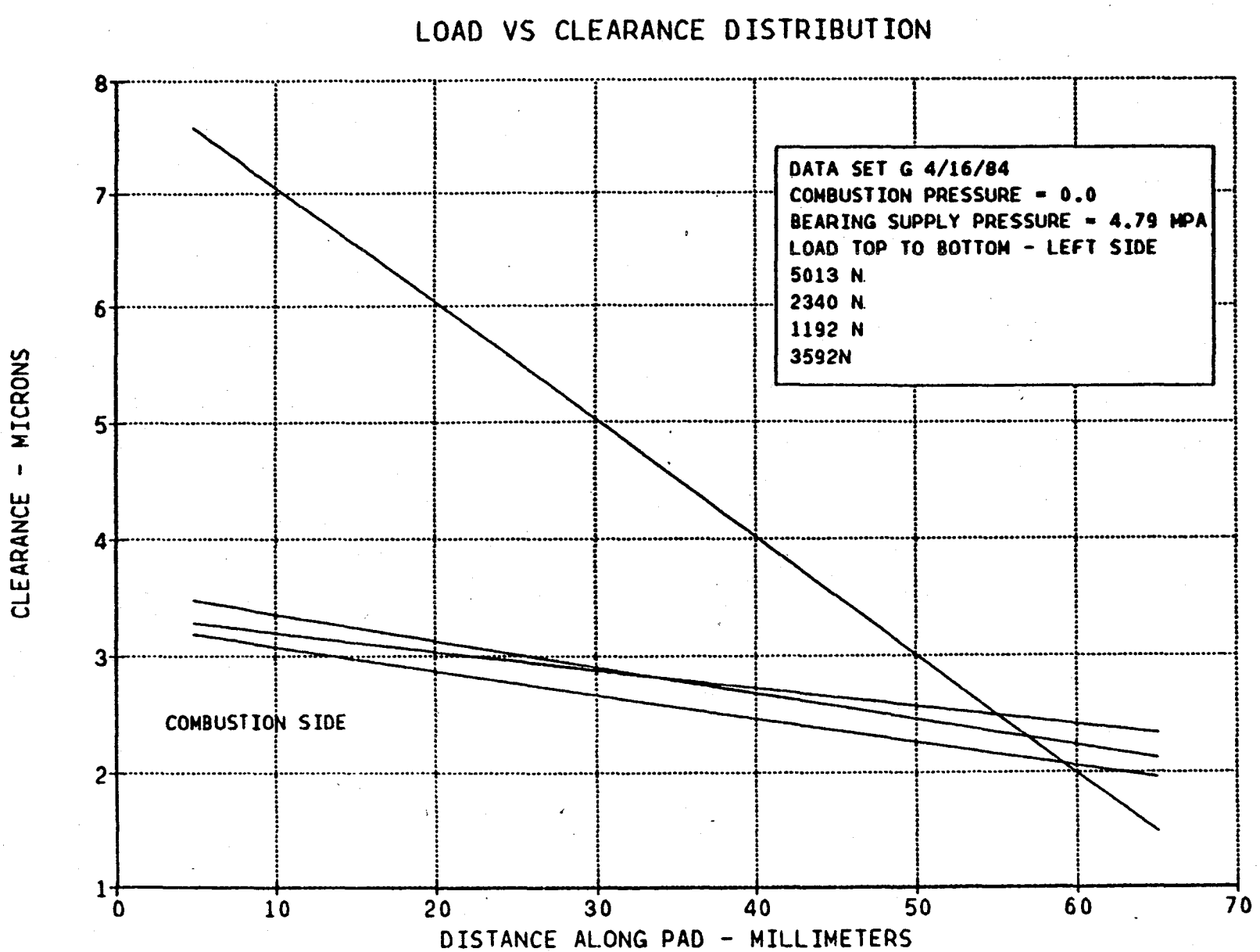
LOAD VS CLEARANCE DISTRIBUTION
DATA SET G 4/16/84
COMBUSTION PRESSURE = 0.0
BEARING SUPPLY PRESSURE = 4.79 MPA
LOAD TOP TO BOTTOM - LEFT SIDE
5013 N.
2340 N.
1192 N
3592N
COMBUSTION SIDE
CLEARANCE - MICRONS
DISTANCE ALONG PAD - MILLIMETERS
1
2
3
4
5
6
7
8
0
10
20
30
40
50
60
70

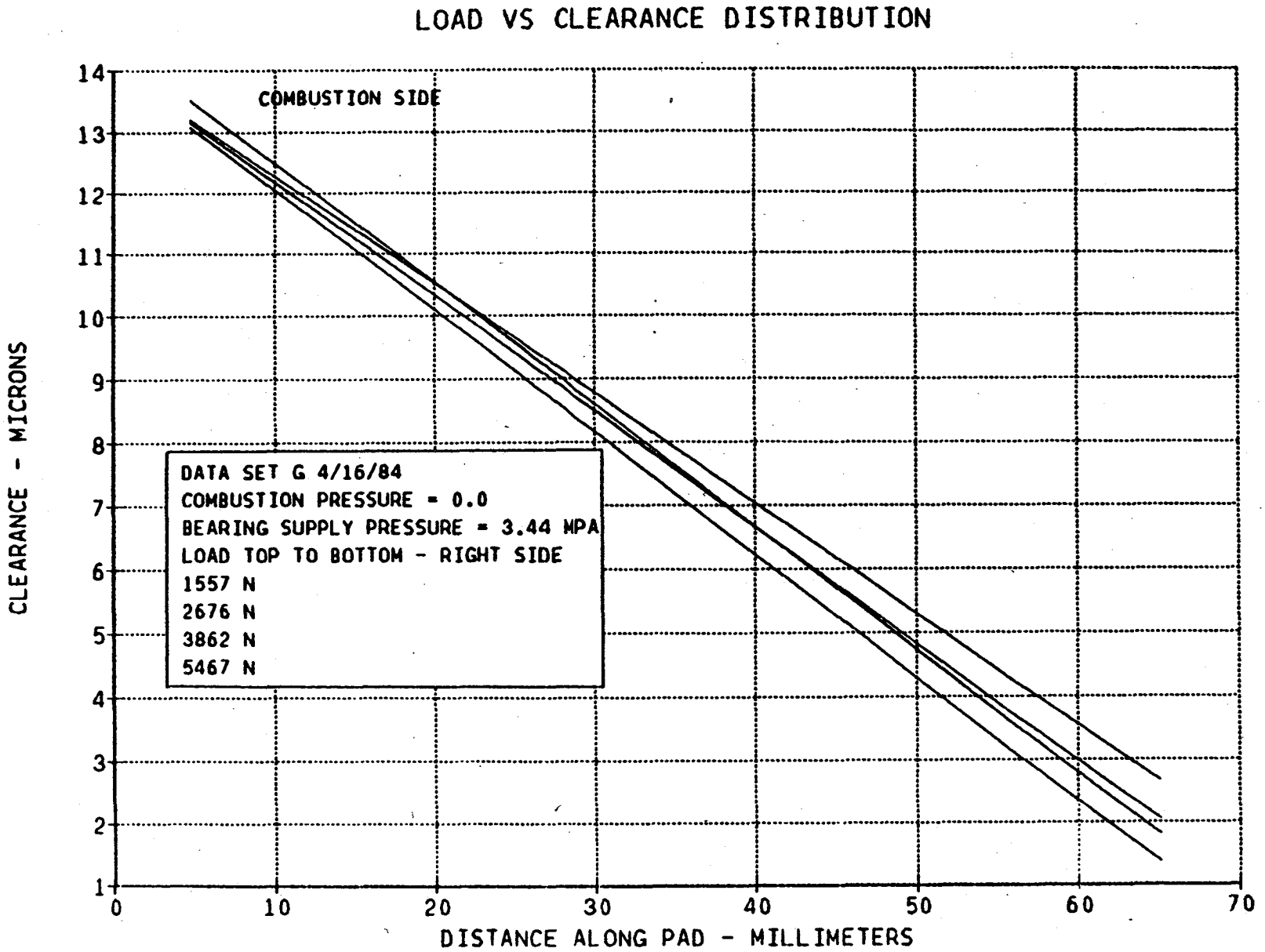
LOAD VS CLEARANCE DISTRIBUTION
COMBUSTION SIDE
DATA SET G 4/16/84
COMBUSTION PRESSURE = 0.0
BEARING SUPPLY PRESSURE = 3.44 MPA
LOAD TOP TO BOTTOM - RIGHT SIDE
1557 N
2676 N
3862 N
5467 N
CLEARANCE - MICRONS
DISTANCE ALONG PAD - MILLIMETERS
1
2
3
4
5
6
7
8
9
10
11
12
13
14
0
10
20
30
40
50
60
70

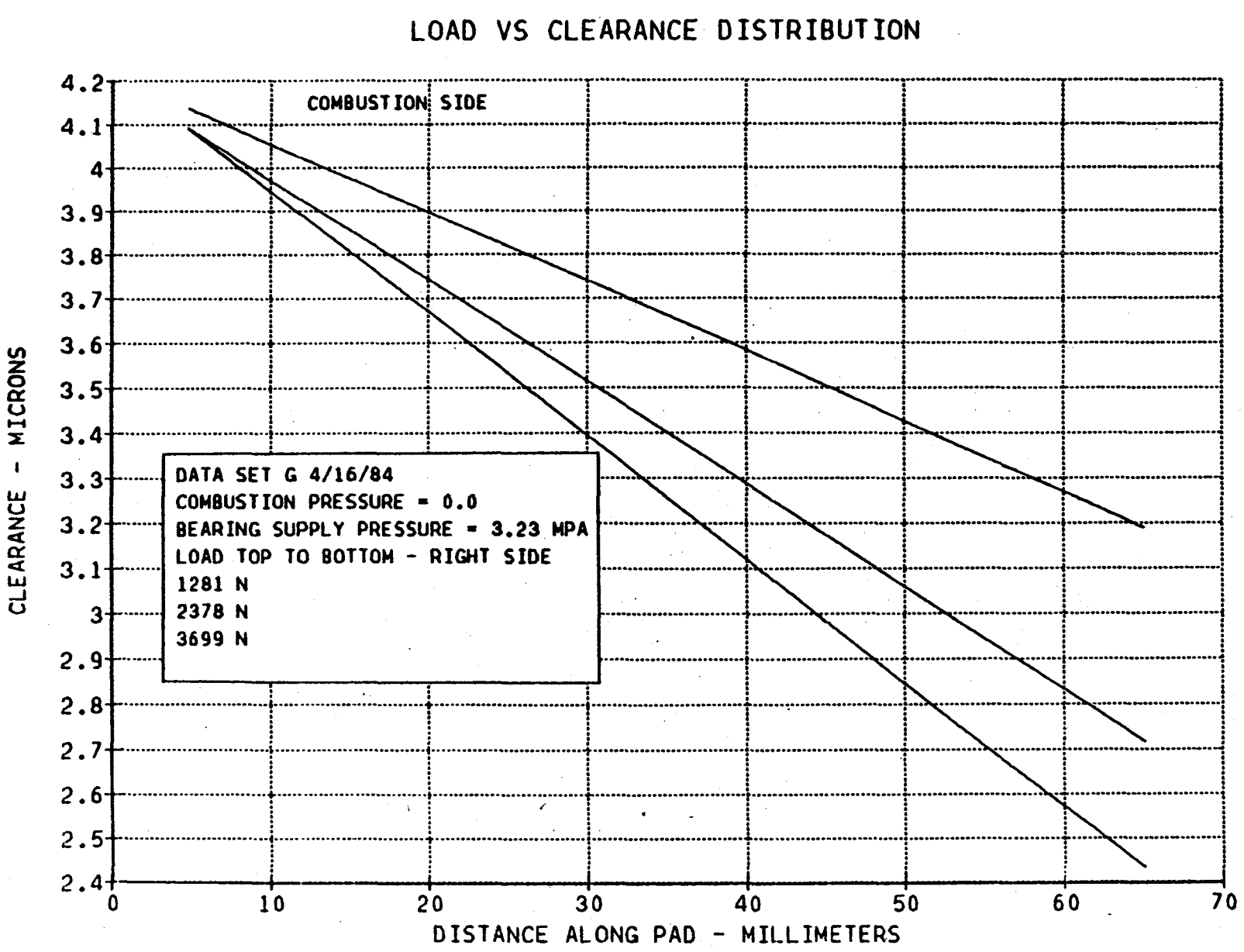
LOAD VS CLEARANCE DISTRIBUTION
COMBUSTION SIDE
DATA SET G 4/16/84
COMBUSTION PRESSURE = 0.0
BEARING SUPPLY PRESSURE = 3.23 MPA
LOAD TOP TO BOTTOM - RIGHT SIDE
1281 N
2378 N
3699 N
CLEARANCE - MICRONS
4.2
4.1
4
3.9
3.8
3.7
3.6
3.5
3.4
3.3
3.2
3.1
3
2.9
2.8
2.7
2.6
2.5
2.4
0
10
20
30
40
50
60
70
DISTANCE ALONG PAD - MILLIMETERS

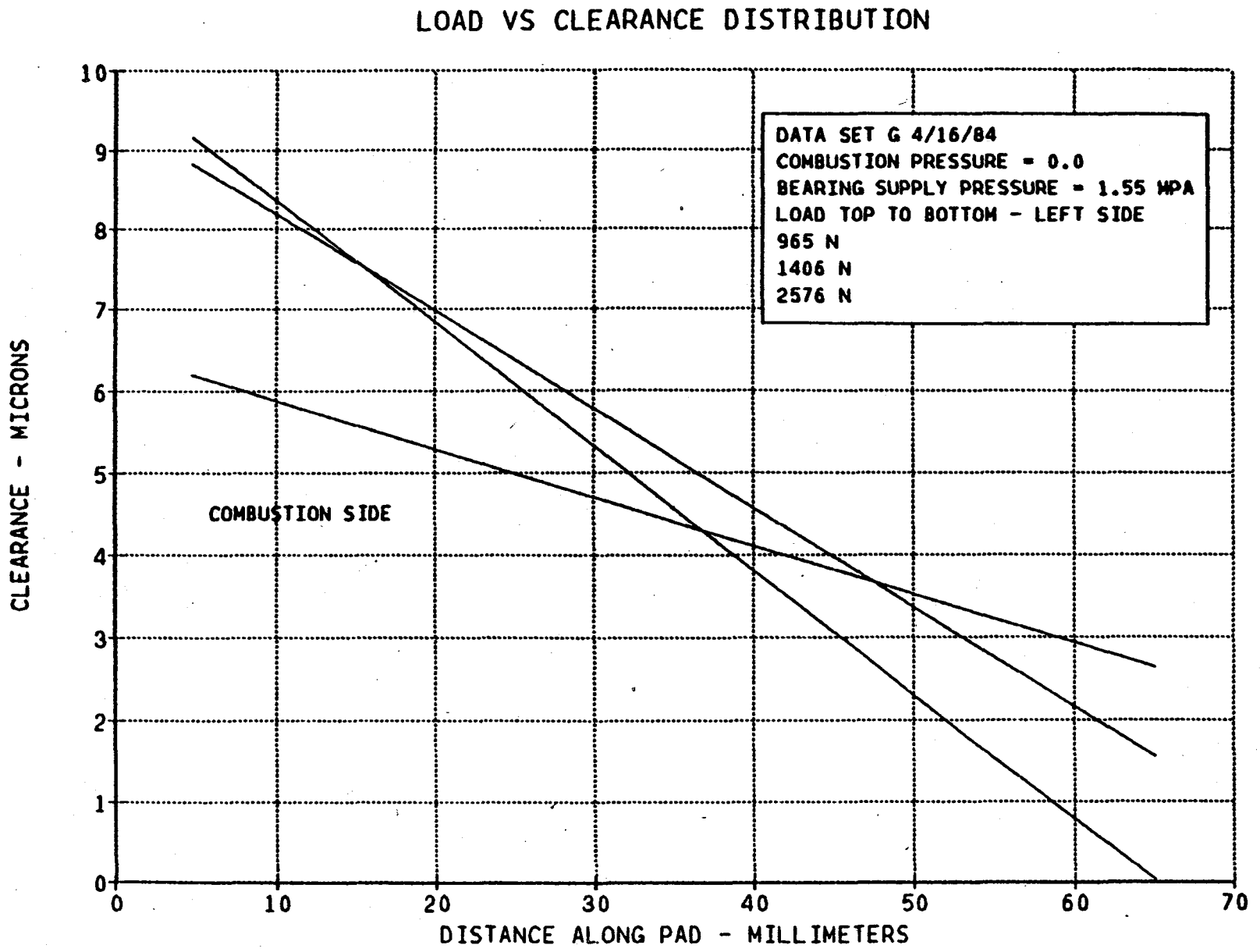
LOAD VS CLEARANCE DISTRIBUTION
DATA SET G 4/16/84
COMBUSTION PRESSURE = 0.0
BEARING SUPPLY PRESSURE = 1.55 MPA
LOAD TOP TO BOTTOM - LEFT SIDE
965 N
1406 N
2576 N
COMBUSTION SIDE
CLEARANCE - MICRONS
DISTANCE ALONG PAD - MILLIMETERS
0
1
2
3
4
5
6
7
8
9
10
0
10
20
30
40
50
60
70

APPENDIX C

RIG DRAWINGS

MECHANICAL TECHNOLOGY INCORPORATED
Latham, New York

PL 649E017
SHEET 1 OF 3

TITLE

CUMMINS DIESEL PISTON RING TEST RIG

SYM	REVISIONS	DATE	APPROVED
A	ISSUED	2 MAY 1990	E. Bruce
B	REVISED PER ECN 649-001	5 SEPT 1990	E. Bruce
C	REVISED PER ECN 649-007	9 DEC 1990	E. Bruce

DRAWN	E. Bruce 17 APR. 1990	CODE IDENT. NO. 26741
CHECKED	PDF... 21 APRIL 1990	PL 649E017 C
APPROVED	W. ... 23 APRIL 1990	SHEET 1 OF 3 REV

MECHANICAL TECHNOLOGY INCORPORATED
Latham, New York

PL649E017
SHEET 2 OF 3

TITLE

CUMMINS DIESEL PISTON RING TEST RIG

QTY./GROUP 4	3	2	1	ITEM NO.	PART NO.	DESCRIPTION
			X	1	649E017G1	ASSEMBLY
			X	2	649C018G1	SPANNER WRENCH
				3		
				4		
				5		
			1	6	649D009P1	BASE
			1	7	649E008P1	PISTON
			1	8	649C014G1	END CAP COMB. PRESS. INLET
			1	9	649C003G1	END CAP BRG. PRESS. SUPPLY
			1	10	649E011P1	CYLINDER
			2	11	649D 02G1	END MOUNTING BRACKET
			4	12	649C004 G1	PEDESTAL
			2	13	649D005G1	JACKSCREW SUPPORT
			4	18	649B006P1	DIFFERENTIAL SCREW
			4	19	649C007 P1	STRAIN GAGE - JACKSCREW
			12	20	10C000229	CAPACITANCE PROBE - M.T.I INST. DIV
				21		
				22		
				23		
				24		

		SYM	REVISIONS	DATE	CODE IDENT. NO. 26741
DRAWN	E Bruso 17 APR. 1980		SEE SHEET 1		PL649E017 C
CHECKED	P.DeFrancesco 21 APRIL 1980				SHEET 2 OF 3 RE
APPROVED	[illegible] 23 APR 80				

MECHANICAL TECHNOLOGY INCORPORATED
Latham, New York

PL649E017
SHEET 3 OF 3

TITLE

CUMMINS DIESEL PISTION RING TEST RIG

QTY./GROUP 4	3	2	1	ITEM NO.	PART NO.	DESCRIPTION
			2	26	*2-038N674-70	"O" RING, PARKER
			2	27	*2-165N674-70	"O" RING, PARKER
			12	28	B-400-1-4BT	MALE CONN., SWAGELOK
			1	29	B-1010-1-8	MALE CONN. 5/8 X 1/2 NPT, SWAGELOK
			1	30	B-1010-1-6	MALE CONN. 5/8 X 3/8 NPT, SWAGELOK
			1	31	B-1010-1-12BT	MALE CONN. 5/8 X 3/4 NPT, SWAGELOK
			4	32		SEAL RING (TETRASEAL #TS33-158-BUNA N GOSHEN RUBBER CO. OR EQ.)
				33		
			4P	34		TAPE, GRAFOIL (.005/.010 THK. SEALOL OR EQ.)
			AR	35		LOC TITE ANTI SEIZE (OR EQUIV.)
			12	36		HEX. SOC. HD. CAP SCR. ALLOY STL. 1/4-20UNC-2A X 7/8 LG.
			12	37		HEX. SOC. HD. CAP. SCR. ALLOY STL. 1/4-20UNC-2A X 1 3/8 LG.
			6	38		HEX. SOC. HD. CAP. SCR. ALLOY STL. 3/8-16UNC-2A X 1 3/8 LG.
			12	39		HEX. SOC. HD. CAP. SCR. ALLOY STL. 3/8-16UNC-2A X 1 1/8 LG.
			4	40	CS-16	HEX. SOC. NO-MAR SET SCR., PIC
			2 SETS	41	649D029G1	PISTON RING FINAL MACHINING
				X	649D025	SEGMENT ROUGH MACHINING
				X	649B022	INSERT, BACK FACE
				X	649C023	INSERT, FRONT FACE, TOP
				X	649C024	INSERT, FRONT FACE, BOTTOM

		SYM	REVISIONS	DATE	CODE IDENT. NO. 26741
DRAWN	E. Crook 17 APR. 1980		SEE SHEET 1		PL649E017 C
CHECKED	P DeFranco 21 APRIL 1980				SHEET 3 OF 3 REV
APPROVED	[signature] 22 APR 1980				

REVISIONS		SIZE E	649E017	REV B
LTR	DESCRIPTION	DATE	APPROVED
A	ISSUED	12-29-79	E Arnold
B	REVISED PER E.C.N. 644-001	11-13-80	E Arnold

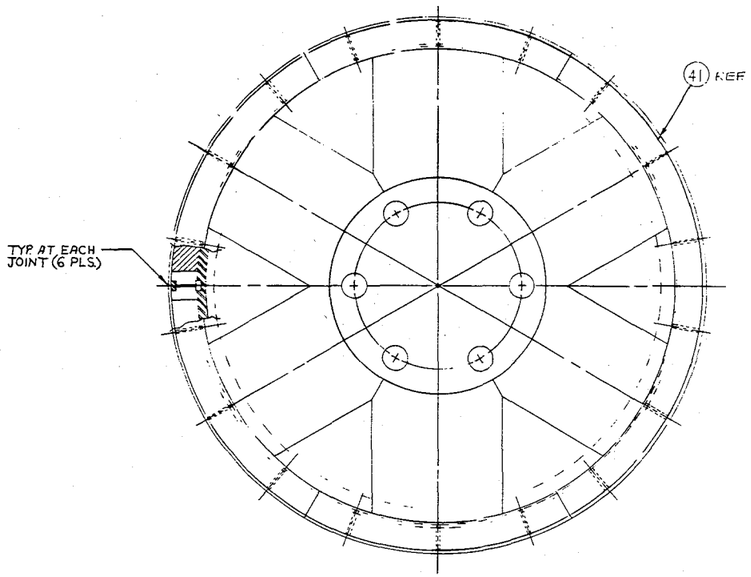

SECTION E-E
(SCALE: 2/1)
TYPICAL 2 PLACES

NOTES:
1. PISTON AND CYLINDER ASSEMBLY IS MOUNTED TO END MOUNTING BRACKET (ITEM 11) AS SHOWN. SHIM AS REQUIRED BETWEEN BRACKET AND PISTON TO OBTAIN SPECIFIED CLEARANCE.
2. TOP SURFACE OF DIFFERENTIAL SCREW (ITEM 18) SHALL BE FLUSH WITH BOSS ON JACKSCREW SUPPORT ASSEMBLY (ITEM 13). INSTALL JACKSCREW (ITEM 13) WITH CLEARANCE TO CYLINDER COUNTERBORE .030-.060 GAP AT JACKSCREW TIP.
3) MEASURE GAP BETWEEN FRONT FACE INSERTS OF PISTON THRUST SETS (ITEM 41). FILL GAP WITH GRAFOIL TAPE ITEM 34, .003-.005 OR .010 THK TAPE AS REQ'D. DO NOT COMPRESS TAPE MORE THAN .003.

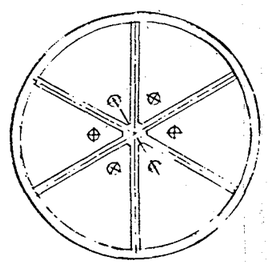

SECTION D-D

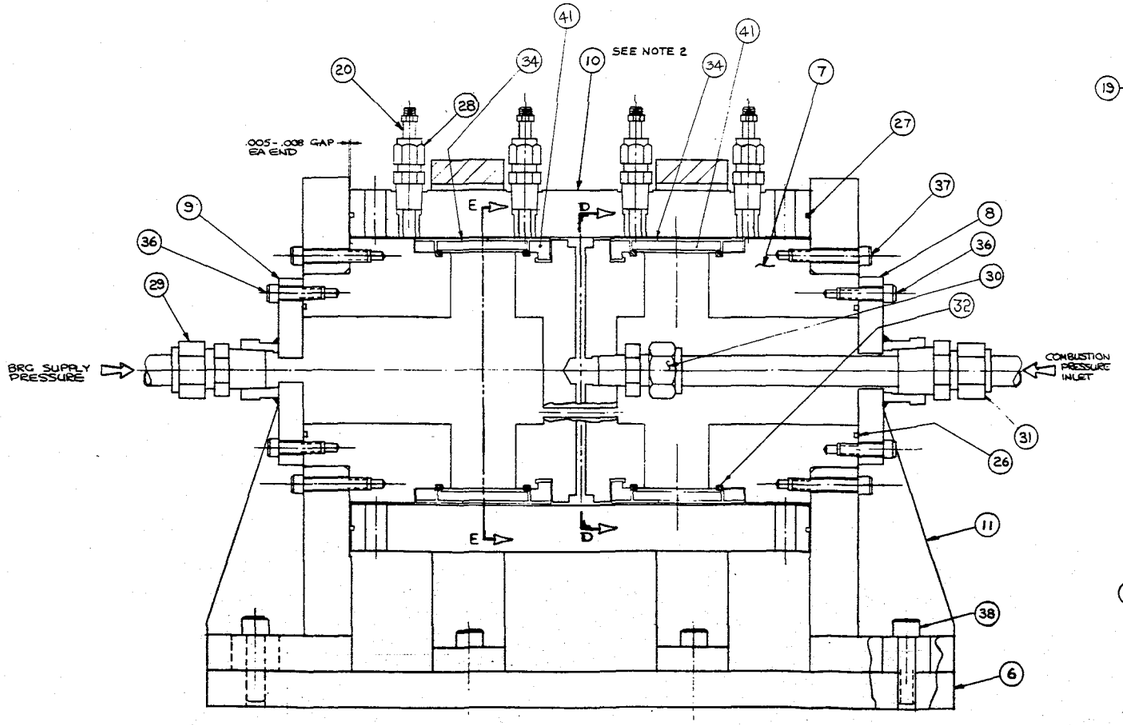

(G1) USE ITEM 35 (ANTI SEIZE CMPD) ON ALL THREADS EXCEPT PIPE THREADS.

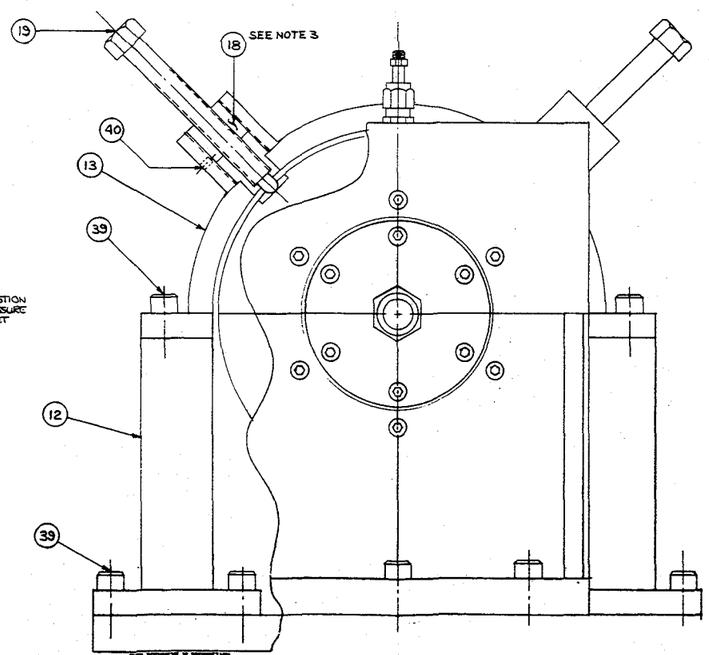

REVISIONS		D649D002	A
A	ISSUED		

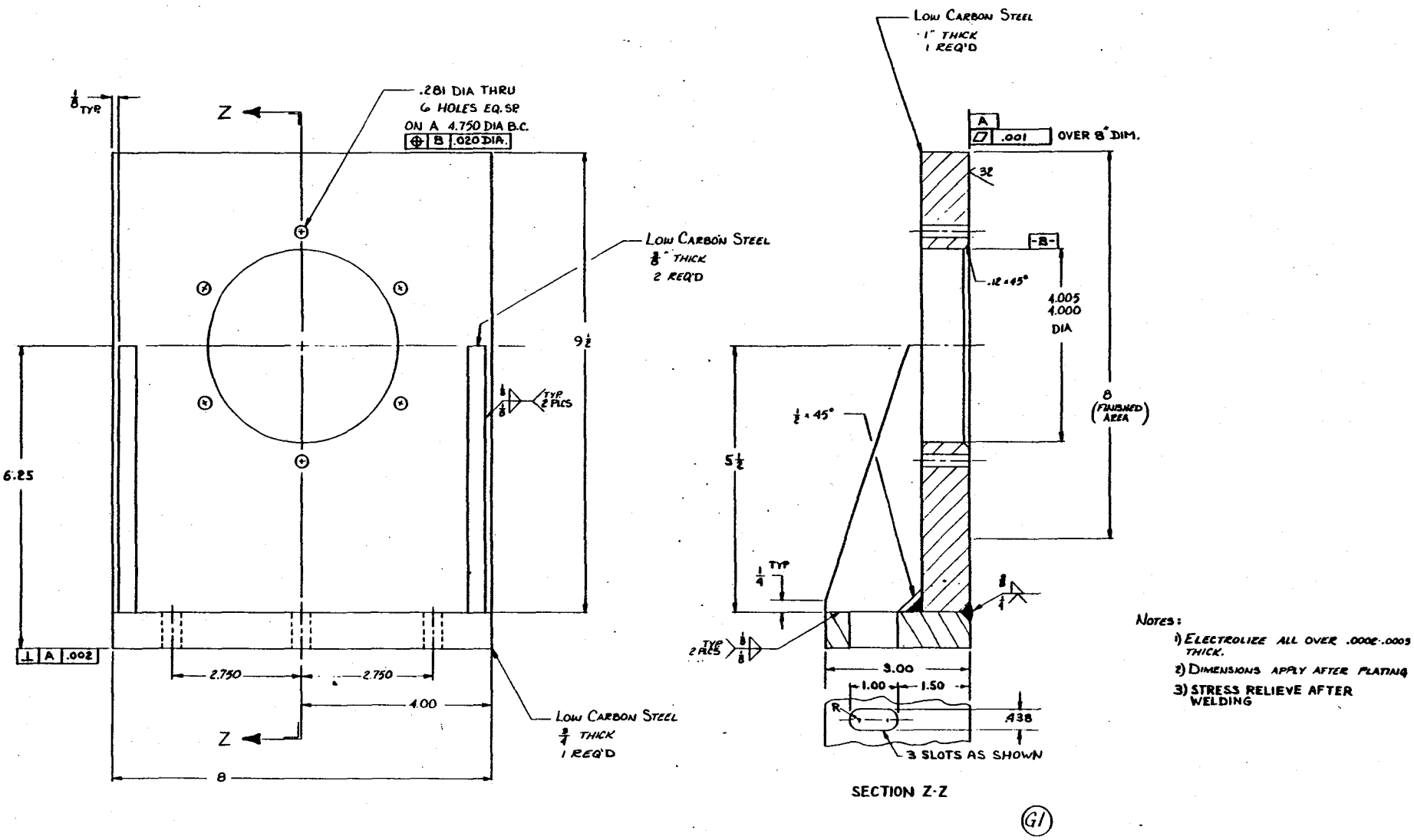

Notes:

1) ELECTROLIZE ALL OVER .0002-.0003 THICK.
2) DIMENSIONS APPLY AFTER PLATING
3) STRESS RELIEVE AFTER WELDING

(G1)

185

841118

REVISIONS		SIZE C	649C003	REV. A
SYM.	DESCRIPTION	DATE	APPROVAL	
A	ISSUED	2AA7 12Dc	E Burt	

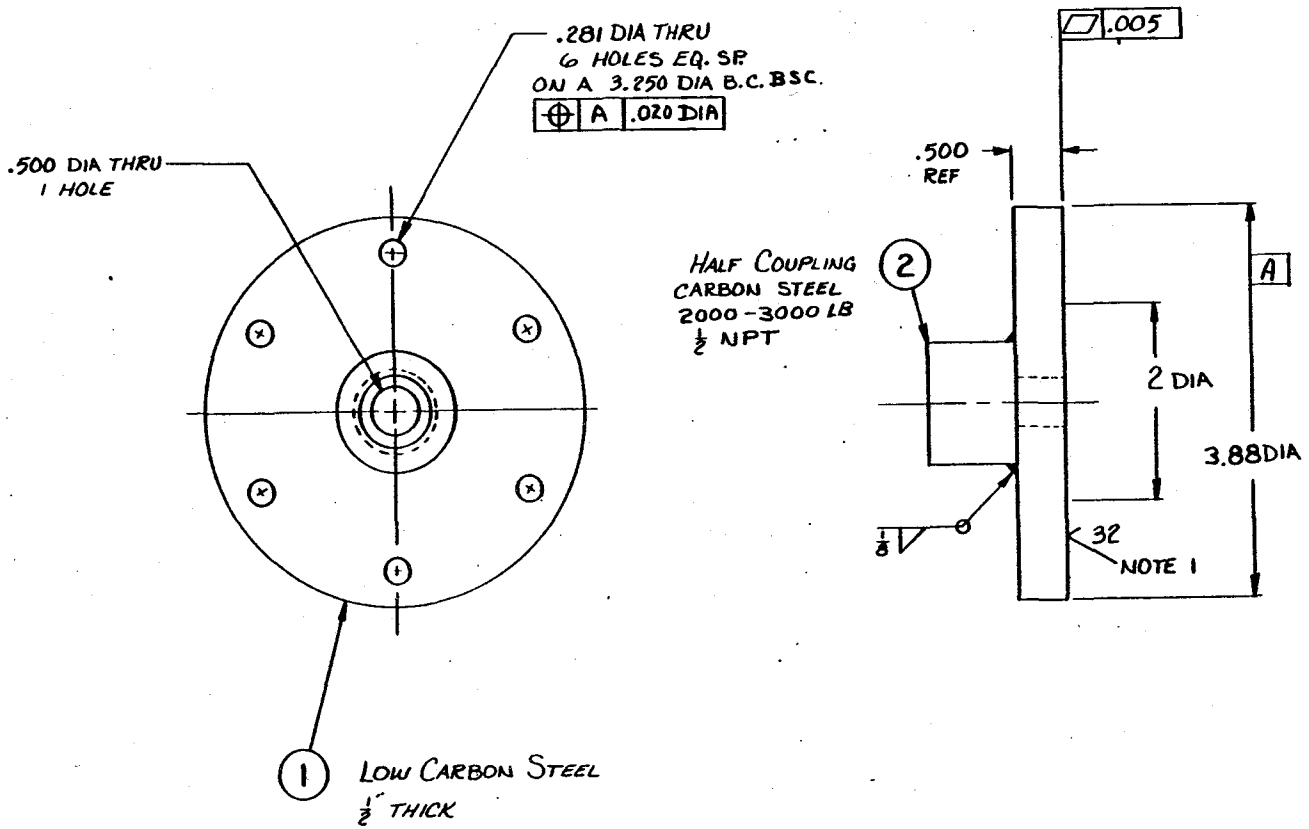

NOTES:

1) 32 FINISH REQUIRED BETWEEN 2 DIA AND 3.88 DIA.
2) BLACK OXIDE PER AMS 2485 ALL OVER AFTER FINAL MACHINING.
3) STRESS RELIEVE AFTER WELDING

REVISIONS		SIZE C	649C004	REV. A
SYM.	DESCRIPTION		DATE	APPROVAL
A	ISSUED		2 MAY 1280	E Rust

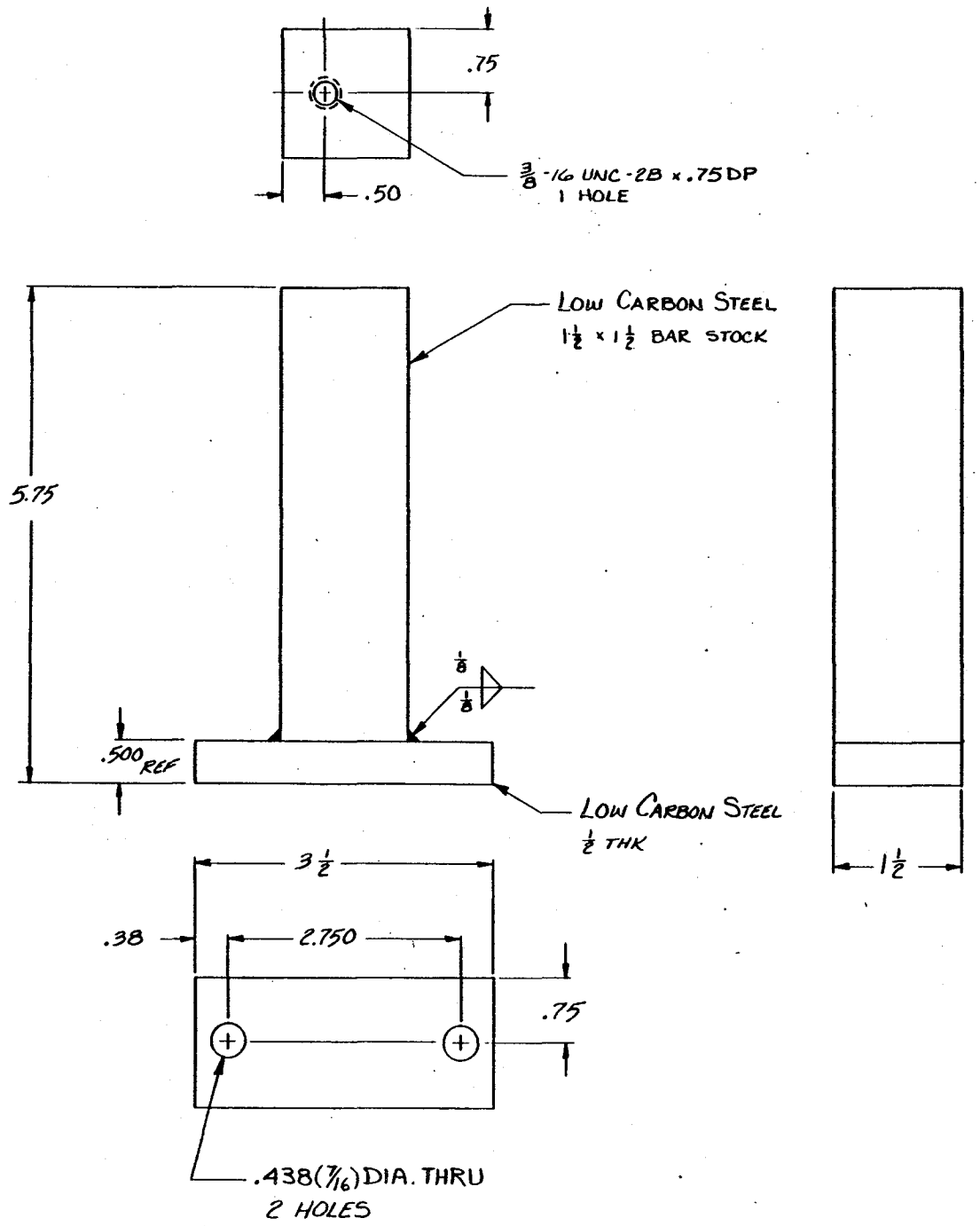

NOTES:
1) BLACK OXIDE PER AMS 2485 ALL OVER AFTER FINAL MACHINING
2) STRESS RELIEVE AFTER WELDING

REVISIONS			649D005	A
REV	DESCRIPTION	DATE	APPROVED	
A	ISSUED	1-26-87		

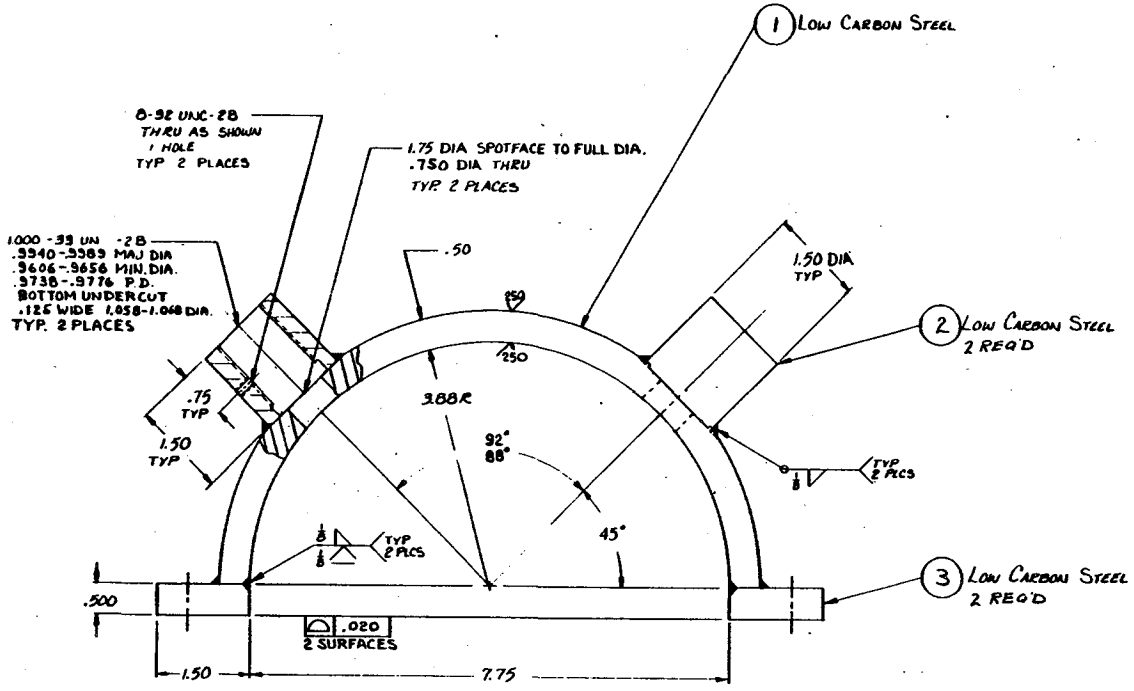

NOTES:

1. BLACK OXIDE PER AMS 2485 ALL OVER AFTER FINAL MACHINING
2. STRESS RELIEVE AFTER WELDING

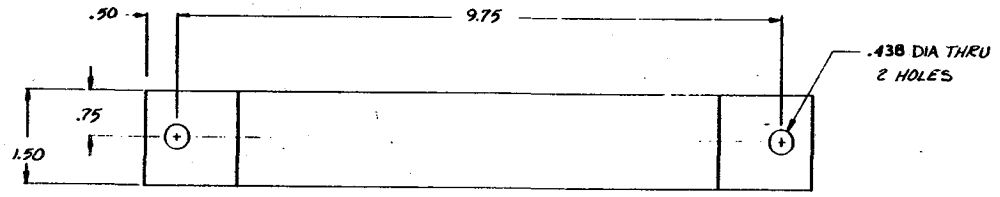

(G1)

REVISIONS		SIZE E	6498006	REV. A
SYM.	DESCRIPTION		DATE	APPROVAL
A				

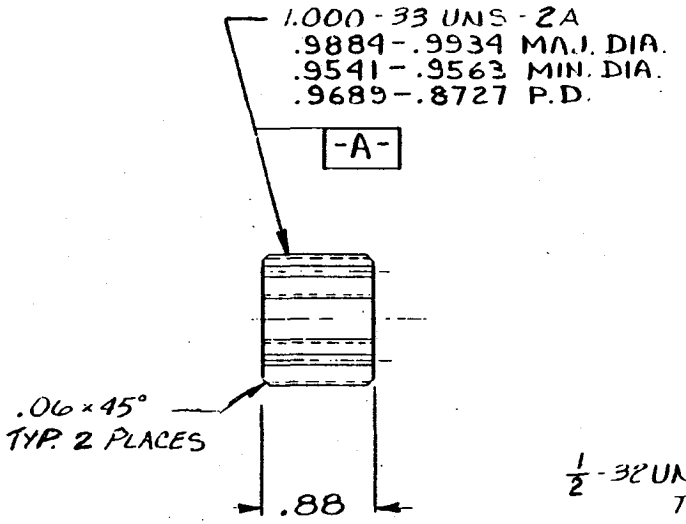

SECTION Z-Z

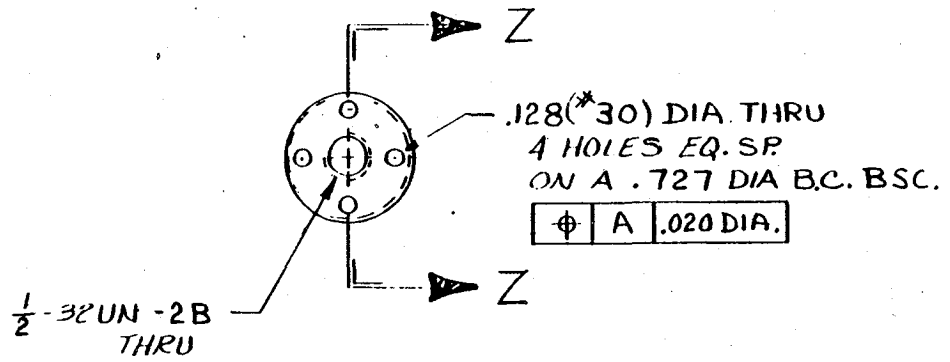

REVISIONS		SIZE C	649C007	REV. A
SYM.	DESCRIPTION	DATE	APPROVAL	
A	ISSUED	2 MAY 1961	C. Burst	

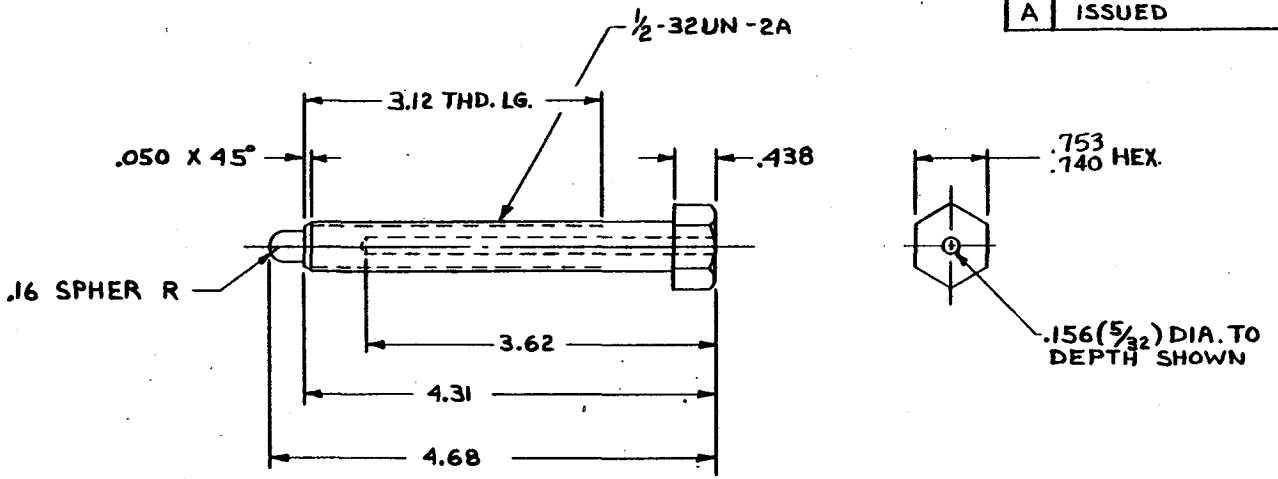

(P1) BOLT
MATL: SAE 4140
HEAT TREAT TO R_C 32-38
FIN: BLACK OXIDE

P1 THIS DWG (1)

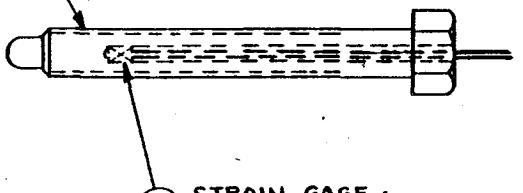

(2) STRAIN GAGE
120 OHM QUARTER BRIDGE, 150°F
CALIBRATION TO 10,000 LBS
TYPE C CONNECTOR TERMINATION
WITH TYPE C PLUG AND CABLE ASSY.
STRAINSERT CO.

(G1)

REVISIONS		E	649E006	G
LTR	DESCRIPTION		DATE	APPROVED
A	ISSUED		7-64	E. Bennett
B	REVISED PER E.C.N. 649-004		21 JUNE 1965	E. Bennett
C	REVISED PER ECN 649-002		13 DEC 72	E. Bennett
D	REVISED PER ECN 649-009		14 FEB 73	E. Bennett
E	REVISED PER ECN 649-010		12 APR 73	E. Bennett
F	REVISED PER ECN 649-011		27 APR 73	E. Bennett
G	ECN CHANGE 649-013		17 OCT 73	E. Bennett

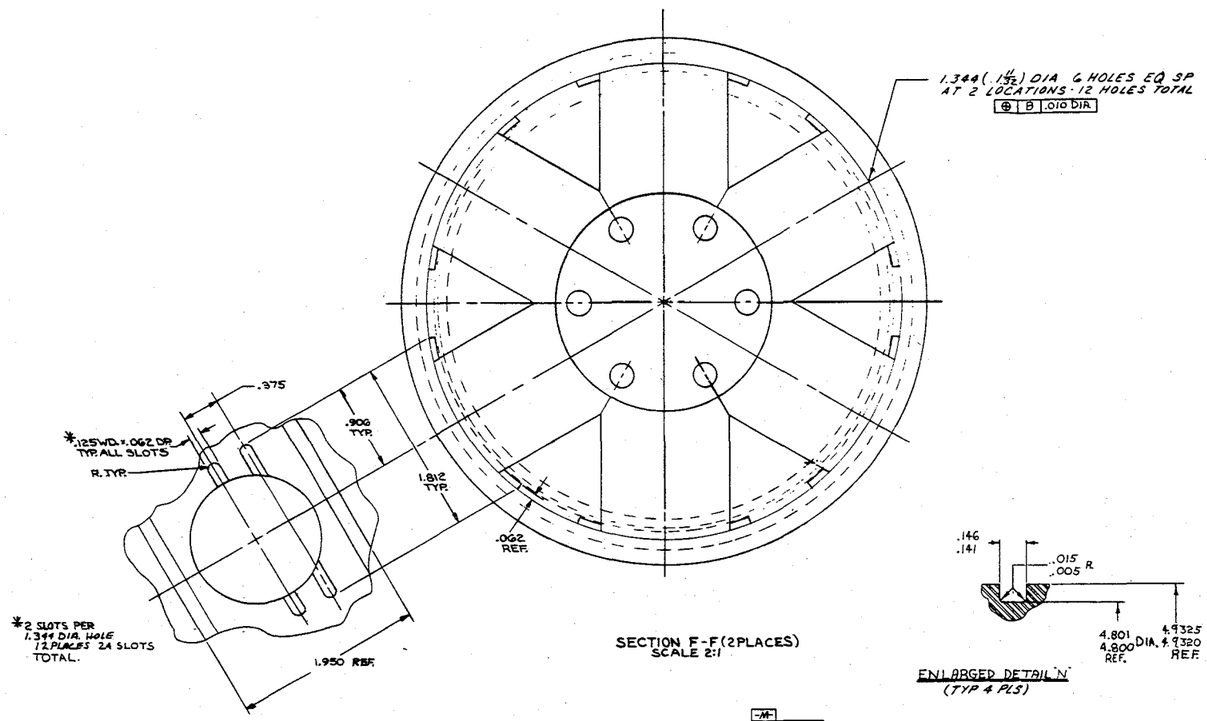

SECTION F-F (2 PLACES)
SCALE 2:1

ENLARGED DETAIL "N"
(TYP 4 PLS)

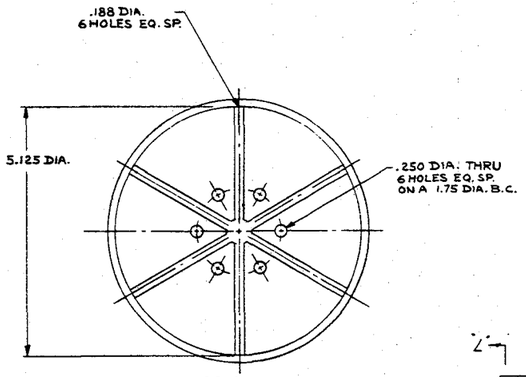

SECTION H-H

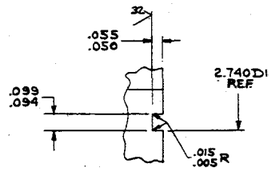

DETAIL "K" (2 PL)
SCALE 4:1

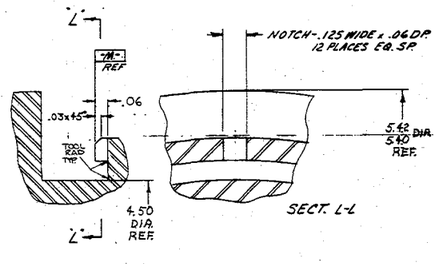

ENLARGED DETAIL "R" (TYP 2 PLS.)

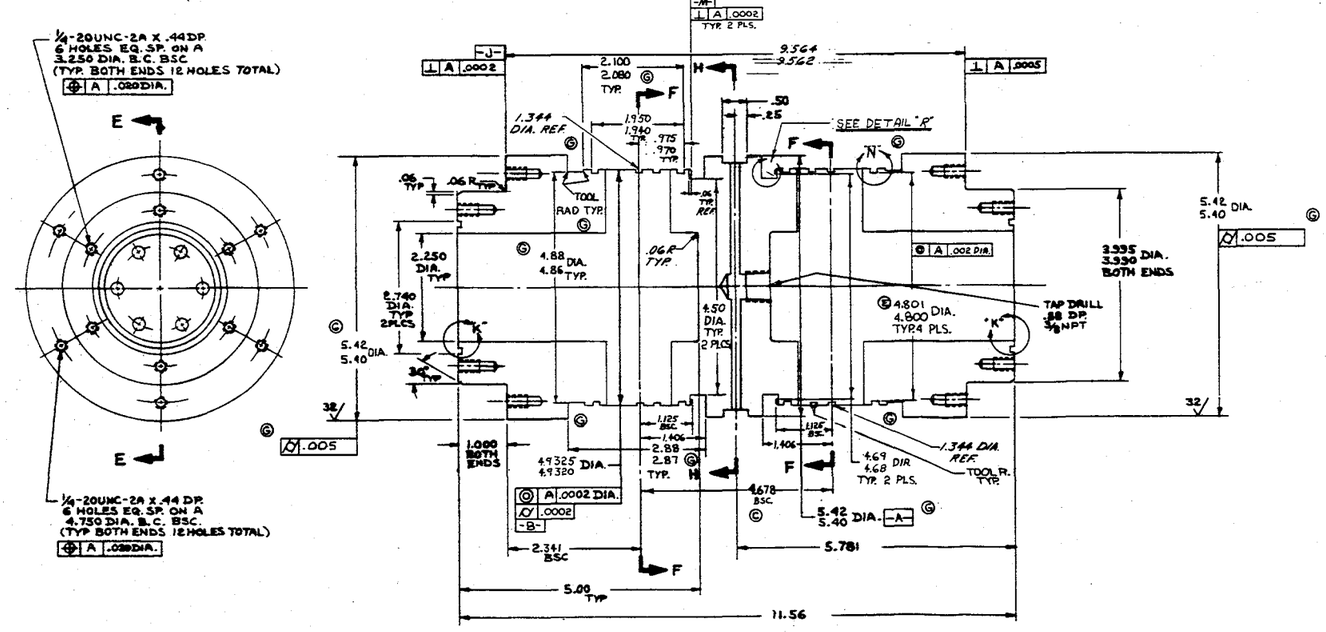

SECTION E-E

NOTES:

1- UNLESS OTHERWISE SPECIFIED ALL DIAMETERS TO BE CONCENTRIC TO DATUM -A- .010 DIA.

2- ELECTROLIZE ALL OVER, EXCEPT THREADED HOLES, 50-100 μ IN. THK.

3- DIMENSIONS APPLY AFTER PLATING

4- STRESS RELIEVE BEFORE FINAL MACHINING

(1)

842438

MTI-21954

REVISIONS		DWG D 649D009	REV A
REV	DESCRIPTION	DATE	APPROVED
A	ISSUED	8-24-47	

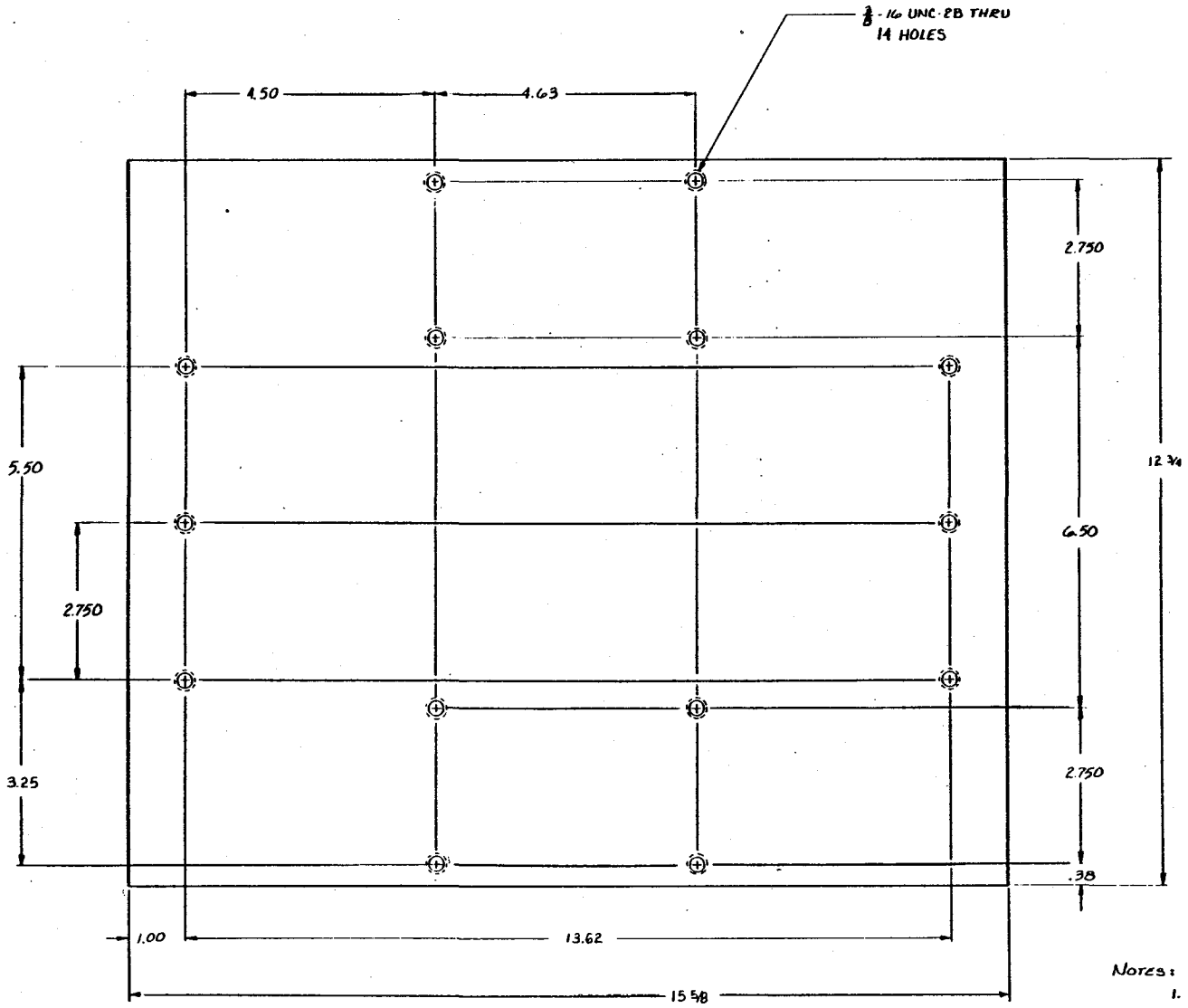

Notes:

1. LOW CARBON STEEL FLAT GROUND STOCK, OIL HARDENING GRADE STEEL OR STRIPPER PLATE

842440

REVISIONS	E	649E011	B
A	ISSUED		
B	ECN CHANGE 649-012		

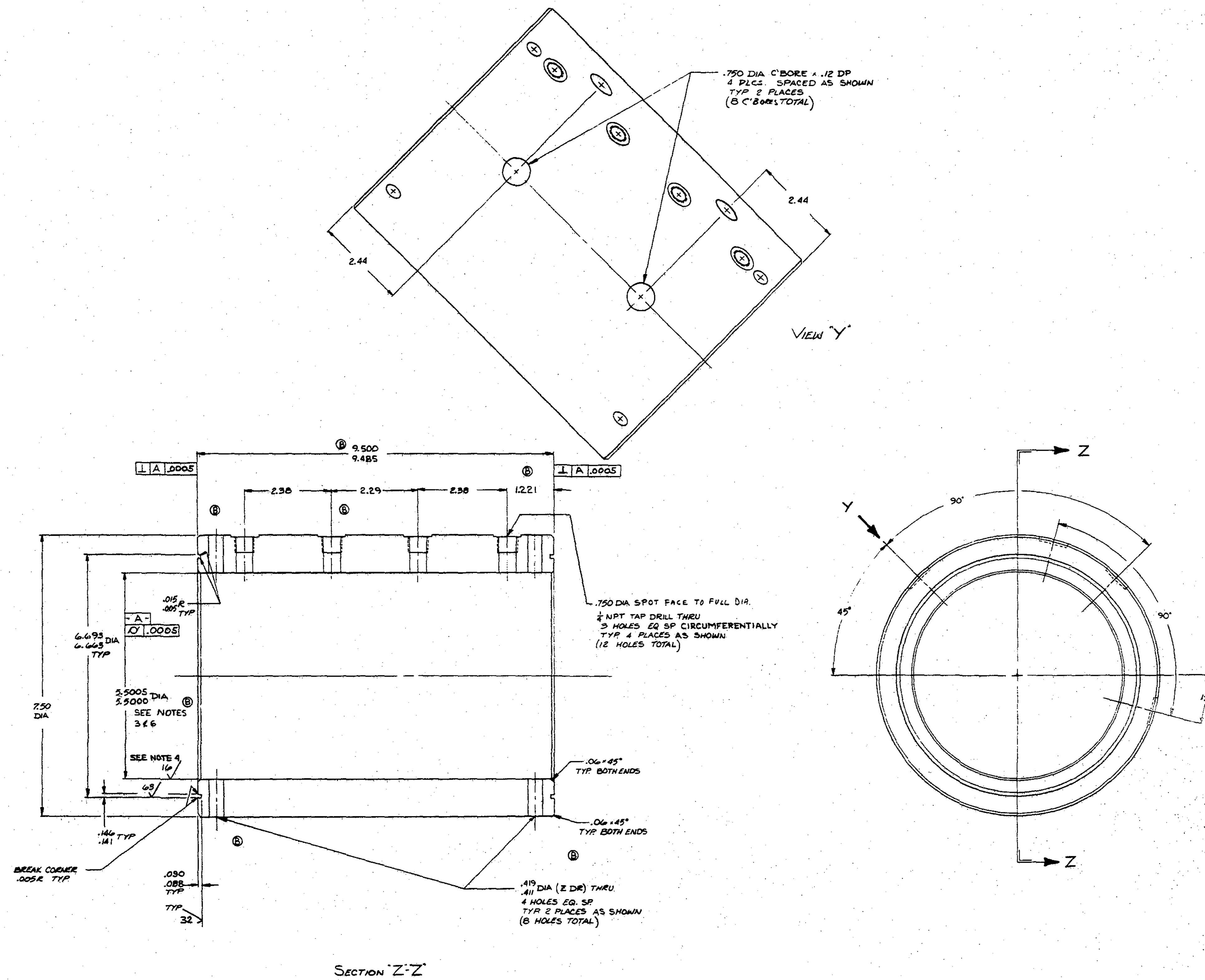

NOTES:

1) PART TO BE IN FULL ANNEALED CONDITION BEFORE FINAL MACHINING

(B) 2) ~~ELECTROLIZE ALL OVER .0002-.0003 THICK EXCEPT THREADED HOLES~~

3) DIMENSIONS APPLY AFTER PLATING

4) UNLESS OTHERWISE SPECIFIED ALL DIAMETERS TO BE CONCENTRIC WITHIN .010 DIA.

5) SURFACE FINISH NOTED APPLIES BEFORE PLATING

(B) 6) ELECTROLESS NICKEL PLATE CYL I.D. ONLY. .005-.006 THK PLATING SHALL BE IN ACCORDANCE WITH AMS 2404

REVISIONS		SIZE C	649C014	REV. A
SYM.	DESCRIPTION		DATE	APPROVAL
A	ISSUED		2 MAY 1980	L Brandt

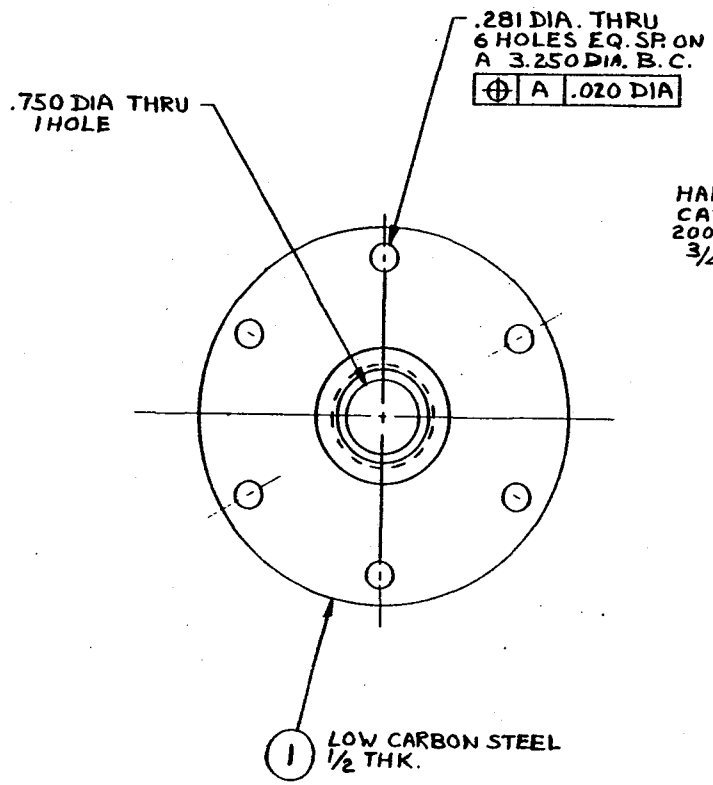

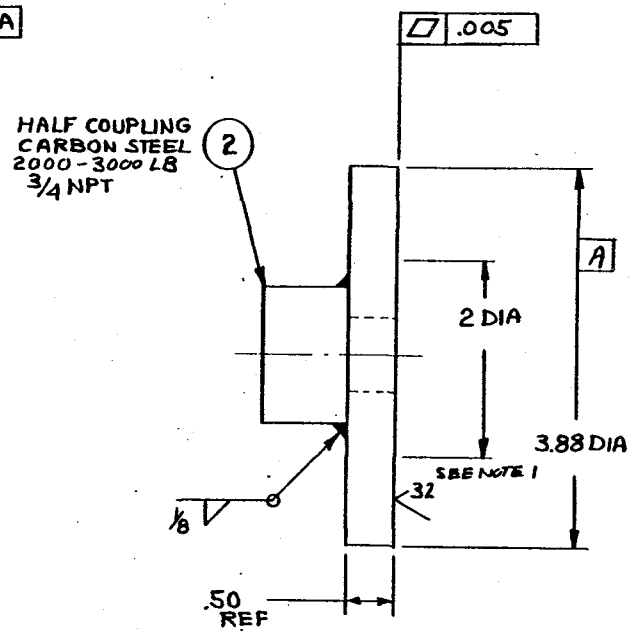

NOTES

1. 32 FINISH REQUIRED BETWEEN 2 DIA. AND 3.88 DIA.
2. BLACK OXIDE PER AMS 2485 ALL OVER AFTER FINAL MACHINING
3. STRESS RELIEVE AFTER WELDING

(61)

REVISIONS		SIZE C	649C018	REV. A
SYM.	DESCRIPTION	DATE	APPROVAL	
A	ISSUED	2 MAY 73	C. Brandt	

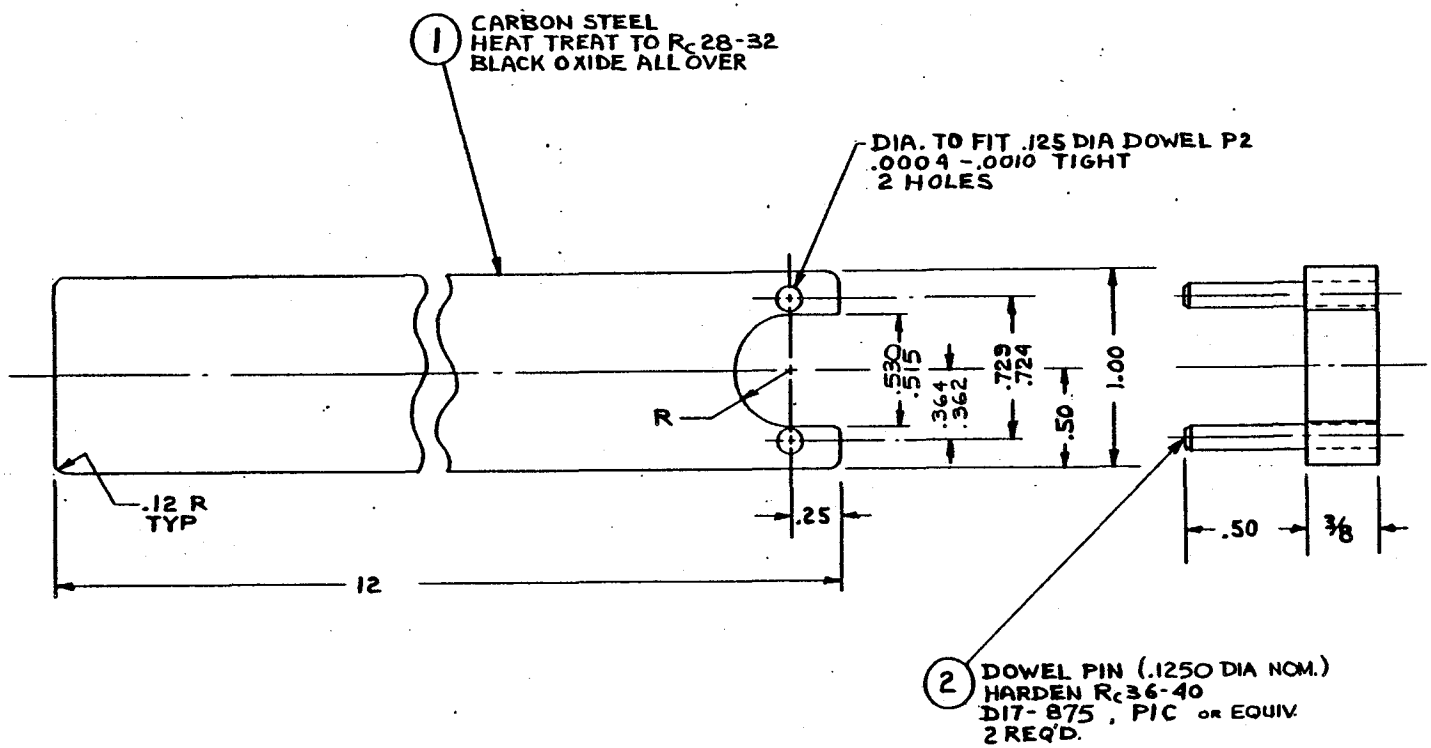

G1

198

842441

REVISIONS		SIZE C	649C023	REV. C
SYM.	DESCRIPTION	DATE	APPROVAL	
A	ISSUED	6 SEPT. 1980	E Brant	
B	REVISED PER ECN 649-003	8 OCT. 1980	E Brant	
C	REVISED PER ECN #649-008	3 DEC. 1980	E Brant	

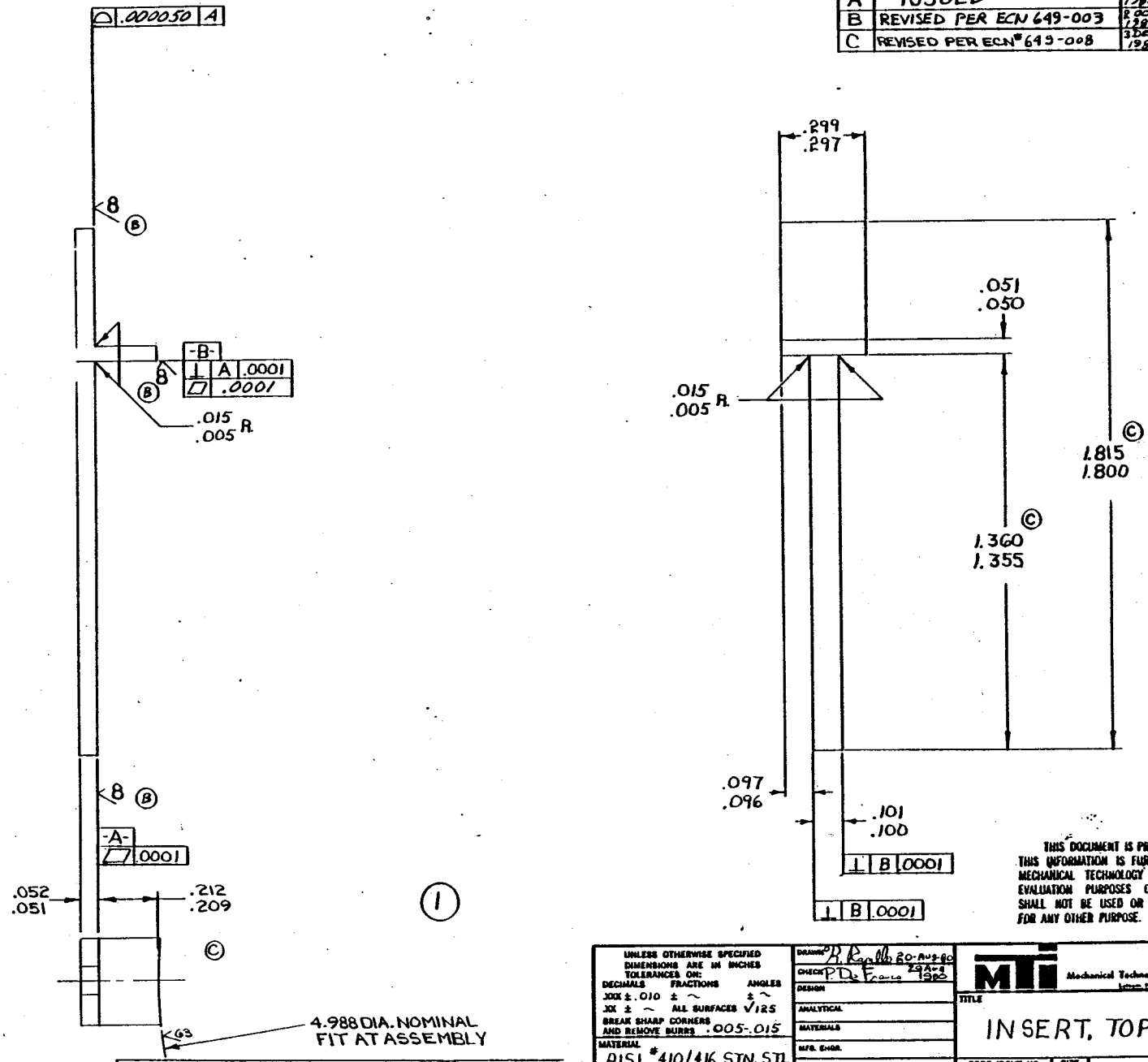

(1)

COMPANY CLASSIFICATION	
PROPRIETARY V	NAME AND TITLE E. Brant Mfgl. Engr
NON-PROPRIETARY	DATE 5 Sept. 1980

UNLESS OTHERWISE SPECIFIED DIMENSIONS ARE IN INCHES
TOLERANCES ON:
DECIMALS FRACTIONS ANGLES
.XXX ± .010 ± ~ ± ~
.XX ± ~ ALL SURFACES √125
BREAK SHARP CORNERS AND REMOVE BURRS .005-.015

MATERIAL: AISI #410/416 STN. STL.

TREATMENT: ANNEALED

DRAWN R. Rapelli 20-AUG-80
CHECK P.D. Evans 29 Aug 1980
DESIGN
ANALYTICAL
MATERIALS
MFG. ENGR.
PROJ. ENGR.
QUALITY CONTROL
H. Jones 9/3/80

Mechanical Technology Incorporated
Latham, New York

TITLE: INSERT, TOP FRONT

CODE IDENT NO.	SIZE	
26741	C	649C023

ISSUED	SCALE	WT.
5 SEPT. 80	4X	ACT. CALC.

REVISIONS		SIZE C	649C024	REV. C
SYM.	DESCRIPTION	DATE	APPROVAL	
A	ISSUED	5 SEPT. 1980	E Brault	
B	REVISED PER ECN 649-003	20 OCT. 1980	E. Brault	
C	REVISED PER ECN# 649-008	5 DEC. 1980	E Brault	

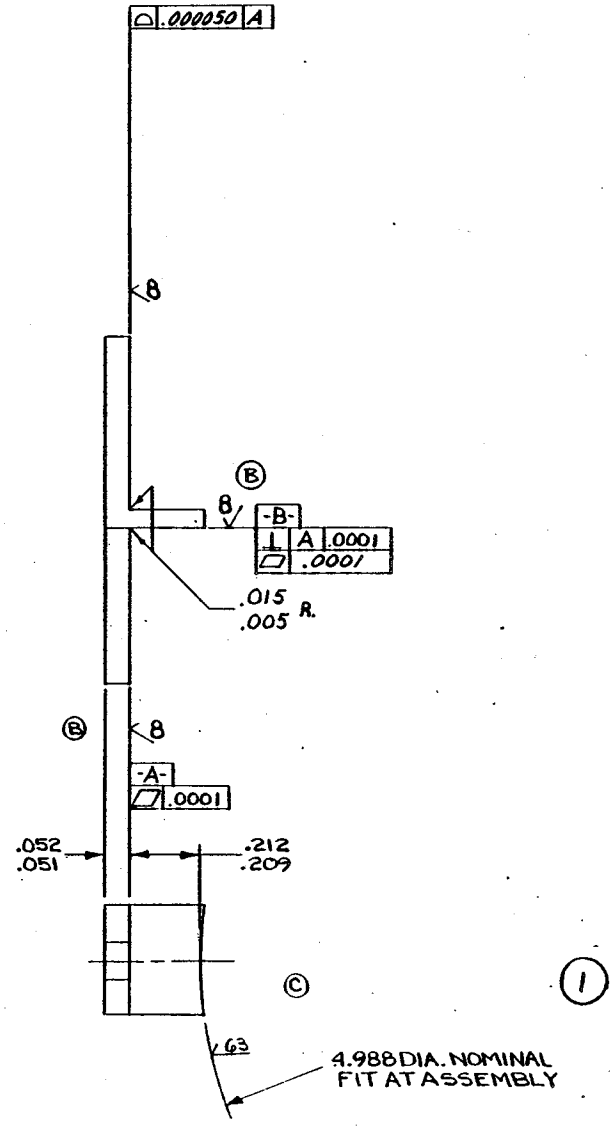

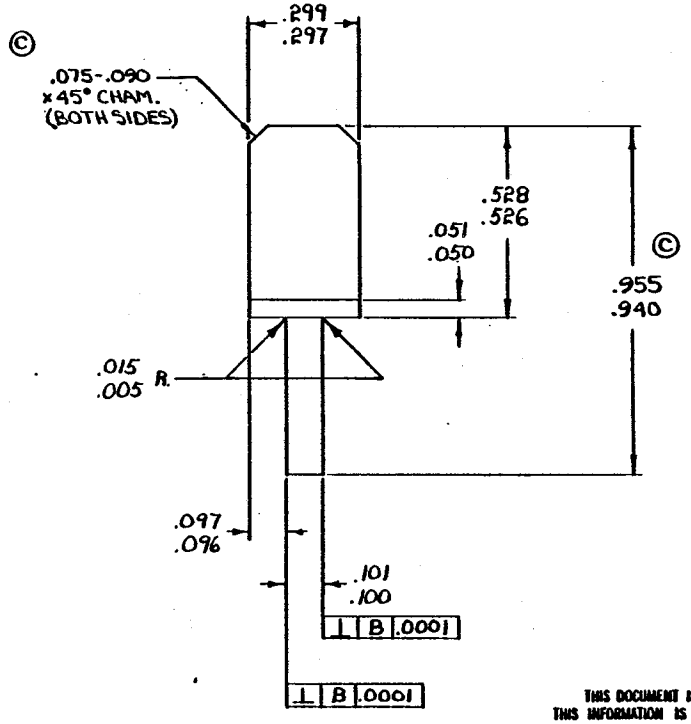

1

200

COMPANY CLASSIFICATION	
PROPRIETARY ✓	NAME AND TITLE E. Brault Draft Eng.
NON-PROPRIETARY	DATE 5 Sept 1980

UNLESS OTHERWISE SPECIFIED DIMENSIONS ARE IN INCHES
TOLERANCES ON:
DECIMALS FRACTIONS ANGLES
XXX ± .010 ± ~ ± ~
XX ± ~ ALL SURFACES √125
BREAK SHARP CORNERS AND REMOVE BURRS .005 - .015

MATERIAL: AISI #410/416 STN. STL.

TREATMENT: ANNEALED

DRAWN	R. Paulk 20 Aug 80
CHECK	PD&F 29 Aug 1980
DESIGN	
ANALYTICAL	
MATERIALS	
MFG. ENGR.	
PROJ. ENGR.	
QUALITY CONTROL	H. Jones 9/3/80

Mechanical Technology Incorporated
Latham, New York

TITLE: INSERT, BOTTOM FRONT

CODE IDENT NO.	SIZE	
26741	C	649C024

ISSUED 5 SEPT. 80 | SCALE 4-X | WT. ACT. CALC.

BRUNING 40-105 221-05-5

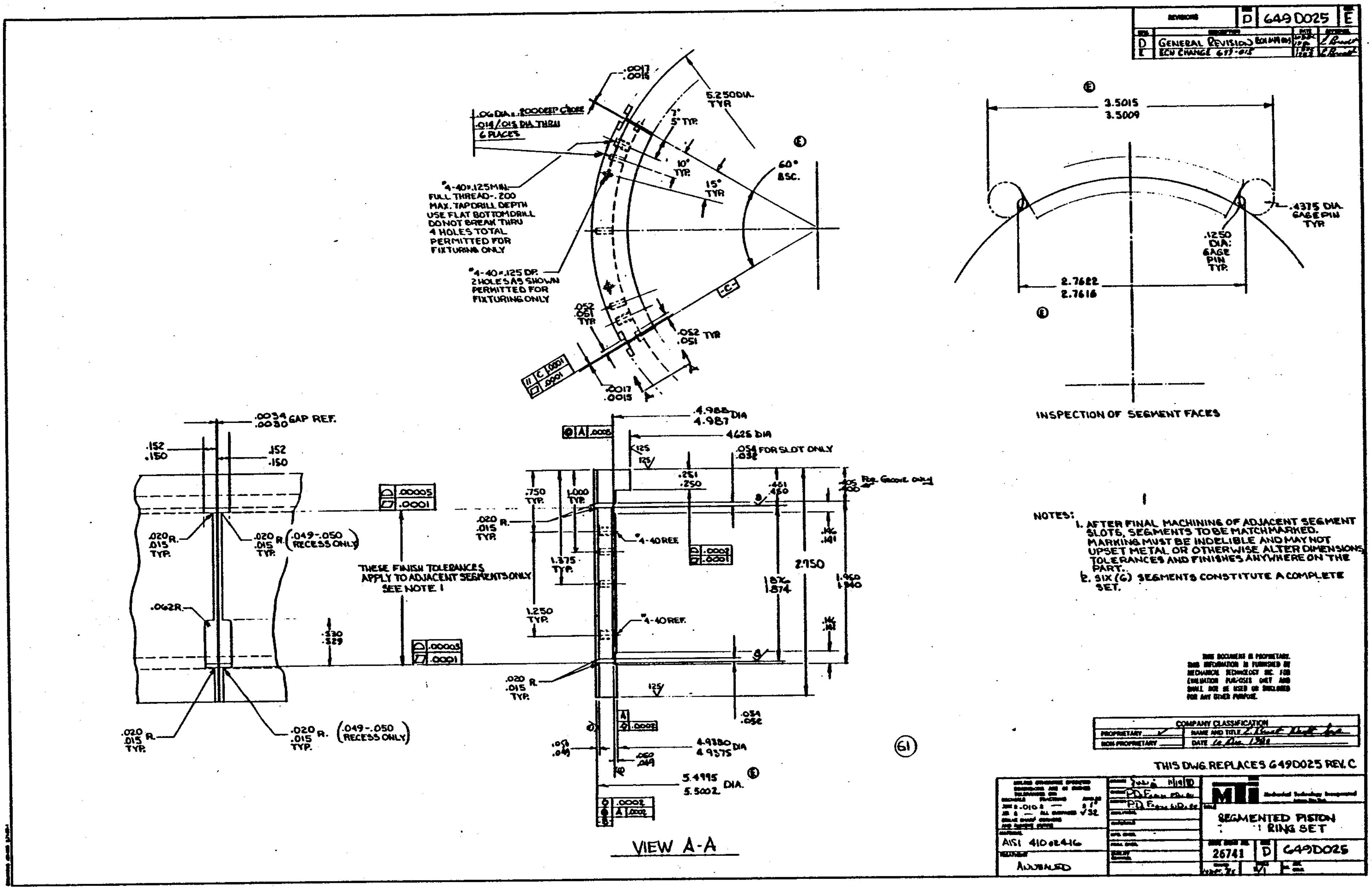
REVISIONS
D 649D025 E
D GENERAL REVISION
E ECN CHANGE
5.2500 DIA. TYP.
.0017 .0015
.06 DIA. x .200 DEEP C'BORE .014/.015 DIA THRU 6 PLACES
7° 5° TYP.
10° TYP.
15° TYP.
60° BSC.
#4-40 x .125 MIN. FULL THREAD - .200 MAX. TAP DRILL DEPTH USE FLAT BOTTOM DRILL DO NOT BREAK THRU 4 HOLES TOTAL PERMITTED FOR FIXTURING ONLY
#4-40 x .125 DP. 2 HOLES AS SHOWN PERMITTED FOR FIXTURING ONLY
.052 .051 TYP.
.052 .051 TYP.
.0017 .0015
3.5015 3.5009
.4375 DIA. GAGE PIN TYP.
.1250 DIA. GAGE PIN TYP.
2.7622 2.7616
INSPECTION OF SEGMENT FACES
.0034 .0030 GAP REF.
.152 .150
.152 .150
.020 .015 R. TYP.
.020 .015 R. (.049-.050 RECESS ONLY) TYP.
.062 R.
.330 .329
.00005 .0001
.00005 .0001
THESE FINISH TOLERANCES APPLY TO ADJACENT SEGMENTS ONLY SEE NOTE 1
.020 .015 R. TYP.
.020 .015 R. (.049-.050 RECESS ONLY) TYP.
4.988 4.987 DIA
4.625 DIA
.054 .032 FOR SLOT ONLY
.251 .250
.451 .450
.405 .400 FOR GROOVE ONLY
.750 TYP.
1.000 TYP.
#4-40 REF.
1.375 TYP.
1.250 TYP.
#4-40 REF.
1.876 1.874
2.750
1.960 1.940
.020 .015 R. TYP.
.054 .032
4.9380 4.9375 DIA
5.4995 5.5002 DIA.
VIEW A-A
NOTES:
1. AFTER FINAL MACHINING OF ADJACENT SEGMENT SLOTS, SEGMENTS TO BE MATCHMARKED. MARKING MUST BE INDELIBLE AND MAY NOT UPSET METAL OR OTHERWISE ALTER DIMENSIONS, TOLERANCES AND FINISHES ANYWHERE ON THE PART.
2. SIX (6) SEGMENTS CONSTITUTE A COMPLETE SET.
COMPANY CLASSIFICATION
PROPRIETARY
NON-PROPRIETARY
THIS DWG. REPLACES 649D025 REV. C
61
AISI 410 or 416
ANNEALED
MTI
SEGMENTED PISTON RING SET
26741 D 649D025

REVISIONS			D	G49D023	B
REV	DESCRIPTION	DATE	APPROVED		
A	ISSUED	9-24-86	L Brandt		
B	ECN CHANGE 649-016	11-21-88	L Brandt		

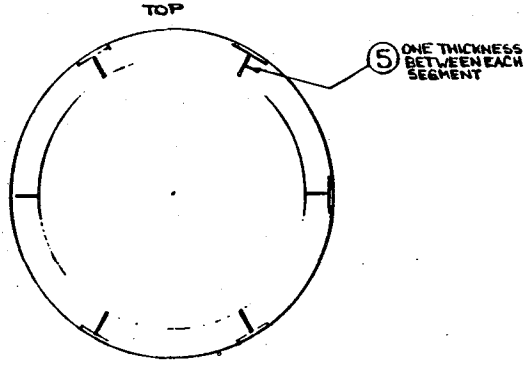

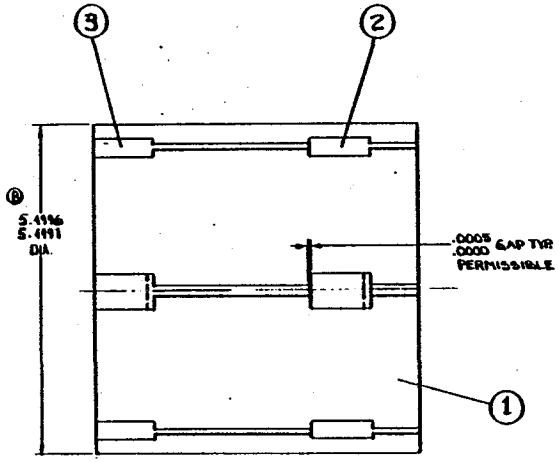

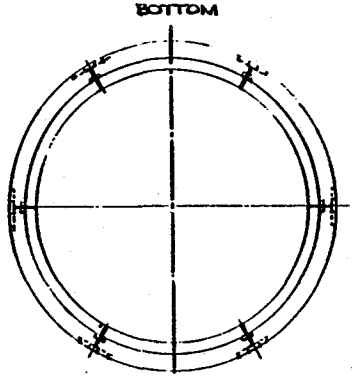

6

FINAL MACHINING PROCEDURE

1) ALL FRONT FACE INSERTS (ITEM 2,3) ARE TO BE FITTED TO RING SET (ITEM 1)
2) ALL FITTED INSERTS TO BE MATCH MARKED WITH SEGMENTS. MARKING MUST BE PERMANENT AND LEGIBLE AFTER FINAL FINISHING. NO UPSET METAL, DIMENSIONAL OR SURFACE FINISH CHANGES ARE PERMITTED BY MARKING PROCESS.
3) WITH AN EXTERNAL RING FIXTURE, DRY LAP O.D. OF ASSY. UNTIL INSERTS CONFORM TO O.D. SURFACE OF PISTON RING SET, AND DIAMETER IS TO DIMENSION SHOWN.
4) FIT PROTRUDING ENDS OF ITEM 2,3 FLUSH TO DIA. OF .111-.116 REF. WIDE GROOVE WITHIN ±.0002.
5) BACK FACE INSERT (ITEM 4) IS NOT MACHINED OR MARKED AT THIS OPERATION, BUT IS INCLUDED IN COMPLETED PISTON RING ASSY.

ITEM DWG.	PART No.	DESCRIPTION
AR 5		SHIM STOCK, .003-.0035 THK.
G 4	G49B022 P1	INSERT, BACK FACE
G 3	G49C023 P1	INSERT, FRONT FACE, TOP
G 2	G49C024 P1	INSERT, FRONT FACE, BOTTOM
1 1	G49D025 G1	PISTON RING SET

COMPANY CLASSIFICATION	
PROPRIETARY	NAME AND TITLE L Brandt Mgr Eng
NON PROPRIETARY ✓	DATE 9 Dec 1986

THIS DWG. REPLACES G49E026 REV. C

MTI

PISTON RING FINAL MACHINING

SIZE	DWG. NO.	REV
	26741	D G49D023

1. Report No.	2. Government Accession No.	3. Recipient's Catalog No.
NASA CR-174746		

4. Title and Subtitle	5. Report Date
Development of Gas-Lubricated Pistons for Heavy Duty Diesel Engine Technology Program	July 1984
	6. Performing Organization Code

7. Author(s)	8. Performing Organization Report No.
Wilbur Shapiro	MTI 84TR58
	10. Work Unit No.

9. Performing Organization Name and Address	11. Contract or Grant No.
Mechanical Technology Incorporated 968 Albany-Shaker Road Latham, New York 12110	DEN 3-309
	13. Type of Report and Period Covered
12. Sponsoring Agency Name and Address	Contractor Report
U.S. Department of Energy Office of Vehicle and Engine R & D Washington, D.C. 20585	14. Sponsoring Agency Code DOE/NASA/0309-1

15. Supplementary Notes

Final Report. Prepared under Interagency Agreement DE-A101-80CS50194. Project Manager, Howard Yacobucci, Transportation Propulsion Division, NASA Lewis Research Center, Cleveland, Ohio, 44135.

16. Abstract

Static testing of a segmented, gas-lubricated, piston-ring was accomplished. The ring utilizes high-pressure gas generated during the diesel cycle to energize a hydrostatic gas film between the piston and cylinder liner. The configuration was deficient in overall performance, because all segments of a ring set failed to form a fluid-film simultaneously, when exposed to internal preload. The difficulty was traced to the delicate moment balance required to prevent the segments from overturning and contacting the cylinder walls. Some individual sectors formed a film and performed well in every respect including load capability to 6,000 N. These results produce optimism as to the ultimate feasibility of hydrostatic, gas-lubricated piston rings. In addition to test results, the principles of operation, and theoretical developments are presented. Breathable liner concepts are suggested for future consideration. In these configurations, solid hydrostatic pistons are coupled with flexible liners that elastically deform to form a gas-film under hydrostatic pressurization. Breathable liners afford the mechanical simplicity required for mass produced engines, and initial examination indicates satisfactory operation.

17. Key Words (Suggested by Author(s))	18. Distribution Statement
Hydrostatic bearing Gas-lubrication Adiabatic diesel engine Self-adjusting clearance	Unclassified-Unlimited STAR Category 85 DOE Category UC-96

19. Security Classif. (of this report)	20. Security Classif. (of this page)	21. No. of pages	22. Price*
Unclassified	Unclassified	210	A10

*For sale by the National Technical Information Service, Springfield, Virginia 22161